The Seismic Response of Drilled Shaft Foundations

A thesis submitted in partial fulfilment of the requirements for the degree

of

Doctor of Philosophy

By

Alastair Chambers

Department of Civil Engineering

University of Canterbury

Christchurch

New Zealand

1999

ABSTRACT

During earthquakes, drilled shaft foundations are subjected to dynamic variations in load. These loads have been found to reduce the shaft capacity, with failure occurring at loads less than the design capacity of the foundation. The loads are applied as inertial loads at the head of the shaft and as predominantly horizontal shear loads along the buried length of the shaft. The seismic loads are of a cyclic nature, with significant frequencies ranging from 0.1 Hz to 10Hz. The duration of loading is usually less than 30 seconds.

This study experimentally determines the effect that the different forms of seismic loading have on the capacity of a drilled shaft foundation. A model drilled shaft of 95 mm diameter by 1450 mm buried length is constructed in a homogeneous deposit of cohesionless soil and is tested under cyclic loading that is representative of a seismic event. The study is performed in two separate stages. The first stage of tests has combinations of mean and cyclic load applied axially to the head of the shaft while the soil around the shaft is static. The second stage of tests has different axial loads applied to the head of the shaft while the soil around the shaft is shaken by a shaking table.

The stage 1 tests have shown that cyclic axial loading about zero mean load has the most detrimental effect on the stability of the model drilled shaft. A parameter called the Level of Load Reversal has been developed to quantify this result. A conceptual shear-zone model as also been developed to illustrate the behaviour of the soil around the drilled shaft during cyclic axial loading.

The stage 2 tests have shown that shaking of the soil increases the uplift capacity of the drilled shaft by increasing the density and stiffness of the soil mass. If a constant axial load is applied to the drilled shaft while the soil is shaken then the shaft will fail in uplift at considerably lower loads than the equivalent static capacity. The axial load magnitude causing uplift failure will also depend upon the level of shaking, with greater levels of shaking bringing greater reductions in uplift capacity during shaking.

If a constant axial load is applied to the drilled shaft while the soil is shaken then the shaft will also fail in uplift at considerably lower loads than the equivalent static capacity. The axial load magnitude causing uplift failure will be greater than that of the constant axial load and this difference may depend upon the cumulative displacement during each type of loading. The cyclic displacements will be smaller because each half cycle of uplift load is offset by each half cycle of compressive load. The effect of phase difference between peak uplift load and peak soil displacement is unclear from these tests.

This study has shown that drilled shaft foundations may fail during an earthquake at loads that are considerably lower than their design capacity. It is recommended that further experimental research be carried out in the area of seismic capacity of drilled shaft foundations. Particular emphasis should be placed upon the mechanisms and the soil properties that dictate the minimum level of foundation support during a seismic event.

ACKNOWLEDGEMENTS

I would like to thank the following people for their help in bringing this research together:

Kevin McManus – for his supervision, his guidance and his much needed pep talks.

The Technical staff of the Department of Civil Engineering, particularly John Maley – for their practical assistance, their innovation, their humour and their many rescue efforts.

The University of Canterbury and the French Government under Projet Nationale FOREVER – for the funding that made this research possible.

I would also like to thank the following people for making my time at University so enjoyable:

Nigel, Nathan, Jason and Graham – for all the highbrow and all the lowbrow times. I thank you for some of the best memories so far. I will treasure them and I look forward to many more.

Roger Dawe – for the peace that he has brought to my life.

Rob, Erica, Nick, the R'trays and all the people that have come and gone in the last eight years – for all the fun both on and off the field.

Rob Davis – for taking the risk and, in doing so, allowing me to experience the great enjoyment of teaching.

I would finally like to thank the following people for the wonderful life that I have had:

Mum – for being such a gorgeous, peaceful soul and for sharing yourself so generously with us all.

Dave, Bindy, Kathy, Jo and Kirsty – for laughing at me just when I needed it and for laughing with me just when I needed that too.

Charlotte Louise – for softening a grumpy old bear with your boundless love. Thank you for making me so happy.

Table of Contents

List of Figures

List of Tables

List of Symbols

English Letters – Upper Case

A_{loop}	area of hysteresis loop
A_t	area of tip of foundation
APSS	average peak shear strain
B	diameter of foundation
CLRL	critical level of repeated load
CSD	cyclic stability diagram
CYC	cyclic axial loading
D	depth of foundation
D_{10}	particle size with 10 % finer by mass
D_{60}	particle size with 60 % finer by mass
EI	flexural stiffness of foundation
E_s	subgrade modulus
G	soil shear modulus
G*	maximum (low strain) shear modulus
G_{sec}	secant shear modulus
G_{tan}	tangent shear modulus
H	depth of soil layer
K	coefficient of horizontal soil stress
[K]	soil spring stiffness matrix
LLR	level of load reversal
[M]	soil mass matrix
MC	monotonic compression
MU	monotonic uplift
N	number of lumped masses in soil layer, number of cycles of load
N_γ	bearing capacity factor
N_q	bearing capacity factor
P_o	magnitude of mean component of foundation load
P_c	amplitude of cyclic component of foundation load

Q_c	capacity in compression
Q_{cs}	static compressive capacity
Q_{cside}	side resistance in compression
Q_{ctip}	tip resistance in compression
Q_{side}	side resistance
Q_{tip}	tip resistance
Q_u	monotonic uplift capacity
Q_{ud}	static uplift capacity after soil shaking
Q_{us}	static uplift capacity before soil shaking
Q_{uu}	static uplift capacity during soil shaking
Q_{uside}	side resistance in uplift
Q_{utip}	tip resistance in uplift
S	stable
U	unstable
W	weight of foundation

English Letters – Lower Case

a	soil reaction degradation parameter, radius of hole
c	viscous damping coefficient, data not recorded
[c]	soil damping matrix
d	failed in uplift prior to test completion
d_p	displacement accumulated during cyclic loading
d_{ppl}	peak to peak displacement for first cycle of load
d_{ppf}	peak to peak displacement for final cycle of load
e	equipment failure
e_{min}	minimum void ratio
e_{max}	maximum void ratio
h	depth between lumped masses
m	change in uplift capacity after cyclic loading
p'	effective normal stress
p	longitudinal seismic wave, lateral soil reaction

p_N	cyclic soil reaction for N cycles of load
p_1	cyclic soil reaction for first cycle of load
q	vertical effective stress at tip of foundation
r	radial cylindrical coordinate
s	transverse seismic wave
u	horizontal relative soil displacement
$\dot{u}$	horizontal relative soil velocity
$\ddot{u}$	horizontal relative soil acceleration
$\ddot{u}_b$	horizontal bedrock acceleration
u_g	horizontal bedrock displacement
x	depth along foundation, horizontal cartesian coordinate
x*	normalised deflection of laminar tank
y	lateral foundation displacement, horizontal cartesian coordinate
z	vertical cartesian coordinate, vertical cylindrical coordinate
z*	normalised depth of laminar tank

Greek Letters

ε	volumetric strain
$\bar{\phi}$	soil effective stress friction angle
ϕ_{ss}	steady state friction angle
γ	shear strain
γ_c	maximum shear strain
γ_r	resilient shear strain
ρ	soil mass density
ρs	density of solid particles
σ_h	horizontal effective stress
σ_r	radial effective stress
σ_θ	tangential effective stress
$\overline{\sigma_v}$	vertical effective stress

τ	shear stress
τ_c	maximum shear stress
τ_{max}	maximum shear stress
$\tau_{r\theta}$	horizontal shear stress
θ	tangential cylindrical coordinate
ξ	equivalent linear damping ratio
ζ_{qd}	bearing capacity modification factor
ζ_{qr}	bearing capacity modification factor
ζ_{qs}	bearing capacity modification factor

Chapter 1

INTRODUCTION

Most foundations will be subjected to variations in load over their design life. The variations may be due, in part, to high winds, vehicular loads or earthquakes. The understanding of foundation behaviour under statically varying loads is well established but little is known about the behaviour of foundations under dynamically varying loads. Recent research has shown that deep foundations may undergo a degradation in load carrying capacity when subjected to cyclically varying axial loads.

This study examines the specific case of drilled shaft foundations in cohesionless soil, subjected to the dynamic loading that is typical of a seismic event. Drilled shaft foundations are often used to support structures with high aspect ratios, including many bridges, high-rise buildings and elevated tanks. Earthquake loading in such cases tends to induce large cyclic axial loads on the drilled shafts, as shown in Figure 1.1. In many cases, net uplift loading of the foundations will result.

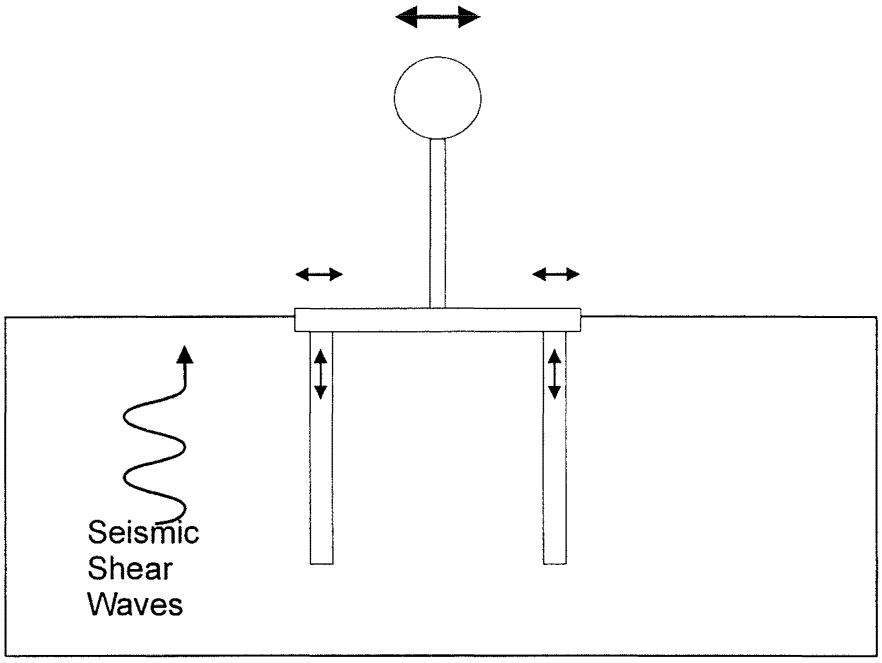

Figure 1.1 – Earthquake Induced Axial Loads on Drilled Shafts

Observations after the 1985 Mexico City earthquake (Girault 1986) indicated that some 25 buildings supported on friction piles suffered sudden settlements during the earthquake. At least one building overturned (Mendoza and Auvinet 1988), with several of the friction piles having pulled out of the soil. Zeevaert (1991) concluded that cyclic axial loading during the earthquake mobilised the side capacity of the piles, allowing plunging deformation to occur. It is not clear from these observations, however, whether the failures were caused by simple overloading of the piles by the earthquake induced axial forces, or by degradation of the side friction capacity of the piles during cyclic loading. This study aims to identify the mechanisms that cause instability during seismic loading and to quantify the parameters that are critical to the stability of the drilled shaft.

This chapter introduces the drilled shaft foundation and outlines the methods used to predict its load carrying capacity. The methods are taken from Turner & Kulhawy (1987) and McManus & Kulhawy (1991). A summary is given of the present knowledge concerning the fundamental behaviour of drilled shaft foundations under dynamic loading. A summary is also given of the behaviour of cohesionless soils under cyclic loading. Finally, the scope of this study is outlined and the overall research methodology is explained.

1.1 DRILLED SHAFT FOUNDATIONS

A drilled shaft is essentially a cylindrical hole in the ground that is filled with concrete. The concrete may be reinforced, and the bottom can be belled in certain soils, although only straight-sided shafts are considered herein. In most cohesionless soils, the drilling of the hole is preceded by driving a steel casing into the ground. The soil within the casing is excavated with the drill, leaving the casing to provide lateral support for the soil around the hole. The casing may or may not be removed after the concrete has been placed. Details of the various construction methods and equipment may be found in Greer and Gardner (1986).

Drilled shaft foundations develop resistance to axial loads from a combination of side resistance, Q_{side} and tip resistance, Q_{tip}, as shown in Figure 1.2. The resisting forces must be in equilibrium with the applied load, so the compressive capacity, Q_c is given by:

$$Q_c = Q_{cside} + Q_{ctip} - W \tag{1.1}$$

where the subscript c refers to compression and W is the weight of the drilled shaft. Similarly, the uplift capacity Q_u of the drilled shaft is given by:

$$Q_u = Q_{uside} + Q_{utip} + W \tag{1.2}$$

where the subscript u refers to uplift.

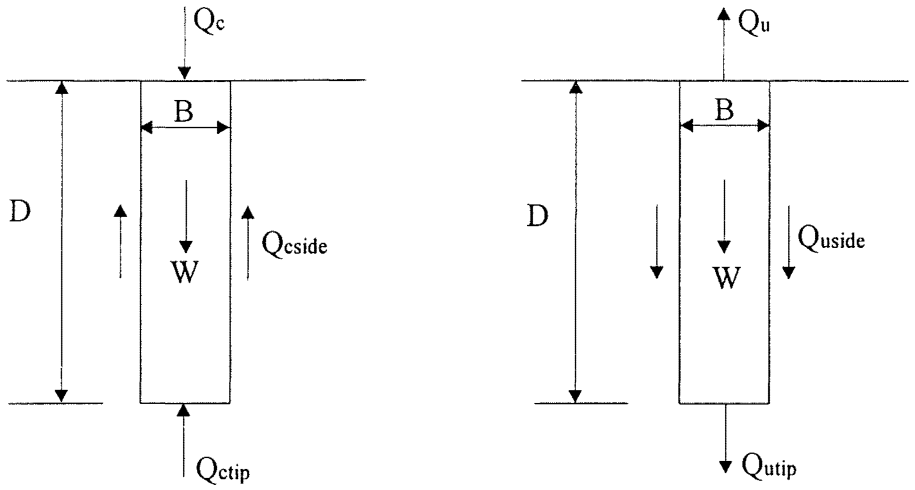

a) Compression **b) Uplift**

Figure 1.2 – Equilibrium Forces Acting on a Drilled Shaft Foundation

A comprehensive research programme by Stewart and Kulhawy (1981) and Kulhawy (1981), which included analytical and experimental modeling of drilled shafts in

uplift, has shown that the side resistance of straight-walled drilled shafts results from friction acting over a cylindrical surface that forms close to the soil/concrete interface.

Methods for predicting the side resistance of drilled shafts are based on fundamental effective stress concepts. For long-term or static loading, under drained conditions, the side resistance is given by:

$$Q_{side} = \int_{surface} \tau(z)dz \tag{1.3}$$

where $\tau(z)$ is the shearing resistance with depth along the side of the foundation and the integral is a summation of the shear stresses over the contact area of the foundation. The side resistance of a straight-walled drilled shaft is therefore given by:

$$Q_{side} = \pi B \int_0^D K(z)\overline{\sigma_v}(z)\tan\bar{\phi}(z)dz \tag{1.3}$$

where K is the coefficient of horizontal soil stress, $\overline{\sigma_v}$ is the vertical effective stress, $\bar{\phi}$ is the soil effective stress friction angle, B is the diameter of the shaft, D is the depth of the shaft and $Q_{side} = Q_{uside} = Q_{cside}$.

For shafts in compression, the tip capacity develops from a bearing capacity mechanism beneath the tip. Vesic (1977) observed that the failure zone consists of a highly compressed conical wedge that forces its way through the soil mass, as shown in Figure 1.3.

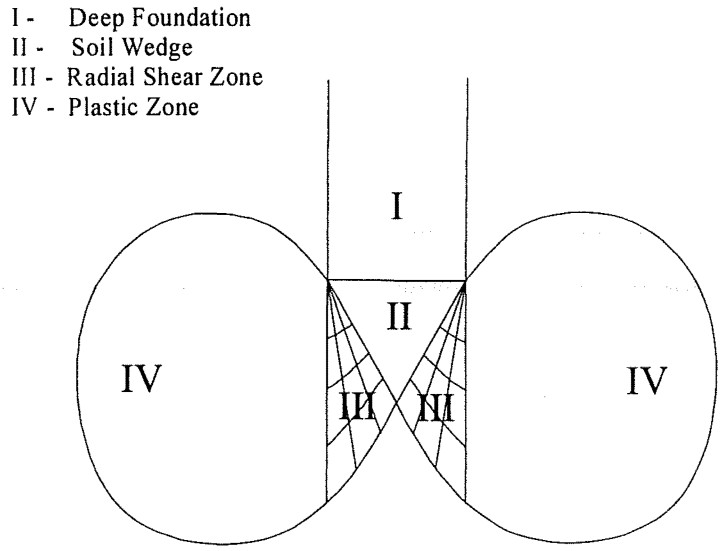

Figure 1.3 – Failure Mode Beneath the Tip of a Deep Foundation (from Vesic (1977))

The ultimate compressive tip capacity, Q_{ctip}, for a drilled shaft in cohesionless soil during drained loading, neglecting the N_γ term which commonly is small by comparison, can be approximated by:

$$Q_{ctip} = A_t \; q \; N_q \; \zeta_{qr} \; \zeta_{qs} \; \zeta_{qd} \tag{1.4}$$

where A_t is the area of the tip, q is the value of vertical effective stress at the level of the tip and N_q is a bearing capacity factor. The ζ terms are modification factors, where the subscript q indicates the portion of bearing capacity from the soil overburden above the tip and the second subscripts indicate the reason for modification. Equation 1.4 is subject to the stipulations of vertical foundation, vertical concentric loading, horizontal ground surface and horizontal foundation tip. The bearing capacity and modification factors may be found in Vesic (1977).

1.2 CYCLIC SOIL RESPONSE

The behaviour of soils under cyclic loading appears to be highly complex and, to date, even the most sophisticated models cannot provide accurate predictions of the behaviour under generalised cyclic stress conditions. There are, however, a number of characteristic properties that are exhibited by all soils under cyclic loading.

Cyclic loading of a soil brings about stress reversals as the load changes from increasing load to decreasing load and vice versa. Each stress reversal brings a change in the stiffness of the soil and each cycle of loading generates energy losses, causing the soil to undergo both hysteretic but recoverable strain and residual or non-recoverable strain. An idealisation of this behaviour is shown in Figure 1.4.

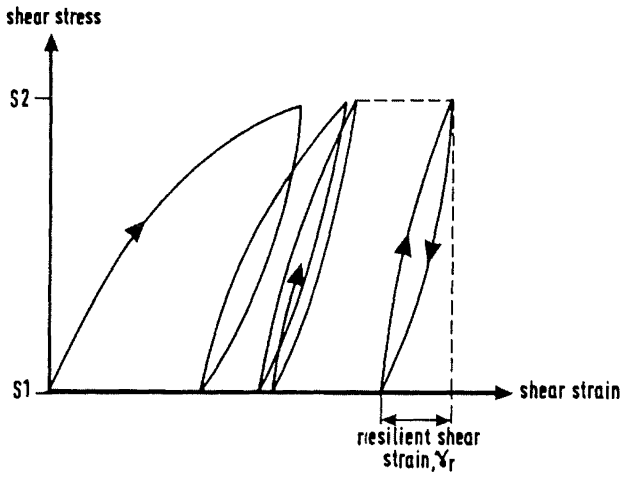

Figure 1.4 – The Typical Development of Shear Strain During a Cyclic Load Test (From O'Reilly & Brown (1991))

The magnitude of the recoverable strain remains fairly constant during each cycle while the irrecoverable strain tends to decrease with increasing numbers of load cycles. The decrease in irrecoverable strain occurs as the soil particles rearrange themselves into a fabric that is resilient to the loading. If the cyclic load amplitude is constant, then the soil will eventually reach a state of quasi-elastic or resilient response. The load amplitude must then be increased if further permanent strains are to occur.

The magnitude of the recoverable strain and the area of each stress-strain hysteresis loop depend upon both the magnitude of the shear strain at each cycle and the normal effective stress of the soil. The effect of shear strain magnitude is shown in Figure 1.5 by a decrease in soil shear modulus with increasing shear strain. A decrease in shear modulus will increase the peak-to-peak shear strain over each cycle and increase the area of the hysteresis loop. Changes in the shear modulus with increasing normal effective stress (shown as p') will also change the shape of the hysteresis loop, thus affecting the magnitude of the resilient shear strain.

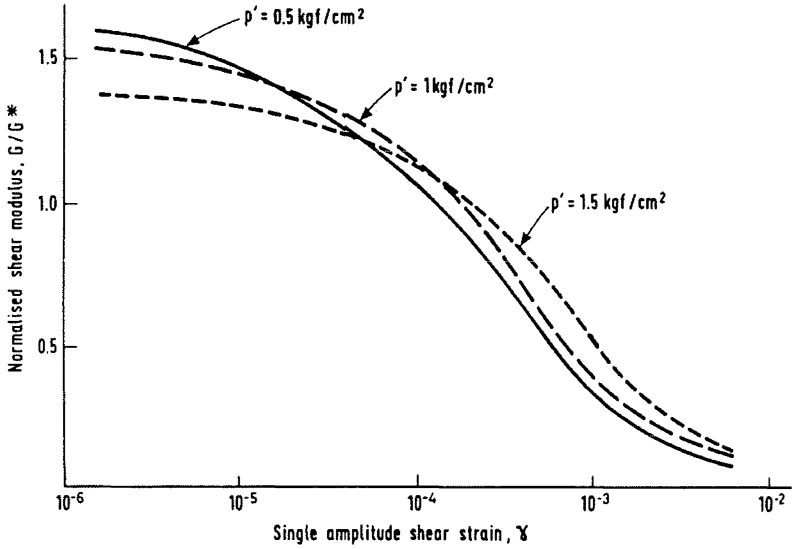

Figure 1.5 – The Influence of Shear Strain Magnitude and Mean Normal Effective Stress on the Shear Modulus of Dry Toyoura Sand (From O'Reilly & Brown (1991))

1.3 CYCLIC FOUNDATION CAPACITY

Very little information is available on the behaviour of deep foundations under cyclic axial loads and there is a distinct lack of information on the capacity of deep foundations under seismic shear loading. A review of the cyclic axial load data is given in Chapter 2 but may be summarised by the following:

1. All but the very lowest levels of repeated loading (as low as 10 to 20 percent of the static capacity in the few reported studies) show continuing deformation without any limit.
2. Two-way repeated loads and repeated uplift loads generally lead to capacity reduction while repeated compression loads have less effect on capacity.

SCOPE OF STUDY

This study focuses on the changes in uplift capacity of a drilled shaft foundation in cohesionless soil during and because of cyclic variations in both axial load and soil shear load. The study is performed in two distinct stages. The first stage has model drilled shaft foundations tested in a static soil deposit under cyclic axial loads. The second stage has model drilled shaft foundations tested in a soil deposit that is undergoing cyclic shear loading on a shaking table. The model drilled shaft is simultaneously subjected to different combinations of mean and cyclic axial load.

The first stage of testing involves the preparation of a homogeneous soil deposit and the construction of a model drilled shaft within that soil deposit. Loads are applied to the head of the drilled shaft with a hydraulic actuator. Different combinations of mean and cyclic load are applied and the response of the drilled shaft is measured directly during each test. The change in capacity under each combination of axial load is compared with the capacity of the drilled shaft when no cyclic load has been applied. Details are given in Chapter 3 of the laboratory procedures used to prepare the soil deposit and to construct the model drilled shaft. The loading apparatus, the instrumentation of each sample and a summary of the test results are given in Chapter 4. Analysis of the test results and interpretations of those results are given in Chapter 5.

The second stage of testing also involves the preparation of a homogeneous soil deposit and the construction of a model drilled shaft within that soil deposit. It was necessary to construct a special tank for these tests so that the soil deposit could deform in shear when subjected at its base to cyclic shear loading on the shaking table. Details of the tank design and construction and the laboratory procedures used

to prepare each soil deposit are given in Chapter 6. Also given is a summary of the performance of the tank under cyclic shear loading. The loading apparatus, the instrumentation of each sample and a summary of the test results are given in Chapter 7. Analysis of the test results and interpretations of those results are given in Chapter 8. A summary of the findings of this study is given in Chapter 9 and further test details are appended.

REFERENCES

GIRAULT, P. (1986), "Analyses of Foundation Failures", Proc. Int. Conf. The Mexico City Earthquakes, ASCE, 1985.

GREER, D.M. and GARDNER, W.S. (1986), "Construction of Drilled Pier Foundations", John Wiley and Sons, New York.

KULHAWY, F.H. (1981), "Analysis of Drilled Shaft Foundations in Uplift: A Summary Report", Contract Report B-49(7), Niagara Mohawk Power Corporation, Syracuse, August 1981.

McMANUS, K.J. and KULHAWY, F.H. (1991). "Cyclic Axial Loading of Drilled Shafts in Cohesive Soil for Transmission Line Structures" Report EL-7161, Electric Power Research Inst., Palo Alto. Calif.

MENDOZA, M.J. and AUVIVET, G. (1988), "The Mexico Earthquake of September 19, 1985 – Behavior of Building Foundations in Mexico City", Earthquake Spectra, Vol. 4, No. 4, EERI.

O'REILLY, M.P. & BROWN S.F. (1991). "Cyclic loading of soils", Blackie, Glasgow & London. Van Nostrand Reinhold, New York (1991)

STEWART, J.P. and KULHAWY, F.H. (1981), "Experimental Investigation of the Uplift Capacity of Drilled Shafts in Cohesionless Soil", Contract Report B-49(6), Niagara Mohawk Power Corporation, Syracuse, May 1981.

TURNER, J.P. and KULHAWY, F.H. (1987). "Experimental Analysis of Drilled Shaft Foundations Subjected to Repeated Axial Loads under Drained Conditions," Report EL-5325, Electric Power Research Inst., Palo Alto. Calif.

VESIC, A.S. (1977), "Design of Pile Foundations", Synthesis of Highway Practice 42, Transportation Research Board, Washington, 1977.

ZEEVAERT, L. (1991), "Seismosoil Dynamics of Foundations in Mexico City Earthquake, September 19, 1985", Journal of the N.Z. Society for Earthquake Engineering, Vol. 26, No. 1.

Chapter Two

SEISMIC LOADS ON DEEP FOUNDATIONS

INTRODUCTION

When an earthquake occurs, the ground shakes and everything in contact with the ground shakes with it. This chapter describes how earthquakes occur and how the energy of an earthquake is transmitted through the earth and up to the surface, where it is felt as strong ground motion. The complex nature of seismic ground motion is illustrated and general simplifications of that motion are presented. These simplified ground motions are useful for engineering design in so much as they describe the general nature of ground motion while simplifying the actual ground actions and the reactions of any structure under design.

It has been found that the ground motion at the surface depends upon the properties of the soil near the surface. This chapter describes two simple models that may be used to analyse the behaviour of a soil layer under strong ground motion.

When the ground shakes, so too do the structures in contact with that ground. The shaking of a structure must be resisted by its foundations but this resistance generates loads in the foundations. This chapter describes the different types of loads that are exerted on the foundations by the shaking of the structure and by the ground itself. The effects of the loads are discussed and a summary is given of previous research into the actions of the soil and foundation during seismic loading. Where applicable, analytical models are also presented for determining the behaviour of deep foundations during seismic loading.

2.1 EARTHQUAKES

The surface of the earth is covered by a crust of solid geological material. The crust has a thickness ranging from as little as 5 km beneath the oceans to as much as 40 km beneath the continents. Rather than being one continuous shell, the crust is made up of a number of smaller, interlocked plates called tectonic plates. The different plates are shown in Figure 2.1.

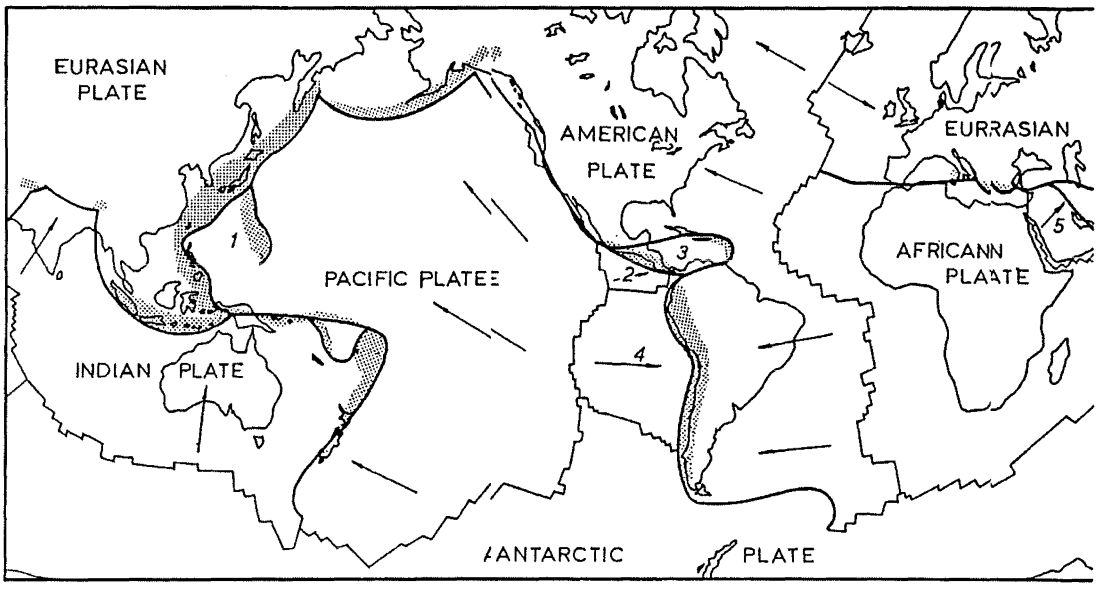

Figure 2.1 – The Earth's Tectonic Plates, with Vectors showing their Relative Movement (From Eiby (1989))

Beneath the semi-rigid tectonic plates lies a viscous, semi-molten layer called the mantle. The mantle has a thickness of approximately 2850 km, with a temperature ranging from 3600°C at its lower boundary to around 1000°C at the upper, crustal boundary. The temperature gradient across the mantle generates internal convection currents, moving the semi-molten material in a circular manner. The movement of the material creates drag forces on the underside of the crustal plates and these drag forces create stresses along the plate boundaries as the plates try to move with respect to each other. If the stresses between the plates exceed the material strength then the plate boundary will rupture, releasing the stored strain energy. The released energy radiates out from the point of rupture and is felt at the surface as an earthquake.

The energy of an earthquake is radiated as seismic waves. There are two general classes of seismic wave; body waves and surface waves. As their names suggest, body waves travel through the interior of the earth while surface waves are confined to travel in a region close to the surface.

There are two types of body waves. The first is the longitudinal (p) wave, which has particle motion that is parallel to the direction of wave propagation. The second is the transverse or shear (s) wave, which has particle motion that is perpendicular to the direction of wave propagation.

There are also two types of surface waves. The first is the Rayleigh wave, which has particle motion in a vertical plane as the wave propagates across the surface. The second is the Love wave, which has particle motion in a horizontal plane as the wave propagates across the surface. The direction of particle motion in the Love wave is perpendicular to the direction of wave propagation.

All types of seismic wave are produced during an earthquake, but it is the shear waves that carry the most energy and pose the greatest risk to engineered structures. If a shear wave is propagating vertically, then the associated soil or rock displacements are horizontal, and horizontal displacements bring horizontal ground accelerations. If a structure is in contact with the ground then those accelerations will be transmitted to the structure and will generate horizontal inertial loads within the structure. While most structures are designed to account for increases in vertical load, many are not designed to allow for increased horizontal loads, so the horizontal inertial loads may then cause the structure to fail.

Horizontal ground accelerations are also produced by horizontally propagating Love waves but these carry less energy than shear waves so, while they increase the inertial loads on a structure, the amount by which they do so is not as significant.

If all the shear waves radiated out in straight paths, then very few of them would actually travel vertically and the horizontal accelerations would be minor. Unfortunately this is not the case, because the waves are refracted towards the vertical as they approach the surface. The ground near the surface of the earth is generally less

dense than that at depth so, when the seismic waves travel upward from a denser layer to a less dense layer, they are refracted to a more vertical direction. This behaviour is shown schematically in Figure 2.2. Because of the refraction, a greater proportion of the total seismic energy actually reaches the surface in the form of vertically propagating shear waves.

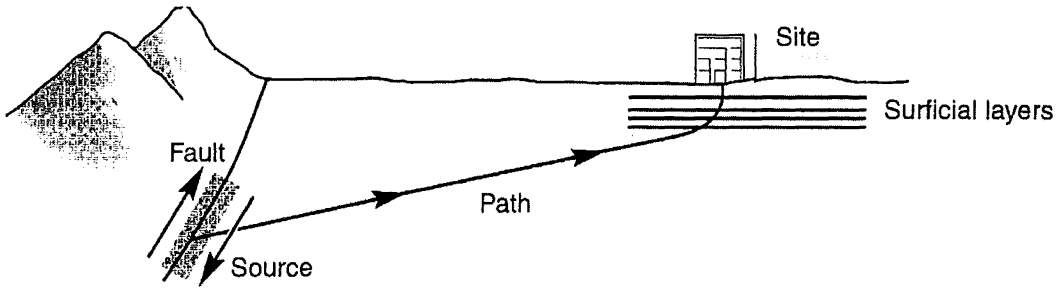

Figure 2.2 – Refraction of Seismic Waves due to Layering near the Surface (From Kramer (1996))

2.2 STRONG GROUND MOTION

The most important aspect of an earthquake, from an engineering perspective, is the nature of the strong ground motion. The seismic energy that is released during an earthquake causes the ground to move and the accelerations associated with these ground motions generate inertial loads in any structure that is in contact with the ground. If the ground beneath a structure undergoes an acceleration, then the acceleration will generate inertial forces within the structure itself and, if the inertial forces become great enough, then the structure may fail.

In order to fully describe the ground motion at a point, recordings must be made of the three components of ground translation and the three components of ground rotation. In practice, the rotations are usually neglected and an array of three orthogonal seismographs is used to measure displacements in the East-West, North-South and vertical directions. Each seismograph, in its simplest form, consists of a

damped, single-degree-of-freedom oscillator that traces out its displacement during an earthquake event. The trace can be corrected for the motion of the oscillator and the true ground motion can then be found. Nowadays, seismographs have generally been superseded by electronic accelerometers that measure the ground acceleration directly. The results are displayed as accelerograms, with each component of ground acceleration plotted as a function of time. Figure 2.3 shows a typical set of accelerograms, recorded at Gilroy, California during the 1989 Loma Prieta earthquake.

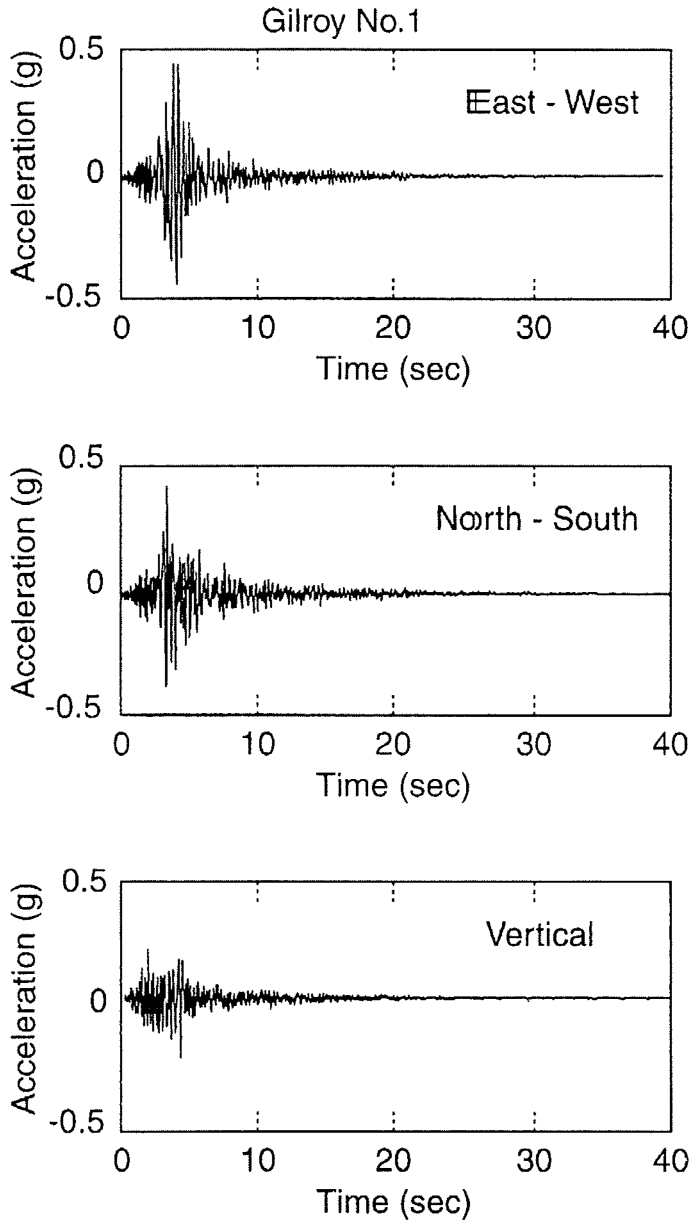

Figure 2.3 – Recorded Ground Accelerations at Gilroy No. 1, California, during the 1989 Loma Prieta Earthquake (From Kramer (1996))

The accelerograms shown in Figure 2.3 illustrate that the ground motion during an earthquake is quite complex, but there are particular features of these plots that describe the ground motion in enough detail to show its engineering significance. The most important features, taken from Kramer (1996), are:

1. The Peak Amplitude – which gives an indication of the peak inertial load induced in the structure.
2. The Frequency Content - Every structure has its own natural frequency and loads applied at or around the natural frequency will cause the structure to resonate.
3. The Duration – The damage caused by one cycle of loading may not be significant but the cumulative damage caused by many cycles may be catastrophic.

It is not possible to check the design of a structure against every conceivable earthquake, so the strong ground motion features shown above can be used to simplify the event and provide general ground motions for engineering design.

Further simplifications may also be made so that design calculations may be kept to economically prudent levels, whilst retaining the important features of the seismic loading.

The first simplification is that the vertical component of strong ground motion is often ignored. The vertical component is often smaller than either of the horizontal components, as it is in Figure 2.3, and its effects are usually integrated into the design. This is because structures are usually designed to withstand variations in vertical load, either by incorporating live or short-term loads into the design or by using over-strength factors during the design stage. On the other hand, variations in horizontal load are not inherent to the design so they may not be ignored.

The second simplification, particularly for research and development, is to model the strong ground motion as a sinusoidal motion. No two earthquakes will ever be the same, but the cyclic nature of the loading is common to all, so a given sinusoidal motion should produce the same effect as a number of different earthquakes. A simple procedure has been developed by Seed et al. (1975) in order to do this. The amplitude of each load cycle is measured off the acceleration or shear stress trace. Different

conversion factors are assigned to each cycle, depending on its relationship to the maximum amplitude, then an equivalent number of cycles of uniform amplitude is found. The choice of amplitude for the uniform cycles is arbitrary but is commonly chosen as 65 % of the maximum recorded amplitude. Figure 2.4 shows the results of the Seed model for a number of previous earthquakes, showing that the equivalent number of cycles increases non-linearly with earthquake magnitude.

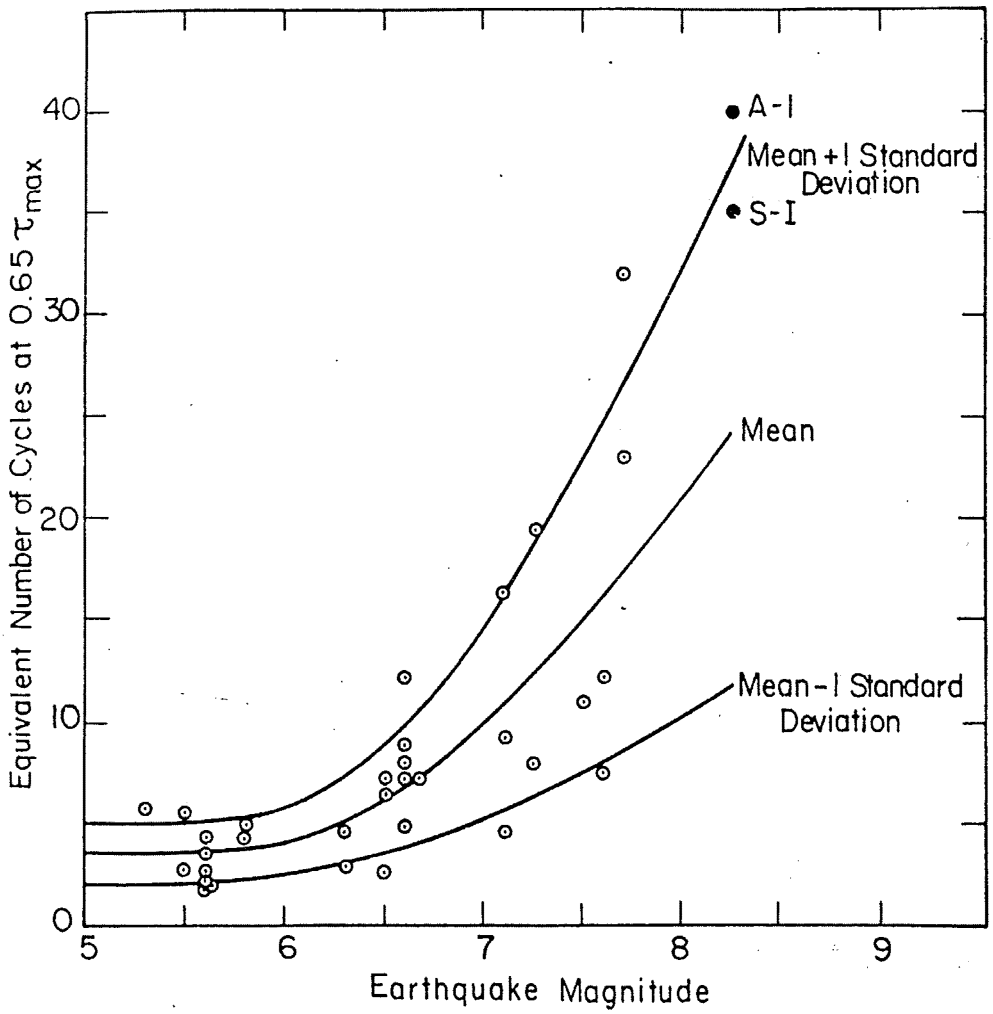

Figure 2.4 – Equivalent Numbers of Uniform Stress Cycles based on Strongest Components of Ground Motion (From Seed et al. (1975))

The Seed et al. method of representing earthquake loads accounts for two of the three ground motion characteristics mentioned above, but it does not account for the frequency content of the event. One reason for this is that the method was developed

for liquefaction analysis, where the nature of the frequency content is not critical. In order to account for the effects of different frequencies, the same sinusoidal motions and numbers of cycles can be used, with the frequency and corresponding amplitudes altered to maintain the same ground accelerations.

Strong ground motion can, therefore, be expressed as a series of one-dimensional sinusoidal cycles of horizontal acceleration. The factors which dictate the severity of the motion are the amplitude and frequency of the wave and the number of cycles of loading.

2.3 GROUND RESPONSE ANALYSIS

When vertically incident shear waves are propagating towards the surface of the earth, they will produce horizontal accelerations within the rock or soil in which they are travelling. Observations have shown that the magnitude of those accelerations will depend upon the properties of the rock or soil in which the waves travel.

An example of the influence of ground conditions comes from the Mexico City earthquake of 1985. Mexico city was originally built around the shores of Lake Texcoco and was largely founded on rock and firm soil. When the area was overtaken by the Spanish, the lake was drained and buildings were erected on the land that had previously been the lake-bed. The lake area, near the modern city centre, consists of a thick deposit of very soft, high-water-content sand and clay. On the 19^{th} of September, 1985, a magnitude 7.8 earthquake struck Mexico city and observations showed that several buildings in the old lake-bed area suffered extensive damage, while those founded on rock or firm soil suffered relatively less damage. Accelerometers placed at different points around the city showed that the peak horizontal acceleration on firm ground was around 4 % of gravity while the peak horizontal acceleration in the lake zone was up to 40 % of gravity.

In order to analyse the response of a soil layer to strong ground motion, it is necessary to create a model of the layer. The most simple model consists of a level, uniform layer of isotropic, linear elastic soil overlying level, rigid bedrock. The model, with its

boundary conditions, is shown schematically in Figure 2.5. The seismic loading involves applying the simplified, vertically incident, shear waves as a one-dimensional bedrock displacement $u_g(t)$. The model will therefore be used to calculate the one-dimensional response of a uniform, linear elastic soil layer.

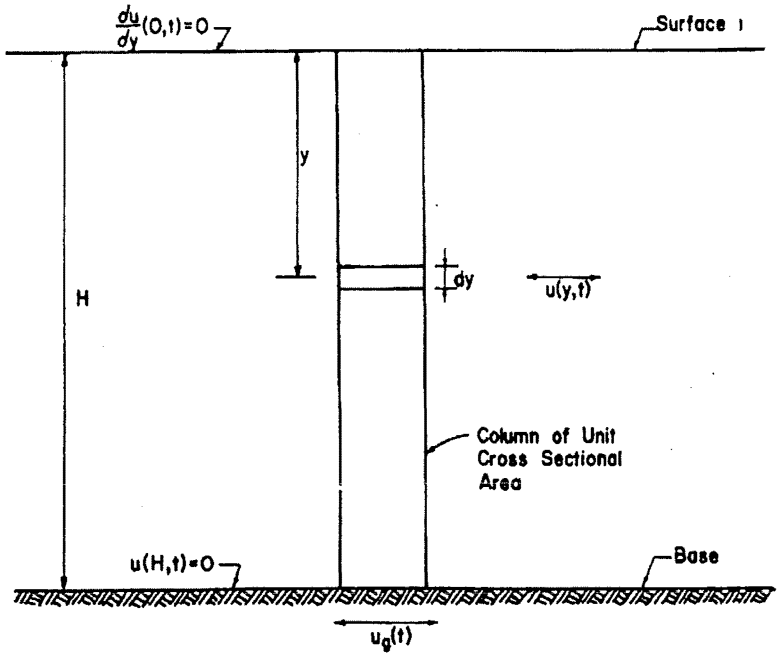

Figure 2.5 – Model of a Linear Elastic, Uniform Density Soil Layer subjected to a Horizontal Seismic Motion at its Base (From Idriss & Seed (1968))

Closed form solutions have been derived for the seismic response of the simple soil layer shown in Figure 2.5. An example, taken from Idriss and Seed (1968), is for the bedrock being subjected to a horizontal seismic motion, $u_g(t)$. The equation of motion is given by:

$$\rho(y)\frac{\partial^2 u}{\partial t^2} + c(y)\frac{\partial u}{\partial t} - \frac{\partial}{\partial y}\left[G(y)\frac{\partial u}{\partial y}\right] = -\rho(y)\frac{\partial^2 u_g}{\partial t^2} \qquad (2.1)$$

in which $\rho(y)$ is the mass density at depth y; $c(y)$ is the viscous damping coefficient at depth y; $G(y)$ is the shear modulus at depth y; and $u(y,t)$ is the relative displacement at depth y and time t.

Solutions to the equation of motion have been developed for soil layers with constant or regularly varying material properties. These solutions are available in Idriss & Seed. (1968). If the properties of the soil layer are irregularly varying, however, then a general solution cannot be found for the equation of motion. Instead, the response of the soil layer can be analysed by discretising the layer into a series of lumped masses, as shown in Figure 2.6. Each mass is connected to the next by a damped shear spring. The equation of motion can then be represented in matrix form by:

$$[\mathrm{M}]\{\ddot{u}\} + [\mathrm{c}]\{\dot{u}\} + [\mathrm{K}]\{u\} = [\mathrm{M}]\ddot{u}_b(t) \tag{2.2}$$

where [M], [c] and [K] are the mass, damping and spring stiffness matrices respectively, $\ddot{u}_b$ is the acceleration vector at the base of the deposit, and $\ddot{u}$, $\dot{u}$ and u are the acceleration, velocity and displacement vectors relative to the base. The vectors have order N, where N is the number of lumped masses used to idealise the soil layer. The equation of motion may then be solved by determining the mass, damping and stiffness values for, and between, each lumped mass. These may be used, with the base acceleration, to determine the acceleration at any other point; particularly at the surface.

The difficulty with using the closed form solution or the lumped mass model is that these models incorrectly assume that the soil behaves in a linear elastic manner. Figure 2.7 shows a plot of shear stress versus shear strain for a soil under cyclic shear loading and it is clear that the soil behaviour is non-linear under these loads.

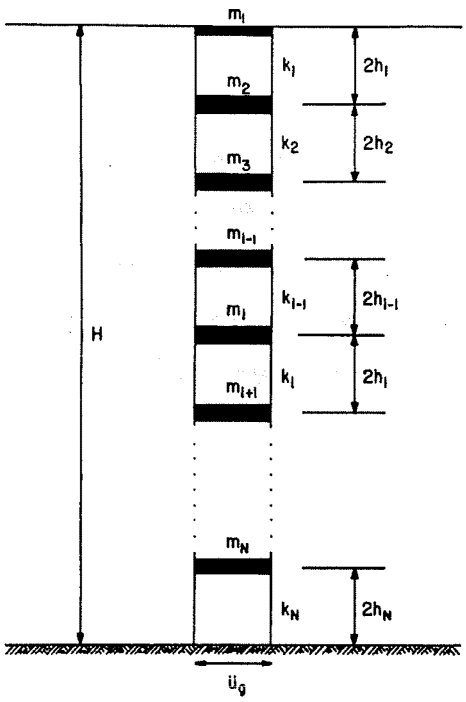

Figure 2.6 – Lumped Mass Model of a Linear Elastic Soil Layer subjected to a Horizontal Seismic Motion at its Base (From Idriss & Seed (1968))

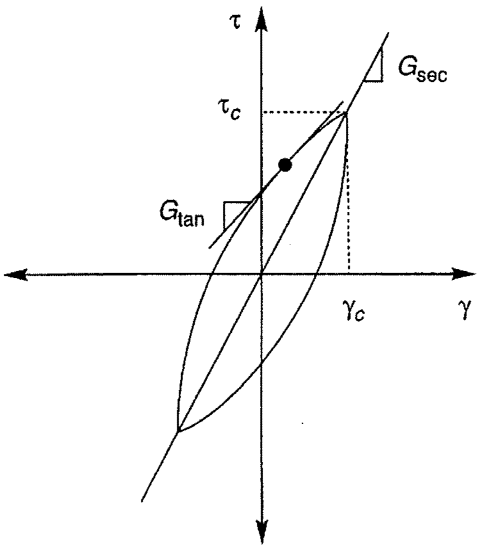

Figure 2.7 – Plot of Shear Stress versus Shear Strain for a Soil under Cyclic Shear Loading (From Kramer (1996))

The previous models can still be used to analyse the seismic response if equivalent linear parameters are found for the soil. Equivalent linear systems have been found to provide reasonably satisfactory evaluations for the dynamic behaviour of soil layers. The equivalent linear soil parameters are found from stress-strain curves like the one shown in Figure 2.7. The stiffness of the soil is taken to be the secant shear modulus, G_{sec}. The stiffness is usually given by the tangent shear modulus, G_{tan}, (shown as the slope of the curve in Figure 2.7) but the variation of G_{tan} with shear strain is obvious so it can be averaged out to an equivalent linear value by using the secant shear modulus, G_{sec}, which is given by:

$$G_{sec} = \frac{\tau_c}{\gamma_c} \tag{2.3}$$

τ_c and γ_c are the maximum shear stress and the maximum shear strain, respectively, as shown in Figure 2.7. Similarly, the equivalent linear damping ratio, ξ, can be found by calculating the area under the hysteresis loop, A_{loop}, then calculating the damping ratio, ξ, as:

$$\xi = \frac{1}{2\pi} \frac{A_{loop}}{G_{sec}\gamma_c^2} \tag{2.4}$$

It must be noted that the equivalent linear soil parameters are a function of the peak shear strain, γ_c, so any analysis using these parameters will only be relevant for shear strains in the range of γ_c.

A further refinement of the model can be made by adjusting the equivalent linear soil parameters for their shear strain dependency. To do this, an iterative procedure is required to ensure that the chosen soil properties are compatible with the computed shear strains at each point. The iterative procedure is taken from Kramer (1996) and operates as follows:

1. Initial estimates of G and ξ are made for each layer. The initially estimated values usually correspond to the same stain level; the low-strain values are often used for the initial estimate.
2. The estimated G and ξ values are used to compute the ground response, including time histories of shear strain for each layer.
3. The effective shear strain in each layer is determined from the maximum shear strain in the computed shear strain time history.
4. From this effective shear strain, new equivalent linear values, $G^{(i+1)}$ and $\xi^{(i+1)}$ are chosen for the next iteration.
5. Steps 2 to 4 are repeated until differences between the computed shear modulus and damping ratio values in two successive iterations fall below some predetermined value.

So the accelerations within a soil layer can be determined if the accelerations of the bedrock are known and if the dynamic soil properties are known. The accelerations of the soil layer can then be used to determine the actions of any structure that is in contact with the soil. The accelerations at depths below the surface are particularly useful in determining the actions of deep foundations embedded in the soil layer.

2.4 SEISMIC LOADS ON DEEP FOUNDATIONS

Drilled shaft foundations are often used to support structures with high aspect ratios, including many bridges, high-rise buildings and storage tanks. During an earthquake, the strong ground motion, and the reaction of the superstructure itself, can result in substantial loads being exerted on the foundations. Figure 2.8 shows that seismic waves, in the form of vertically incident cyclic shear waves, will induce horizontal inertial loads in the superstructure. If the structure is to remain stable, then these loads must be resisted by the foundations.

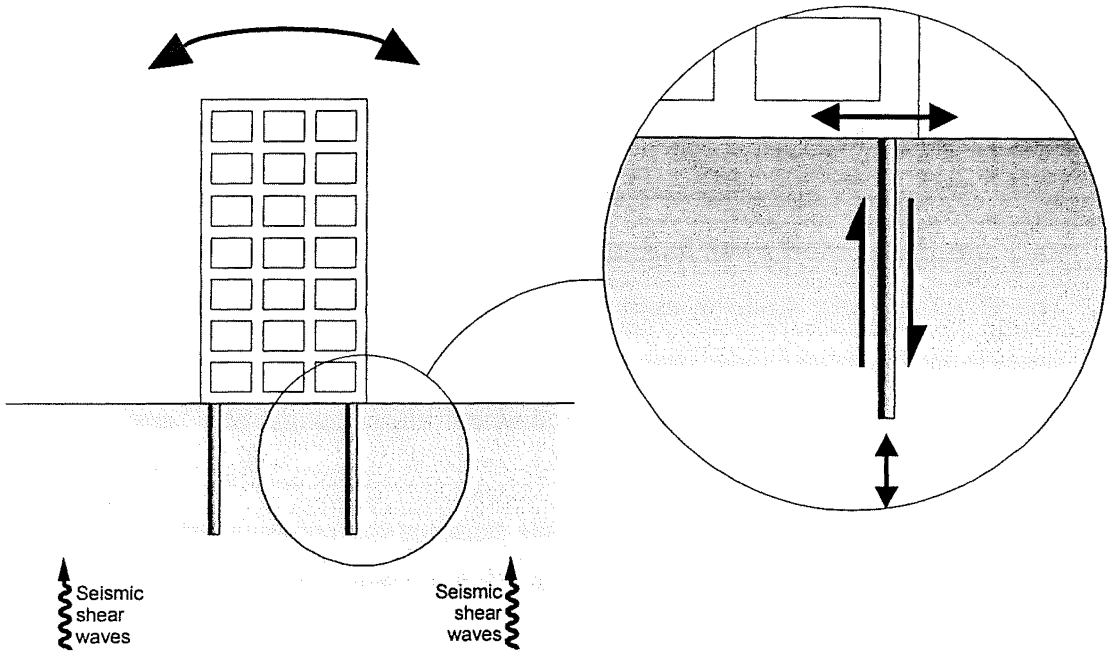

Figure 2.8 – Inertial Loads due to Vertically Incident Seismic Shear Waves

Inertial loads are generated in the superstructure by the accelerations of the ground beneath it. The inertial loads are transferred to the head of the foundation as cyclic lateral and cyclic axial loads. The horizontal translation of the structure generates lateral loads at the foundation head and the rotation of the structure generates axial loads at the foundation head. Further dynamic loading occurs along the length of the foundation as the soil itself displaces in shear.

2.4.1 Inertial Lateral Loads

As a structure displaces laterally under a seismic load, its movement must be resisted by the foundation beneath it. The displacement of the structure induces a lateral load in the head of the foundation and this lateral load is transferred to the surrounding soil as a passive pressure along the length of the foundation shaft.

Observations from deep foundation tests have shown that the magnitudes and distributions of the passive pressures developed under cyclic loading are similar to those developed under monotonic loading. However, the tests also showed that the

peak lateral foundation displacements are significantly greater for cyclic loading than they are for monotonic loading. Lateral foundation displacements are greater under cyclic loading because each half cycle of loading creates permanent strains in the soil around the foundation. The accumulation of these permanent strains allows the foundation to displace relatively freely through the middle of each lateral strain cycle.

The displacements required to mobilise the peak lateral capacity can be rather substantial and, in many cases, these will be greater than the serviceability limits of the foundation. For this reason, it is often peak displacement, rather than load capacity, that is the governing criterion for the design of laterally loaded deep foundations.

The most common model used for deep foundations under cyclic lateral loading follows from the model used for monotonic lateral loading. The model idealises the foundation as a beam-on-elastic-foundation, as explained in Chapter 1, with the governing differential equation for the foundation given by:

$$EI\frac{d^2y}{dx^2} = p(x) \tag{2.5}$$

EI = the flexural stiffness of the foundation, y = the lateral displacement, x = the depth along the foundation and p = the lateral soil reaction. The solution of Equation 2.5 requires the determination of a relationship between the soil reaction and the lateral displacement of the foundation. ie. developing a *p-y* curve for the system. The slope of the *p-y* curve is known as the subgrade modulus, E_s, and is defined by:

$$E_s = -\frac{p}{y} \tag{2.6}$$

If the subgrade modulus cannot be found as a function of depth, then the system can be discretised into soil sections and each section modelled using the Winkler springs described in Chapter 1. *p-y* curves can be found for each soil section and the

foundation loads can then be determined discretely, with equation 2.5 ensuring continuity between each section.

Cyclic lateral loading is allowed for by adding a subgrade degradation parameter to the static value of E_s. The effect of this is to reduce the load capacity for a particular displacement if the foundation has undergone repeated cyclic loading. One such example, from Little and Briaud (1988), reduces the static soil resistance according to:

$$p_N = p_1.N^{-a} \tag{2.7}$$

where p_N = the cyclic soil resistance for N cycles of load, p_1 = the value of p for the first cycle of load, and a = a degradation parameter determined from the results of cyclic pressuremeter tests.

2.4.2 Inertial Axial Loads

As a structure accelerates laterally, an overturning moment is induced about its base. As shown in Figure 2.8, the overturning moment is resisted by axial load couples in the foundation. The axial load is transferred to the surrounding soil as a shear stress along the sides of the shaft and as a compressive or tensile stress beneath the tip of the shaft.

Very little information is available on the behaviour of deep foundations under repeated axial loads. A review of the available data, by Turner et al. (1987) suggests that:

1. All but the very lowest levels of repeated loading (as low as 10 to 20 percent of the static capacity in the few reported studies) show continuing deformation without any limit.
2. Two-way repeated loads and repeated uplift loads generally lead to capacity reduction while repeated compression loads have less effect on capacity.
3. Repeated loads producing axial displacements greater than about 5 percent of the shaft diameter may lead to static capacity reductions.

4. Low levels of repeated load on deep foundations in contractive soils under drained conditions may lead to increases in static capacity.
5. Drainage of excess pore water stress results in some recovery of static capacity. However, this recovery may be lost after relatively few additional repeated loads.

To date, no model has been developed which identifies the stress distribution around a deep foundation under cyclic axial loading. At present, research is focussed on identifying the parameters that are critical to the stability of the foundation during loading. The Turner research has identified a parameter called the Critical Level of Repeated Load (CLRL) which identifies a percentage of the static capacity, above which a deep foundation will undergo continuing displacement without any apparent limit. The CLRL was found to be heavily dependent upon the magnitude and direction of loading, with two-way loading and repeated uplift loading being more detrimental to the stability of the foundation than repeated compression loading.

Research by Poulos (1988) also noted the importance of the level of repeated load. Poulos summarised the effects of repeated axial loading into the Cyclic Stability Diagram (CSD). The CSD is shown in Figure 2.9 and has the cyclic axial load amplitude plotted against the mean axial load. Three regions are identified within the possible bounds of the diagram. They are:

1. The stable zone - in which cyclic loading has no effect on foundation capacity.
2. The metastable zone - in which cyclic loading causes some limited reduction of load capacity.
3. The unstable zone - in which cyclic loading will result in failure of the foundation within a specified number of cycles.

The CSD provides a useful means of defining the response of a deep foundation to various combinations of mean and cyclic load.

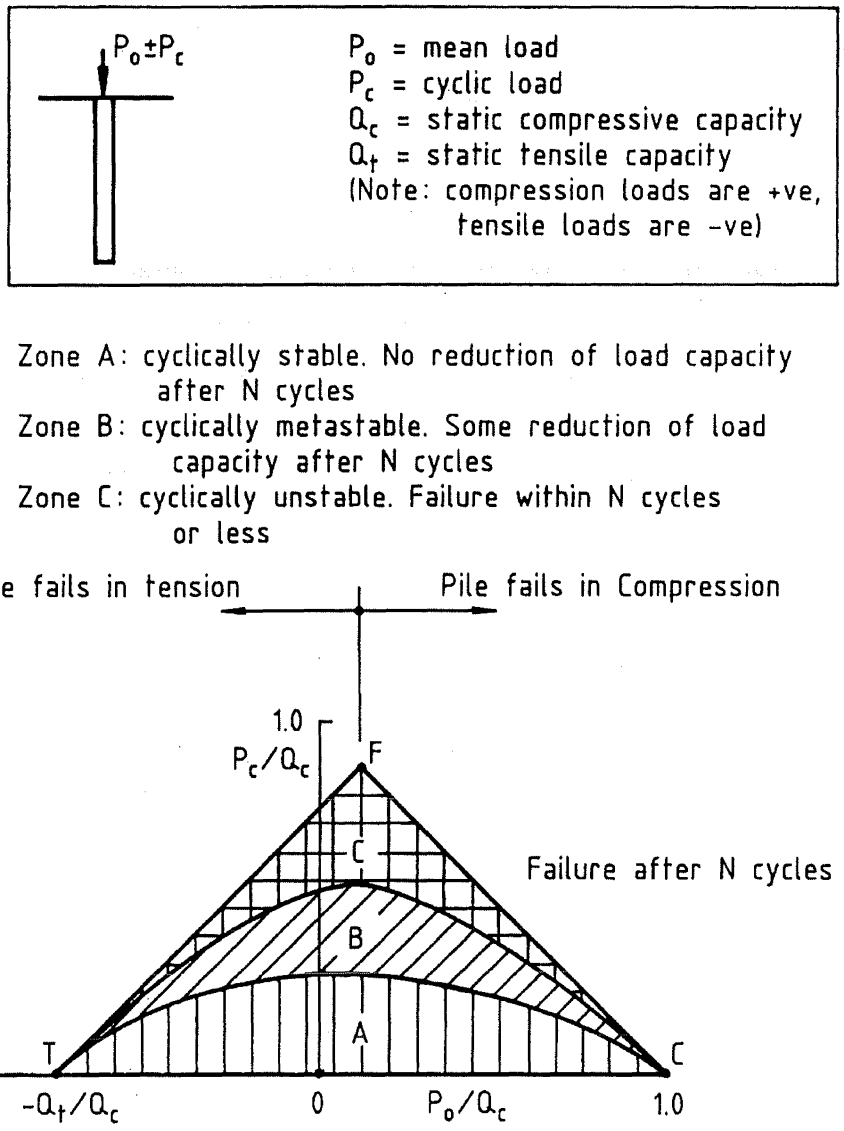

Figure 2.9 – Cyclic Stability Diagram (From Poulos (1988))

2.4.3 Combined Inertial Loads

Cyclic axial and cyclic lateral loads do not act independently during a seismic event. The application of one alters the effect of the other.

A summary of research observations by Turner (1987) shows that combined loading causes a decrease in both axial load transfer and axial side resistance by moulding away the soil along the top of the foundation. Increased bending moments are also

observed, as a result of axial compression loads being superimposed on top of lateral loads.

No analytical model exists for predicting deep foundation response to combined cyclic loads as little research has been done in this field. Turner (1987) summarised that "Much research still is needed. For example, failure modes for combined loading need to be defined as a function of soil type, foundation geometry, ratio of axial to lateral load, and whether the axial loading is uplift, compression, or both."

2.4.4 Dynamic Soil Loads

There is a significant difference between seismic excitation of the ground and foundation, and cyclic loading of the foundation head. If the foundation head is loaded, then the head is the only point of load application and there is only a near-field reaction in the soil immediately surrounding the foundation. If, however, the soil undergoes seismic excitation, then the whole soil mass moves in a free-field response to the loading and load is applied over the full length of the foundation. An illustration of seismic excitation of the soil mass and foundation is shown in Figure 2.10.

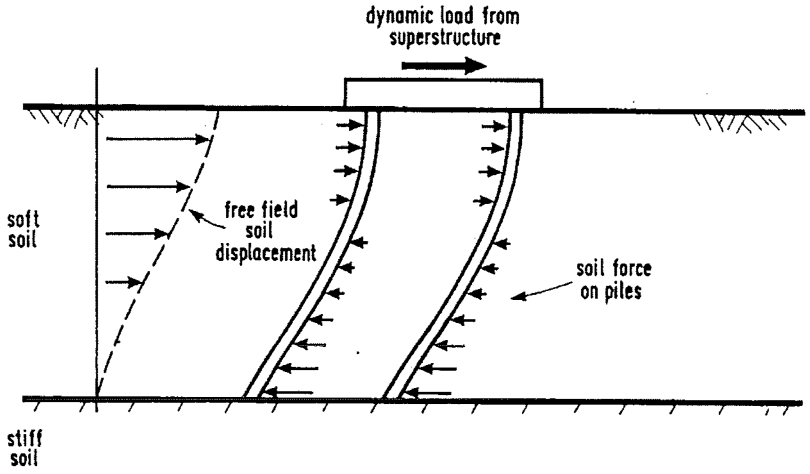

Figure 2.10 – Dynamic Soil Loads due to Seismic Loading of Soil Mass (From O'Reilly & Brown (1991))

If the foundation is flexible compared to the soil then the effect of the soil displacement will be minimal. If, however, the foundation is stiff, such as a drilled shaft or pier, then it will be subjected to significant loads as it resists the soil displacement.

The behaviour of deep foundations under dynamic soil loads can be modelled with the Winkler model shown in Figure 2.11. The model consists of horizontal Winkler springs, which provide horizontal resistance over the length of the foundation, and a rotational spring at the foundation head, which provides a restraint to rotation. The difference between this model and that used to analyse inertial lateral loads is the point of application of load. In the inertial lateral load case, the load is applied at the head of the foundation and the supports of the Winkler springs are considered to be rigidly fixed. In the dynamic lateral load case, the load is applied at all points along the shaft and the supports of the Winkler springs are considered to move in compliance with the free-field soil displacement. The model therefore consists of a free-field soil displacement superimposed upon the near-field soil-spring reactions.

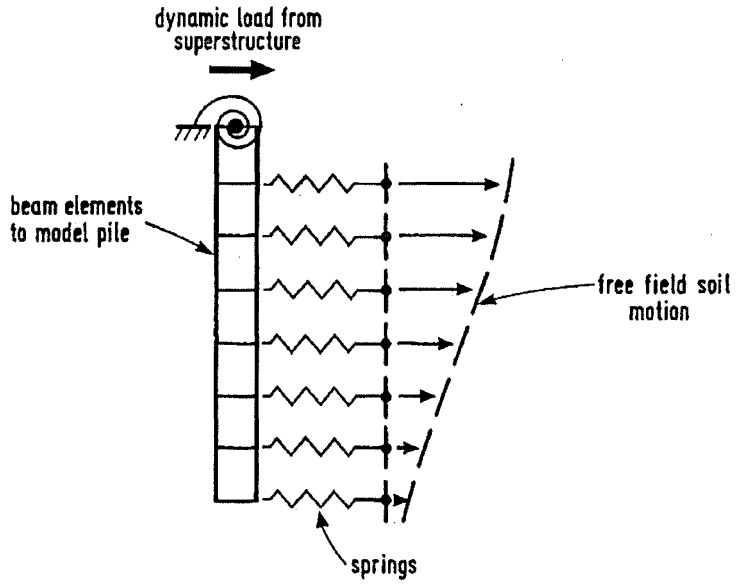

Figure 2.11 – Winkler Spring Model for Dynamic Soil Loads
(From O'Reilly & Brown (1991))

To determine the loads and displacements on the foundation, the first step is to calculate the deflected shape of the free-field soil profile. The next step is to

determine the characteristics of each Winkler spring. The stiffness and damping are required, as are any non-linear effects, yield points and cyclic degradation factors. The flexural stiffness (*EI*) of the foundation is also required because the loads, displacements and bending moments will all depend upon the material characteristics of the foundation. When all the required parameters have been found, the analysis is performed by superimposing the deflected shape of the soil profile upon the supports of the Winkler springs, with the simultaneous requirement of continuity along the length of the foundation. The analysis is an iterative procedure, so a computerised procedure is suited to this analysis. One such soil-pile interaction program has been developed and is now in common use. It is called SPASM8 and was developed by Matlock et al. (1978).

SUMMARY

Seismic waves are generated when the surface of the earth ruptures during an earthquake. These waves propagate through the earth and cause strong ground motion when they reach the surface. The nature of the strong ground motion is rather complex but, for engineering purposes at least, they can be simplified into one-dimensional sinusoidal motion, with the intensity of shaking being represented by the amplitude, frequency and duration of the sinusoidal motion.

Observations from recorded earthquakes have shown that the ground motion at the surface depends upon the soil or rock near the surface. Simple models have been developed to analyse the behaviour of a soil layer under seismic excitation of the underlying bedrock. These models take the soil material properties into account in order to determine the actions under seismic loading.

If a structure is in contact with a soil layer undergoing seismic loading then that structure will also undergo seismic loading. The loads that are generated in the structure must be resisted by the foundations, so seismic loads are then exerted on the head of the foundation. The displacements of the soil around the foundation also exert loads along the length of the foundation. Research into the behaviour of deep foundations under seismic loading has shown that both lateral and axial loading bring

about a reduction in foundation performance. Repeated lateral loads have been found to degrade the stiffness of the surrounding soil, allowing increasingly large lateral displacements to occur. Repeated axial loads have been found to degrade the strength of the surrounding soil, allowing increasingly large axial displacements to occur. The degradation of soil strength was found to be more pronounced if the mean load on the foundation was in uplift.

When the soil around a deep foundation is subjected to seismic loading, then the displacements of the soil will exert loads along the full length of the foundation. The flexural stiffness of the foundation and the restraint offered at its head may increase these loads even further. Research into the behaviour of foundations under dynamic soil loading has shown that the response very much depends upon the material properties of the soil and of the foundation. Flexible foundations in stiff soils will generally follow the response of the soil layer while stiffer foundations in softer soils will remain essentially rigid, with the soil distorting around them.

Few models have been developed to analyse the behaviour of deep foundations under seismic loads. The most commonly used model incorporates an analytical model for soil response with a Winkler spring model for lateral foundation displacement. The model follows an iterative procedure that requires continuity of the soil, the structure and the foundation loads and displacements. To date, no model exists that analyses the response if a deep foundation under repeated axial loading.

REFERENCES

EIBY, G.A. (1989). "Earthquakes", Heinemann Reed, Auckland, 1989.

IDRISS, I.M., and SEED, H.B. (1968). "Seismic Response of Horizontal Soil Layers", J. Soil Mech. and Found. Div., ASCE, Vol. 94, No. SM4, July, 1968.

KRAMER, S.L. (1996). "Geotechnical Earthquake Engineering", Prentice Hall, New Jersey, 1996.

LITTLE, R.L. and BRIAUD, J-L. (1988). "Full Scale Cyclic Lateral Load Tests on Six Single Piles in Sand", Miscellaneous Paper GL-88-27, Geotechnical Div., Texas A&M Univ., College Station, Texas.

MATLOCK, H., FOO, S.H.C. and BRYANT, L.M. (1978) "Simulation of Lateral Pile Behaviour Under Earthquake Motion", Proc., EQ Eng. and Soil Dyn., ASCE Specialty Conference, Pasadena, CA., pp. 601-619.

O'REILLY, M.P. & BROWN S.F. (1991). "Cyclic loading of soils", Blackie, Glasgow & London. Van Nostrand Reinhold, New York (1991)

POULOS, H.G. (1988). "Cyclic Stability Diagram for Axially Loaded Piles", J. Geotech. Engrg., ASCE, Vol. 114, No.8, August, 1988.

SEED, H.B., IDRISS, I.M., MAKDISI, F. and BANERJEE, N. (1975), "Representation of Irregular Stress Time Histories by Equivalent Uniform Stress Series in Liquefaction Analyses", Report No. EERC 75-29, College of Engineering, UoC. Berkeley, California, October, 1975.

TURNER, J.P., KULHAWY, F.H. and CHARLIE, W.A. (1987), "Review of Load Tests on Deep Foundations Subjected to Repeated Loading", Report No. EL-5375, Electric Power Research Institute, Palo Alto, California, August, 1987.

Chapter Three

CONSTRUCTION OF MODEL DRILLED SHAFTS FOR CYCLIC AXIAL LOAD TESTS IN A STATIC SOIL DEPOSIT.

INTRODUCTION

This chapter provides details of the construction of each model drilled shaft and static soil deposit. Details are given of the tanks used to contain the soil deposit, the soil used for the tests and the materials used to construct each drilled shaft foundation. An outline is also given of the apparatus and procedures used to prepare each soil deposit and model drilled shaft.

3.1 TANK CONSTRUCTION

Two cylindrical tanks, each 1.00 m diameter by 1.99 m high, were constructed from 6 mm plate steel that was rolled and welded into a tube. Details of the tanks are shown in Figure 3.1. Two tanks were built so that the soil could be transferred from one to the other, thus avoiding double handling of the soil and the need for a storage tank. A sheet of perforated steel plate was welded to the base of each tank to allow the soil to flow out. To control the flow of soil, another identical plate was fitted beneath the first so that when the holes in the two plates were aligned the soil could flow. The sliding bottom plate was controlled by a simple screw mechanism which, when turned, would control the rate of flow of the soil.

The tanks were lifted and moved with a travelling overhead crane. To overcome the height restrictions imposed by lifting one 2 m high tank over the other, a lifting beam was designed to fit inside the top tank. The beam could be removed when the tank was to be used as the test container.

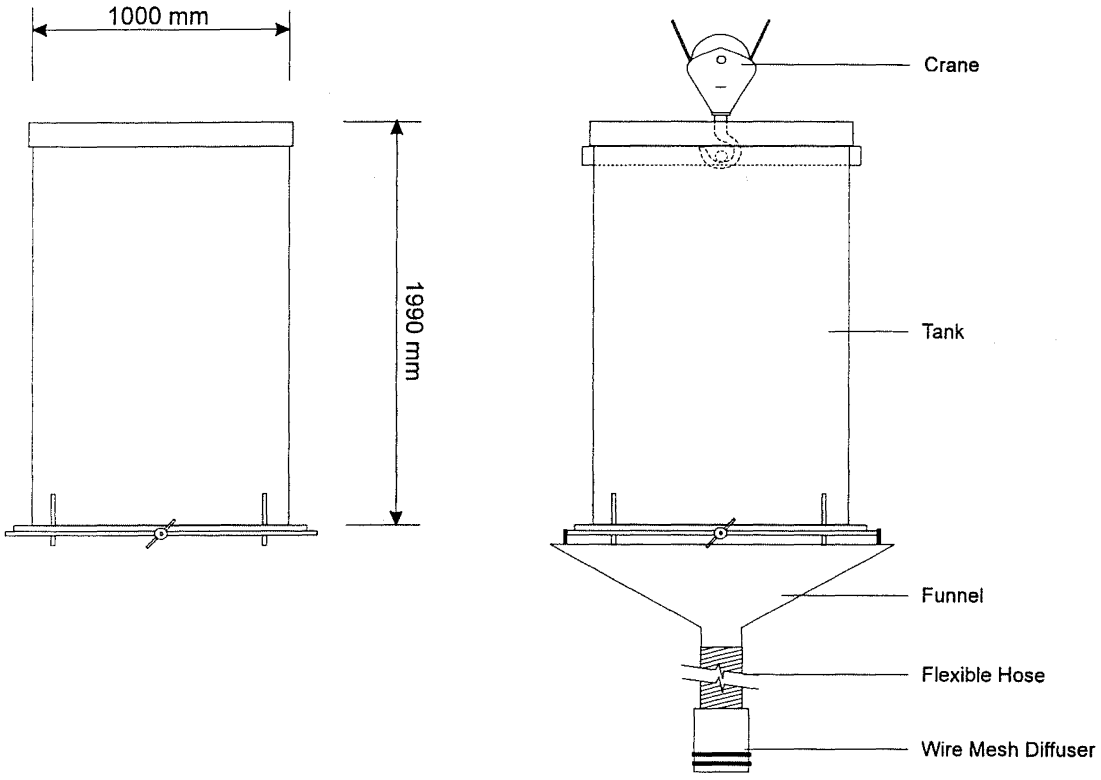

Figure 3.1 - Steel Sand Tanks

3.2 SOIL

The soil chosen for these tests was an industrial grade 30/60 silica sand. The properties of this sand are given in Table 3.1. The material was supplied by Commercial Minerals Ltd, Auckland, New Zealand.

The reasons for selecting this soil were:

a) It is a generic particulate material that should qualitatively simulate the behaviour of a range of different soils.
b) It is suitable for air pluviation.
c) It is suitable for being reused many times without degradation.
d) It should be possible to obtain additional supplies of the material for future testing.
e) It is very clean and minimal dust is generated during air pluviation.

Table 3.1 – Soil Properties

Property	Symbol	Value
Density of Solid Particles	ρ_s	2.65 t/m^3
10% finer	D_{10}	0.30 mm
60% finer	D_{60}	0.45 mm
minimum voids ratio	e_{min}	0.53
maximum voids ratio	e_{max}	0.83
Steady State Friction Angle	ϕ_{ss}	33°

Note: Derivations of the soil properties are given in Appendix A.

3.3 PREPARATION OF SOIL DEPOSIT

The soil deposits were prepared by air pluviation. To prepare each soil deposit, one full tank of sand was lifted over an empty tank and the perforated steel gate was opened. The sand flowed out through the gate and collected in a funnel that had been suspended beneath the top tank, as shown in Figure 3.1. The sand flowed down a 95 mm diameter flexible hose, discharging through a wire mesh diffuser into the bottom tank.

The diffuser was made from a 100 mm diameter by 300 mm long section of plastic tube that was packed with wire mesh. The amount of wire mesh could be adjusted to produce the desired relative density of the soil deposit. Homogeneity of the soil deposit was achieved by holding the diffuser at a constant 50 mm above the rising soil surface so that the energy of deposition remained constant. Richards et al. (1990) showed that air pluviation with a constant height of deposition produces near-homogeneous soil deposits. A similar diffuser has also been used successfully by Iai (1991) to prepare homogeneous sand deposits.

Samples of soil were taken as each soil deposit was prepared. The density of each sample was found in order to check the density and homogeneity of each deposit. The results are shown in Table 3.2.

Table 3.2 – Soil Deposit Density Tests

Weight of sample (gm)	Density (t/m^3)	Voids Ratio	Relative Density (%)
199.65	1.53	0.73	0.33
200.49	1.53	0.73	0.33
197.40	1.51	0.75	0.27
197.33	1.51	0.75	0.27
202.93	1.56	0.70	0.43
197.93	1.51	0.75	0.27
200.52	1.53	0.73	0.33
196.10	1.49	0.78	0.17
198.57	1.52	0.74	0.30
199.71	1.53	0.73	0.33
198.79	1.52	0.74	0.30
198.08	1.51	0.75	0.27
201.08	1.54	0.72	0.37
199.42	1.53	0.73	0.33

The average relative density for the static soil deposits was 31 percent. A loose sand was chosen for these tests to reduce the effects of soil dilation. The model test results are then more readily applicable to full-scale tests, where the confining pressures are greater and dilation is more suppressed. This is in accordance with the principal of 1-g modelling described by Scott (1989).

3.4 CONSTRUCTION OF DRILLED SHAFT

A drilled shaft foundation is usually constructed by drilling a hole in the soil, inserting a reinforcing cage then filling the hole with concrete. If the drilled shaft is constructed in a loose non-cohesive material then a casing may be required to maintain stability of the hole. If so, the casing is first driven into the soil then the soil is drilled out. The casing may be removed once the concrete has been placed.

Since the present tests were performed using prepared soil deposits, it was much simpler to construct the soil deposits around the shaft casing than it was to drill into the dry sand. The shaft casing was made from 1 mm thick galvanised sheet metal that had been rolled and riveted into a tube. The dimensions of the casing were 95 mm diameter by 1500 mm long. The casing was suspended in the bottom tank and the sand poured around it by controlling the direction of the diffuser. Care was taken to avoid disturbing the shaft casing as this would tend to disturb and possibly densify the soil around it.

The model drilled shafts, nominally 95 mm diameter by 1450 mm long, were constructed by pouring concrete into the drilled shaft casing. Each shaft was reinforced using a single 16 mm diameter deformed steel bar. Steel pins were fixed radially top and bottom to help centre the bar inside the casing. A 70 mm diameter steel plate was fixed to the bottom of the bar to provide some confinement to the relatively "green" concrete during load testing (the model drilled shafts were tested after only 24 hours curing). The reinforcing bar was threaded at the top to allow fixing to the load actuator.

Details of the concrete mix used are given in Table 3.3. The mix design gives a water:cement ratio of 0.4 and a crushing strength of 12 MPa after 24 hours. Each batch of concrete was mixed in a bucket then trowelled into the shaft casing, taking care not to disturb the casing and the surrounding soil. The concrete was lightly tamped at one third and two thirds heights then, when the placing was finished, the overhead crane was used to pull the shaft casing out. Removal of the casing caused

the level of the concrete to drop by approximately 20 mm. The concrete was then left to cure for 24 hours before load testing the shaft.

Table 3.3 – Model Drilled Shaft Concrete Mix Design

Item	Details	Quantity
Aggregate	$d_{10} = 0.15$ mm, $d_{60} = 0.53$ mm	15 kg
Cement	Rapid Hardening Portland	6.62 kg
Plasticiser	Daracem 100	18 ml
Water		2.65 l

REFERENCES

IAI, S. (1991). "A Strain Space Multiple Mechanism Model For Cyclic Behavior of Sand and its Application," Research Note No.43, Earthquake Engineering Research Group, Port and Harbour Research Institute, Ministry of Transport, Japan. May 1991.

RICHARDS, R. Jr., ELMS, D. G., and BUDHU, M. (1990). "Dynamic Fliuidization of Soils," Journal of Geotechnical Engineering, ASCE, Vol.116, No. 5, May 1990.

SCOTT, R.F. (1989). "Centrifuge Modelling Technology; A Survey", Rev. Francaise de Geotechnique, Vol. 48, pp 15-34.

Chapter Four

TESTING OF MODEL DRILLED SHAFTS UNDER CYCLIC AXIAL LOADS IN A STATIC SOIL DEPOSIT.

INTRODUCTION

This chapter gives details of the cyclic axial load tests performed in static soil deposits. Cyclic axial load tests were performed on model drilled shafts, under different combinations of mean and cyclic axial load amplitude. The uplift capacity of each shaft was found after cyclic loading and compared with the uplift capacity without cyclic loading. The effects of cyclic loading could then be determined.

The results show that some model drilled shafts remained stable during loading while others became unstable. Examples are given for each type of shaft response and stability criteria are determined for the model drilled shaft. All the load/displacement curves for these tests are included in Appendix B.

4.1 LOAD TEST PROGRAM

The first tests performed on the model drilled shafts were monotonic load tests. Monotonic uplift and monotonic compression tests were performed to establish the static uplift and the static compressive capacities with no cyclic loading. The capacities were used as benchmarks, by which the capacities after cyclic axial loading could be compared.

The remaining tests were performed with various combinations of mean and cyclic axial load being applied to the shaft. Upon completion of the cyclic axial loading, each shaft was failed in uplift to determine its residual uplift capacity.

4.2 LOADING RIG AND INSTRUMENTATION

Axial loads were applied to the model drilled shafts with a servo controlled hydraulic actuator, as shown in Figure 4.1. The actuator was attached to the shaft reinforcing rod with a clevis and pin and was supported by a reaction frame that was bolted to the steel tank. The hydraulic actuator was controlled by a Moog model 73-233 servo-valve and an MTS 443.11 closed-loop servo-hydraulic system, as illustrated in Figure 4.2. The required load signals were generated by a PC and downloaded to a Hewlett-Packard random waveform generator (model HP33120A), as shown in Figure 4.3. Data acquisition was via a Hewlett-Packard VXI system digital voltmeter and multiplexer interfaced with the PC.

Vertical shaft displacement was measured using a Linear Variable Displacement Transducer (LVDT) mounted on the hydraulic actuator. Applied shaft loads were measured using a Precision Transducers LPC 2.5 tonne load cell mounted between the actuator and the drilled shaft head. Horizontal soil stress was measured using a Kyowa BE-2KC Soil Pressure Transducer buried in the soil approximately 20 mm away from the side of the shaft at various depths.

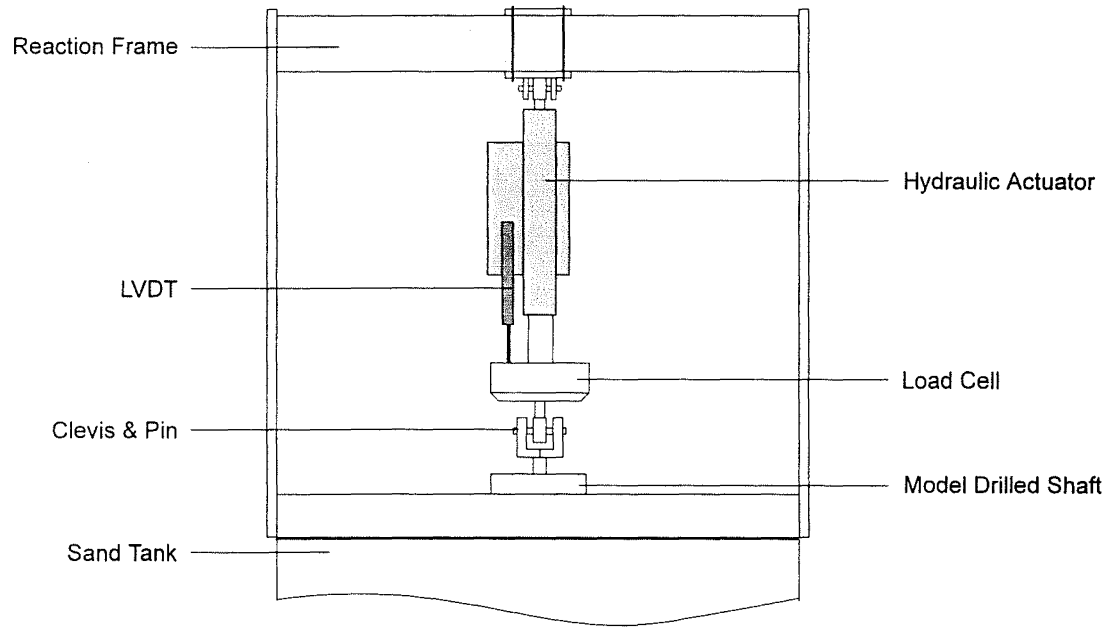

Figure 4.1 - Axial Loading System

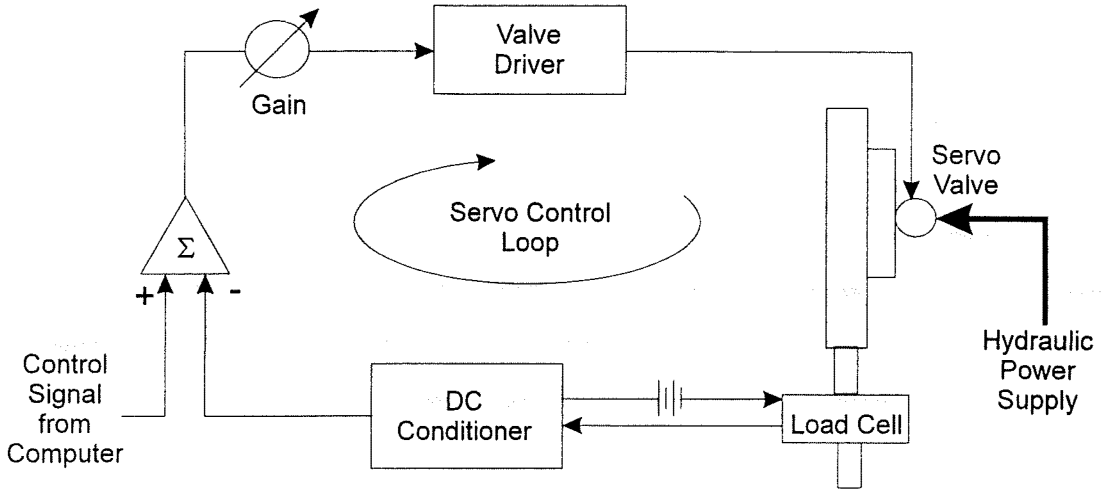

Figure 4.2 - Load Controlled Electro-Hydraulic Test System

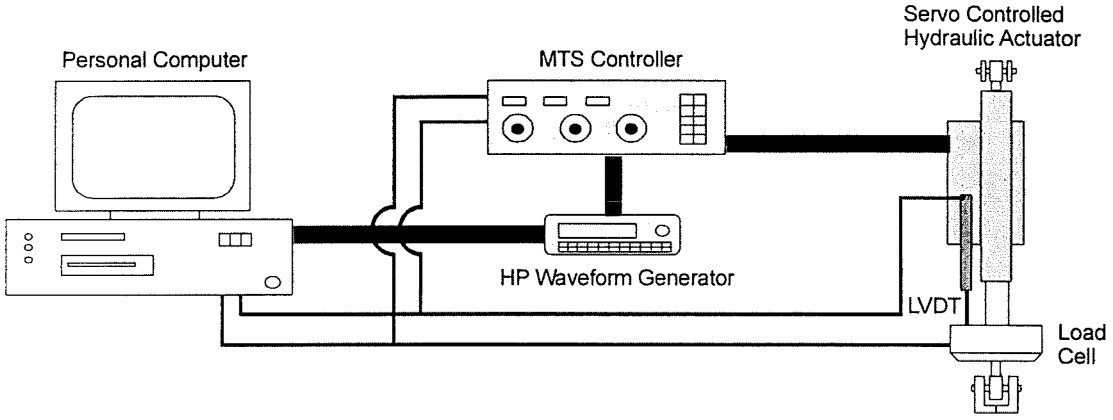

Figure 4.3 - Actuator Control and Data Acquisition Systems

4.3 MONOTONIC LOAD TEST RESULTS

4.3.1 Monotonic Uplift Capacity

Three monotonic uplift tests were performed on model drilled shafts. A typical load/displacement response (for test 017) is shown in Figure 4.4. The load/displacement response is typical for a drilled shaft uplift failure, showing a peak load reached at a relatively low displacement. The load then decreases with increasing displacement, eventually reaching a "steady state" strength of approximately 80 percent of the peak load.

The uplift capacities for monotonic tests 015, 016 and 017 were found to be 1.56 kN, 1.68 kN and 1.52 kN respectively, so the average monotonic uplift capacity of the model drilled shaft was taken to be Q_{us} = 1.59 kN.

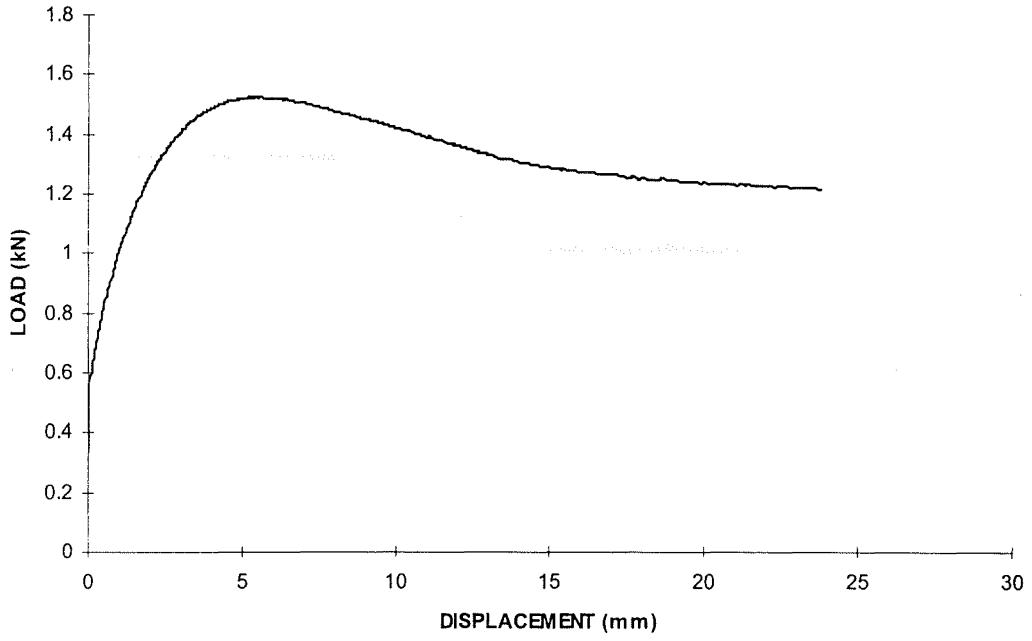

Figure 4.4 - Load versus Displacement for Monotonic Uplift Test 017

4.3.2 Monotonic Compressive Capacity

Two monotonic compression tests were performed on model drilled shafts. A typical load/displacement response (for test 035) is shown in Figure 4.5. The

load/displacement response is typical for a drilled shaft compressive failure, with no definite peak load shown. A difficulty then arises in interpreting the actual "ultimate compressive capacity".

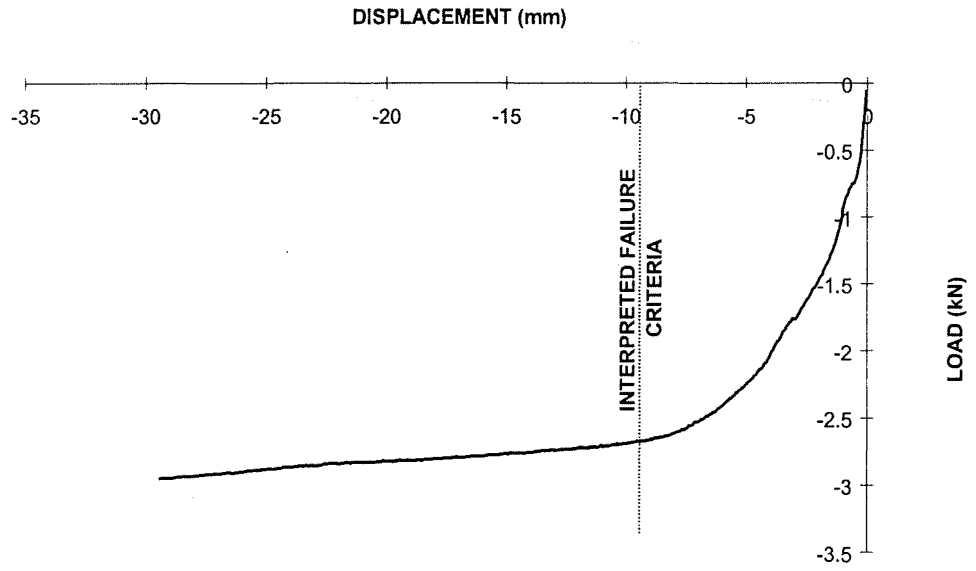

Figure 4.5 - Load versus Displacement for Monotonic Compression Test 035

The problem of interpreting compressive capacity has been examined by Hirany and Kulhawy (1988). The authors compared forty-one different methods for interpreting load test data and found the various methods to be very inconsistent in their interpretation of the compressive capacity for drilled shaft foundations. The authors found that the interpretation methods fell into three main categories – settlement limitation, graphical construction and mathematical model. A detailed discussion of each method is given in Hirany and Kulhawy (1988).

For this study, the interpreted compressive capacities were determined using a settlement limitation method. Settlement limitation methods generally dictate that the interpreted capacity is taken to be that load required to produce or exceed some pre-determined amount of settlement of the shaft. A settlement limitation method was chosen because it is the least susceptible to individual judgement, since the only parameter choice is that of critical settlement and once its value has been chosen it remains constant for all tests. The graphical construction and mathematical model

methods were disregarded because they both involve fitting curves to the data, which introduces greater individual judgement and possible bias.

The particular method chosen for this study was the Diameter-Dependent Settlement Limitation method. In this method, the critical settlement is selected as a percentage of the shaft diameter. The choice of a diameter-dependent method was based on a statement by Terzaghi (1942) where it was stated that "the failure load is not reached unless the penetration of the pile is at least equal to 10 percent of the diameter of the tip of the pile". One of the drawbacks of this settlement limitation method is that it may produce different interpreted capacities for different diameter shafts, even when they produce exactly the same load/displacement curves. However, the drawback is not relevant to the present tests because all tests are performed on identical shafts in a near-constant homogeneous soil deposit.

For the present study, the critical settlement was taken as 10 percent of the shaft diameter. The choice of 10 percent follows from Terzaghi (1942) and from Weltman (1980) who interpreted their shaft capacities as the load on the shaft when the settlement is equal to 10 % of the shaft diameter. The choice of 10 percent was rather arbitrary (values ranging from 2 percent to 25 percent have been used by others) because the aim of the test regime was to observe the **changes** in capacity under different loads rather than any absolute values. As long as the failure parameter stayed the same then all results would be relative to each other, thus enabling valid comparisons to be made.

For these model shafts, a critical settlement of 10 percent of the shaft diameter equates to a shaft displacement of 9.5 mm. The failure displacement is indicated in Figure 4.5 and illustrates that the selected definition of failure is appropriate for this test. When the displacement reaches –9.5 mm, the response of the shaft has become highly non-linear. It has moved through a transition zone from linear-elastic behaviour and is now almost fully plastic, indicating that failure has occurred. (Note that compression is taken as negative and uplift as positive).

For the chosen failure criterion, the interpreted compressive capacity for Test 035 was found to be 2.66 kN. The capacity of Test 042 was 2.69 kN so the average interpreted compressive capacity of the model drilled shaft was taken to be Q_{cs} = 2.68 kN.

4.4 CYCLIC AXIAL LOAD TESTS

The remainder of axial load tests were performed under various combinations of mean and cyclic axial load. The general shape of each simulated earthquake load history is illustrated in Figure 4.6. The first stage of loading involved slowly applying the dead or mean load as a constantly increasing "ramp" function. The mean load was held constant for 100 seconds to allow for the majority of creep effects to dissipate, then the "earthquake" load was applied as a series of 20 cycles of sinewave at a frequency of 1 Hz, oscillating about the mean load. When the cyclic load test was completed, the shaft was failed in uplift to determine the uplift capacity. The uplift capacity could then be compared with the monotonic uplift capacity to determine the effect of the cyclic axial load.

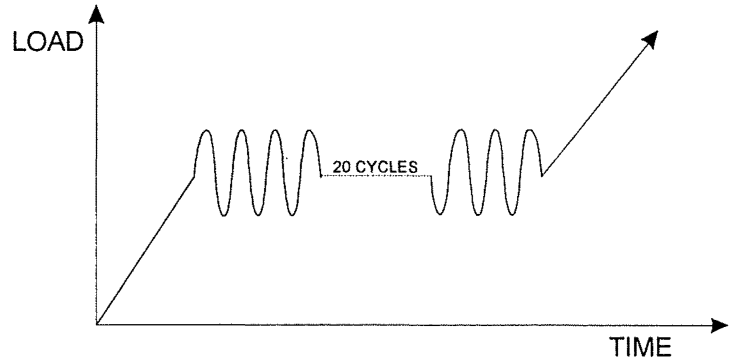

Figure 4.6 - Simulated Earthquake Load History

The results from the cyclic axial load tests are summarised in Table 4.1. The results show three different patterns of shaft response: The shaft may remain stable during the test or it may become unstable and fail, either in compression or in uplift.

Table 4.1 – Model Drilled Shaft Axial Load Test Results

Test	Load	P_c (kN)	P_o (kN)	Q_u (kN)	m	d_p (mm)	d_{ppl} (mm)	d_{ppf} (mm)	Result
15	MU	-	-	1.563	-	-	-	-	-
16	MU	-	-	1.677	-	-	-	-	-
17	MU	-	-	1.524	-	-	-	-	-
18	CYC	1.00	0.00	1.744	1.1	-4.50	1.91	0.94	S
19	CYC	1.00	0.00	C	c	-4.25	2.39	1.03	S
20	CYC	1.20	0.00	D	d	60	3.28	d	U
21	CYC	1.00	0.20	1.598	1.0	-2.71	2.67	1.26	S
22	CYC	1.20	0.20	d	d	D	2.25	10	U
23	CYC	1.00	-0.20	1.327	0.8	-5.89	3.12	0.77	S
24	e	e	e	e	e	E	e	e	-
25	CYC	1.20	-0.20	1.568	0.9	-5.08	3.33	1.08	S
26	CYC	1.40	-0.20	D	d	D	5.85	d	U
27	CYC	0.50	-1.00	C	c	-1.83	1.41	0.10	S
28	CYC	2.00	-1.00	1.173	0.7	-	12.11	3.48	U
29	e	e	e	e	e	e	e	e	-
30	CYC	2.15	-1.15	d	d	18.50	19.76	4.11	U
31	CYC	0.50	0.00	c	c	-0.38	0.29	0.22	S
32	CYC	0.75	0.00	c	c	-1.9	1.03	0.48	S
33	CYC	0.40	0.20	c	c	-0.06	0.46	0.18	S
34	CYC	0.70	0.20	1.517	0.9	-1.25	0.80	0.52	S
35	MC	-	-	-	-	-	-	-	-
36	CYC	0.60	0.40	1.545	0.9	2.47	1.86	0.66	S
37	CYC	1.00	0.30	1.723	1.0	-0.42	1.81	1.23	S
38	CYC	1.20	0.40	d	d	d	d	d	U
39	CYC	1.50	-0.60	1.436	0.9	-8.60	-4.38	-2.14	U/S
40	CYC	1.50	-1.00	1.003	0.6	-9.61	-4.26	-0.63	U
41	CYC	1.50	-0.80	1.292	0.8	-9.34	-4.00	-1.02	U
42	MC	-	-	-	-	-	-	-	-
43	CYC	1.20	-0.80	0.941	0.5	-6.90	-3.41	-0.60	S

Symbol	Description
P_c	magnitude of cyclic component of load
P_o	mean or dead load component (+ = tension)
Q_u	ultimate uplift capacity
m	change in uplift capacity after cyclic loading (Qu/Qt)
d_p	Displacement accumulated during cyclic loading (+ = upwards)
d_{ppl}	peak to peak displacement for first cycle of load
d_{ppf}	peak to peak displacement for final cycle of load
MU	monotonic uplift
MC	monotonic compression
CYC	cyclic axial loading
S	Stable
U	Unstable
c	data not recorded
d	Failed in uplift prior to test completion
e	Equipment failure

4.4.1 Stable Behaviour

Some of the model drilled shafts remained stable during the load tests. The load/displacement response of a typical stable test (test 021) is shown in Figure 4.7. The shaft had a mean axial load of 0.2 kN and a cyclic axial load amplitude of 1.0 kN.

Figure 4.7 shows that the shaft undergoes a hysteretic cyclic response to the axial load combination, with the peak cyclic load amplitude reached on each half cycle. The shaft displaces into the soil mass with each successive cycle but the displacement per cycle decreases and the stiffness of the soil/shaft system increases as the test progresses.

The final stage of loading for Test 021 has the shaft loaded to failure in uplift. The residual uplift capacity for Test 021 was found to be 1.60 kN, or 101 percent of the benchmark monotonic capacity Q_{us}. Therefore, the cyclic loading had no significant effect on the uplift capacity in this test.

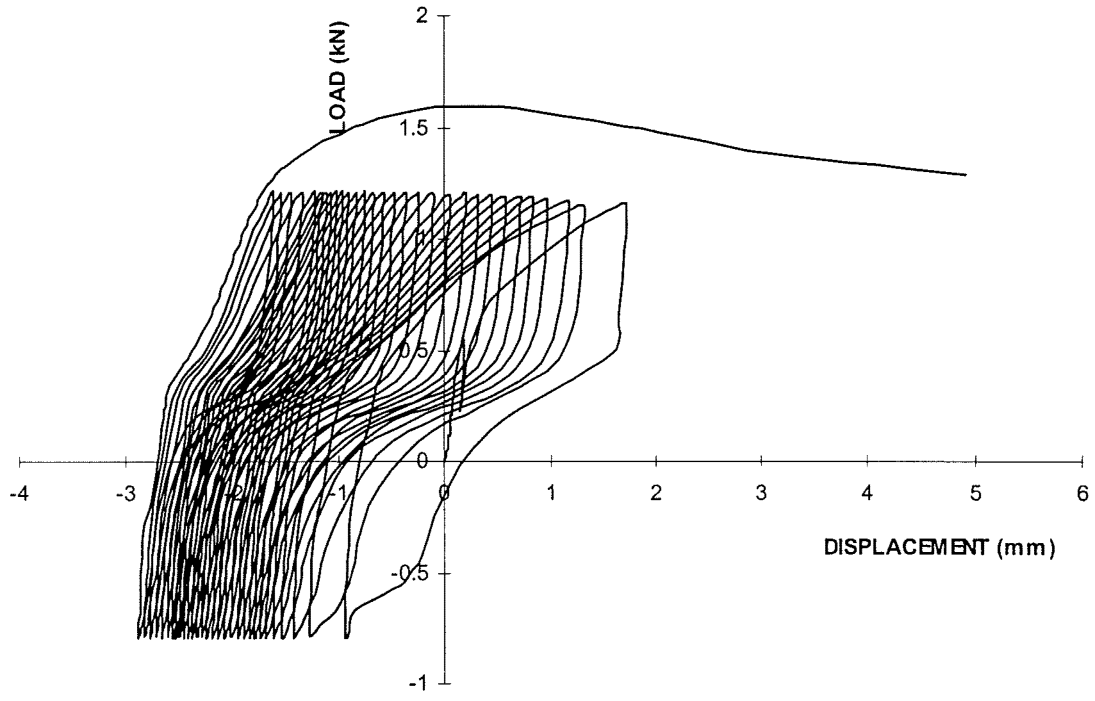

Figure 4.7 - Load versus Displacement for Cyclic Axial Load Test 021

4.4.2 Uplift Failure

An example of an uplift failure is shown in Figure 4.6, for test 022. In the first six cycles of loading the response is similar to stable test 021, with the shaft undergoing a hysteretic response to the cyclic axial load. However, during these cycles the shaft does not progressively displace downward into the soil mass. Instead, it quickly reaches a minimum average displacement, cycles about the minimum for five cycles then, in the seventh cycle of loading, the shaft begins to work its way up and out of the soil. Each subsequent cycle brings an increasing upward displacement as the shaft moves out of the soil. The increasing cyclic displacements reach a point where the required load can no longer be sustained during the cycle. Any attempt to apply greater load simply brings larger upward displacements and the test is eventually terminated when the maximum displacement is reached on the hydraulic actuator.

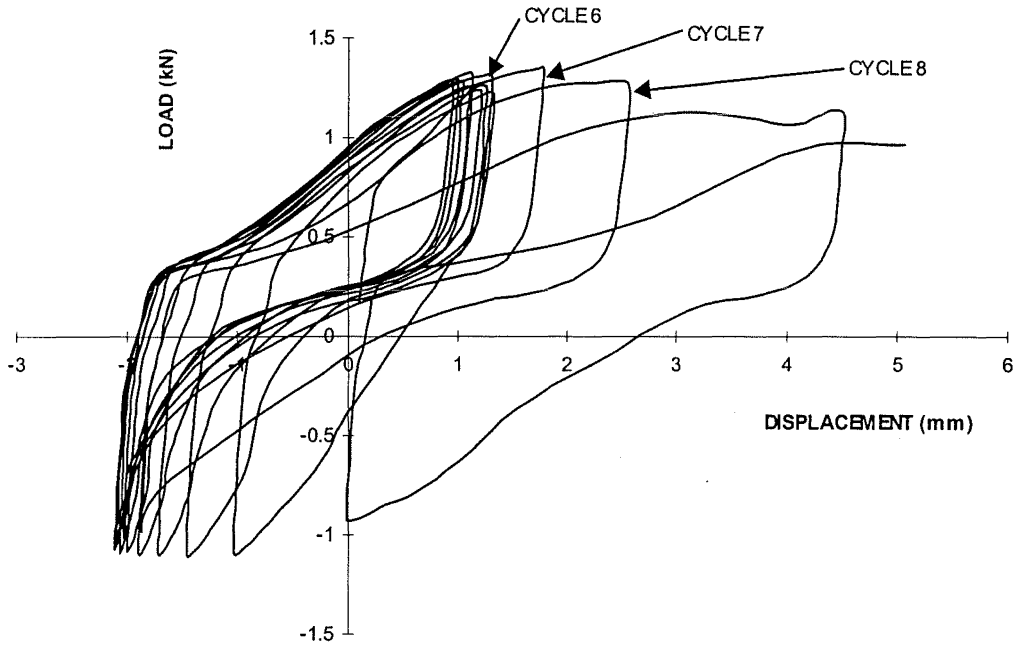

Figure 4.8 - Load versus Displacement for Cyclic Axial Load Test 022

4.4.3 Compressive Failure

An example of a compressive failure is shown in Figure 4.8, for test 041. The shaft response is generally similar to that of stable test 021 in that the load is maintained for each cycle and the displacement increment per cycle decreases as the test progresses. However, the model drilled shaft in test 041 has failed in compression because the cumulative settlement has exceeded the defined failure criterion of 9.5 mm.

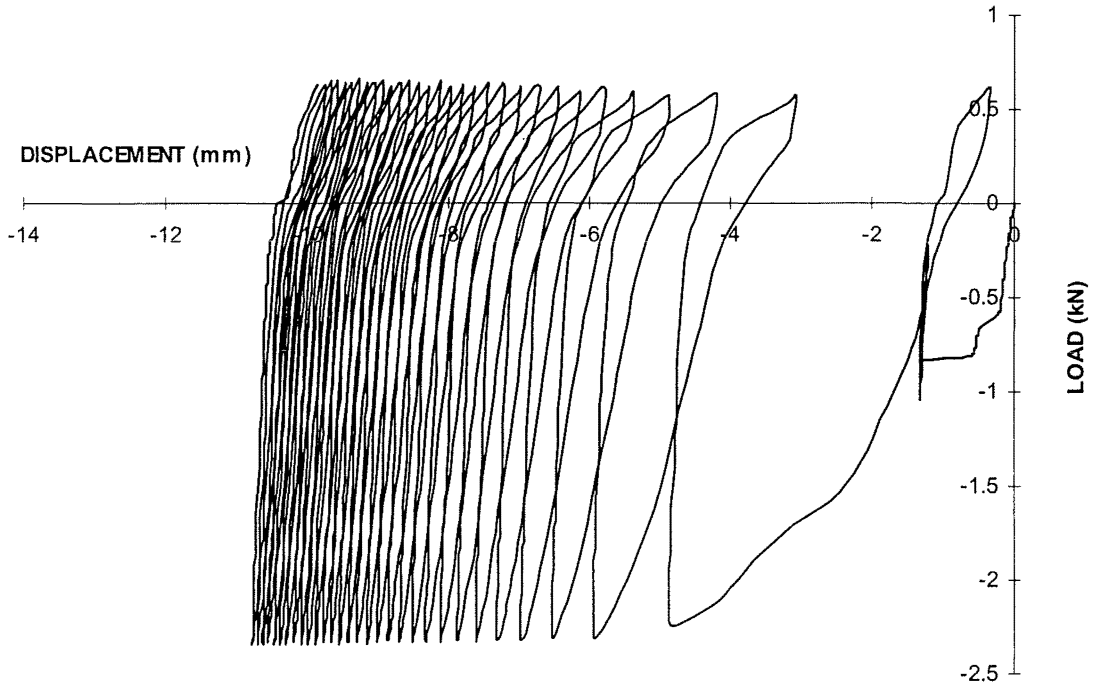

Figure 4.9 - Load versus Displacement for Cyclic Axial Load Test 041

4.5 CYCLIC STABILITY CRITERIA

The present set of tests show that, in most cases, the foundation is able to withstand the applied loads. Failure in these tests has usually come as a result of excessive displacement, either in uplift or in compression. For this reason, it is judicious to set stability criteria that are governed by displacement.

Poulos (1989) and Turner & Kulhawy (1990) found a correlation between cyclic uplift stability and cyclic displacement (the displacement of the foundation in one half cycle of loading). They found that the foundation becomes unstable in uplift if its displacement exceeds a certain critical level during cyclic axial loading. The Poulos tests show that significant degradation of the limiting skin friction (and therefore shaft failure) occurs if the cyclic displacement amplitudes exceed the displacement at peak load under static loading conditions. The Turner and Kulhawy tests show that the shaft becomes unstable if the cyclic displacement amplitude exceeds 3-4 mm, regardless of the geometry of the shaft or the soil density.

If the Poulos stability criterion is applied to the present study then instability is predicted for cyclic displacements exceeding approximately 4 mm. The Turner and Kulhawy criterion is set at 3-4 mm, so the critical cyclic displacement for the present study would be expected at 3-4 mm. A comparison of the cyclic responses of tests 021 and 022 (shown in Figures 4.7 and 4.8 respectively) shows that the shaft is stable when the cyclic displacement is 2.7 mm but unstable when the cyclic displacement reaches 3.1 mm. The results of two other tests performed under similar loading conditions show instability occurring at similar cyclic displacement. Test 019 had a cyclic displacement of 2.4 mm and remained stable while test 020 had a cyclic displacement of 3.6 mm and became unstable during the test. **The critical cyclic displacement was therefore set at 3 mm for uplift stability in the present study.**

The compressive stability criterion chosen for the present study is also displacement dependent. The compressive failure shown in Figure 4.9 shows that the model drilled shaft is certainly able to withstand the applied loads but, from a serviceability point of view, the shaft has undergone excessive displacement during the test. It has, therefore,

been deemed to have become unstable. The limits of "excessive displacement" are highly subjective and depend upon the end use of the drilled shaft foundation. However, if quantifiable comparisons are to be made then those settlement limits must be set. **The cumulative settlement limit has therefore been set for the present study as 10 percent of the shaft diameter, or 9.5 mm**. This follows from the interpreted monotonic compressive capacity discussed in section 4.3.2, where the shaft response became highly non-linear when the displacement exceeded 10 percent of the shaft diameter.

SUMMARY

Axial load tests were performed on 27 identical model drilled shaft foundations that were embedded in a static soil deposit. The first tests were monotonic uplift and monotonic compression tests, performed to determine the equivalent static capacities of the drilled shaft. The uplift capacity of the drilled shaft was found to be 1.59 kN and the compressive capacity was found to be 2.68 kN.

The remaining tests were cyclic axial load tests, performed with different combinations of mean and cyclic axial load applied to the shaft. The tests produced three distinct responses to the applied loading. Some of the shafts remained stable during loading while others failed either in uplift (excessive upward displacement) or in compression (excessive downward displacement).

Stability criteria were determined for the model drilled shafts, based on the displacement magnitudes observed during loading. The limits of stable displacement were set at 3.5 mm per cycle for uplift stability and a cumulative displacement of 9.5 mm for compressive stability.

REFERENCES

HIRANY, A. and KULHAWY, F.H. (1988). "Conduct and Interpretation of Load Tests on Drilled Shaft Foundations," Report EL-5915, Volume 1, Electric Power Research Inst., Palo Alto. Calif. July, 1988.

TERZAGHI, K. (1942). "Discussion of Committee on the Bearing Value of Pile Foundations," Proceedings, ASCE, Vol. 68, No. 2, February, 1942.

TURNER, J.P. and KULHAWY, F.H. (1990). "Drained Uplift capacity of Drilled Shafts under Repeated Axial Loading," J. Geotech. Engrg., ASCE, Vol. 116, No.3, March, 1990.

WELTMAN, A.J. (1980) "Pile Load Testing Procedures" Report PG7, Construction Industry Research and Information Association (CIRIA), London, 1980, 53 p.

Chapter Five

THE CYCLIC AXIAL LOAD RESPONSE OF MODEL DRILLED SHAFTS IN STATIC SOIL DEPOSITS.

INTRODUCTION

The results from the cyclic axial load tests performed in a static soil deposit, are summarised in this chapter. A Cyclic Stability Diagram is constructed from the results providing a clear illustration of the effects of cyclic axial loading on the stability of the drilled shaft. Analysis of the diagram leads to the development of a parameter called the Level of Load Reversal (LLR). The LLR can be used to determine whether a particular combination of mean and cyclic load will cause a drilled shaft to become unstable during loading.

A conceptual soil/shaft system model is developed from the results of these tests and from the cyclic axial load tests of others. The model has a dilating shear zone that is generated around the drilled shaft under cyclic loading. Changes to the shear zone and the surrounding soil mass bring about shaft failure as the shear zone dilates and contracts under the induced shear strains and the surrounding soil mass contracts and stiffens. Hoop stresses may be generated within the soil mass if it is able to contract sufficiently. Hoop stresses reduce the confining stress around the shaft by creating an arching effect in the soil mass, thus reducing the overall strength of the soil/shaft system.

A short series of tests was performed on drilled shafts in higher density soil deposits. The results from these tests are given, showing that the model drilled shaft is more prone to failure under cyclic loading when the relative density of the soil is increased. The conceptual shear zone model is then used to explain the reduction in cyclic stability at increased soil density.

5.1 THE CYCLIC STABILITY DIAGRAM

The Cyclic Stability Diagram was developed by Poulos (1988) to illustrate the effects of cyclic loading on the capacity of a drilled shaft. (Details and an illustration of the Cyclic Stability Diagram are given in Chapter 2.) The Cyclic Stability Diagram is a plot of the cyclic axial load amplitude versus the mean axial load for a series of cyclic axial load tests. The region bounded by the diagram is divided into stable, metastable and unstable regions, indicating the effect that each axial load combination has on shaft stability.

A Cyclic Stability Diagram has been constructed for the cyclic axial load tests in the static soil deposit and is shown in Figure 5.1. The load combinations that caused instability are plotted as filled squares and the stable load combinations are plotted as unfilled squares. Test 039 is shown as a grey square because this test fell on the boundary between stable and unstable behaviour. The stable/unstable boundary has been drawn in as a solid line.

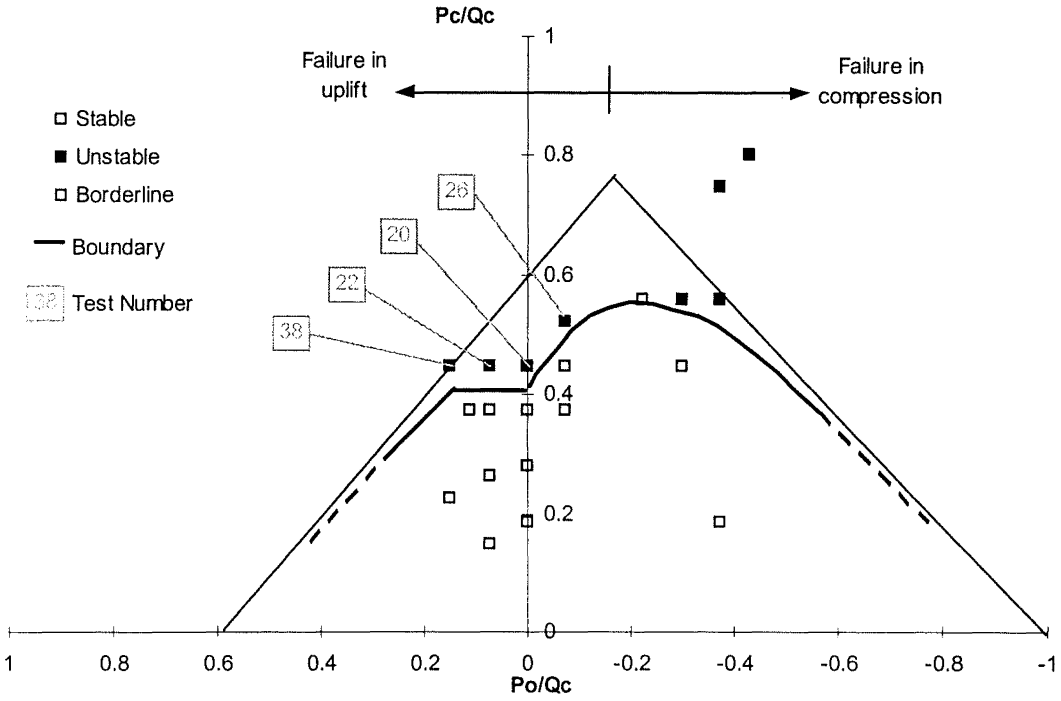

Figure 5.1 - Cyclic Stability Diagram for Cyclic Axial Load Tests in a Static Soil Deposit

The Cyclic Stability Diagram shows that the capacity of a drilled shaft is reduced during cyclic axial loading. In the worst cases (Tests 020 and 026) it was found that the capacity was reduced to approximately 57 percent of the static compressive capacity (Q_c).

There are two notable differences, however, between the Poulos Cyclic Stability Diagram and this Cyclic Stability Diagram. The first difference is that no metastable zone, as defined by Poulos, was found in the present tests. The second difference is that there is a pronounced "dip" in the stable/unstable boundary around zero mean load. These differences will be discussed in the following two sections.

5.1.1 The Metastable Zone

The metastable zone is the area of the plot where the applied loads cause a reduction in uplift capacity (Q_u) after loading, but the shaft remains stable during the load test. No metastable zone has been identified in the present diagram because there were no significant reductions in Q_u after any of the tests. The change from stable to unstable behaviour occurs over a very small change in cyclic axial load amplitude so, if a metastable zone does exist, then it must be very narrow.

The lack of a metastable zone is not a new development. Poulos (1988) had already found that "for very soft soils, there is almost no metastable zone". The soil deposits used in the present tests may be considered very soft, as they had an average relative density of 31 percent. No metastable zone would then be expected.

The lack of a metastable zone may also be attributed to the stiffness of the drilled shaft. Poulos found that "short stiff piles may fail very abruptly, with little prior warning, after small increases in cyclic load above the stable zone." The model drilled shaft used for these tests may be considered both short and stiff by Poulos' measure (a length of 1450 mm and a stiffness of 8.53×10^{10} Nmm^2) so no metastable zone would then be expected for these tests.

Further evidence of a narrow metastable zone is found from cyclic load tests performed by McManus & Kulhawy (1994). These tests, performed in over-consolidated clay, also show a rapid change from stable to unstable behaviour. In two of these tests (their K and L) a change of 13 percent of Q_u was sufficient to change the load response from stable to unstable. The drilled shafts used in these tests were also made from steel reinforced concrete with similar dimensions to the present model drilled shaft, so the lack of a metastable zone concurs with the Poulos observation for very stiff piles.

5.1.2 The Level Of Load Reversal

A pronounced "dip" in the stable/unstable boundary is evident where it crosses the $P_0/Q_c = 0$ axis (ie. around zero mean load). In other respects the boundary largely follows the idealised shape predicted by Poulos. The dip, however, is significant because it indicates that the Level of Load Reversal (LLR) is a significant parameter in predicting the uplift stability of a drilled shaft under cyclic axial loading.

The LLR is described as the **minimum** amount by which the load changes orientation, either from compression to uplift or from uplift to compression. The LLR is defined in Equation 5.1.

$$LLR = \frac{P_c - |P_o|}{Q_u} \tag{5.1}$$

where P_c is the cyclic axial load amplitude, P_o is the mean axial load and Q_u is the static uplift capacity.

Load tests 20, 22, 26 and 38 all failed in uplift and all plot very close to the stable/unstable boundary, as shown in Figure 5.1. Details of the cyclic load applied to each are shown graphically in Figure 5.2. All the drilled shafts shown in Figure 5.2 were unstable during the test, but they failed at different peak uplift loads. In Test 038 the peak uplift load was 100 percent of Q_u and, as expected, the drilled shaft failed.

However, in Test 022 the peak uplift load was only 88 percent of Q_u and the drilled shaft failed. The worst case load combinations occurred in Tests 020 and 026, where the peak uplift load was only 75 percent of Q_u and the drilled shaft failed during the test.

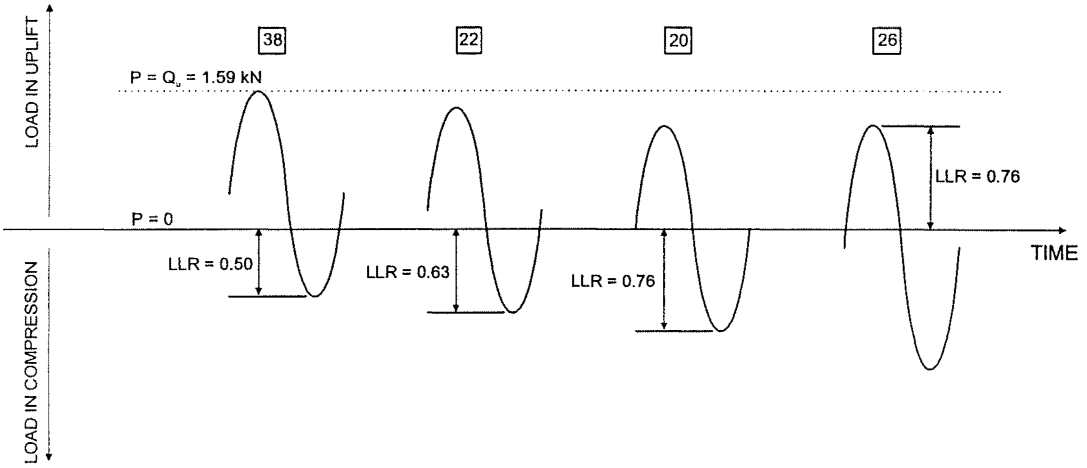

Figure 5.2 – Unstable Cyclic Load Tests around Zero Mean Load

The LLR may be useful for predicting whether a particular load combination is stable in uplift or not. The diagram shown in Figure 5.2 illustrates that as the LLR increases the peak uplift load causing instability decreases. Test 038 has an LLR of 0.50 and fails at 100 percent of Q_u, Test 022 has an LLR of 0.63 and fails at 88 percent of Q_u, and Tests 020 and 026 both have an LLR of 0.76 and both fail at 75 percent of Q_u.

The significance of the LLR has been indirectly noted in previous research. A review of cyclic load tests by Charlie et al. (1985) found that two-way repeated loading had a more severe degrading effect on strength than did one-way loading. If this observation is expressed in terms of the LLR then loading with non-zero LLR (two-way loading) had a more severe degrading effect on strength than loading with zero LLR (one-way loading). Such an observation agrees with the present study.

The Level of Load Reversal has been plotted versus peak uplift load in Figure 5.3 for all the model drilled shaft tests that failed in uplift. A clear boundary exists between

the stable and unstable test results and has been indicated as a straight line. The stable region may then be defined by the following relationship:

$$P_c < 0.67Q_u + \frac{|P_o| - P_o}{2} \tag{5.2}$$

The obvious limitation that the total peak load (P_c+P_o) be less than the static uplift capacity (Q_u) must also apply. Therefore, for mean load levels in uplift, the cyclic load amplitude causing failure in uplift is predicted by the following equations:

$$P_c = 0.67Q_u, \qquad P_c + P_o < Q_u \tag{5.3}$$

For low mean load levels in compression, the cyclic load amplitude causing failure in uplift is predicted by the following equation:

$$P_c = 0.67Q_u + |P_o|, \qquad |P_o| < 0.2Q_u \tag{5.4}$$

For greater mean loads in compression, plotting in the compression failure zone of the cyclic stability diagram, the stable/unstable boundary has not been fully determined. However, the following equation appears to predict the cyclic load amplitude causing failure and has been derived from the stable/unstable boundary shown as a dashed line in Figure 5.1.

$$P_c = 0.7(Q_c - |P_o|), \qquad |P_o| > 0.2Q_c \tag{5.5}$$

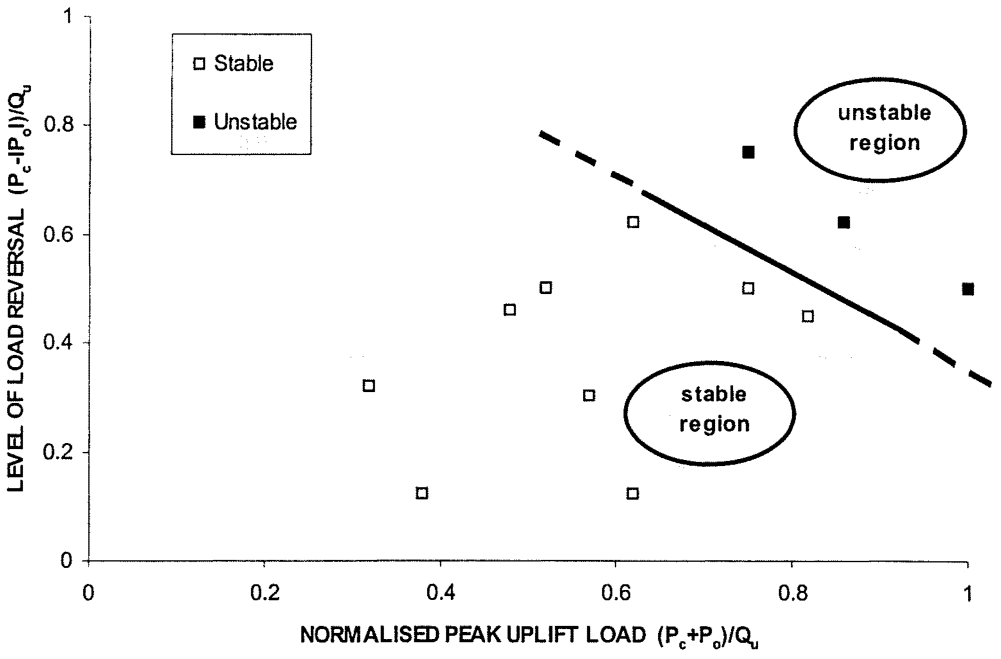

Figure 5.3 – Level of Load Reversal versus Total Peak Load for Tests in Uplift Failure Region

5.2 SOIL/SHAFT SYSTEM BEHAVIOUR

Having quantified the loads that cause instability of the model drilled shafts, the next step is to identify the mechanisms that cause that instability. A model may then be developed that incorporates the failure mechanisms and qualitatively describes the failure of the drilled shaft under cyclic axial loading.

In order to develop a conceptual model for the uplift failure of drilled shaft foundations, it is necessary to first describe those aspects of soil behaviour that are relevant to the soil/shaft system. The following sections describe those relevant aspects, then group them together to form a conceptual system model. Note that the focus of this work is on uplift failure, so the component of strength offered by the tip of the shaft has been largely ignored in the following analysis.

5.2.1 Soil Shearing Zone

Beech and Kulhawy (1987) reasoned that when a drilled shaft foundation fails in uplift it does so, not at the soil/shaft interface, but in the soil mass itself. Inspection of the failure surface shows that a shear zone develops in the soil grains adjacent to the shaft and that most of the shear strain occurs in this zone.

Shear zone formation has been identified in simple shear tests performed by Uesugi et al. (1986). In these tests, concrete surfaces of various roughness were tested against sands of different grain size and density. The results show that as the roughness of the concrete increases, so the failure surface moves away from the sand/concrete interface and into the sand layer itself. Measurements of the peak angle of friction confirm that the failure surface develops within the sand, since the peak angle of friction was found to be equal to that of the sand mass, rather than a reduced interface angle associated with sand and concrete.

Uesugi et al. used enlarged photographs of their specimens to observe the formation of the shear zone during each test. Figure 5.4(a) shows the variation in particle displacement during a typical monotonic shearing test. The unfilled circles show the position of individual soil particles before any load was applied and the filled circles show the corresponding particles after the interface had been sheared by a distance of 16 mm. This distance is indicated by position C in the diagram. Positions A and B are those corresponding to the displacement at peak load and the displacement at initial steady state response (see Figure 5.4(b)).

It is clear from Figure 5.4(a) that a shear zone is formed in the particles adjacent to the interface and that failure occurs within this region. Beyond the failure point, the movement of the particles within the shear zone tends to become random while the movement of those outside the shear zone tends to become normal to the shearing surface. The normal displacements illustrated in Figure 5.4(a) show that dilation is occurring in the shear zone.

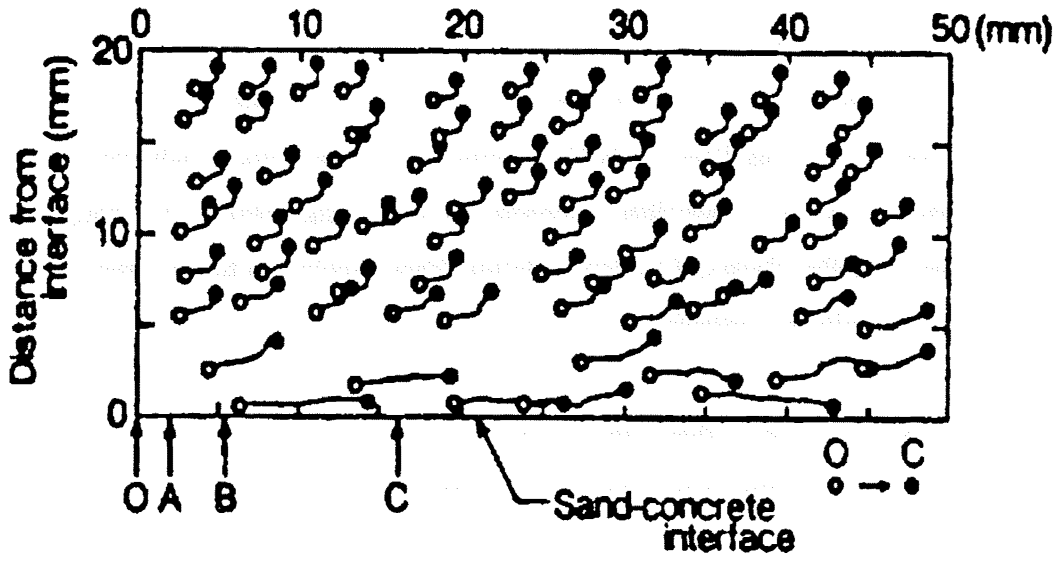

Figure 5.4 (a) – Particle Displacement Near a Rough Sand-Concrete Interface under Monotonic Loading (from Uesugi et al. (1990))

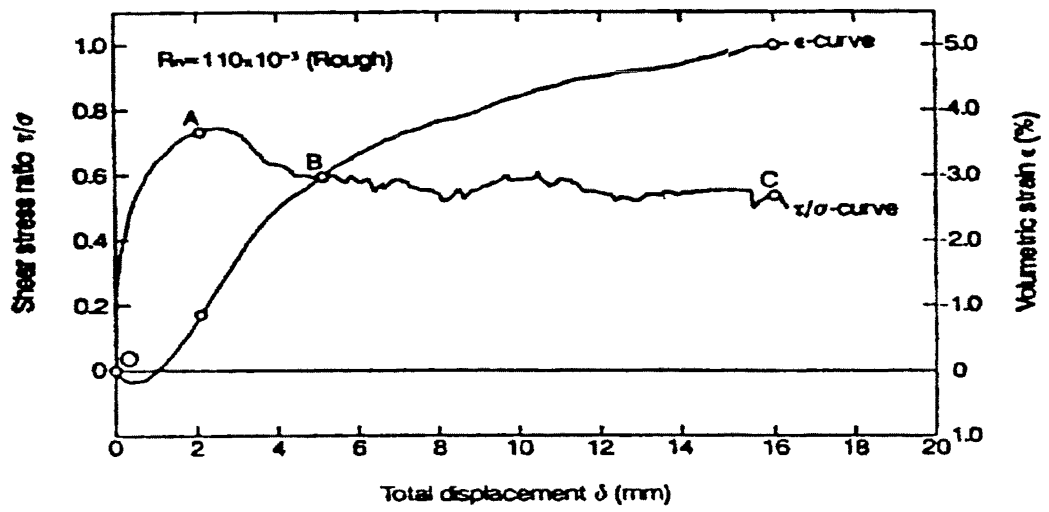

Figure 5.4 (b) – Monotonic Loading Trace of the Particle displacement near a rough sand-concrete interface under monotonic loading (from Uesugi et al. (1990))

Similar materials were used for the Uesugi tests and the present study, so it is likely that the failure surfaces were similar also. The rough sand-concrete interface that was

tested by Uesugi was inherently tested in the present tests because the drilled shafts were cast in-situ. By casting in this manner, the sand around the shaft acts as a mould for the wet concrete so when the concrete sets it has a roughness similar to the surrounding sand. The roughness is further increased by sand grains adhering to the concrete surface as it sets. Therefore, according to the Uesugi results, the roughness created around a drilled shaft indicates that failure should occur in the soil mass itself, rather than at the soil/shaft interface.

Further indication of a soil shear zone is given by the relative density of the soil deposits. Uesugi found that when the relative density of the sand was reduced to approximately 50 percent, then shear failure would take place within the sand, even at low roughness. The present tests were performed at an average relative density of 30 percent so this indicates that shaft failure should occur in the sand mass itself, regardless of the roughness of the model drilled shaft.

5.2.2 Dilation

The Uesugi results show that soil dilation occurs during shearing tests. The dilation is shown in Figure 5.4(b) by an increase in sample volume as the soil is sheared. Dilation occurs as the soil particles attempt to slide past each other along the developing failure plane. In order for the soil particles to slide past each other, they must slide and roll up and over each other. Their upward movement increases the overall volume of the soil sample as they compel the rest of the sample to move in a direction perpendicular to the plane of shearing. ie. the sample dilates under the shearing action.

Further to the overall volume change, Uesugi also observed that the increase in volume generally occurred in the shear zone. The increase was due to a decrease in shear zone density after failure, with the density of the soil outside the shear zone changing little during the test.

The dilation seen in the Uesugi tests has been observed in small-size pile tests performed by Turner and Kulhawy (1988). These tests show an increase in pile strength during uplift loading and it was noted that "the primary cause is an increase in the horizontal stress as the filter sand undergoes dilation when sheared during uplift loading".

The effects of soil dilation are also noted in full-scale pile tests performed by Lehane et al. (1993). Lehane found that "at peak shear resistance the radial effective stress is (approx) 1.4 times its stationary equilibrium value". Such an increase in radial effective stress is due to dilation and the associated increase in soil volume.

The observations of Turner and Lehane highlight an important difference between dilation during simple shear tests and dilation during actual pile tests. In simple shear tests the normal stress is kept constant and dilation is allowed to occur freely. However, in pile tests any dilation is resisted by an increase in horizontal soil stress, which in turn increases the peak load required to shear the soil.

5.2.3 Hoop Stress

The stress at a point, within a soil mass, is commonly stated in terms of cartesian coordinates x, y and z. It may just as easily be stated in terms of cylindrical coordinates r, θ and z, as shown in Figure 5.5. A cylindrical coordinate system is used in the following section to explain the development of hoop stresses around a drilled shaft during cyclic axial loading.

Hoop stress is the component of stress that acts tangentially about a point. It is denoted in Figure 5.5 as σ_θ. For an undisturbed soil sample, the hoop stress in a horizontal plane is equivalent to the horizontal soil stress, σ_h.

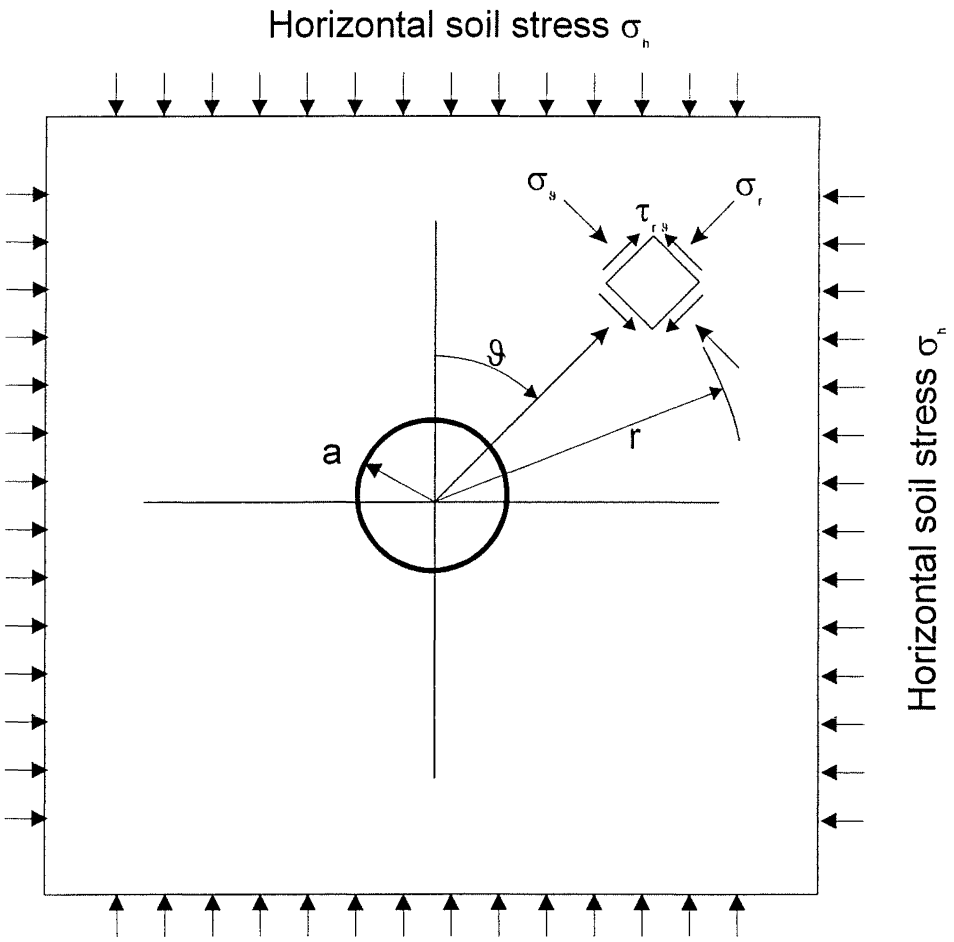

Figure 5.5 – Plan View of the Stresses Surrounding a Vertical Circular Hole in a Soil Mass

If a disturbance is created at a point in the soil mass then that disturbance will act as a stress concentration and alter the stress field within the soil mass. Let the disturbance be a vertical hole of radius a, as shown in Figure 5.5. Terzaghi (1943) found the elastic solutions for the soil stresses around the vertical hole to be:

$$\sigma_r = \sigma_h(1 - a^2/r^2) \tag{5.6}$$

$$\sigma_\theta = \sigma_h(1 + a^2/r^2) \tag{5.7}$$

$$\tau_{r\theta} = 0 \tag{5.8}$$

where σ_r is the radial stress, σ_θ is the tangential or hoop stress, $\tau_{r\theta}$ is the shear stress in the radial plane and σ_h is the horizontal shear stress far from the hole.

The boundary conditions around the unsupported vertical hole dictate that the radial stress σ_r at the edge of the hole must be zero because the hole is unsupported, and the shear stress must be zero at all points in a horizontal plane because the surrounding or "far-field" stress is symmetric at all points in a horizontal plane. The first boundary condition is satisfied by equation 5.6, where $\sigma_r = 0$ when $r = a$. The second boundary condition is satisfied by equation 5.8, where $\tau_{r\theta}$ is zero everywhere. Equation 5.7. however, shows that the tangential stress σ_θ has altered in order to maintain equilibrium. The equation shows that $\sigma_\theta = 2\sigma_h$ at the edge of the hole (when $r = a$) so hoop stresses have been developed in order to maintain equilibrium of the hole.

The development of hoop stresses around a hole can be visualised as an arching action between the soil particles. As the hole is drilled and the drilled material removed, the soil particles adjacent to the hole are able to relax inward. As they relax they simultaneously bear upon, yet support one another, which creates a circular arch or hoop around the hole. Eventually the hole becomes self-supporting and the radial stress within the hole goes to zero.

Results from these tests indicate that hoop stresses may be developed around the drilled shaft during cyclic axial loading. The results show that the radial soil stress undergoes a marked reduction during the downward part of the loading cycle. The actual reduced value is not known because it was not possible to record the absolute values of radial stress during the tests – only changes in radial stress could be recorded. However, similar measurements were taken by Turner and Kulhawy (1987) and their measurements did have a zero reading. Radial soil stress measurements taken from their test S4 are shown in Figure 5.6 and they show that the radial stress at the soil/shaft interface approaches zero during part of the loading cycle. It is likely, therefore, that hoop stresses are developed in order to maintain equilibrium of the system.

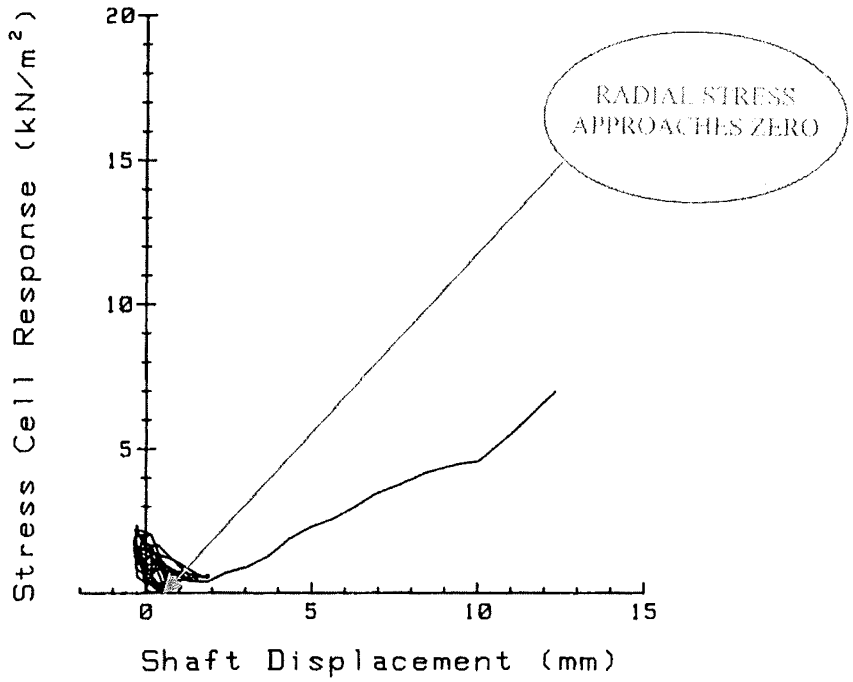

Figure 5.6(a) – Radial Soil Stress measurements from Turner & Kulhawy Test S4 (Depth of Stress Cell = 254 mm)

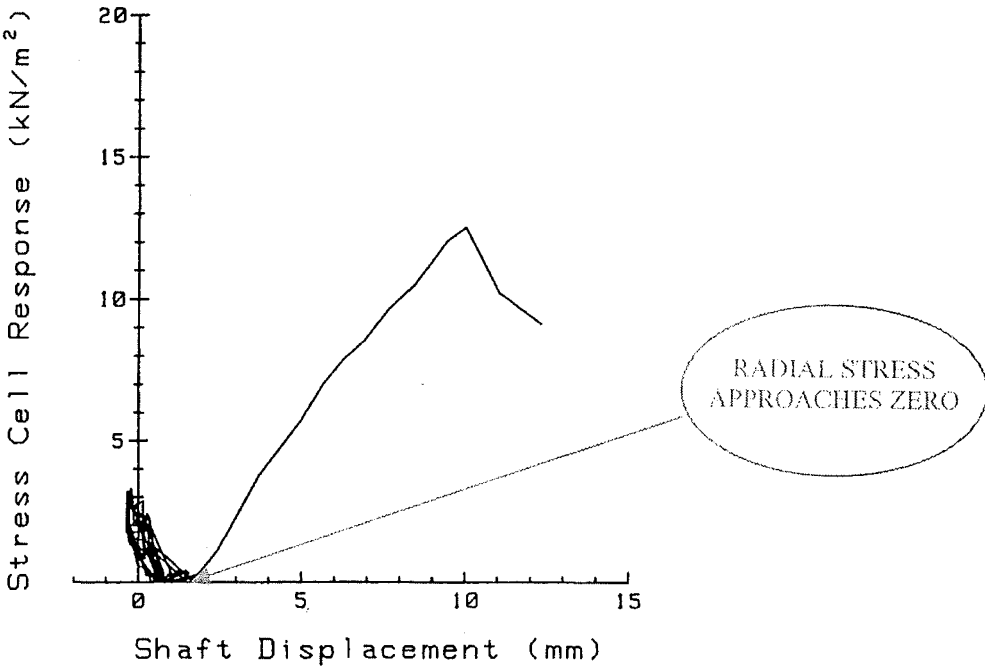

Figure 5.6(b) – Radial Soil Stress measurements from Turner & Kulhawy Test S4 (Depth of Stress Cell = 381 mm)

5.3 SOIL/SHAFT SYSTEM MODEL

Having described the relevant patterns of behaviour around the drilled shaft, a conceptual model is next constructed that describes the behaviour of a drilled shaft under cyclic axial loading. It must be emphasised that this model is somewhat speculative. It is based upon the observations of these and other cyclic axial load tests and no rigorous attempt has been made to verify it, experimentally or otherwise.

The model consists primarily of a dilating shear zone that forms around the shaft during cyclic loading. The model is shown in Figure 5.7. Inside the dilating shear zone, the drilled shaft cycles as a rigid surface with a roughness that is similar to that of the soil. Outside the dilating shear zone, the soil mass reacts elastically to the applied shear and normal loads and may become partially self-supporting if the dilating shear zone contracts sufficiently.

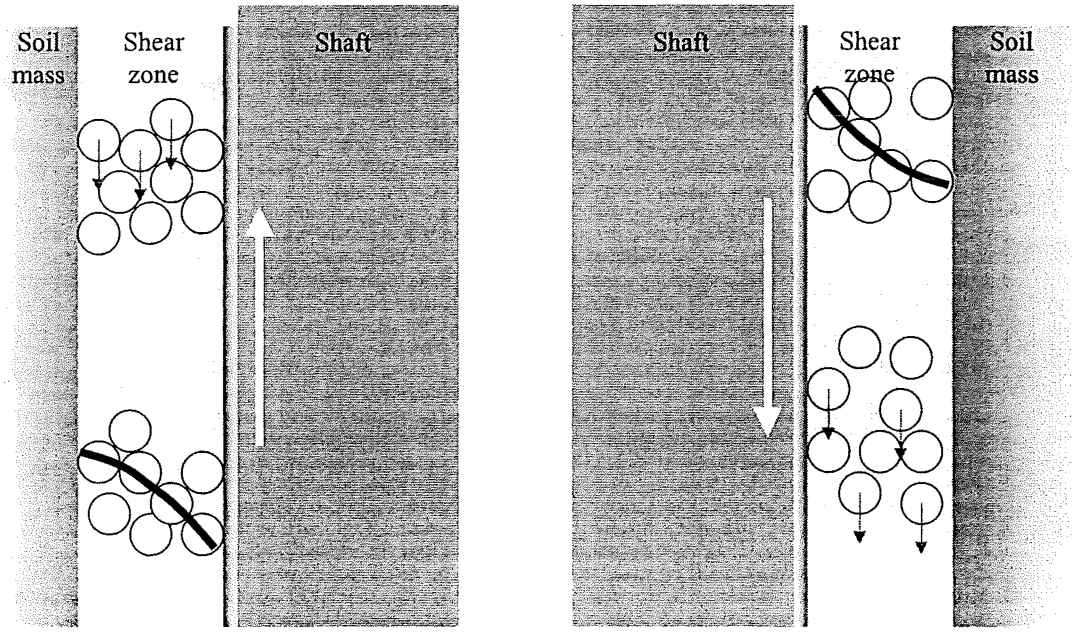

(a) Upward Displacement (b) Downward Displacement

Figure 5.7 – Soil/Shaft System Model

The behaviour of the model is best explained by proceeding through a typical loading cycle. Figure 5.8(a) shows the load/displacement trace from the fifth cycle of loading in Test 020. The load has been cycling at up to approximately 88 percent of the static uplift capacity and the response is stable at this point. Figure 5.8(b) shows the change in horizontal soil stress, the load and the displacement plotted versus time.

The change in soil stress was measured by a transducer buried at a depth of 920 mm and at a radial distance of 20 mm from the surface of the shaft. A true zero reading could not be taken before the transducer was buried so the trace only shows the soil stress relative to that at the start of the test. The estimated horizontal soil stress at this depth, before loading and assuming a K_0 of 0.5, is equal to 7.0 kPa.

The following sections outline the relevant observations from each part of the loading cycle then discuss those observations in terms of the conceptual shear zone model. Indicators A-F refer to those in Figures 5.8(a) and 5.8(b).

A – B

Load/Disp: The load is increasing in uplift and the shaft is displacing upwards. Figure 5.8(a) shows that the stiffness is high initially then reduces shortly before B.

Soil Stress: The stress is increasing and reaches a peak at B.

Model Behaviour: The soil around the shaft is dilating as it is sheared. The dilating soil increases in volume, causing the radial soil stress to increase.

B – C

Load/Disp: The load continues to increase and the rate of displacement increases. Figure 5.8(a) shows that the stiffness is reduced in this section. Both load and displacement peak at point C.

Soil Stress: The soil stress initially reduces then maintains an approximately constant value.

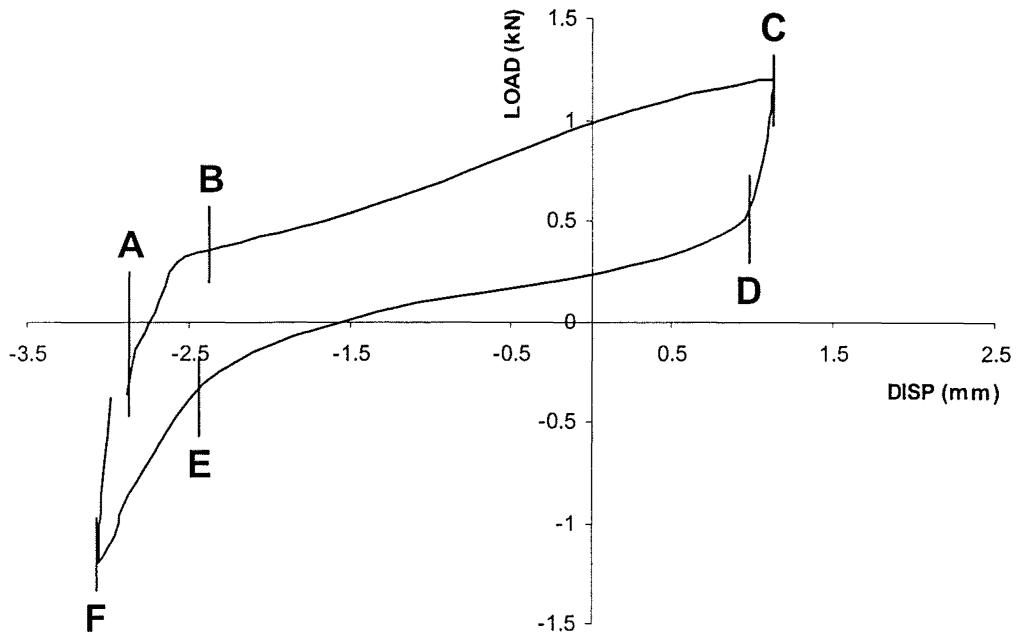

(a) Load versus Displacement

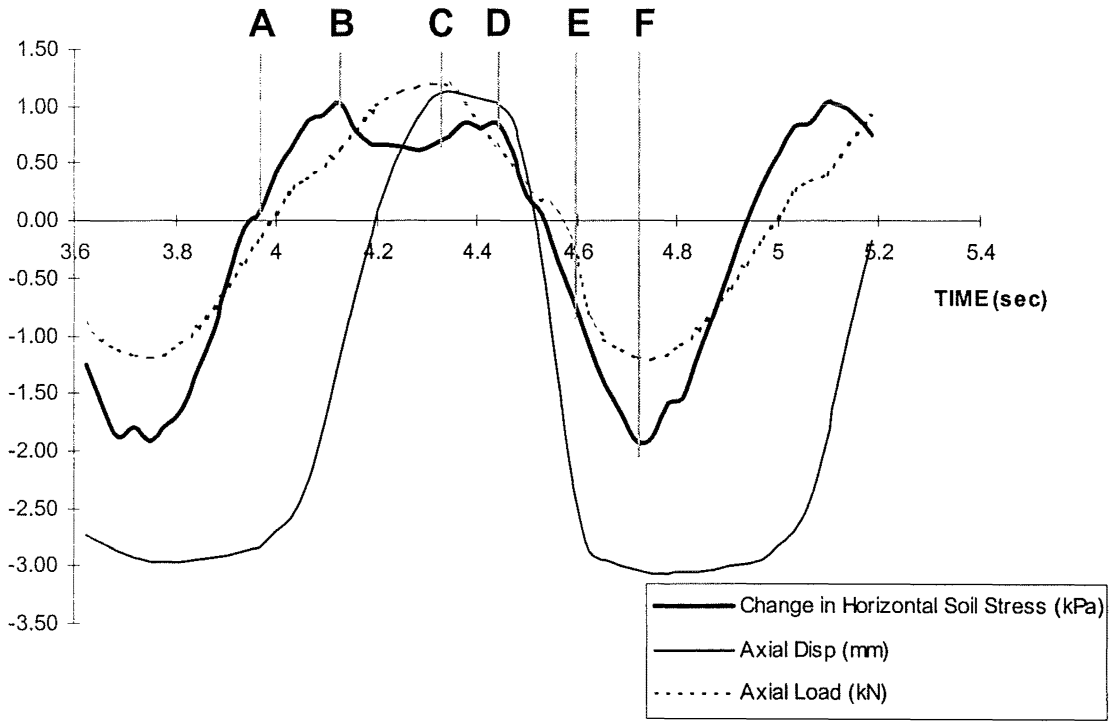

(b) – Soil Stress, Displacement and Load versus Time

Figure 5.8 – Results from Fifth Cycle of Cyclic Axial Load Test 020

Model Behaviour: The soil has exceeded peak dilation and fails along a developing shear-zone failure surface. Continuing shear brings a decrease in shear-zone volume, with a corresponding decrease in radial soil stress. Eventually, the shear-zone soil begins to shear at constant volume and, in doing so, it maintains a constant radial stress on the surrounding soil mass.

C – D

Load/Disp: The uplift load is reduced and there is a small downward displacement. The apparent stiffness is high.

Soil Stress: The radial stress increases again, reaching a peak at point D.

Model Behaviour: The displacement reversal causes the shear-zone material to interlock and the soil begins to dilate again as the direction of shear displacement is reversed. The dilation is shown as a second increase in soil stress.

D – E

Load/Disp: The load continues to decrease and becomes compressive while the rate of downward displacement increases markedly. The apparent stiffness is low.

Soil Stress: The radial stress decreases steadily.

Model Behaviour: The soil exceeds peak dilation and again fails along a developing shear-zone failure surface. Beyond peak dilation, the volume of the shear-zone material reduces and the horizontal soil stress reduces accordingly. However, instead of the soil stress reaching an approximately constant level as it did during upward displacement, rather it continues to decrease with increasing downward displacement. The difference between upward and downward displacement may be explained by referring to Figure 5.7. When the shaft is displacing upward, dilation occurs and the shear-zone particles interlock. They tend to form arches between the shaft and the soil mass, as shown in

Figure 5.7(a). Beyond peak dilation, these arches break down but the self-weight of the particles works to constantly rebuild further arches. The particles tend to lodge themselves between the shaft and the soil mass. They push outward on the soil mass and inward on the shaft and so maintain a moderate level of radial soil stress.

When the shaft begins to displace downward, the soil response is initially similar to that of upward displacement. The shear zone and the soil mass dilate as they shear, and the stiffness is similar to that of upward displacement. The response changes, however, when peak dilation is exceeded on the downward cycle, as shown in Figure 5.7(b). Beyond peak dilation, the soil-particle arches break down as before but now there is a lower tendency for them to re-build. The reason for the instability is that the self-weight of the shear-zone particles now acts in the same direction as the displacement of the shaft. Any displacement of the shaft now serves to extend and collapse the arches rather than compress and support them.

The soil-particle arches continue to collapse as further shaft displacement occurs. The collapsing shear zone reduces in volume, thus reducing the radial stress on both the shaft and the soil mass. With a reduced radial stress on the soil mass, it is able to relax inwards so **hoop stresses may develop**. As the soil mass relaxes inward it begins to support itself and, in doing so, it reduces the confinement of the shear zone and shaft. The shear-zone material is then able to shear more easily so the shear-zone material and the shaft tend to collapse and fall into the "hole" created by the partially self-supporting soil mass.

E - F

Load/Disp: The load is increasing in compression and there is a reduction in the rate of downward displacement. The apparent stiffness slowly increases. The load and the displacement reach a minimum at point F.

Soil Stress: The radial stress continues to decrease until reaching a minimum at the corresponding minimum load and displacement (point F).

Model Behaviour: The radial soil stress continues to decrease (and hoop stresses presumably continue to increase) until the shaft reaches maximum downward displacement at point F. Figure 5.8(a) shows, however, that the system stiffens up considerably when the load becomes compressive. The likely reason for this stiffness increase is that the load can now be resisted by the tip of the shaft as well as the side-walls. Some of the axial load is transferred from a shear stress along the side-wall to a compressive stress beneath the tip of the shaft. Further evidence of the transfer of load may be interpreted from the displacement trace shortly after point E. At this point there is a distinct change in the slope of the displacement trace as the load increases in compression. The change in slope is probably due to the extra resistance offered by the tip and it may also be due to the compressive resistance beneath the tip being stiffer than the post-peak-dilation shear resistance offered by the side-walls.

The load cycle ends with a displacement reversal at peak compressive load and then unloading in compression. The load cycle has had a permanent effect on the soil/shaft system because at least some of the soil around the drilled shaft has undergone inelastic shear deformation during the cycle. The ability of the soil/shaft system to withstand further cycles of load will now depend on the cumulative effect of the previous load cycles. The following section uses the conceptual shear zone model to illustrate how the uplift stability of the drilled shaft is affected by the cyclic axial loading.

5.4 UPLIFT FAILURE DURING CYCLIC AXIAL LOADING

As shown in Chapter 1, a drilled shaft foundation will fail in uplift when the total uplift load exceeds the capacity of the shaft. The Poulos Cyclic Stability Diagram and the Cyclic Stability Diagram from these tests have both shown that the uplift capacity of the shaft also depends on the nature of the applied load. The diagrams show that the uplift capacity may decrease if the applied load is cyclic. The conceptual shear-zone model can be used to offer a possible explanation of the reduction in uplift capacity under cyclic axial loading.

Figure 5.9 shows the response from a typical unstable cyclic load test. In this test, the drilled shaft failed in uplift at a load amplitude of 57 percent of the equivalent static capacity.

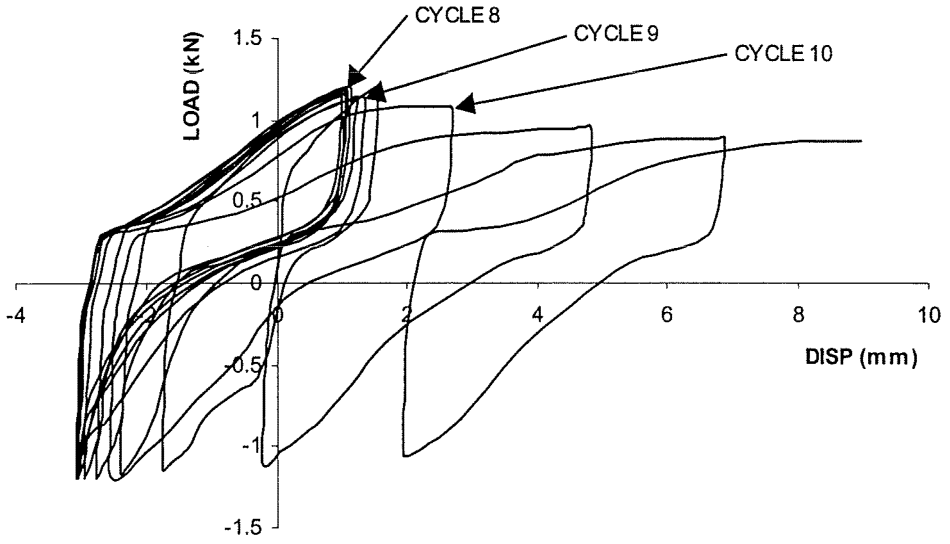

Figure 5.9 – Load versus Displacement for Cyclic Axial Load Test 020

Figure 5.9 shows that the shaft appears to be stable during the first eight cycles of loading. During these cycles the shaft quickly settles into a steady load/displacement response with elastic and inelastic displacements occurring about a reasonably steady mean displacement. However, in the ninth cycle the load does not reach the intended magnitude of 1.2 kN. Instead, the shaft undergoes a greater upward displacement as the load approaches 1.2 kN. The load then decreases and the shaft returns to the same

downward displacement as previous cycles. Further cycles of load bring greater reductions in peak load and increases in upward displacement. The overall upward displacements quickly become excessive and the shaft fails in uplift.

Failure in uplift can be explained with the conceptual shear zone model. The behaviour is best explained by proceeding through the loading cycles leading up to failure. Figure 5.10 shows the change in horizontal soil stress and the axial shaft displacement leading up to failure. The axial load has been omitted to simplify the diagram but it is sinusoidal with a 1.2 kN amplitude and a zero mean. Peak uplift load occurs at peak upward displacement.

The following sections outline the relevant observations from each of the load cycles then discuss those observations in terms of the conceptual shear zone model.

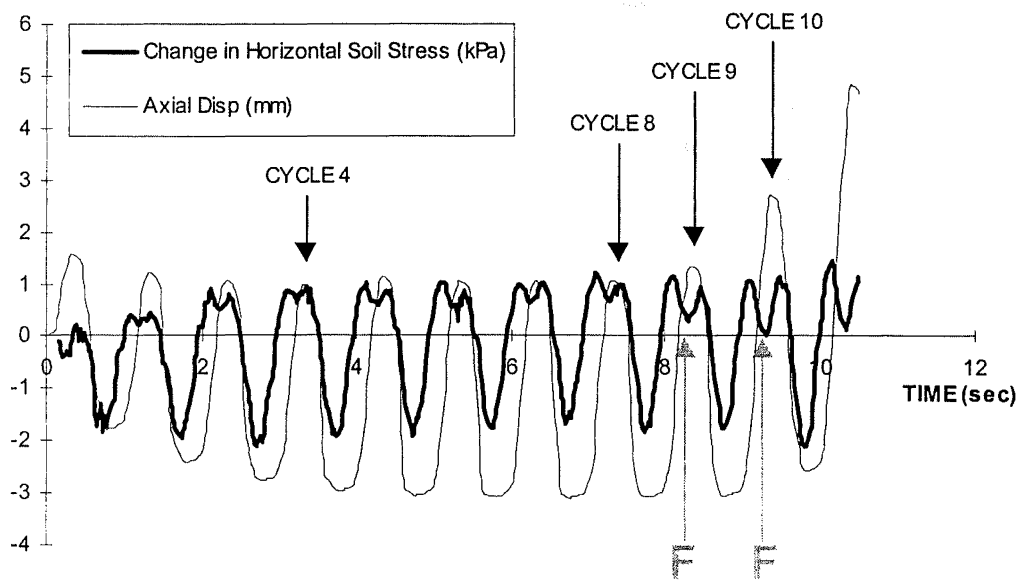

Figure 5.10 – Soil Stress and Axial Displacement versus Time for Cyclic Axial Load Test 020

CYCLES 1 – 4

Disp: The shaft cycles about a decreasing mean displacement as it settles into the soil mass.

Soil Stress The stress response is similar to that discussed in Section 5.3 with peaks occurring at the displacement reversals and a notable stress reduction or trough after the second peak. The magnitudes of the two peaks increase with increasing numbers of cycles while the magnitude of the second trough appears to reach a fairly constant value from the first cycle.

Model Behaviour: The behaviour is similar to that discussed in Section 5.3 with the shear zone material dilating at each displacement reversal then contracting after peak dilation on each half cycle. The magnitude of the downward stress reduction indicates that hoop stresses may be developing from the first cycle. These cycles are notable for the small stress peaks during dilation of the shear zone. This indicates that the shear zone may be able to shear with little increase in volume and/or the surrounding soil mass is compacting, allowing the zone to shear with little increase in normal stress. Increasing numbers of cycles bring greater dilation peaks and smaller peak-to-peak displacements as the soil/shaft system stiffens up, reaching a quasi steady state by the fourth cycle.

The overall downwards movement of the shaft is probably due to compaction of the soil beneath the tip of the shaft since the tip resistance is mobilised from the very first cycle. This is shown by the large reduction in horizontal soil stress seen from the very first cycle.

CYCLES 5 – 8

Disp: The shaft cycles about a steady mean displacement.

Soil Stress The stress response is generally steady-state, with peaks occurring at each of the displacement reversals and a trough occurring during the downward part of each cycle.

Model Behaviour: The soil/shaft system appears to have reached a steady state response. The maximum and minimum stresses do not appear to be changing as the shear zone dilates and contracts under elastic and inelastic shearing. The minimum radial stresses are not changing significantly so the soil mass also appears to have reached a steady state.

CYCLES 9 – 11

Disp: The maximum upward displacement increases in the ninth cycle. Large increases in upward displacement occur in the tenth and subsequent cycles and the shaft fails in uplift.

Soil Stress The soil stress is much the same as previous cycles except after the first peak during upward displacement. At this point (indicated as point F in Figure 5.10) the stress reduction increases with each successive cycle.

Model Behaviour: The drilled shaft fails in uplift during these cycles because **the surrounding soil mass no longer offers the necessary confinement after peak dilation.** Each cycle of loading causes the soil mass to displace radially outward during dilation and to displace radially inward during contraction. As is the case with all soils, these soil displacements are not completely elastic so the soil mass does not return to the same point when it contracts. Contractions are further resisted by hoop stresses that develop within the soil mass.

As upward displacement begins, the shear-zone material dilates and shears while under the confining stress of the soil mass. Beyond peak dilation, the shear-zone material contracts and the soil mass contracts around it. However, each time this occurs the soil mass stiffens up and contracts by a smaller amount, thus reducing the confinement of the shear zone and the capacity of the drilled shaft. If the number of load cycles is sufficient then the capacity of the drilled shaft will be reduced to that of the applied load and the shaft will fail in uplift.

Uplift failure through the loss of confinement is underlined when the unstable test results are compared with those from a stable test. Figures 5.11a and 5.11b compare the displacement traces and soil stress traces respectively from unstable test 020 and stable test 025. Test 020 was performed with a zero mean axial load and a cyclic axial load amplitude of 1.2 kN while Test 025 was performed with a mean axial load of 0.2 kN in compression and a cyclic axial load amplitude of 1.2 kN.

The first four cycles of unstable Test 020 are shown in Figure 5.11a and show an increasing peak-to-peak displacement and an overall downward displacement for the drilled shaft. The peak-to-peak and overall displacements remain fairly constant for cycles five to eight then from cycle nine onwards the peak-to-peak displacement increases rapidly and the shaft fails in uplift. By comparison, stable Test 025 shows a decreasing peak-to-peak displacement and an overall downward displacement from the first cycle onwards.

Figure 5.11b shows the corresponding changes in horizontal soil stress. The first four cycles of loading show an increase in the average stress for Test 020 but little change in average stress for Test 025. The different average stresses may arise from the different initial conditions around the stress transducer. They may also arise from the different mean loads on the drilled shaft. Test 025 has a lower mean load and therefore a lower peak uplift load so the dilation levels will be lower and the mean horizontal stress would be expected to be lower. Lower minimum stresses during the downward displacement of Test 025 may also be due to the different mean load. Test 025, with its lower mean load, will have greater compressive loads. These loads are transferred away from the sidewall and into the tip of the shaft so the horizontal stress will be expected to be lower during peak compressive load.

From cycle four to cycle eight the unstable test shows an approximately constant response. There is a small reduction in soil stress after peak upwards dilation and a large reduction in soil stress after peak downwards dilation. The apparent stability breaks down, however, in cycle nine when the stress reductions after upwards dilation begin to increase and the shaft fails in uplift. By comparison, the stable test also

shows stress reductions after peak dilation in each direction but the reductions and the stress response as a whole, remain approximately constant throughout the test.

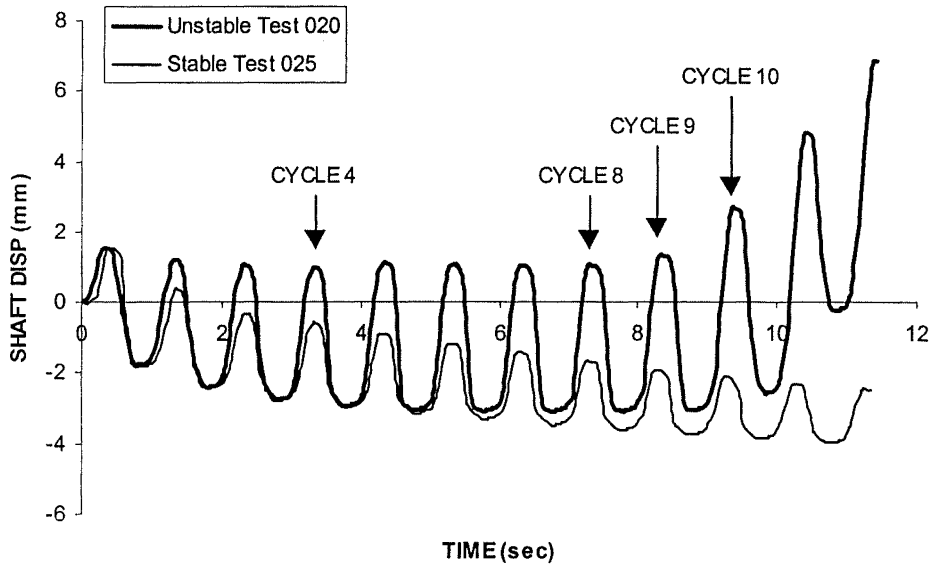

Figure 5.11a – Shaft Displacement versus Time for Cyclic Axial Load Tests 020 & 025

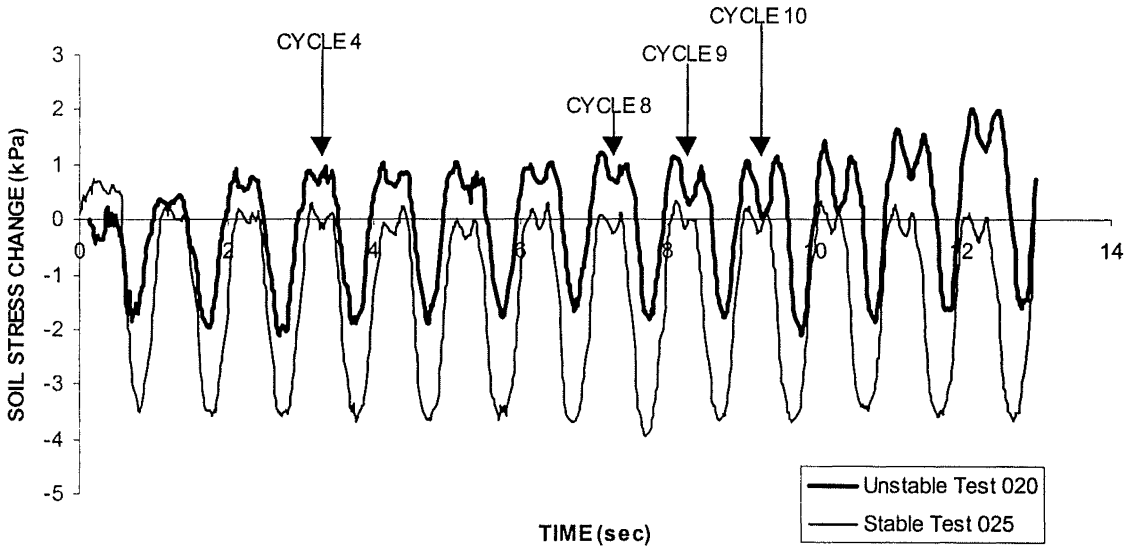

Figure 5.11b – Change in Soil Stress versus Time for Cyclic Axial Load Tests 020 & 025

The comparisons shown in Figures 5.11a &511b underline the difference between stability and instability. They show that uplift stability depends on adequate confinement during uplift displacement. In terms of the conceptual shear zone model, uplift stability is retained if the shear zone and the drilled shaft continue to be sufficiently confined by the surrounding soil mass. If the soil mass stiffens up, and no longer adequately confines the contracting shear zone after dilation, then the shear zone will shear more readily and the drilled shaft will fail in uplift.

5.5 THE EFFECTS OF SOIL DENSITY

Turner et al. (1990) found that a drilled shaft foundation is more susceptible to failure under cyclic axial loading if the soil density is increased. To check this finding a set of cyclic axial load tests were performed on shafts embedded in a denser soil stratum.

The soil deposits were prepared by air pluviation, as they were in the previous tests, but they were then densified by shaking. This was achieved by preparing the soil deposits in a special laminated tank that was able to deflect in shear. The tank was designed for the second series of tests and will be discussed in detail in Chapter 6. To compact the soil deposits, the tank was attached to a shaking table and shaken at +/- 45 mm for twenty seconds at 1 Hz.

The first tests conducted in the compacted soil deposits were monotonic uplift tests. These tests were conducted to establish the static uplift capacity, Q_{ud}, after densification. Results from the monotonic tests show that the static uplift capacity increased as a function of the shaking amplitude. The relationship is given in Chapter 7 and shows that the uplift capacity for these tests had increased from 1.28 kN to 3.89 kN. The relative density of the soil deposit had also increased from 31 percent to 68 percent. The monotonic uplift test (Test 316) corresponding to this level of shaking is given in Figure 5.12.

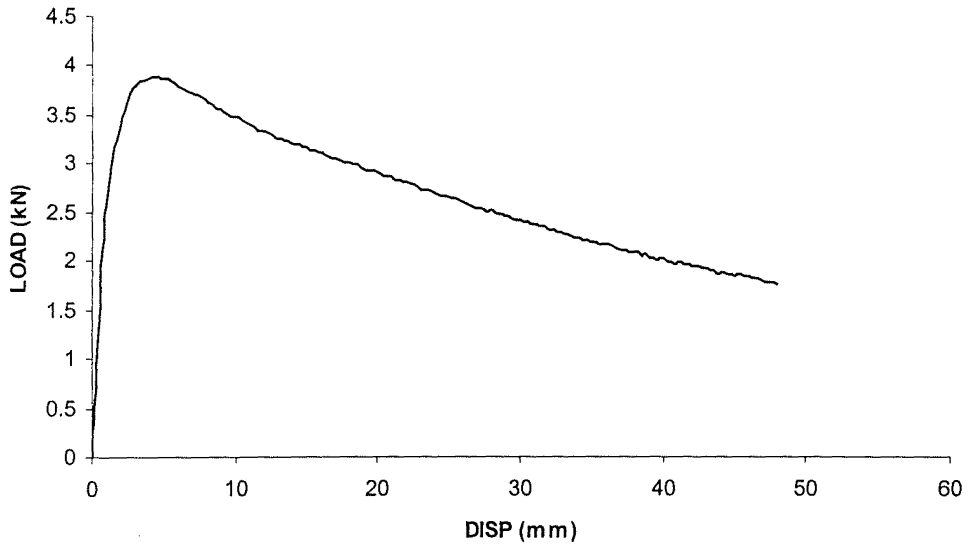

Figure 5.12 – Load versus Displacement for Monotonic Uplift Test 316

A series of cyclic axial load tests were then performed on shafts in the densified soil deposits. All the tests were performed at zero mean load, as this had been found earlier to be the worst case load configuration for cyclic axial loading. The results of these tests are shown in Table 5.1.

Table 5.1 – Cyclic Axial Load Tests in a Compacted Soil Deposit

Test No.	Mean Load ($\% Q_{ud}$)	Cyclic Load (kN)	Cyclic Load ($\%Q_{ud}$)	Stable/Unstable
317c	0	2.31	59	Failure
317d	0	1.65	42	Failure
318c	0	0.99	25	3.73
318d	0	1.28	33	0.52e

The first test was performed at 2.31 kN or 59 percent of the new static capacity, Q_{ud}. The second test was performed at 1.65 kN or 42 percent of Q_{ud}. Both shafts failed in the first few cycles of loading.

The third test was performed at 0.99 kN or 25 percent of Q_{ud} and the shaft remained stable during the test. A further test was performed at 1.28 kN or 33 percent of Q_{td} and the shaft was unstable. Interpolation of these results showed that cyclic instability now occurred at 1.1 kN or 28 percent of the equivalent static capacity, Q_{ud}, when the relative density was 68 percent. This compares with instability occurring at 67 percent of the equivalent static capacity when the relative density was 31 percent The test results therefore concurred with Turner et al. who had found that shafts in denser soils were more susceptible to cyclic degradation.

The susceptibility of denser soils to cyclic degradation is readily explained with the shear zone model. If the surrounding soil mass is loose, then it will more readily compress under the radial stress increase associated with shear zone dilation. The drilled shaft will therefore have a lower monotonic uplift capacity but it will be more stable under cyclic loading because the soil mass is less able to become self-supporting through the development of hoop stresses. The reason for this is that a lower density soil mass will have to contract further radially inwards before the soil particles begin to form arches and develop hoop stresses. If hoop stresses do not develop, then a higher confining stress is maintained on the shear zone, lower shear strains are possible and the shaft is less likely to become unstable.

Conversely, a drilled shaft in a dense soil will have a higher monotonic uplift capacity but it will be more susceptible to cyclic degradation. A denser soil mass will require a smaller inward radial displacement before the soil particles begin to form arches and hoop stresses develop. As the hoop stresses develop the confining stress on the shear zone decreases. Greater shear strains are then possible and the drilled shaft is more likely to become unstable.

SUMMARY

Cyclic axial load tests were performed on model drilled shaft foundations in a homogeneous soil mass. In the worst case loading configuration, cyclic axial loading was found to reduce the shaft uplift capacity to 67 percent of the equivalent static capacity.

The results from all the tests have been conveniently presented in a Cyclic Stability Diagram, with the cyclic axial load plotted against the mean axial load. The Cyclic Stability Diagram illustrates that the worst case loading occurs at zero mean load, where the shaft may fail in uplift at a load of only 67 percent of the static uplift capacity. At loads either side of zero mean load the shaft may sustain greater cyclic load amplitudes.

Analysis of the tests shows that the Level of Load Reversal (LLR) may govern the stability of the drilled shaft during cyclic axial loading. The LLR is the minimum amount by which the load magnitude is reversed. LLR relationships have been determined for all combinations of mean and cyclic load.

A conceptual soil/shaft system model has been developed from these and other test results. It describes a dilating and contracting shear zone that forms around the shaft. When an axial load is applied to the shaft, the shear-zone soil dilates. In doing so, it increases in volume, thus increasing the radial stress on the surrounding soil mass. The soil mass displaces radially outward under the stress increase then, after peak dilation, the shear zone contracts and the surrounding soil mass contracts around it. The radially inward contraction may develop hoop stresses in the soil mass, thus reducing the confining stress on the shear zone. The shear zone may then shear more easily so the uplift capacity of the drilled shaft is reduced. If the reduction in uplift capacity per cycle is great enough, and the number of degrading load cycles is great enough then the shaft will not be able to withstand further loading and it will fail in uplift.

A series of similar cyclic axial load tests were performed on a drilled shaft in a denser soil. It was found that the cyclic uplift capacity dropped from 67 percent of the

equivalent static capacity to only 28 percent of the equivalent static capacity when the soil relative density was increased from 31 percent to 68 percent. This result agrees with previous research by others, who had found that shafts in denser soils were more susceptible to cyclic degradation. The effect of soil density on cyclic uplift stability is also explained using the shear zone model. Denser soils may be more susceptible to cyclic degradation because the soil mass is more readily able to develop hoop stresses. The surrounding soil mass is already more compact so smaller radial strains may be required for the soil mass to become self-supporting and so reduce the confining stress on the shear zone.

REFERENCES

BEECH, J.F. & KULHAWY, F.H. (1987). "Experimental Study of the Undrained Uplift Behavior of Drilled Shaft Foundations", Report EL-5323, Electric Power Research Inst., Palo Alto. Calif.

CHARLIE, W.A., TURNER, J.P. and KULHAWY, F.H. (1985). "Review of Repeated Axial Load Tests in Deep Foundations," Drilled Piers and Caissons II, Ed. C.N. Baker, Jr. ASCE, New York.

LEHANE, B.M., JARDINE, R.J., BOND, A.J. and FRANK. R. (1993)."Mechanisms of Shaft Friction in Sand from Instrumented Pile Tests," ASCE, Vol. 119, No. 1, January, 1993.

McMANUS, K.J. and KULHAWY, F.H. (1994). "Cyclic Axial Loading of Drilled Shafts in Cohesive Soil" J. Geotech. Engrg., ASCE, Vol. 120, No.9, September, 1994.

POULOS, H.G. and LEE, C.Y. (1988). "Model tests in grouted piles in calcareous sediment," Proc., Int. Conf. in Calcareous Sediments, Perth, Australia, Vol. 1.

POULOS, H.G. (1988). "Cyclic Stability Diagram for Axially Loaded Piles", J. Geotech. Engrg., ASCE, Vol. 114, No.8, August, 1988.

SEED, H.B. and IDRISS, I.M. (1970). "Soil Moduli and Damping Factors for Dynamic Response Analysis," Report No. EERC 70-10, Earthquake Engineering and Research Center, College of Engineering, U of C Berkeley, Dec. 1970.

TERZAGHI, K. (1943). "Theoretical Soil Mechanics," John Wiley and Sons, Inc. New York.

TURNER, J.P. and KULHAWY, F.H. (1987). "Experimental Analysis of Drilled Shaft Foundations Subjected to Repeated Axial Loads under Drained Conditions," Report EL-5325, Electric Power Research Inst., Palo Alto. Calif.

TURNER, J.P. and KULHAWY, F.H. (1990). "Drained Uplift capacity of Drilled Shafts under Repeated Axial Loading," J. Geotech. Engrg., ASCE, Vol. 116, No.3, March, 1990.

UESUGI, M., KISHIDA, H. and UCHIKAWA, Y. (1990). "Friction Between Dry Sand and Concrete under Monotonic and Repeated Loading," Soils and Foundations Vol.30, No.1, 115-128, Mar. 1990.

Chapter Six

CONSTRUCTION OF MODEL DRILLED SHAFTS FOR CYCLIC AXIAL LOAD TESTS IN SHAKING SOIL DEPOSITS.

INTRODUCTION

In order to load test model drilled shafts in a shaking soil deposit, a special laminar tank was designed for use on the University of Canterbury Shaking Table. The tank was designed so that the soil with in it could be used to model the free-field response of a horizontal soil layer during seismic shear loading. To do this, the tank had to fulfil two basic requirements. Firstly, it had to deflect with the soil deposit when they were both shaken and secondly, the deflection of the tank was not to impinge on the preferred deflection of the soil.

This chapter outlines relevant design features from previous tanks, then details the design and construction of the laminar tank used for these tests. Descriptions are also given of the model drilled shafts used for the tests, the methods employed for preparing each soil deposit and drilled shaft, and the instrumentation used to collect data from each test. Finally, a summary is given of the performance of the laminar tank during shaking.

6.1 SHAKING TABLE

The Department of Civil Engineering, at the University of Canterbury, operates a unidirectional, horizontal shaking table. The characteristics of the table are given in Table 6.1. The shaking table is driven by a closed-loop, servo-controlled hydraulic actuator. The system was originally controlled by an MTS model M1000 controller but this was replaced by an MTS model Teststar 2 controller, that was then used for the second stage of the test programme.

Each test was performed under displacement control, with the cyclic table displacements generated by entering the required amplitude, frequency and number of cycles into the PC-based control system.

Table 6.1 – Characteristics of the University of Canterbury Shaking Table

Property	Value
Dimensions	4.0 m x 2.0 m
Maximum Allowable Load	200 kN
Maximum Horizontal Force	200 kN
Maximum acceleration with a mass of 5 tonne	2.7 g
Maximum Speed	1.0 m/s
Maximum Displacement	0.30 m

6.2 TANK CONSTRUCTION

The tank was designed so that it would allow the soil within it to deflect in such a way that it would model the response of a semi-infinite horizontal soil layer under seismic horizontal shear loading. The intension was to create a free-field response to the shear loading, with a minimum of boundary effects imparted on the soil deposit by the actions of the tank. To achieve this, the tank was designed to deflect during shaking, allowing shear strains to occur in the soil deposit as they would in the free field.

6.2.1 Previous Tank Designs

The primary considerations of any tank design are firstly that it should contain the soil and secondly that it should not impinge on the preferred response of the soil during shaking.

The most basic form of shaking table tank has rigid end-walls. This design certainly contains the soil during the test, but it also imposes severe boundary effects on the soil

response. Rigid end-walls reflect the incident shear waves and prevent shear strains within the soil during shaking, so the response is not equivalent to that of the free-field.

To reduce the boundary effects of the end-walls, whilst maintaining a relatively simple tank set-up, Mizuno et al. (1984) constructed a tank with rigid end-walls, but lined the tank with a urethane foam to absorb the incident shear waves. The tank is shown in Figure 6.1. Similar approaches were taken by Finn & Gohl (1992) and Steedman & Maheetharan (1989), whereby the rigid tanks were lined along the end-walls with Styrofoam and Duxseal, respectively. The latter design is shown in Figure 6.2. Each of these designs assists in absorbing the shear waves, but they still restrict the deflection of the soil mass, so do not allow for true free-field soil response.

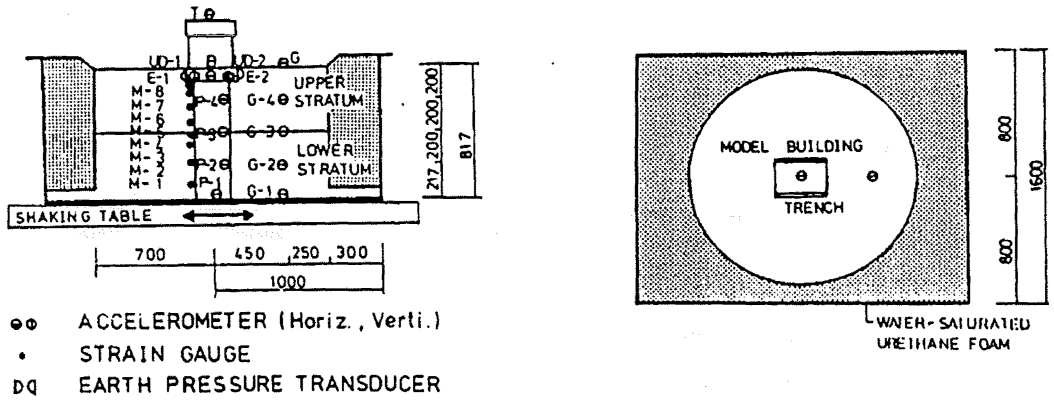

Figure 6.1 – Foam Lined Shaking Table Tank (From Mizuno et al. (1984))

Maruyama (1977) and Iwasaki (1986) overcame the restriction on soil deflection by constructing a tank with hinged end-walls. The walls were hinged at the base so that they could deflect with the soil deposit as it responded to the shaking. The end-walls were also connected to each other with a wire rope so that the soil deposit remained confined during each test.

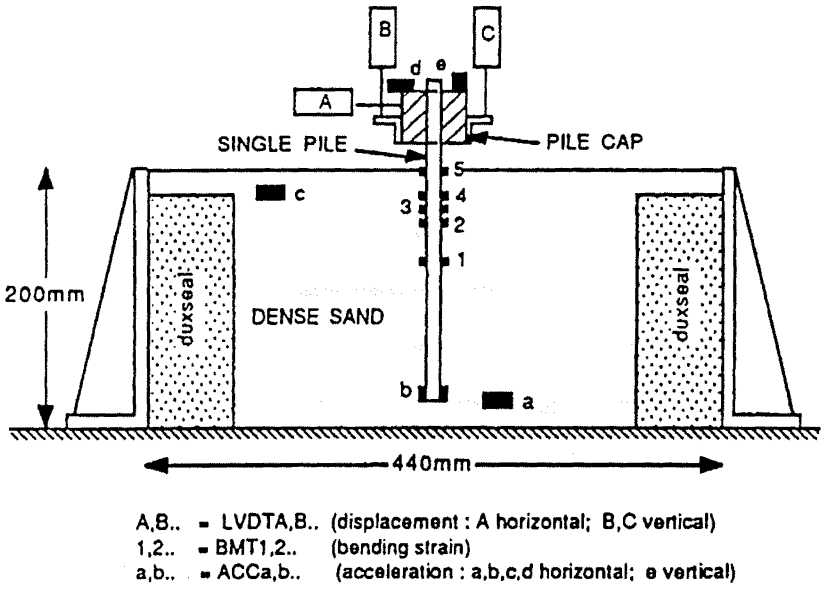

Figure 6.2 – Foam Lined End-walls (From Steedman & Maheetharan (1989))

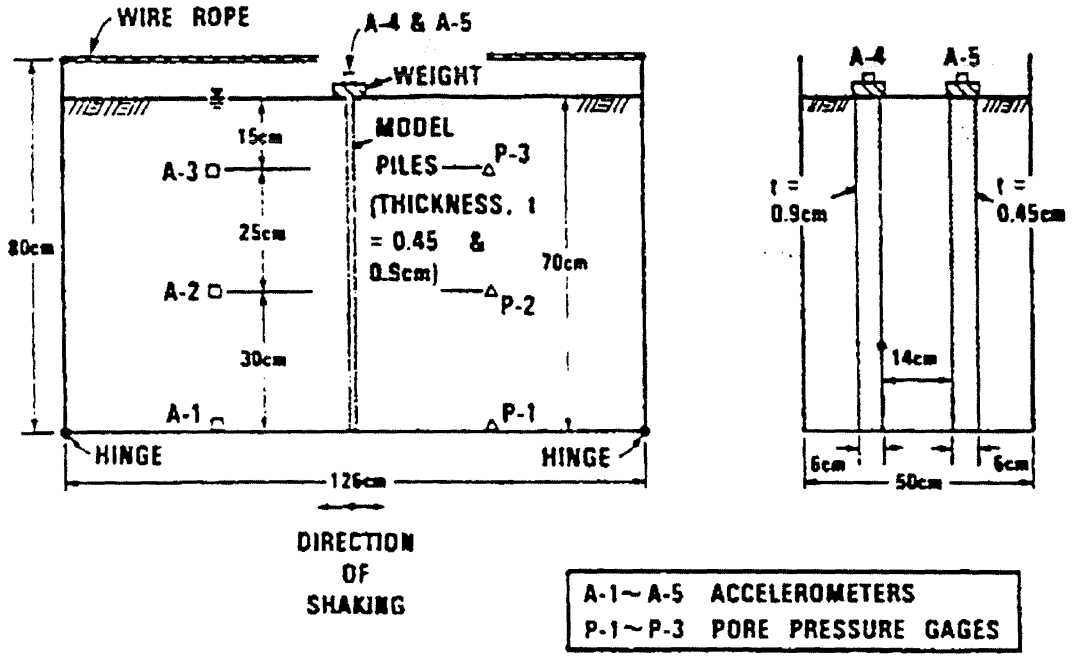

Figure 6.3 – Hinged End-walls (From Maruyama (1977))

The same system was used by Fishman et al. (1995) but was further refined by making the end-walls flexible. Doing so allowed for non-linear shear strains to occur over the soil column. The end-walls were also strain-gauged so that they could act as stress transducers during the shaking table testing.

A different approach has been taken by others, whereby the whole tank moves with the soil mass. In such cases, the tank has been constructed from a stack of laminates that slide over one another and move with the soil column. An example of a laminar tank, by Hushmand et al. (1988), is shown in Figure 6.4. The major problem associated with this type of tank design is that of inter-laminate friction. Hushmand et al. (1988) and Iai (1991) reduced the friction between laminates by fitting steel roller bearings between the laminates of their tanks, while Whitman et al. (1981) reduced the friction between laminates by coating each contact surface with Teflon.

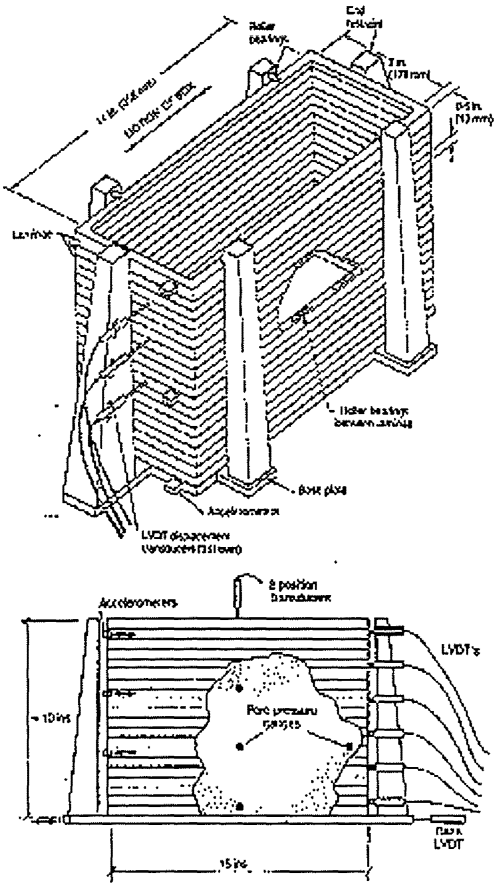

Figure 6.4 – Laminar Tank (From Hushmand et al. (1988))

There are other factors that must be considered when designing a shaking table tank. The shape of the tank and particularly the length-to-depth ratio are important, as are the method of soil confinement and the method of tank support.

The length-to-depth ratio of the tank will affect its response under horizontal shaking. The more slender the tank, the higher are the cantilever bending deformations within the soil column. To reduce these effects and to encourage shear deformations, Hushmand et al. intentionally designed their tank with a length-to-depth ratio of 1.4. Other tanks also had higher length-to-depth ratios, including Fishman et al. with a ratio of 3.5 and Iwasaki with a ratio of 6.3. To further reduce bending and to ensure the laminates stayed together, loads have sometimes been applied to the top of the tank. Whitman et al. placed a cap on the laminates and held it down with spring pressure, while Iai placed a load of 25 kN on the top of the laminates to reduce rocking motion. Such loads, however, must increase the frictional forces between the laminates and therefore affect the response of the soil during shaking. To effectively reduce the confining load while still providing bending resistance when necessary, Hushmand et al. fitted roller bearings to the top of the restraining frame, as shown in Figure 6.4. The bearings were adjusted to apply a small contact force at 1 g but, since the tests were performed in a centrifuge, it was likely that the contact force was reduced to zero during each test. Should the tank began to lift during the test, the laminates would come into contact with the roller bearings and further bending would be resisted.

The restraining frame on the Hushmand tank was also used to support the laminates. By restraining the tank within a frame of vertical supports, the tank was restricted to move in the direction of the shaking table only, with no torsional rotation possible. Neither of the circular tanks had used support frames so it was possible that torsional rotations occurred during these tests. The restraining frame would also act as a support for the laminates when the tank was empty.

Soil confinement is not a significant problem for rigid tanks but laminar tanks must be provided with some measure for preventing the soil from discharging between the laminates. The most common method for confining the soil within the tank has been to line the empty tank with a flexible rubber membrane. The membrane provides

confinement without hindering the displacement of the soil column. Other confinement methods have included a loose plastic liner (Hushmand et al.) and no liner at all (Whitman et al.), but in this case the Teflon sliders forming a continuous seal between each laminate.

6.2.2 University of Canterbury Tank Design

The design chosen for the University of Canterbury laminar tank follows from that of Hushmand et al., and is shown in Figure 6.5. The tank has internal dimensions of 1.8 m long by 1.8 m wide by 2.0 m tall. The dimensions give a length-to-depth ratio of 0.9, which is relatively low but maintains a balance between the need to reduce bending and the need for an appropriate soil volume for testing the drilled shafts.

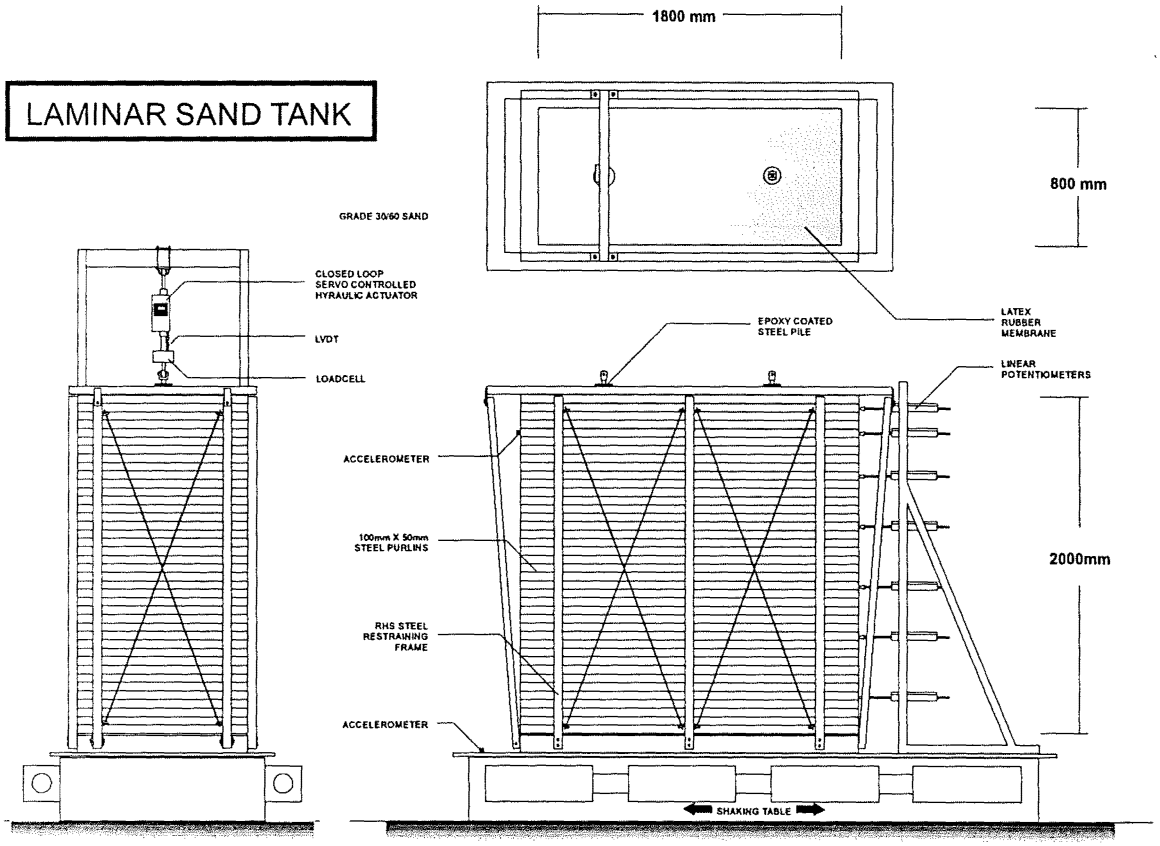

Figure 6.5 – University of Canterbury Laminar Tank

The laminates were made from 100 mm by 50 mm cold formed steel channel that was laid on its flat and welded into rectangular laminates. Teflon was chosen as the most efficient way of separating the laminates, as it was relatively simple to construct and would maintain a constant separation of the laminates, with little or no maintenance. Teflon strips of 150 mm long by 10 mm wide by 1 mm thick were glued to both sides of the laminates at six locations. Tests showed that the strips produced a coefficient of friction of 0.07, indicating that at normal stresses equivalent to those at the base of the tank, the load required to shear the laminates was only 2 percent of the load required to shear the soil mass.

The soil was contained within the tank with a flexible membrane liner. Latex rubber sheets, each 1 mm thick, were draped over the inside of the laminates and glued to the top laminate. The sheets were overlapped and the horizontal soil stress kept the sheets in place during each test.

The laminates were supported by a steel frame that was constructed from 50 mm by 50 mm Rectangular Hollow Section (RHS), with 10 mm diameter rods acting as cross-bracing members. The frame restricted the laminates to move only in the direction of the shaking table and also supported the stack of laminates when the tank was empty. Incorporated into the frame were movable steel end-stops and a steel top-cap. Between tests, the 50 mm by 50 mm RHS end-stops were bolted against the laminates so they would prevent the laminates from moving when the tank was empty. During each test the end-stops were extended out to the end of the frame, so that the tank could deflect in shear. In their extended position, the end-stops could still limit any extreme shear deformations. The steel top-cap was made from 100 mm by 50 mm RHS and was bolted to the top of the restraining frame. It sat over the stack of laminates and could be adjusted at the start of each test to provide a small contact pressure between it and the laminates. Both the top-cap and the side members of the supporting frame were coated with Teflon strips to reduce friction during testing.

The stack of laminates and the supporting frame were fixed to a 100 mm by 100 mm RHS base-frame, which had a 10 mm thick steel plate floor. The tank was bolted to the shaking table with twelve 10 mm diameter bolts.

6.3 SOIL

These tests were performed with the same silica sand that was used for the static soil deposit tests. A description of the sand, the reasons for its selection and its relevant engineering properties are given in Section 3.2.

6.4 PREPARATION OF SOIL DEPOSIT

These deposits were also prepared by air pluviation, but the large mass involved in these tests meant it was not feasible to employ a two-tank handling system. Instead, a hopper and storage bin system was used to fill and to empty the laminar tank. The hopper system is shown in Figure 6.6.

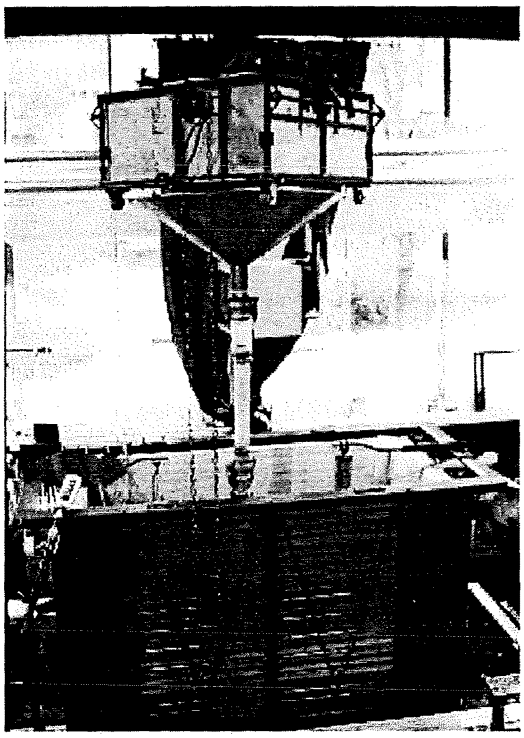

Figure 6.6 – Hopper system for preparing soil deposits (laminar tank also shown)

The 0.5 m^3 hopper was constructed from 12 mm plywood, fixed to a 25 mm square steel tube frame. The base of the hopper contained a gate for the soil to flow through. The gate consisted of two perforated steel plates with a screw mechanism to align the holes in the plates.

Between tests, the sand was stored in a plywood tank. The plywood tank was placed on 1 m high trestles so that the hopper could be rolled underneath it and quickly filled via a wooden gate in the base of the plywood tank. The full hopper was then fitted with the same funnel/hose/diffuser system that was used in the static soil deposit tests then lifted over the laminated tank with the overhead travelling crane. The gate on the hopper was then opened and the sand flowed out. The flow rate of the sand could be adjusted while the hopper was suspended overhead by way of a chain block mechanism, similar to those used on roller type garage doors.

Modifications were made to the original diffuser because the rate of soil deposition with the original diffuser had been particularly slow. The second diffuser was constructed by attaching a set of 200 mm diameter sieves to the flexible hose. Prudent selection of sieve sizes meant that a balance could be found between the desired relative density and an adequate rate of deposition. The sieves chosen for the new diffuser were two 10 mm and two 5.5 mm sieves, which allowed each tank to be filled in approximately 8 hours. The average density of the soil deposit was found by weighing the full tank after each test. Details of the weights are given in Table 6.2, showing that the average relative density of the soil was 46 percent, with a range of +/- 6 percent.

After each test, the laminar tank was emptied and the sand returned to the plywood tank. To empty the tank, it was lifted onto load-skates then wheeled off the shaking table and onto a pair of trestles. A steel sliding gate was opened in the base of the tank and the sand allowed to pour back into the hopper. Each full hopper was then lifted over the plywood storage tank where the hopper gate was opened and the sand returned to storage.

Table 6.2 – Densities of Shaking Table Soil Deposits

Test	Total Mass (kg)	Soil Density (t/m^3)	Void ratio	Relative Density (%)
302	5837	1.55	0.71	40
303	5884	1.57	0.69	46
304	5856	1.56	0.70	43
305	5925	1.58	0.68	51
306	5902	1.57	0.68	49
307	5914	1.58	0.68	50
308	5867	1.56	0.70	44
309	5888	1.57	0.69	47
310	5899	1.57	0.68	48
312	5885	1.57	0.69	46
313	5915	1.58	0.68	50
314	5934	1.58	0.67	52
315	5885	1.57	0.69	46
316	5864	1.56	0.70	44
318	5915	1.58	0.68	50
319	5873	1.56	0.70	45
320	5850	1.56	0.70	42
321	5854	1.56	0.70	43

6.5 CONSTRUCTION OF DRILLED SHAFT

A cast-in-situ concrete drilled shaft was used successfully for the first series of tests but the test schedule was hampered by the need for a 24 hour concrete curing period. During the curing period, neither the drilled shaft nor the soil deposit could be disturbed, so the time became non-productive in terms of achieving test results. To overcome this loss of productive time, an artificial drilled shaft was constructed and used for the shaking table tests. No curing time was necessary for the artificial drilled shaft so it could be tested as soon as the soil deposit had been prepared. The artificial drilled shaft was similar in size to the cast in-situ drilled shaft, with a buried length of

1450 mm and a diameter of 95 mm. It was constructed from hollow steel tube and was coated with a mixture of sand and epoxy resin to simulate the roughness of a cast in-situ drilled shaft. The hollow steel tube had a wall thickness of 1.5 mm which gave the drilled shaft a calculated flexural stiffness of 83600 Nm^2, compared with a calculated flexural stiffness of 85300 Nm^2 for the cast in-situ drilled shaft.

The artificial drilled shaft was prepared by simply suspending the shaft in the empty tank and depositing the sand around it. Again, care was taken to avoid disturbing the shaft while the soil deposit was prepared. When the soil was deposited, the drilled shaft could be tested immediately.

6.6 INSTRUMENTATION OF TANK

The following measurements were made during each test and the results recorded on a PC-based data acquisition system: Calibrations of these instruments are given in Appendix D

- Shaking Table Displacement – with a linear potentiometer attached to the table
- Shaking Table Acceleration – with an accelerometer attached to the table
- Tank Acceleration – with an accelerometer attached to the top of the tank
- Tank Displacement – with an array of linear potentiometers, as shown in Fig. 6.5.
- Soil Surface Settlement - with a linear potentiometer attached to the tank frame

Manual measurements were also made of the total soil settlement at different depths. Indicators were constructed from 150 mm by 150 mm, thin wooden plates that were each laid flat at various depths within the soil deposit, as shown in Figure 6.7. Attached perpendicularly to each plate was a slender steel rod. The rod protruded through the soil to the surface so that, as the soil settled, the change in height of the rod would indicate the settlement at that particular depth.

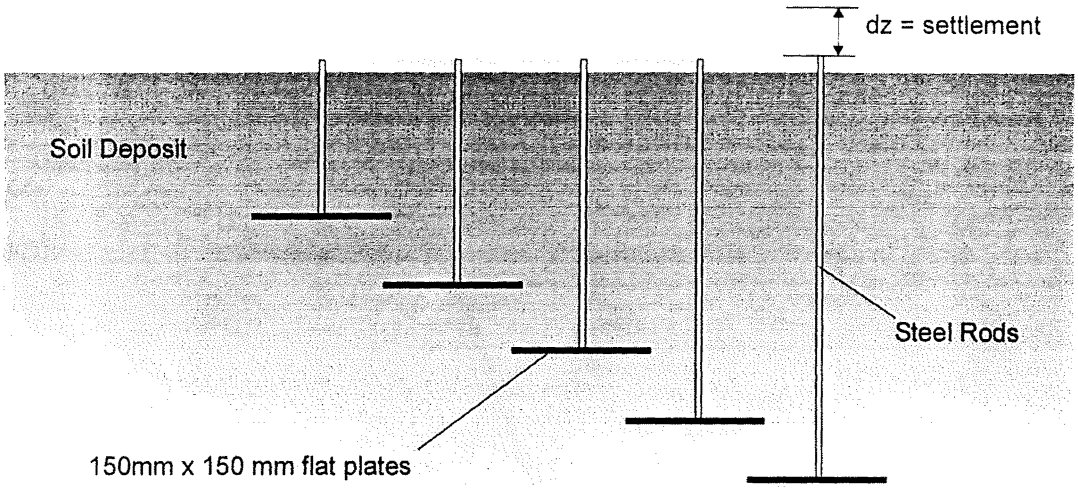

Figure 6.7 – Settlement Indicators

6.7 TANK BEHAVIOUR AND SOIL RESPONSE

The laminar tank was designed so that the soil would model a free-field response to shear loading when the tank and soil deposit were shaken on the shaking table. Observations from video recordings show that the tank responded as designed, in so much as the response to horizontal shaking was predominantly a shear response. Only minor cantilever bending actions were detected during each test. The horizontal displacement of the tank was measured with an array of linear potentiometers and a typical deflected shape is shown in Figure 6.8. In this case, the shaking is cyclic at a frequency of 1 Hz.

Also shown in Figure 6.8 is a theoretical response that was calculated using the SHAKE computer program of Schnabel et al. (1972). The program models the system as a linear visco-elastic soil mass that is subjected to vertically propagating shear waves. The program divides the soil deposit into a selected number of horizontal layers that extend to infinity in the horizontal direction, with the bottom layer being an elastic half-space. Each layer is homogeneous and isotropic and is characterised by a thickness h, a mass density ρ, a shear modulus G, and a damping factor β.

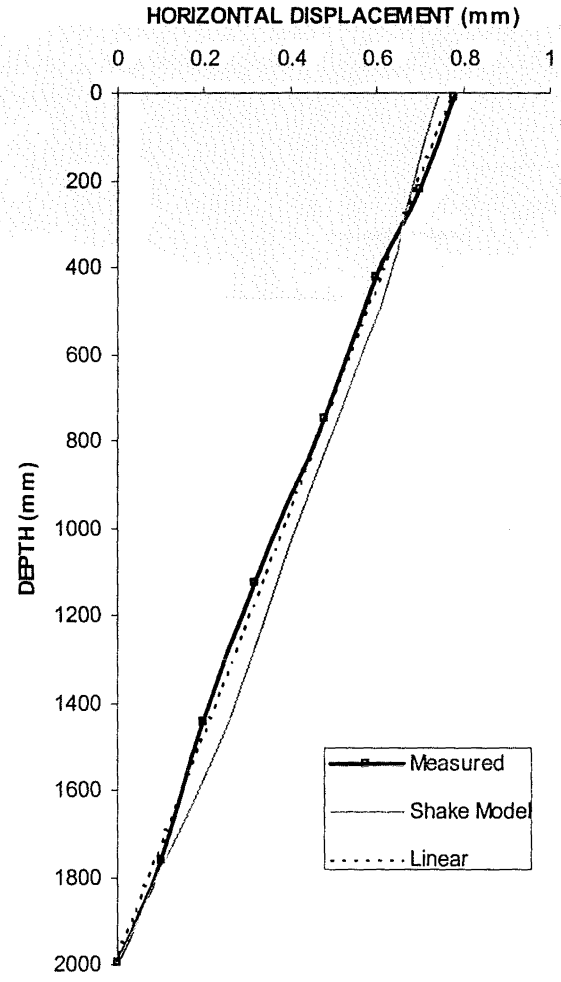

Figure 6.8 – Typical Deflected Shape of Laminar Tank at a Frequency of 1 Hz. (From Yang (1998))

The soil parameters used for the Shake program were calculated from equations by Hardin & Drnevish (1972) then these calculated soil parameters were adjusted for their shear strain and confining stress dependency. The adjustments were calculated from equations by Seed & Idriss (1970). Plots of the adjusted soil modulus and damping ratio are given in Figure 6.9. These plots show that the effective shear modulus is proportional to the square root of depth and the effective damping ratio is nearly constant with depth. Both plots are as expected for a homogeneous soil layer.

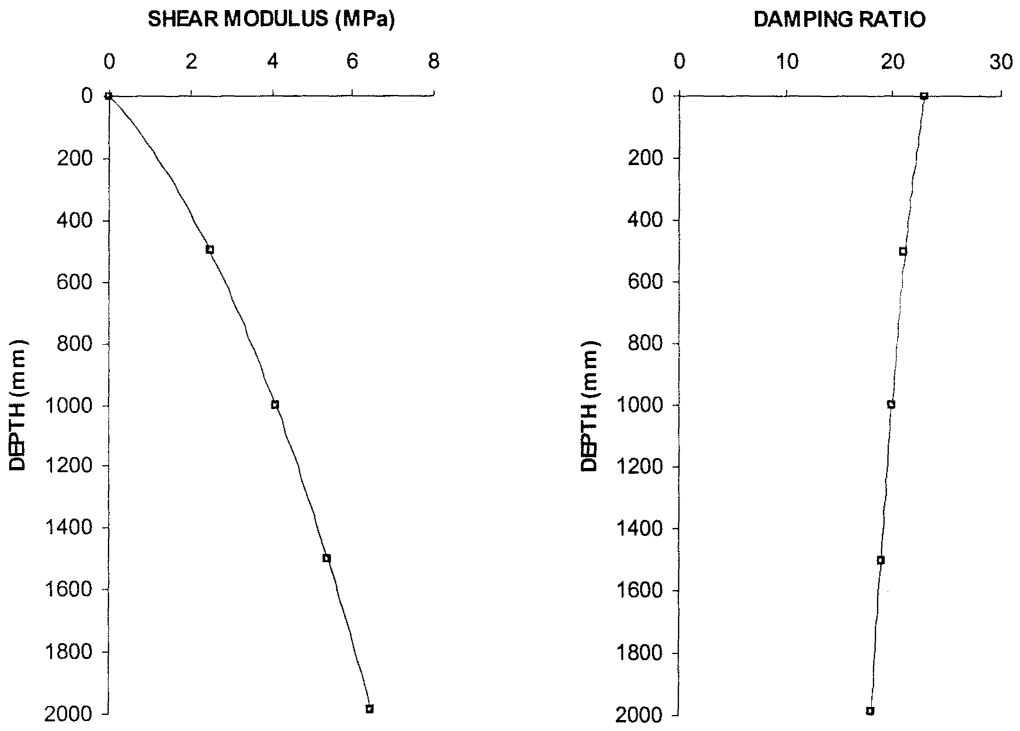

(a) Effective Shear Modulus **(b) Effective Damping Ratio**

Figure 6.9 – Effective Soil Parameters for Soil Deposit at a Frequency of 1 Hz. (From Yang (1998))

The measured deflected shape shown Figure 6.8 shows that the laminar tank appears to have linear response to shaking at 1 Hz. It also shows, however, that the tank has a higher stiffness near its base, when compared to the results from the Shake model. The increased stiffness may be due to crushing of the Teflon sliders, thereby increasing the friction between them. It may also be due to debris becoming trapped between the sliders. However, the zone of increased stiffness is not excessively different from the Shake model (which is only a model) and both show that the laminar tank has a predominantly linear response to cyclic shaking at a frequency of 1 Hz.

The second aspect of soil behaviour that significantly affected the response of the soil layer is that of settlement. Figure 6.10 shows the surface settlement of the soil deposit during a typical load test of 20 cycles at 1 Hz (with a peak table displacement of 45 mm). Figure 6.10 shows that there was a significant amount of settlement in the early cycles of loading but the rate of settlement decreased as the soil compacted.

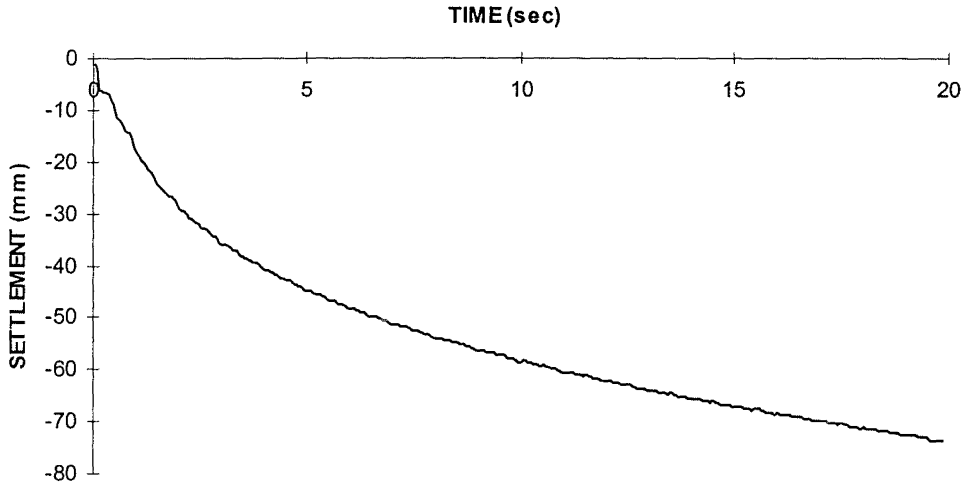

Figure 6.10 – Surface Settlement During 20 Cycles of Loading at 1 Hz. (Peak Table Disp=45mm).

Measurements taken from the buried plates are shown in Figure 6.11, indicating how the overall settlement is distributed over the height of the soil layer. It appears from the linear trend-line overlain in Figure 6.11 that the settlement is reasonably evenly distributed over the soil layer. There does, however, appear to be a smaller amount of settlement near the base of the tank. This region coincides with the region of lower shear displacement that was observed in Figure 6.8 and is consistent with the findings of Silver & Seed (1971) who found that the settlement of a soil layer was proportional to the shear strain in that layer.

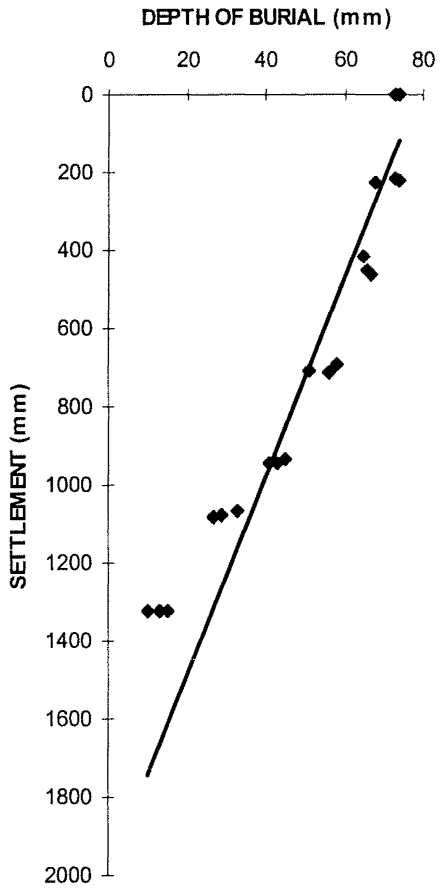

Figure 6.11 – Settlement versus Depth after 20 Cycles at 1 Hz.

The settlement increases the relative density of the soil and, therefore, also the stiffness, resulting in smaller shear displacements as each consecutive cycle of shaking is applied. Figure 6.12 shows the lateral displacement at the top of the tank over 20 cycles of shaking and it is clear that the peak displacement decreases with increasing numbers of cycles. It is likely that this increase in stiffness is due to an increase in density brought about by settlement of the soil during cyclic shaking.

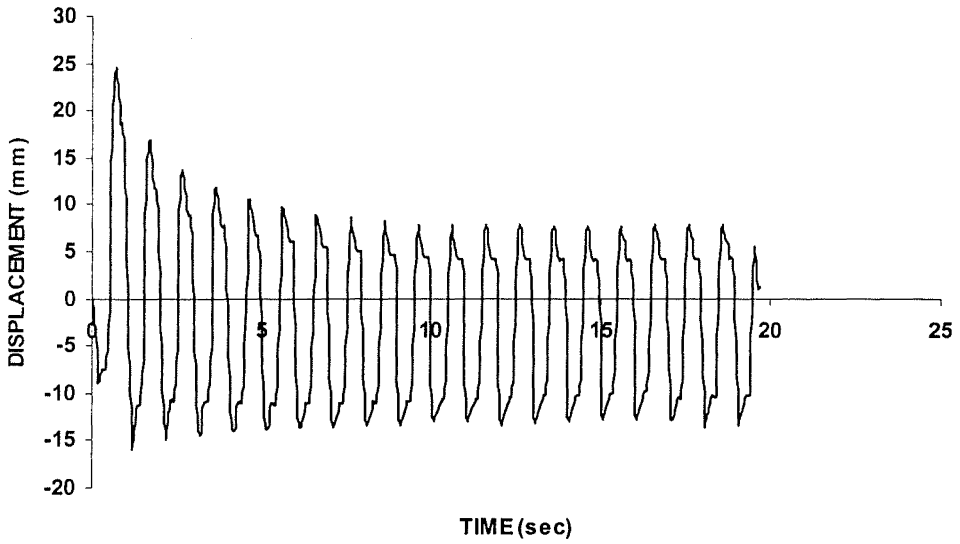

Figure 6.14 –Displacement at Top of Tank During Cyclic Load Test

In order to compare different levels of shaking it is preferable to determine the actual response of the soil rather than the loads, displacements or accelerations that are applied to the soil. If the actual soil response is measured, then any variations in the input or the soil deposit are accounted for.

A parameter called the Average Peak Shear Strain (APSS) has been developed to quantify the actual soil response. The APSS accounts for the deflected shape of the soil deposit and also for the settlement that occurs during shaking. The following steps are used to calculate the APSS:

1. The shear strain of the soil deposit is calculated for all depths and times from the displacement data recorded by the array of potentiometers.
2. The shear strain is averaged over the soil column. The soil deposit is therefore assumed to have a linear deflected shape, which appears justified according to Figure 6.8.
3. The peak shear strain is found at each half cycle of shaking and then these peaks are averaged over the number of half cycles. Averaging the peaks over the whole of the test accounts for the reductions in shear strain as the soil settles and stiffens.

The APSS has been determined for all the shaking table tests and the values range from 0.10 percent for Test 203a to 1.56 percent for Test 302. Further examples of the different APSS values are given in Table 6.3.

Table 6.3 –Examples of APSS Values Determined from Shaking Table Tests

Test	Peak Table Displacement (mm)	Peak Table Acceleration (g)	Surface Settlement (mm)	APSS (%)
211a	30	0.12	-7	0.11
209a	40	0.16	-34	0.38
210a	45	0.17	-42	0.53
212a	50	0.19	-69	0.96
310	45	0.23	-74	1.48

The values in Table 6.3 show that the APSS increases with increasing table acceleration. They also show that the amount of surface settlement increases as the APSS increases. The usefulness of the APSS is highlighted by the differences in Tests 210a and 310. Both tests were performed at the same peak table displacement (and table frequency) but each had a different peak table acceleration. These results show that it more prudent to measure the actual soil response rather than assume a soil response from the input parameters.

Tests 210a and 310 showed different soil responses because they were performed with different controllers on the shaking table. The two controllers were described in Section 6.1. The 200 series tests were performed with the old controller and the 300 series tests were performed with the new controller, the latter producing a greater peak acceleration for the same input table displacement. Again, this highlights the need to measure the actual soil response rather than any input parameter.

SUMMARY

A laminated tank was designed and constructed for use on the shaking table at the University of Canterbury. The tank was used to contain a soil deposit while allowing the soil to displace as it was shaken on the shaking table. The tank was designed to model the free-field response of a horizontal soil layer under simulated seismic loading

A storage and hopper system was constructed to enable each soil deposit to be prepared. The soil was transferred from the storage tank to the hopper then deposited in the laminar tank in a controlled manner. The transfer method allowed homogeneous soil deposits to be repeatedly produced at an average relative density of 46 percent.

An artificial model drilled shaft was constructed for these tests. The drilled shaft was constructed from steel tube and coated with a sand/epoxy resin mixture, giving it a surface roughness that was similar to that of cast-in-situ concrete. The artificial drilled shaft had a flexural stiffness that was similar to the reinforced concrete drilled shaft used for the previous tests.

The response of the laminar tank was similar to that of a theoretical free-field soil response. The deflected shape of the tank could be seen as a simple linear function of depth. The magnitude of tank deflection was a function of the number of cycles of shaking, with the tank stiffening up as successive cycles were applied. The increase in stiffness was most likely due to an increase in soil density due to settlement under repeat cycles of shear strain. The average peak shear strain (APSS) has been developed as a measure of the soil response. The APSS is the peak shear strain of each half load cycle, averaged over the height of the soil column, and over the full number of cycles. The APSS shall be used to quantitatively determine the level of soil shaking when the tank is used to test model drilled shaft foundations.

REFERENCES

FINN, L.W.D. & GOHL, W.B. (1992). "Response of Model Pile Groups to Strong Shaking". ASCE Geotechnical Special Publication No 34, New York, Sept. 13-17, 1992. Ed. Shamsher Prakash.

FISHMAN, K.L., MANDER, J.B. & RICHARDS, R. Jr. (1995) "Laboratory Study of Seismic Free-field Response of Sand". Soil Dynamics and Earthquake Engineering, Vol. 14, pp 33-43.

HUSHMAND, B., SCOTT R.F. & CROUSE C.B. (1988). "Centrifuge liquefaction tests in a laminar box", Geotechnique 38, No 2, 253-262.

IAI, S. (1991). "A Strain Space Multiple Mechanism Model For Cyclic Behavior of Sand and its Application," Research Note No.43, Earthquake Engineering Research Group, Port and Harbour Research Institute, Ministry of Transport, Japan. May 1991.

IWASAKI, T. (1986). "Soil Liquefaction Studies in Japan: State of the Art." Soil Dynamics and Earthquake Engineering, Volume 5, No. 1, PP. 28-33.

MARUYAMA, I. (1977). "Dynamic Behaviour of Piles in Liquefiable Foundation Soils". Thesis presented to Chiro University, Tokyo, Japan. In partial fulfillment of the requirements for the degree of Master of Science.

MIZUNO, H., IIBA, M. & KITAGAWA, Y. (1984). "Shaking Table Testing of Seismic Building-Pile-Two-Layered-Soil Interaction." Eighth World Conference of Earthquake Engineering, San Fransisco, Volume 3. 1984.

SILVER, M.L. & SEED, H.B. (1971), "Volume Changes in Sands During Cyclic Loading" J. Soil Mech. and Found. Div., ASCE, Vol. 97, No.SM9, September, 1971.

SCHNABEL, P.B., LYSMER, J. & SEED, H.B. (1972). "A Computer Program for Earthquake Response Analysis of Horizontally Layered Sites". Report No. EERC72-12. Earthquake Engineering Research Centre, Berkeley.

STEEDMAN, R.S. & MAHEETHARAN, A. (1989). "Modelling the Dynamic Response of Piles in Dry Sand". Proceedings of the Twelfth International Conference on Soil Dynamics and Foundation Engineering. Rio de Janeiro. pp 983-986.

WHITMAN, R.V., LAMBE, P.C. & KUTTER, B.L. (1981). "Initial Results from a Stacked-Ring Apparatus for Simulation of a Soil Profile". Proceedings, International Conference on Recent Advances in Geotechnical Earthquake Engineering and Soil Dynamics, St Louis, Mo., April 26 – May 3, 1981.

YANG, J. (1998). "Kinematic Soil Micropile Interaction". Thesis presented to University of Canterbury, Christchurch, New Zealand. In partial fulfillment of the requirements for the degree of Master of Engineering (Civil).

Chapter Seven

TESTING OF MODEL DRILLED SHAFTS UNDER AXIAL LOADS IN SHAKING SOIL DEPOSITS.

INTRODUCTION

This chapter details a series of tests performed on model drilled shaft foundations in a shaking soil deposit. Different axial loads were applied to each shaft while the surrounding soil deposit was shaken under simulated seismic shear loading. A full list of the test results is given. Examples are also given of the different responses to both soil shaking and to the applied axial loads. Graphical summaries are given of the overall shaft displacements and the changes in shaft capacity under different types of axial load and soil shaking.

7.1 LOAD TEST PROGRAM

The first tests were monotonic uplift and monotonic compression tests. The model drilled shaft and the soil density had changed from the earlier tests so monotonic tests were required to reestablish the static uplift and static compressive capacities. The shaft had changed from a cast in-situ reinforced concrete drilled shaft to a sand and epoxy coated steel tube shaft and the relative density of the soil deposit had changed from 31 percent to 47 percent. The capacities found from these tests would act as benchmarks and the capacities after each load test would be compared to them.

The second set of tests were monotonic uplift and compression tests performed after soil shaking. These tests were performed to determine the changes in capacity due to shaking and, particularly, to settlement of the soil. The magnitude of the shaking was varied from test to test and there was zero load on the drilled shaft during shaking.

For the third set of tests, each drilled shaft was subjected to a constant axial load while the soil deposit was shaken. These tests were performed to determine the static

capacity of the drilled shaft during shaking. The magnitudes of both the shaking and the constant axial load were varied from test to test.

For the fourth set of tests, each drilled shaft was subjected to a cyclic axial load while the soil deposit was shaken. These tests were performed to determine the cyclic capacity of the drilled shaft during shaking. The magnitude of the cyclic axial load and the phase difference between peak axial load and peak soil motion were varied from test to test.

7.2 LOADING RIG AND INSTRUMENTATION

Axial loads were applied to the drilled shaft with the same hydraulic actuator that was used for the load tests in static soil deposits, as described in Section 4.2. The reaction frame was modified for these tests so that it could be attached to the laminar tank.

A trigger system was constructed so that the axial loads and the soil motions could be synchronised. The trigger system is shown in Figure 7.1. The system utilised a trigger function within the waveform generator whereby the load signal would be initiated when the waveform generator received a pulse from a triggering device. The triggering device for these tests consisted of a rotary encoder that was wired to the shaking table. The first movement of the shaking table would activate the rotary encoder and trigger the waveform generator.

The results from a typical synchronised test are shown in Figure 7.2. The peak displacement at the top of the tank has been synchronised with the peak axial load on the drilled shaft, giving a phase difference between the two of zero degrees in this case. The generator also had a delay function so the phase difference between soil motion and shaft axial loading could be adjusted from one test to another. The shaking table tests were all performed at a phase difference of either zero degrees or ninety degrees – the maximum and minimum phase differences between axial load and soil motion.

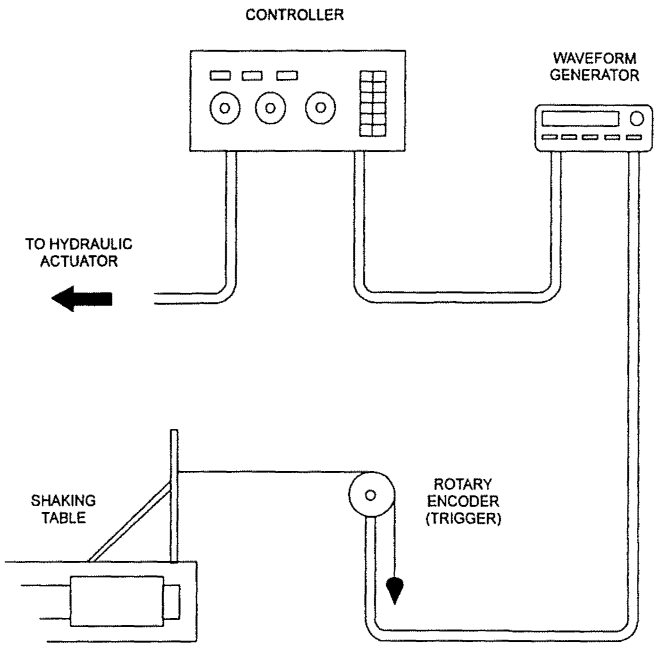

Figure 7.1 – Trigger System for Simultaneous Axial :Loading and Soil Motion

Axial load and axial displacement were measured electronically during each test and recorded on the same PC based data acquisition system used for the earlier tests. Electronic measurements were also taken from a soil pressure transducer that was buried 20 mm from the shaft and at different depths for each test.

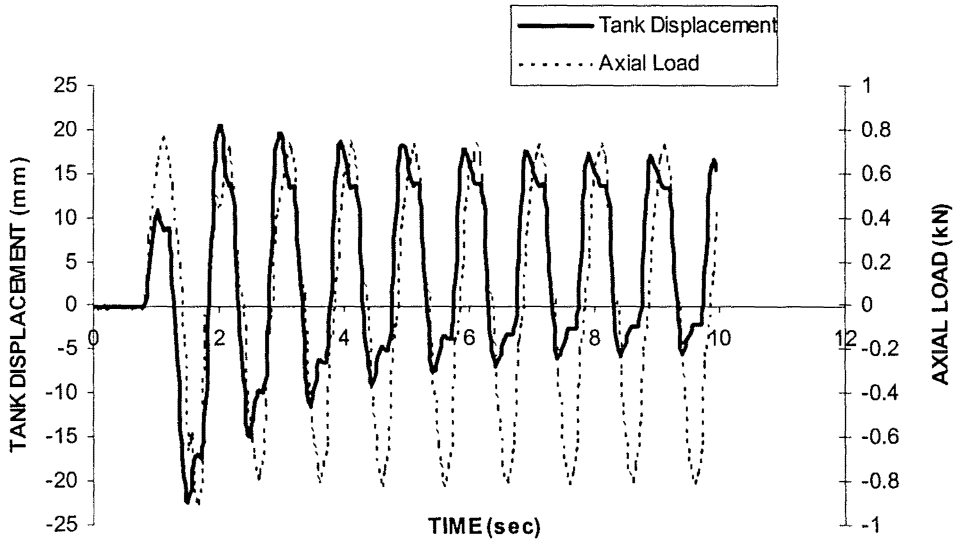

Figure 7.2 – Phase Difference between Tank Displacement and Axial Load for Test 304

7.3 MONOTONIC LOAD TESTS WITHOUT SOIL SHAKING

The results for all the tests performed in the laminar tank are given in Table 7.1.

7.3.1 Monotonic Uplift Capacity

Four monotonic uplift tests (tests 200a, 200b, 201a, 201b) were performed on model drilled shafts in the laminar tank without soil shaking. A typical load/displacement response (for test 200b) is shown in Figure 7.3.

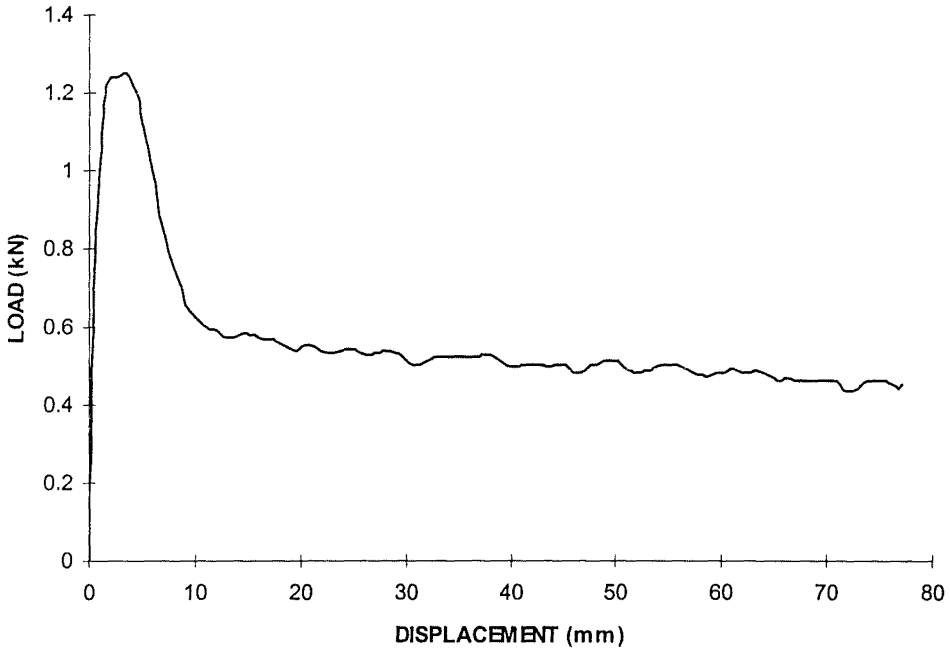

Figure 7.3 – Load versus Displacement for Monotonic Uplift Test 200b

The static uplift capacity (Q_{us}) for Test 200a was found to be 1.30 kN. The capacities for Tests 200b, 201a and 201b were 1.28 kN, 1.25 kN and 1.30 kN, respectively. The average static uplift capacity for the model drilled shaft in the laminar tank without soil shaking was therefore taken to be Q_{us} = 1.28 kN.

The static uplift capacity of the earlier reinforced concrete drilled shaft was 1.59 kN. The difference between the two model drilled shafts may be due to the artificial

drilled shaft not having the same roughness as the reinforced concrete, although this should not have a significant effect according to the research on surface roughness outlined in Chapter 2. Instead, it is possible that the hydrostatic pressure of the column of wet concrete may compress the surrounding soil before it sets, thereby increasing the radial stress on the drilled shaft and increasing the uplift capacity accordingly.

7.3.2 Monotonic Compressive Capacity

Two monotonic compression tests (tests 202a, 202b) were performed on model drilled shafts in the laminar tank without soil shaking. A typical load/displacement response (for test 202b) is shown in Figure 7.4.

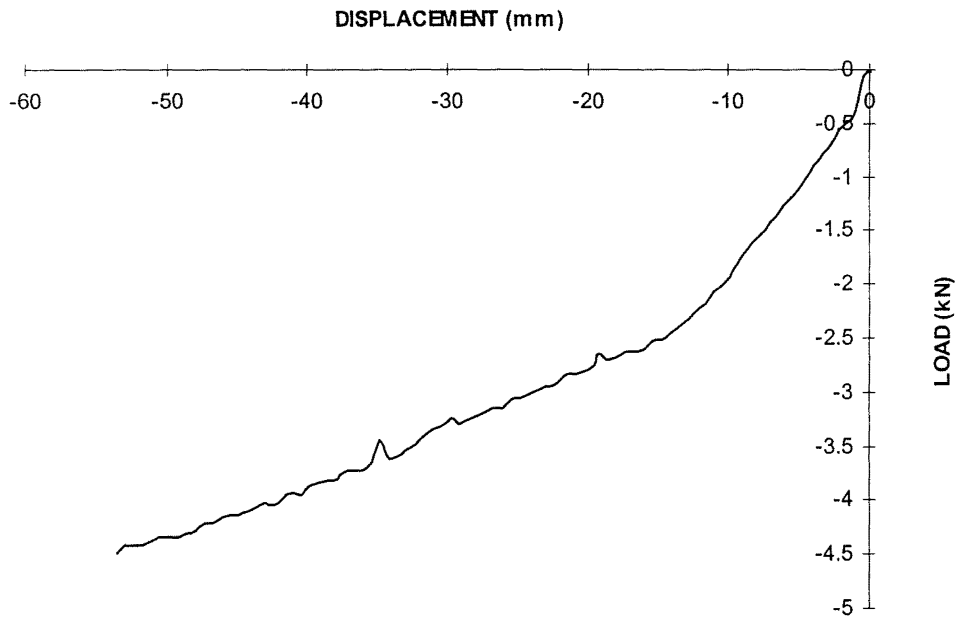

Figure 7.4 – Load versus Displacement for Monotonic Compression Test 202b

The interpreted compressive capacity (Q_{cs}) for Test 202a was found to be 2.00 kN. The capacity for Test 202b was 1.95 kN, so the average interpreted compressive capacity for the model drilled shaft, in the laminar tank, was taken to be Q_{cs}= 1.98 kN.

The static compressive capacity of the earlier reinforced concrete drilled shaft was 2.68 kN. The capacity difference between the two drilled shafts may again be due to stress increases during the casting process. The difference may also be due to the preparation method used for the epoxy coated steel drilled shaft. The shaft was prepared by suspending it in the tank and depositing the soil around it by air pluviation. This method meant that the soil beneath the tip of the shaft was probably very loose because it was not possible to move the diffuser in underneath the shaft during soil preparation. The same problem arises for the reinforced concrete shaft when the soil is prepared around a casing but it is likely that the soil beneath the tip is then compacted when the wet concrete is placed.

Table 7.1 – Load Test Results for Laminar Tank

Test	Table Amplitude (mm)	Axial Load Amplitude (kN)	APSS (%)	Soil Settlement (mm)	Shaft Displacement (mm)	Residual Uplift Capacity (kN)
200a	-	Uplift Failure	-	-	-	1.30
200b	-	Uplift Failure	-	-	-	1.28
201a	-	Uplift Failure	-	-	-	1.25
201b	-	Uplift Failure	-	-	-	1.30
202a	-	Comp Failure	-	-	-	-2.00
202b	-	Comp Failure	-	-	-	-1.95
203a	30	0.32 – constant	0.10	-8	-3	1.99
203b	30	0	0.10	-8	-4	1.48
204a	50	0.32 – constant	0.86	-67	-25	3.60
204b	50	0	0.86	-67	-32	3.30
205a	40	0.32 – constant	0.33	Data Lost	-10	Data Lost
205b	40	0	0.33	.....Data Lost.....		
206a	45	0.32 – constant	0.57	-61	-24	2.95
206b	45	0	0.57	-61	-29	Data Lost
207a	30	0.64 – constant	0.13	-10	-3	1.89
207b	30	0	0.13	-10	-6	1.49
208a	50	0.64 – constant	1.00	-73	-19	4.03
208b	50	0	1.00	-73	-34	3.35
209a	40	0.64 – constant	0.38	-34	-7	2.61
209b	40	0	0.38	-34	-15	2.19

210a	45	0.64 – constant	0.53	-42	-6	2.60
210b	45	0	0.53	-42	-18	2.56
211a	30	0.96 – constant	0.11	-7	1	0.84
211b	30	0	0.11	-7	-4	1.51
212a	50	0.96 – constant	1.02	-69	30	Failure
212b	50	0	1.02	-69	-34	3.28
213a	45	0.86 – constant	0.65	-52	10	0.66
213b	45	0	0.65	-52	-26	2.71
301	45	0.64 – cyclic, d=90°	.....Data Lost.....			3.75
302	45	0.64 – cyclic, d=90°	1.56	-76	-43	3.80
303	45	0.64 – cyclic, d=0°	1.38	-78	-33	4.00
304	45	0.77 – cyclic, d=90°	1.40	-69	-35	3.79
305	45	0.90 – cyclic, d=90°	1.39	-72	-34	3.75
306	45	1.02 – cyclic, d=90°	1.32	-71	-26	3.78
307	45	1.15 – cyclic, d=90°	1.30	-66	-27	4.22
308	45	1.41 – cyclic, d=90°	1.55	-71	-30	3.99
309	45	1.66 – cyclic, d=90°	1.48	-71	-15	4.22
310	45	1.92 – cyclic, d=90°	1.48	-74	27	Failure
311	45	1.92 – cyclic, d=0°	DataLost	-76	35	Failure
312	45	1.664 – cyclic, d=0°	1.44	-71	26	Failure
313	45	1.41 – cyclic, d=0°	1.39	-70	-29	4.58
314	45	1.54 – cyclic, d=0°	1.46	-68	4	1.98
315	45	1.79 – cyclic, d=90°	1.40	-67	14	2.90
316	45	Load not applied	1.50	-73	-33	3.89
317	45	0	-	Data Lost	-36	-
317a	-	2.31 – cyclic	-	-	70	Failure
317b	-	1.65 - cyclic	-	-	70	Failure
318	45	0	1.54	-72	Data Lost	-
318a	-	0.99 - cyclic	-	-	0	3.73
318b	-	1.28 - cyclic	-	-	12	0.52

7.4 MONOTONIC LOAD TESTS AFTER SOIL SHAKING

The laminar tank was bolted to the shaking table for these tests and then subjected to the simulated earthquake event. The event consisted of 20 cycles of sinewave, applied at a frequency of 1 Hz. The sinewave amplitude was kept constant over the 20 cycles, but varied between tests. A typical table motion, with a peak-to-peak displacement of 90 mm, is shown in Figure 7.5.

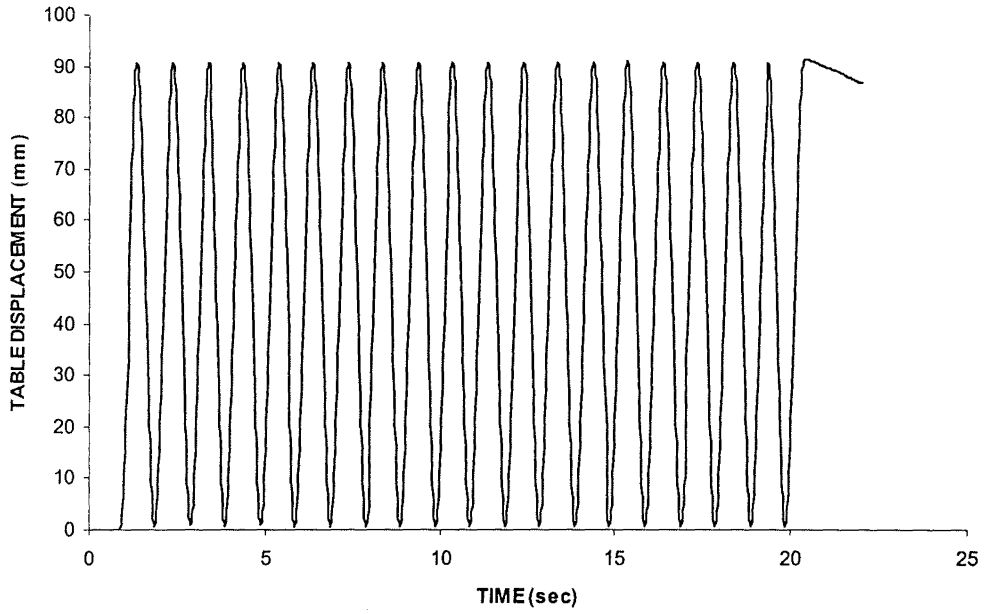

Figure 7.5 – Table Displacement versus Time for Test 206

Twelve monotonic uplift or compression tests were performed on model drilled shafts after shaking of the soil deposit. The results from these tests are summarised in Table 7.2.

Table 7.2 – Monotonic Uplift Test Results after Soil Shaking

Test	Table Amplitude (mm)	Axial Load Amplitude (kN)	APSS (%)	Soil Settlement (mm)	Shaft Displacement (mm)	Uplift Capacity Q_{ud} (kN)
203b	30	0	0.10	-8	-4	1.48
204b	50	0	0.86	-67	-32	3.30
205b	40	0	0.33	.....Data Lost.....		
206b	45	0	0.57	-61	-29	Data Lost
207b	30	0	0.13	-10	-6	1.49
208b	50	0	1.00	-73	-34	3.35
209b	40	0	0.38	-34	-15	2.19
210b	45	0	0.53	-42	-18	2.56
211b	30	0	0.11	-7	-4	1.51
212b	50	0	1.02	-69	-34	3.28
213b	45	0	0.65	-52	-26	2.71
316	45	0	1.50	-73	-33	3.89

The results from these tests are shown in Figure 7.6, with the uplift capacity (Q_{ud}) plotted as a function of the average peak shear strain (APSS) of the soil deposit.

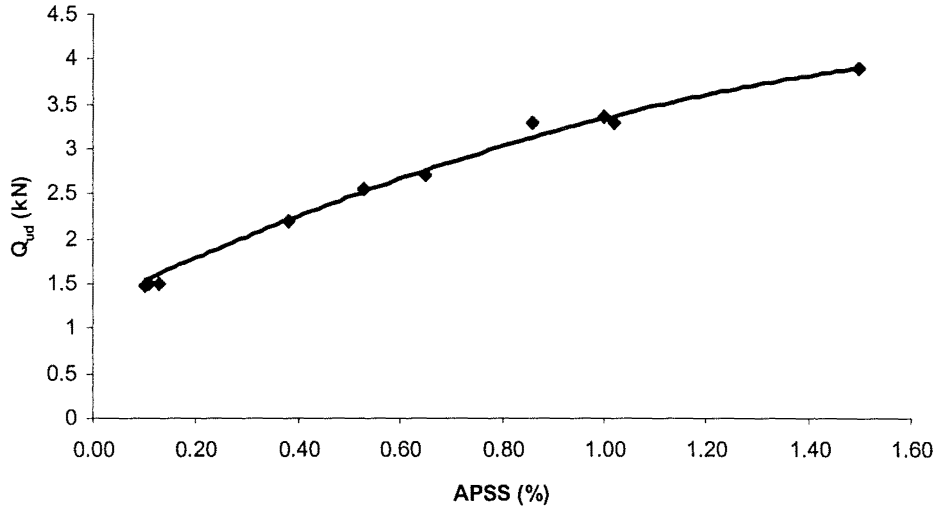

Figure 7.6 –Monotonic Uplift Capacity after Shaking (Q_{ud}) versus APSS

Figure 7.5 shows a close correlation between APSS and uplift capacity (Q_{ud}) with uplift capacity increasing with increasing APSS, although the rate of increase tends to lessen at higher APSS. The smaller rate of increase at higher APSS values may be due to the soil approaching its minimum void ratio. The denser the soil becomes, the less affect the shaking has on density. The best-fit curve shown in Figure 7.5 is given by the relationship:

$$Q_{ud}\,(\text{kN}) = -0.62 * APSS^2 + 2.68 * APSS + Q_{us}\,(\text{kN}) \qquad (7.1)$$

in which Q_{ud} is the uplift capacity after shaking, APSS is the average peak shear strain of the soil deposit during shaking and Q_{us} is the uplift capacity without shaking.

Equation 7.1 shows that there was an increase in drilled shaft uplift capacity that was explicitly due to shaking of the soil deposit. No axial loads were applied to the drilled shaft during these shaking tests so the change in capacity must due to changes in the soil mass during shaking. The correlation shown in Equation 7.1 was used to differentiate between the effects of soil shaking and the effects of applied axial loads during subsequent model drilled shaft tests.

7.5 CONSTANT AXIAL LOAD APPLIED DURING SOIL SHAKING

Constant axial loads were applied to eleven model drilled shafts while the soil deposit was shaken. At the end of shaking, each drilled shaft was tested in monotonic uplift to determine the uplift capacity. The results from these tests are summarised in Table 7.3. Note that all the axial loads were uplift loads because this study focused on the uplift capacity of drilled shafts under simulated seismic loads.

Table 7.3 –Test Results for Constant Axial Load applied during Soil Shaking

Test	Table Amplitude (mm)	Constant Axial Load Amplitude (kN)	APSS (%)	Soil Settlement (mm)	Shaft Displacement (mm)	Uplift Capacity Q_u (kN)
203a	30	0.32	0.10	-8	-3	1.99
204a	50	0.32	0.86	-67	-25	3.60
205a	40	0.32	0.33	Data Lost	-10	Data Lost
206a	45	0.32	0.57	-61	-24	2.95
207a	30	0.64	0.13	-10	-3	1.89
208a	50	0.64	1.00	-73	-19	4.03
209a	40	0.64	0.38	-34	-7	2.61
210a	45	0.64	0.53	-42	-6	2.60
211a	30	0.96	0.11	-7	1	0.84
212a	50	0.96	1.02	-69	30	Failure
213a	45	0.86	0.65	-52	10	0.66

The test results show that some of the drilled shafts were stable during shaking while others either failed in uplift or underwent large reductions in uplift capacity. Changes in uplift capacity were found for all of the drilled shafts after shaking.

The results from a typical stable test (206a) are shown in Figure 7.7. The constant axial load on the drilled shaft was 0.32 kN and the APSS was 0.57 percent. Also shown for comparison in Figure 7.7 is the displacement trace of a drilled shaft (Test206b) at the same APSS but with zero axial load.

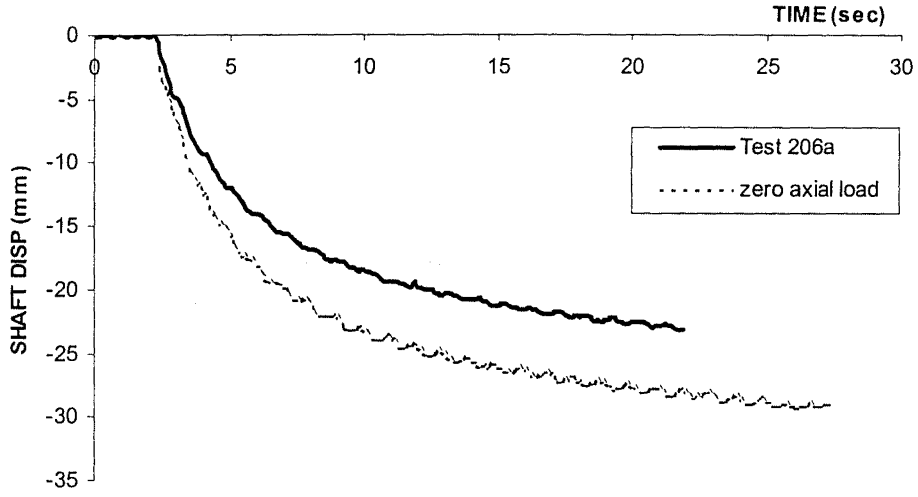

Figure 7.7 – Drilled Shaft Displacement versus Time for Constant Axial Load Test 206a

The results from a typical unstable test (213a) are shown in Figure 7.8. The constant axial load on the drilled shaft was 0.86 kN and the APSS was 0.65 percent.

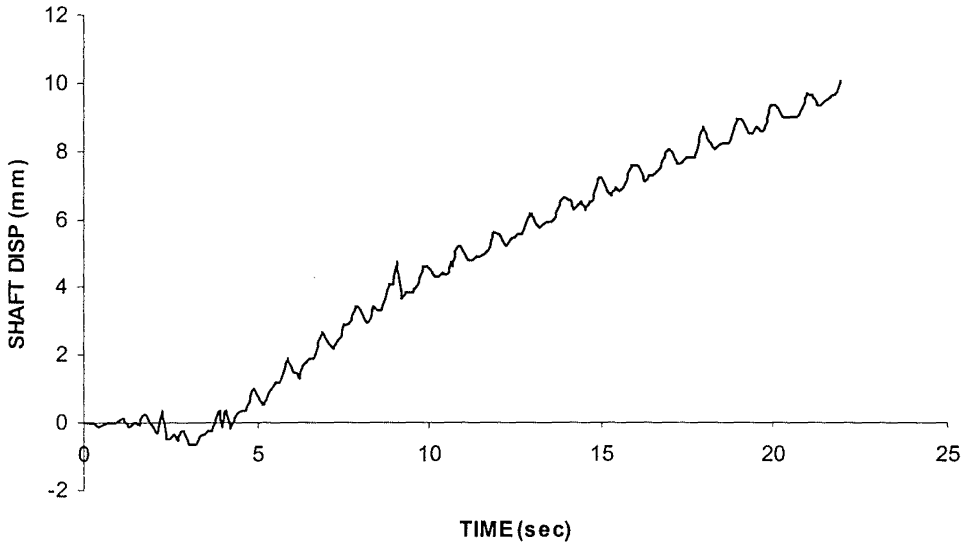

Figure 7.8 – Drilled Shaft Displacement versus Time for Constant Axial Load Test 213a

The displacement results from the constant axial load tests have been summarised in Figure 7.9. The displacement of the drilled shaft after shaking is plotted against the constant axial load. Figure 7.9a has the constant axial load normalised by the static uplift capacity before shaking (Q_{us}) and Figure 7.9b has the constant axial load normalised by the static uplift capacity (Q_{ud}) after the equivalent level of shaking but

with zero axial load. Normalising by Q_{us} presents the axial load as a proportion of the original static capacity (which could be considered as the static design capacity). Normalising by Q_{ud} accounts for the capacity increase due to settlement of the soil during shaking so the results are presented as a proportion of the final static uplift capacity. The test results have been divided into three groups according to the level of soil shaking. The three groups are identified by their corresponding mean APSS. (Note that uplift is plotted as a positive displacement).

Figure 7.9a shows that the shaft undergoes a relatively constant downward displacement with the settling soil if the axial load is less that approximately 50 percent of Q_{us}. If, however, the axial load is greater than approximately 50 percent of Q_{us} then large upward displacements occur as the drilled shaft is pulled out of the soil deposit during shaking. The results show no clear trend with regard to the level of shaking.

Figure 7.9b shows that the level of shaking has an influence on the results. Under weaker shaking, the shaft appears to undergo large upward displacement and pull out of the soil deposit during shaking if the constant axial load exceeds approximately 50 percent of Q_{ud}. If the level of shaking is increased then the same large upward displacements occur but at lower axial loads. At higher shaking levels, the shaft pulls out of the soil mass under a constant axial load of approximately 25 percent of Q_{ud}. It appears therefore that the load required to cause uplift failure during shaking decreases as the level of shaking increases.

It is difficult to determine the actual change in shaft capacity from these results because neither Q_{us} nor Q_{ud} are truly representative of the uplift capacity of the drilled shaft during shaking. They are the static capacities at each end of the test, rather than during the test. Q_{us} underestimates the uplift capacity because it does not account for the soil settlement and Q_{ud} overestimates the uplift capacity because the soil has undergone the full settlement associated with that level of shaking. A more representative static uplift capacity would be somewhere between these two extreme values.

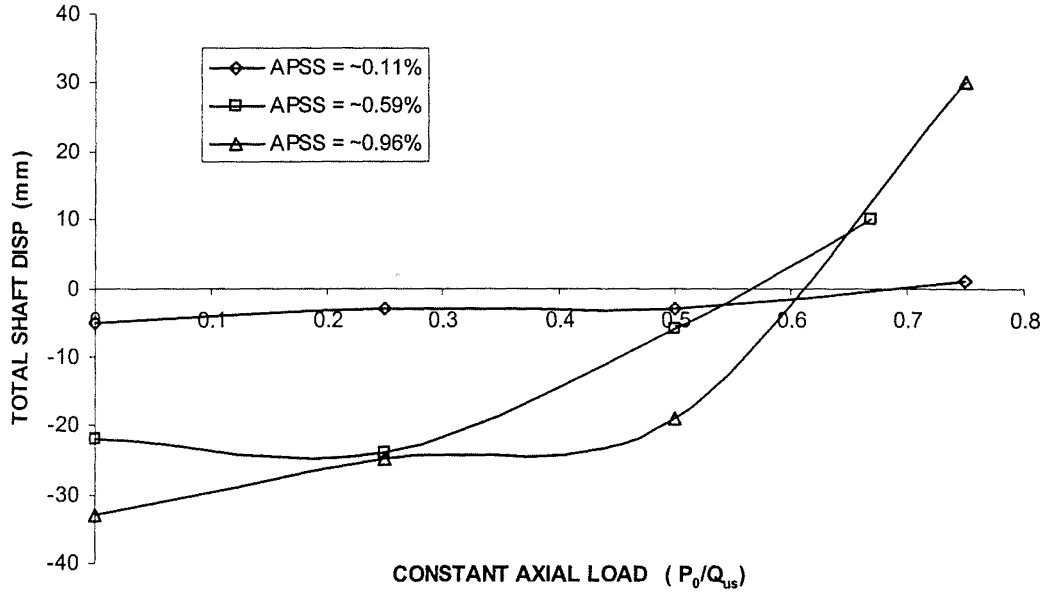

Figure 7.9a – Total Shaft Displacement versus Constant Axial Load Normalised by Uplift Capacity Before Shaking

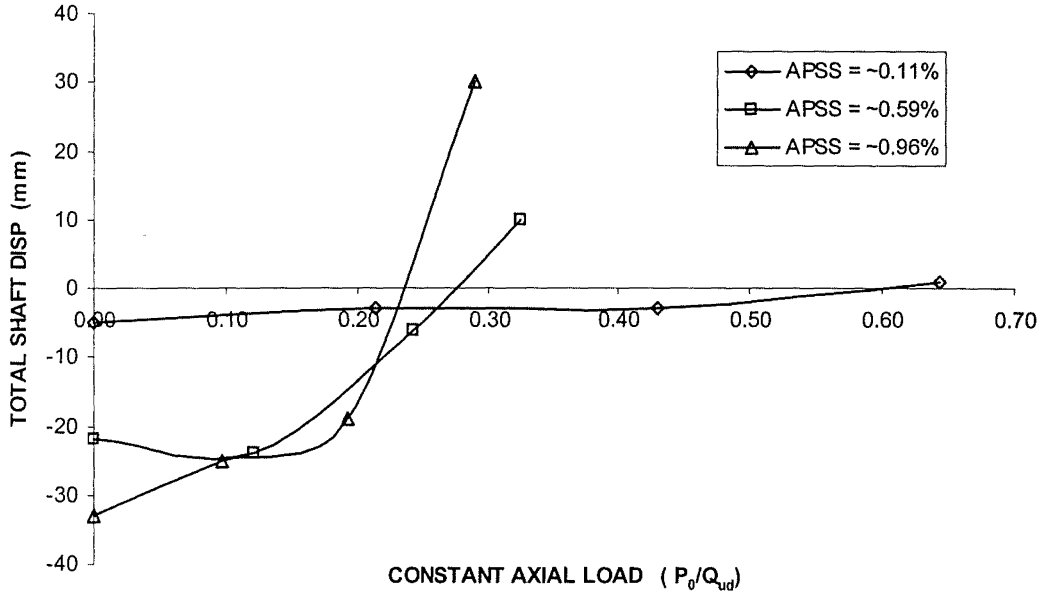

Figure 7.9b – Total Shaft Displacement versus Constant Axial Load Normalised by Uplift Capacity After Shaking Only

Figure 7.7 showed the settlement of the drilled shaft during a load test with no axial load. This graph may be used to arbitrarily define a static uplift capacity during shaking because both the settlement and the uplift capacity after shaking were proportional to the level of shaking. The shape of the graph in Figure 7.7 shows that there is considerable settlement in the first quarter of the shaking then the settlement rate becomes much less over the remainder of the test. If the uplift capacity is assumed to follow the same path from Q_{us} to Q_{ud} then a static uplift capacity during shaking may be defined from Figure 7.7 as follows:

Let the static uplift capacity (Q_{uu}) be arbitrarily selected as the equivalent uplift capacity at the midpoint of the shaking test. At the midpoint of the shaking test, the settlement has typically reached 90 percent of the total settlement. If the increase in uplift capacity is assumed to follow the same shape as the settlement then the static uplift capacity during shaking (Q_{uu}) will be:

$$Q_{uu} = Q_{us} + 0.90(Q_{ud} - Q_{us}) \tag{8.1}$$

Figure 7.10 shows the results of the shaking tests under constant axial load with the axial load normalised by Q_{uu}.

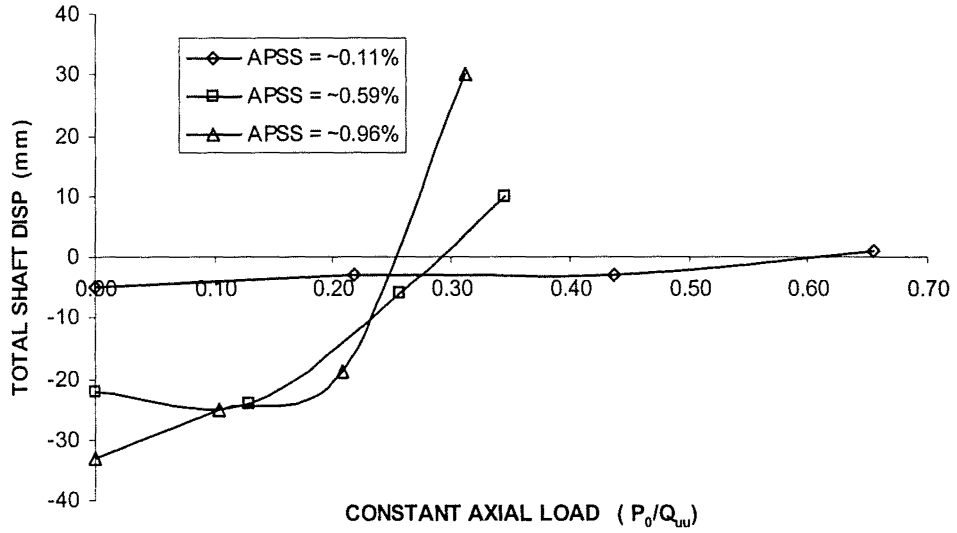

Figure 7.10 – Total Shaft Displacement versus Constant Axial Load Normalised by Uplift Capacity During Shaking

Figure 7.10 shows that large upward displacements occur during shaking at constant axial load levels that are considerably less than the static uplift capacity, Q_{uu}. Again, the axial loads causing these large displacements appear to be proportional to the level of soil shaking, with lower magnitude axial loads causing uplift failure as the level of shaking increases.

The test results also show that the uplift capacity after shaking (Q_u) is affected by the constant axial load applied during shaking. Figure 7.11 shows the results from the monotonic uplift tests performed after soil shaking. The constant axial load (P_0) is normalised by the static uplift capacity during shaking (Q_{uu}). The uplift capacity after shaking with constant axial load (Q_u) has been normalised by the uplift capacity after shaking with no axial load (Q_{ud}). The test results have been divided into three groups according to the level of soil shaking. (The uplift capacity of Test 212a, that failed during the test, has been conservatively estimated at 1.0 kN.)

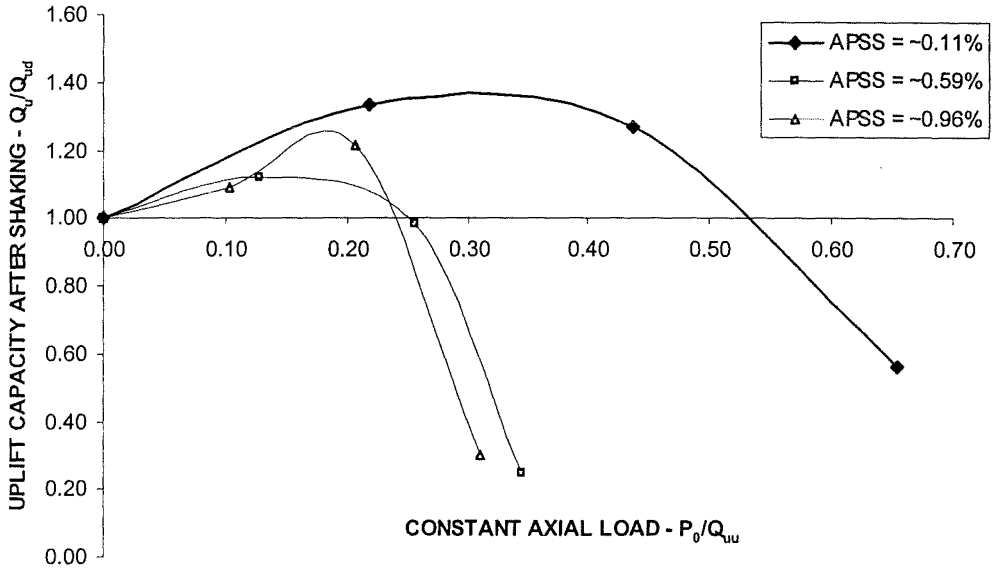

Figure 7.11 –Uplift Capacity Normalised by Uplift Capacity After Shaking Only versus Constant Axial Load Normalised by Uplift Capacity During Shaking

Figure 7.11 shows that, regardless of the level of shaking, there will be an increase in uplift capacity if a low level constant axial load is applied to the drilled shaft during shaking. If the axial load is less than approximately 25 percent of Q_{uu} then the uplift

capacity of the drilled shaft will increase after shaking. If the constant axial load exceeds 25 percent of Q_{uu}, however, then the static uplift capacity will be greatly reduced after strong soil shaking. The reductions in uplift capacity coincide with the large upward displacements seen in Figure 7.10 for the corresponding constant axial loads and levels of shaking.

If the level of shaking is low then the static uplift capacity will continue to increase until the constant axial load exceeds approximately 55 percent of Q_{uu}. If the axial load increases above approximately 55 percent of Q_{uu} at low levels of shaking then large reductions will occur in the uplift capacity of the drilled shaft. Again, the reductions in uplift capacity coincide with the large upward displacements seen in Figure 7.10.

7.6 CYCLIC AXIAL LOAD APPLIED DURING SHAKING

Cyclic axial loads were applied to fifteen model drilled shafts while the soil deposit was shaken. At the end of shaking, each drilled shaft was tested in monotonic uplift to determine the uplift capacity. The results from these tests are summarised in Table 7.4. All the axial loads were applied about a zero mean load because this had been shown from the cyclic tests in a static soil deposit to be the worst case loading configuration. All the tests were performed at approximately the same level of shaking so that the parameters under investigation were limited to the cyclic axial load amplitude and the phase difference between axial loading and soil shaking.

Table 7.4 –Test Results for Cyclic Axial Load applied during Soil Shaking

Test	Table Amplitude (mm)	Cyclic Axial Load Amplitude (kN)	Phase difference (degrees)	APSS (%)	Soil Settlement (mm)	Shaft Displacement (mm)	Uplift Capacity Q_u (kN)
301	45	0.64	90		Data Lost		3.75
302	45	0.64	90	1.56	-76	-43	3.80
303	45	0.64	0	1.38	-78	-33	4.00
304	45	0.77	90	1.40	-69	-35	3.79
305	45	0.90	90	1.39	-72	-34	3.75
306	45	1.02	90	1.32	-71	-26	3.78

307	45	1.15	90	1.30	-66	-27	4.22
308	45	1.41	90	1.55	-71	-30	3.99
309	45	1.66	90	1.48	-71	-15	4.22
310	45	1.92	90	1.48	-74	27	Failure
311	45	1.92	0	DataLost	-76	35	Failure
312	45	1.664	0	1.44	-71	26	Failure
313	45	1.41	0	1.39	-70	-29	4.58
314	45	1.54	0	1.46	-68	4	1.98
315	45	1.79	90	1.40	-67	14	2.90

The test results show that some of the drilled shafts were stable during shaking while others failed in uplift. Changes in uplift capacity were found for many of the drilled shafts after shaking.

The results from a typical stable test (304) are shown in Figure 7.12. The cyclic axial load amplitude was 0.77 kN and the APSS was 1.40 percent. The phase difference between peak axial load and maximum soil displacement was 90 degrees. Also shown for comparison in Figure 7.12 is the displacement trace of a drilled shaft (Test 316) at approximately the same APSS (1.50 percent) but with zero axial load.

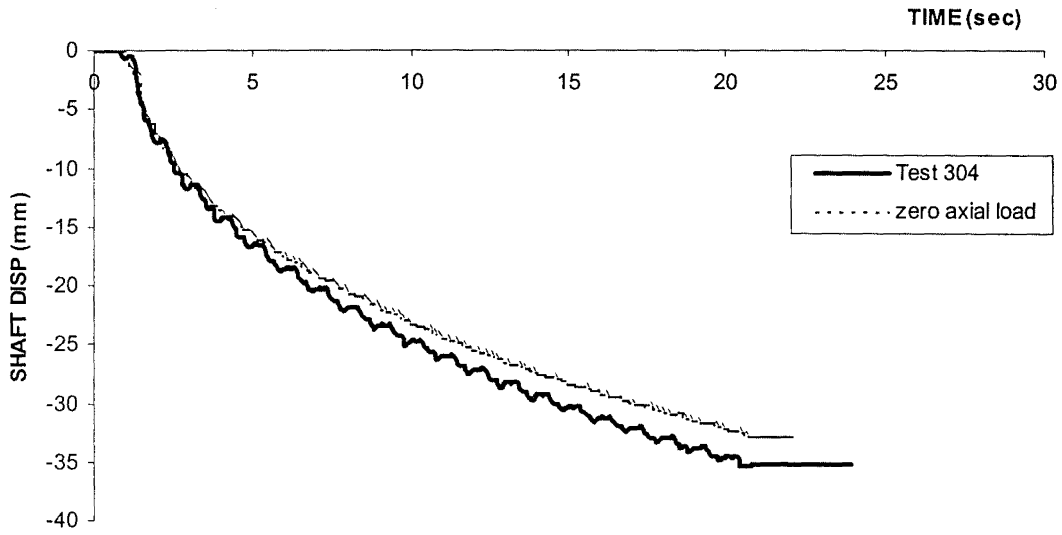

Figure 7.12 – Drilled Shaft Displacement versus Time for Cyclic Axial Load Test 304

The results from a typical unstable test (310) are shown in Figure 7.13. The cyclic axial load amplitude was 1.92 kN and the APSS was 1.48 percent. The phase difference between peak axial load and maximum soil displacement was 90 degrees. The test was terminated when the limit was reached on the hydraulic actuator.

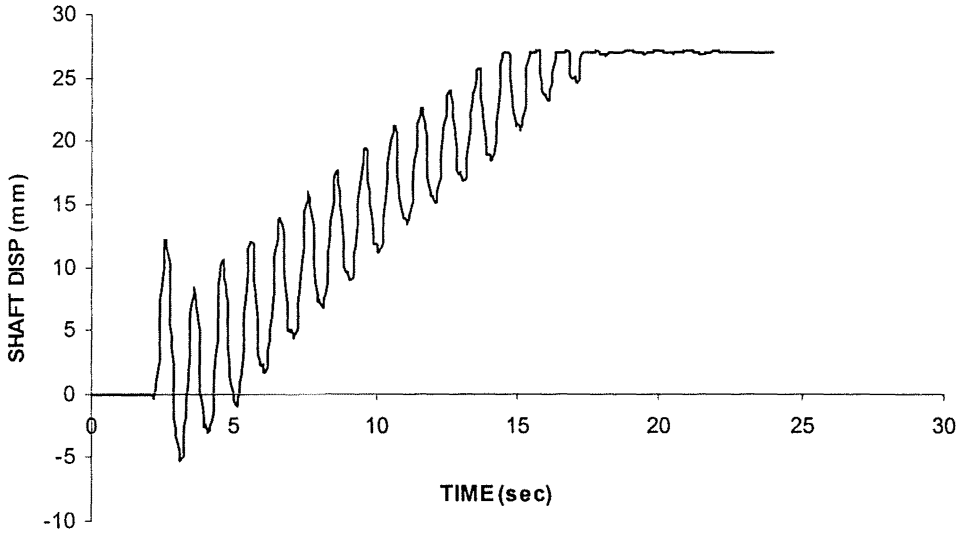

Figure 7.13– Drilled Shaft Displacement versus Time for Cyclic Axial Load Test 310

The displacement results from the cyclic axial load tests have been summarised in Figure 7.14. The displacement of the drilled shaft after shaking is plotted against the cyclic axial load amplitude, with the cyclic axial load normalised by the static uplift capacity during soil shaking (Q_{uu}). The test results have been divided into two groups according to phase difference between peak axial load and peak soil displacement.

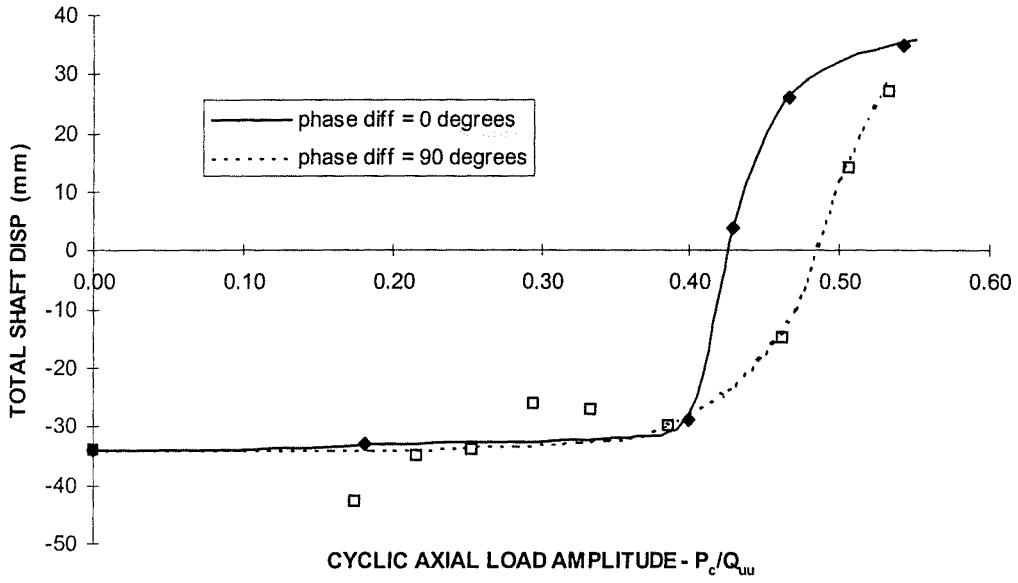

Figure 7.14 - Total Shaft Displacement versus Cyclic Axial Load Amplitude Normalised by Uplift Capacity During Shaking

Figure 7.14 shows that the shaft undergoes a relatively constant downward displacement if the axial load is less than approximately 40 percent of Q_{uu}. If, however, the axial load is greater than approximately 40 percent of Q_{uu} then large upward displacements occur as the drilled shaft is pulled out of the soil deposit during shaking. The results show that phase difference has only a minor effect, with small increases in cyclic axial load above 40 percent causing larger upward displacements when the phase difference is zero. The point of shaft instability changes little when the phase difference is changed from 0 to 90 degrees.

The results from these tests show that the uplift capacity after shaking is affected by the cyclic axial load. Figure 7.15 shows the results from the monotonic uplift tests performed after soil shaking. The cyclic axial load amplitude (P_c) is normalised by the static uplift capacity during shaking (Q_{uu}). The uplift capacity after shaking with cyclic axial load (Q_u) has been normalised by the static uplift capacity after shaking with no axial load (Q_{ud}). The test results have been divided into two groups according to phase difference between peak axial load and peak soil displacement.

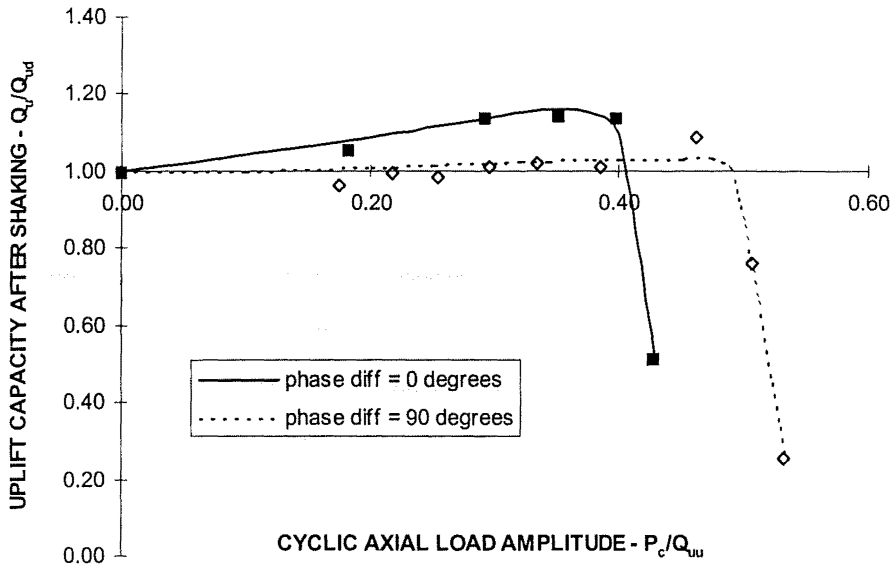

Figure 7.15 – Uplift Capacity Normalised by Uplift Capacity After Shaking Only versus Cyclic Axial Load Normalised by Uplift Capacity During Shaking

The results from these tests show that, like the tests in a static soil deposit, the shaft becomes unstable under cyclic axial loads that are less than the static uplift capacity. The results show that, in the worst case, the shaft undergoes a rapid reduction in capacity if the cyclic axial load amplitude exceeds approximately 40 percent of Q_{uu}. The phase difference between peak axial load and peak soil displacement appears to have a small influence on the point of instability. If the shaking is in phase with the axial load then instability occurs at 40 percent of Q_{uu} but if the shaking is out of phase then instability does not occur until the cyclic axial load amplitude exceeds approximately 50 percent of Q_{uu}. Phase difference also appears to have some effect on the uplift capacity of the stable shafts. For cyclic axial loads that are less than 40 percent of Q_{ud}, there appears to be a significant capacity increase for in-phase loading but very little increase for out-of-phase loading.

The reductions in uplift capacity seen in Figure 7.15 coincide with the large upward displacements seen in Figure 7.14 for cyclic axial loads above approximately 40 percent of Q_{uu}.

SUMMARY

Axial load tests were performed on model drilled shaft foundations while the surrounding soil deposit was shaken under simulated seismic shear loading.

The first tests were monotonic uplift and monotonic compression tests, performed to determine the equivalent static capacities of the drilled shaft. These tests were performed in soil deposits that had not been shaken. The static uplift capacity (Q_{us}) of the drilled shaft was found to be 1.28 kN and the compressive capacity (Q_{cs}) was found to be 1.98 kN.

The second set of tests were performed with no axial load on the drilled shafts while the soil deposits were shaken. These tests were performed to determine the effects of shaking on static shaft capacity. It was found that the uplift capacity (Q_{ud}), increased as the level of shaking increased. The capacity increases were most likely due to increases in soil density that occurred when the soil was shaken. A parameter called the Average Peak Shear Strain (APSS) was developed to quantify the magnitude of soil motion and a correlation was then found between the APSS and the uplift capacity after shaking (Q_{ud}). The correlation between APSS and Q_{ud} allowed the capacity changes due to soil shaking to be distinguished from the capacity changes due to any applied axial loads. The settlement of the soil occurred non-linearly throughout the test so the static uplift capacity changed non-linearly from Q_{us} before the test to Q_{ud} after the test. To account for this, a further parameter was developed as an indication of the static uplift capacity during shaking. The static uplift capacity during shaking, Q_{uu} was arbitrarily taken as the uplift capacity at the mid-point of the test. The capacity was assumed to increase in the same manner as the soil settled so Q_{uu} was taken to be the static capacity, Q_{us}, plus 89 percent of the increase due to shaking.

The third set of tests were performed with constant axial load on the drilled shaft while each soil deposit was shaken. These tests were performed to determine the dynamic uplift capacity of the shaft during shaking. It was found that the shaft failed in uplift during low level shaking if the axial load exceeded approximately 55 percent of the equivalent static capacity, Q_{uu}. If the level of shaking was increased, then the

shaft failed in uplift if the constant axial load exceeded approximately 25 percent of Q_{uu}. The tests showed therefore that an increase in the level of shaking brought a decrease in the uplift capacity of the shaft during shaking. The tests also showed that the capacity of the drilled shaft was found to increase if it did not fail during shaking.

The fourth set of tests was performed with cyclic axial load applied to the drilled shaft while the soil deposit was shaken. The amplitude of cyclic axial load was varied from test to test, as was the phase difference between peak axial load and peak soil displacement. All the tests were performed at zero mean load and at the same level of shaking in order to limit the number of parameters under investigation. The test results showed that the drilled shaft became unstable at a cyclic axial load amplitude of 40 percent of the equivalent static capacity Q_{uu} if the loading was in phase. If the cyclic axial load was out of phase with the soil displacement then the drilled shaft became unstable at a load amplitude of 50 percent of Q_{uu}. The test results also showed that if the drilled shaft remained stable during the test, there was an increase in shaft uplift capacity for in-phase loading but little increase in capacity for out-of-phase loading.

Chapter Eight

THE AXIAL LOAD RESPONSE OF MODEL DRILLED SHAFTS IN SHAKING SOIL DEPOSITS.

INTRODUCTION

The axial load tests in a shaking soil deposit showed that the capacity of a drilled shaft changes if the soil around it is shaken. The tests showed that the capacity increases if there is no axial load on the drilled shaft during shaking but the capacity may decrease if the drilled shaft is simultaneously subjected to a constant or cyclic axial load.

This chapter attempts to explain the response of the drilled shaft under these loads. The explanation makes use of the various test results and ties them in with the conceptual shear zone model developed earlier. In this way a possible mechanism is offered for the axial load response of drilled shaft foundations in a shaking soil deposit.

8.1 SOIL RESPONSE DURING SHAKING

The response of the laminar tank and the soil within it were outlined in Section 6.7. From this, the response under cyclic shaking may be summarised by the following three points:

- The deflected shape of the soil deposit is approximately linear during shaking so the shear strain within the soil is approximately constant over the height of the soil deposit.
- The magnitude of the shear strain depends on the magnitude of table shaking and on the number of cycles of shaking. The soil stiffens up with each successive cycle, thus reducing the peak shear strain.

- The shear strain causes the soil to settle during shaking. It is the settlement that brings about the increase in soil stiffness. The amount of settlement is proportional to the magnitude of shear strain and the distribution of settlement is approximately constant over the height of the soil deposit.

There are two factors that significantly affect the response of the soil deposit. The first is inelastic shear strain and the second is settlement. Inelastic shear strain causes the soil response to soften while settlement stiffens the soil up. The two are therefore opposing in their effect on the soil but they are also interconnected because the settlement is largely a result of the shear strain.

Inelastic shear strains can be determined from the stress/strain response of the soil deposit during shaking. The shear stress and shear strain are calculated using a lumped mass model similar to that shown in Chapter 2. The lumped mass model divides the sand deposit into discrete masses whose depths coincide with the heights of the linear potentiometers, as shown in Figure 8.2. The shear strains are calculated from the relative displacements at the top and bottom of each mass. The shear stresses are calculated from the force required to accelerate each lumped mass. The accelerations of each mass are derived from the second time derivative of the average displacement of each mass.

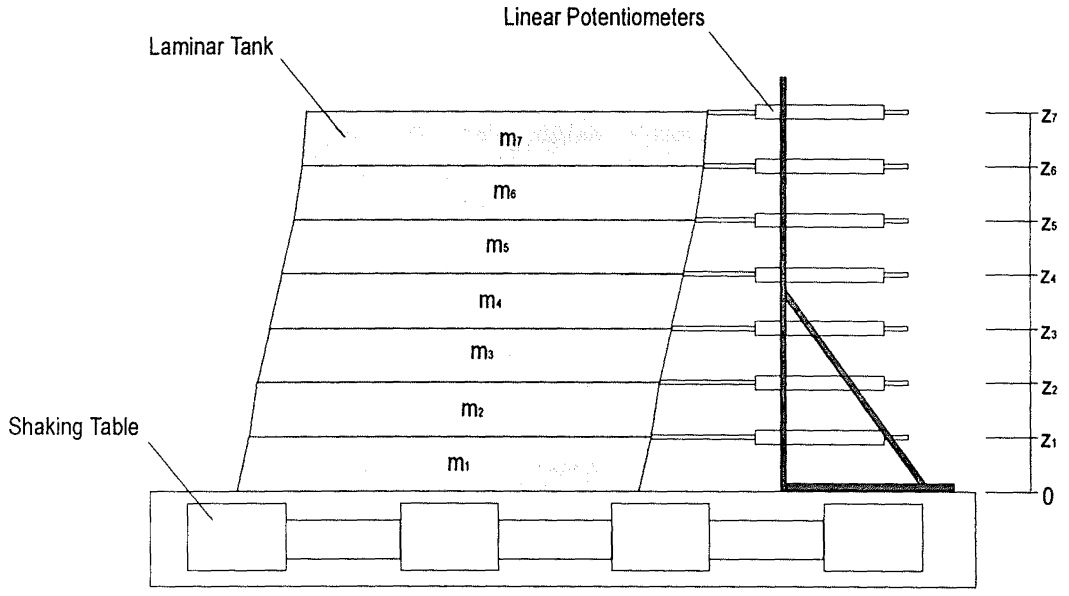

Figure 8.1 – Division of Soil Deposit into Discrete Masses for Lumped Mass Model

The lumped mass model has been used to calculate the stress/strain response of a typical soil deposit and the response is shown in Figure 8.1. The plot shows the stress/strain response at the mid-height of the soil deposit during the fourth cycle of Test 308.

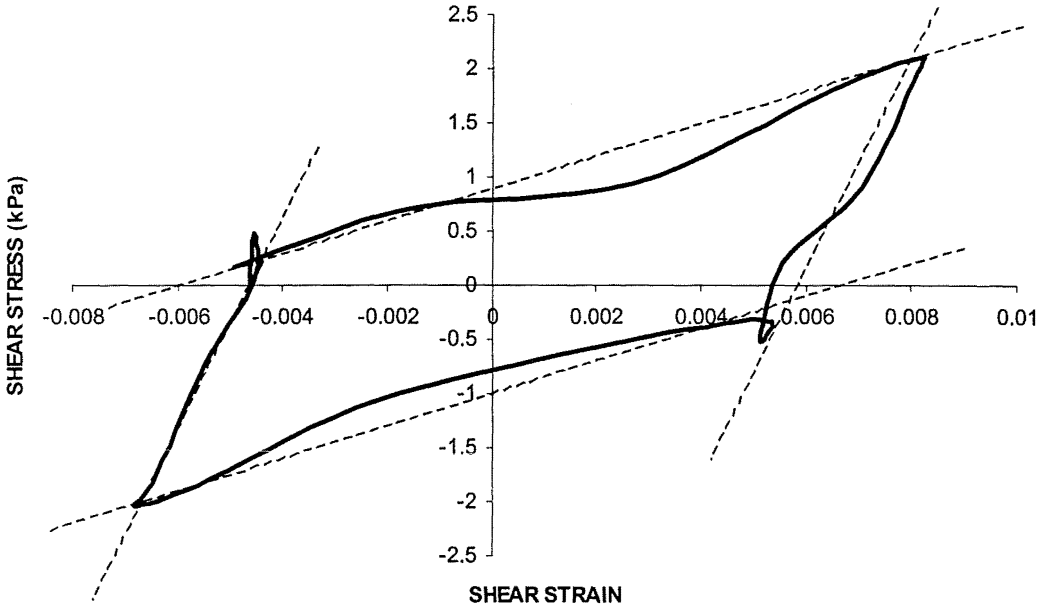

Figure 8.2 – Stress/Strain Response at Mid-height of Soil Layer during Fourth Cycle of Test 308

Figure 8.2 shows that there is a large part of the cycle where the response is inelastic and the stiffness is significantly reduced (the stiffness is shown by the slope of the line). The lower stiffness means that the soil softens during part of the shaking cycle and larger shear strains occur for small increases in shear stress.

Large shear strains cause settlement. As the number of cycles increases, the soil settles further and its density increases accordingly. The increase in density brings a corresponding increase in the overall stiffness of the soil deposit. The increase in stiffness is shown by a reduction in peak shear strain or, similarly, as a reduction in peak soil displacement during the test, as shown in Figure 8.3.

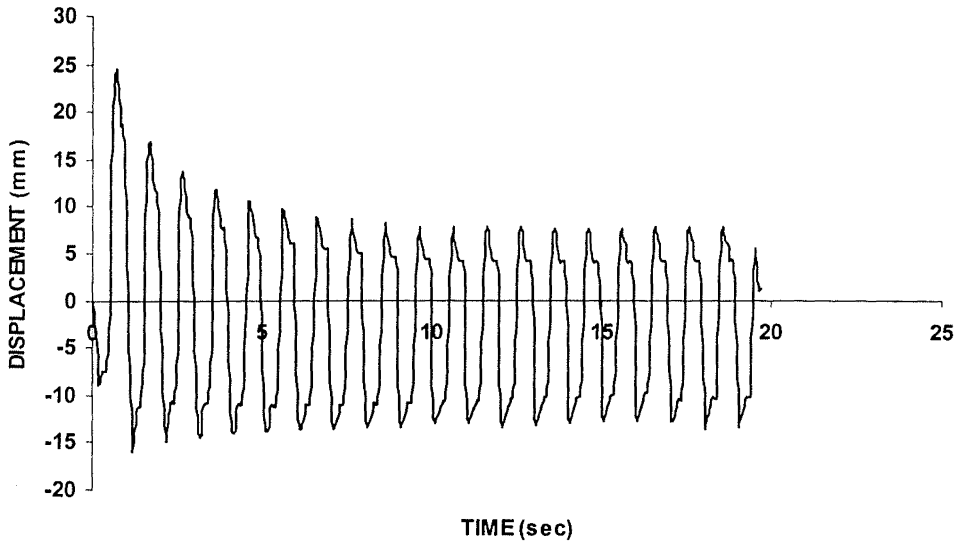

Figure 8.3 –Displacement at Top of Tank During Cyclic Shaking

8.2 SHAFT RESPONSE DURING SHAKING WITH NO AXIAL LOAD

It was shown in Chapter 7 that the static uplift capacity of the drilled shaft increases if the surrounding soil deposit is shaken. The increase in capacity was found to be proportional to the magnitude of soil shaking. The following section explains the increase in capacity in terms of the conceptual shear zone model developed earlier, with reference to particular results collected during the tests.

If no axial load is applied to the head of the drilled shaft then the increase in uplift capacity must come from changes within the soil deposit. Those changes that could affect the stability of the drilled shaft include changes in soil density, soil stiffness and horizontal soil stress.

8.2.1 Soil Density

It has been shown that the density of the soil increases during shaking because the soil settles under the repeat cycles of shear strain. Figure 8.4 shows the settlement after cyclic shaking at an APSS of 1.4 percent. The plot shows that the settlement is reasonably uniform over the height of the soil deposit so the soil deposit could be seen

as a homogenous soil layer of increased density. Superimposed over the soil settlement is the overall settlement of the drilled shaft after the same level of shaking.

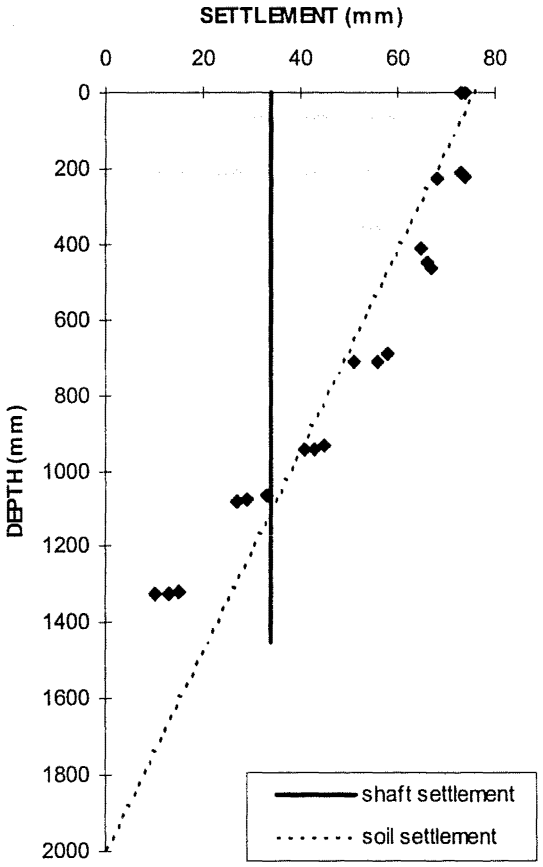

Figure 8.4 – Soil Settlement and Shaft Settlement after Shaking

It is clear from Figure 8.4 that there are varying degrees of differential settlement between the soil and the drilled shaft after shaking. There is only one point on the shaft (at approximately 1100mm) that settles by the same amount as the surrounding soil. The soil settles more than the shaft at all points above this and the soil settles less than the shaft at all points below this. The differential settlement means that there is a relative axial displacement between the shaft and the soil over most of the buried length. It is likely, therefore, that a shear zone develops along the shaft during settlement of the soil deposit because the relative displacement causes the soil to shear. It is also likely that the shear zone will have a different density to the surrounding soil mass because it dilates as it shears so its density decreases.

The soil deposit can therefore be seen as a uniformly densified soil mass that surrounds a lower density shear zone around the drilled shaft.

8.2.2 Soil Stiffness

The soil mass will not only have been densified but it will also have stiffened after the shaking. As shown in Figure 8.3, the peak displacement of the soil mass decreases with each consecutive cycle of shaking so the overall stiffness must be increasing with each cycle. The soil deposit can therefore be seen as a uniformly densified and stiffened soil mass that surrounds a lower density shear zone around the drilled shaft.

8.2.3 Horizontal Soil Stress

The test results do not show the horizontal stress adjacent to the shaft after shaking because no zero axial load tests were performed with the soil stress transducer beside the shaft. However, several tests were performed with the soil stress transducer placed away from the drilled shaft so changes in horizontal stress can be determined for the surrounding soil mass. The results from these tests are shown in Figure 8.5, with the changes compared to the calculated horizontal stress profile before shaking.

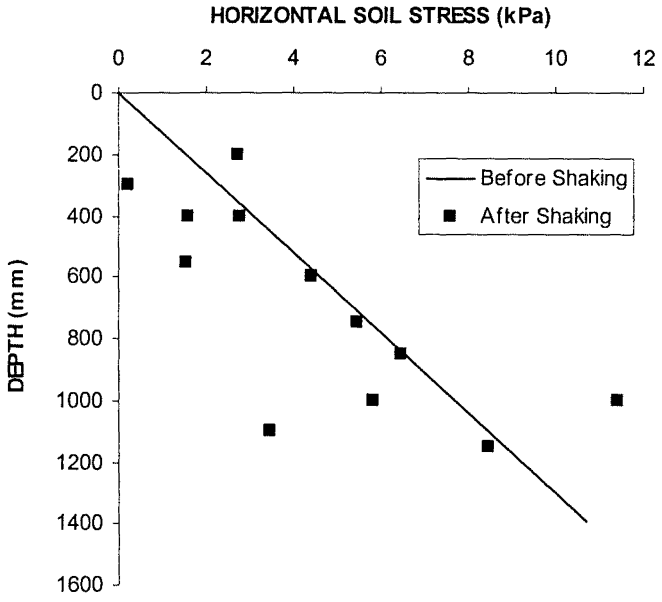

Figure 8.5 – Change in Free-Field Horizontal Soil Stress after Shaking

Figure 8.5 shows that there is no significant trend in the horizontal soil stress change over the depth of the soil deposit after shaking. Some of the measurements show an increase and some show a decrease but in general there is no significant trend. The larger changes may be due to abnormal initial conditions around the stress cell during soil placement.

The changes in soil density, soil stiffness and horizontal soil stress can now be brought together to describe the soil deposit and the embedded drilled shaft after soil shaking. The soil mass after shaking can be seen as a uniformly densified soil mass with an increased stiffness but with a similar horizontal soil stress profile. The soil mass surrounds a lower density shear zone that has undergone varying degrees of shear strain over the length of the drilled shaft. The shear zone surrounds the drilled shaft, that has settled uniformly during shaking.

The increase in static uplift capacity after shaking can now be explained. The monotonic axial load is applied to the drilled shaft in the shaken soil deposit and the shear zone around the shaft dilates as the shaft displaces upward. However, there is now a greater resistance to the dilation because the stiffness and density of the surrounding soil mass have increased. A greater axial load must therefore be applied to cause the drilled shaft to fail in uplift.

8.3 SHAFT RESPONSE DURING SHAKING WITH CONSTANT AXIAL LOAD

It was shown in Chapter 7 that the drilled shaft failed in uplift under strong soil shaking at constant axial uplift loads that were as little as 25 percent of the equivalent static capacity. The decrease in uplift capacity was found to be proportional to the magnitude of soil shaking. The following section explains the decrease in capacity in terms of the conceptual shear zone model developed earlier, with reference to particular results collected during the tests.

The loss of uplift capacity seen under constant axial load is to be expected because there are considerable differences between the soil conditions during shaking and the

soil conditions either before or after shaking. During shaking, the soil is under dynamic conditions and, as shown by the stress/strain curve in Figure 8.1, the soil behaves inelastically for a significant part of the shaking cycle. During the inelastic response the stiffness is markedly reduced so the soil is able to undergo large shear strains for relatively small increases in shear stress. The reduction in stiffness during shaking means that the drilled shaft is able to shear more readily so a lower load is required to fail the shaft in uplift.

These test results show that the shear zone model is still applicable in a shaking soil deposit. The presence of a shear zone is indicated by the abrupt change from stable to unstable response and the low residual uplift capacity if the drilled shaft fails during loading. The abrupt change from stable to unstable response is due to failure of the shear zone during axial loading. If there were no shear zone then there would be a more gradual failure region as increasing axial loads brought increasing amounts of upward displacement during the inelastic shear straining of each shaking cycle. The low residual uplift capacity of the shaft is also due to failure of the shear zone. If there were no shear zone then each half cycle of inelastic shear strain would remould the soil around the drilled shaft. Any changes, due to the axial load, during the previous half cycle would then be erased and the residual uplift capacity of the drilled shaft would remain the same as that under zero axial load.

The shear zone model works as follows during shaking: As the axial load is applied, the material in the shear zone begins to dilate and increase in volume. Under static soil conditions, the surrounding soil mass confines the dilating shear zone, opposing the volume increase and providing the drilled shaft with its static axial capacity. Under dynamic soil conditions, the mechanism is similar but the amount of shear zone confinement has changed. When the soil is undergoing inelastic shear strains during each shaking cycle, it has a much lower stiffness so it provides less confinement to the dilating shear zone. The shear zone can increase in volume more readily and a lower magnitude axial load is therefore required to fail the drilled shaft in uplift.

8.4 SHAFT RESPONSE DURING SHAKING WITH CYCLIC AXIAL LOAD

The behaviour of the drilled shaft during shaking under cyclic axial load is an extension of the behaviour under constant axial load. In terms of the conceptual shear zone model, the surrounding soil mass undergoes inelastic shear strains which cause the soil mass to settle and increase in stiffness over consecutive cycles of shaking. During these cycles, the shear zone forms around the drilled shaft as the soil settles by different amounts at different depths. Any axial load that is applied to the drilled shaft must then be resisted by the shear zone and the softened soil mass.

In the case of cyclic axial load, the shear zone dilates as the direction of displacement is reversed on each half cycle. If the surrounding soil mass is sufficiently stiff then the dilation will be resisted and the drilled shaft will remain stable. A clear illustration of this can be seen in Figure 8.5, where the soil mass is initially too soft and the drilled shaft begins to fail in uplift. However, in the fourteenth cycle of shaking the soil mass reaches the required stiffness through settlement and the drilled shaft restabilises.

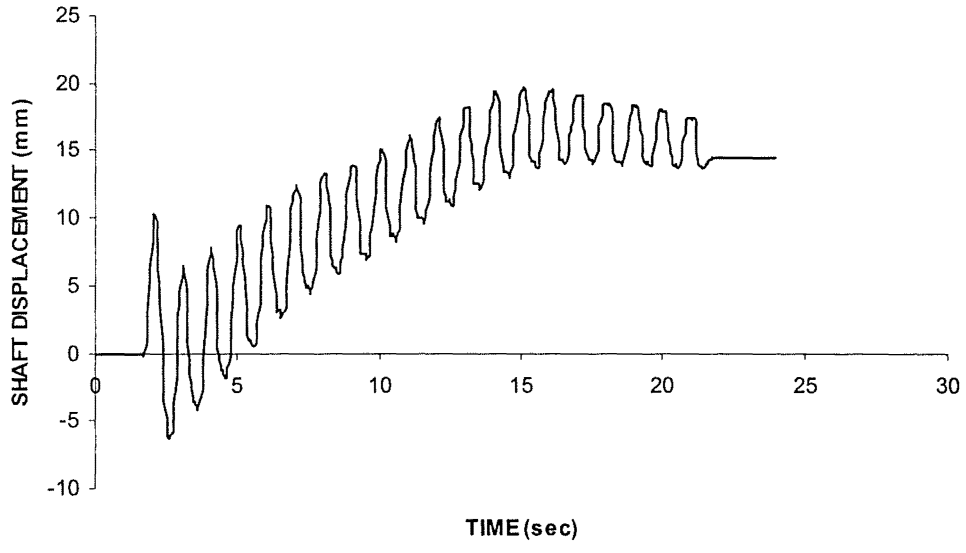

Figure 8.5 – Axial Shaft Displacement versus Time for Cyclic Axial Load Test 315.

Although Test 315 restabilised during the shaking test, its static uplift capacity after shaking was still reduced. The reason for this may be that the shear zone had failed by exceeding peak dilation during cyclic axial loading. When the monotonic uplift was applied after shaking, there was less dilation of the shear zone so the uplift capacity was less than the static uplift capacity without cyclic axial loading. This is despite the surrounding soil mass having densified and stiffened during shaking.

The reason that the cyclic axial load tests were more stable than the constant axial load tests may be because the overall or mean load during the cyclic tests was zero. For each half cycle in uplift there was a corresponding half cycle in compression so the upward displacements during shaking were partially countered by the downward displacements. With lower overall displacements of the drilled shaft there would be a lower overall amount of uplift shearing within the shear zone so the uplift capacity after shaking would be greater than that for constant axial loads.

The reason for the different in-phase and out-of-phase shaft responses is unclear from the test results but may possibly be due to a reduction in tip resistance during the compression part of out-of-phase loading. For out-of-phase loading, the soil undergoes inelastic shear strain as the axial load reaches peak compression. The inelastic response of the soil is softer so there is less resistance beneath the tip of the drilled shaft. A reduction in tip resistance allows greater downward displacement during compression loading so the overall shearing within the shear zone is less than for in-phase loading. Lower overall shear strain would mean that the drilled shaft would remain stable at higher cyclic axial load amplitudes.

SUMMARY

Axial load tests were performed on model drilled shaft foundations in a shaking soil deposit. A number of tests were performed with zero axial load on the drilled shaft and the uplift capacity after shaking was found to have increased. Further tests were performed with either constant or cyclic axial loads on the drilled shaft during shaking and the drilled shaft was found to fail at axial load magnitudes that were considerably lower than the equivalent static capacity.

Observations from the tests have been presented in conjunction with the conceptual shear zone model developed earlier. Together they are used to offer a possible mechanism for the behaviour of the drilled shaft during shaking.

When the soil is shaken, it settles under the repeat cycles of shear strain. The settlement profile is reasonably linear over the depth of the soil deposit while the settlement of the rigid drilled shaft is constant. This differential settlement may lead to the development of a shear zone around the shaft while the surrounding soil mass settles by differing amounts. The settlement of the soil mass causes its density to increase and its stiffness to increase also.

When the drilled shaft is failed in monotonic uplift at the end of shaking the increased stiffness of the surrounding soil mass offers a greater resistance to dilation of the shear zone. So, for drilled shafts with zero axial load during shaking, a greater peak load is then required to fail the shaft in uplift.

If a constant axial load is applied to the drilled shaft during shaking then, in most cases, the capacity will differ from that of a drilled shaft under the same level of shaking but with zero axial load. At axial loads of only 25 percent of the static uplift capacity, the drilled shafts were found to fail in uplift during strong shaking. The reduction in uplift capacity may arise from a reduction in stiffness of the soil mass during shaking. The peak shear strength of the shear zone is reduced because it can dilate more readily so the drilled shaft fails during loading at lower axial loads. Its uplift capacity after shaking is also reduced to a residual capacity because the shear zone has exceeded the peak dilation during shaking.

The response of the drilled shaft during shaking and cyclic axial loading is an extension of the response under constant axial load. As the cyclic axial load is applied, the shear zone dilates and expands against the softer soil mass. Less resistance is offered by the softer soil mass so the drilled shaft fails at lower axial load amplitudes than it does under static soil conditions. The load amplitude causing failure is greater for cyclic axial loads than for constant axial loads. The reason for this may be that the cumulative displacement is less for cyclic loading because each half cycle of upwards displacement is offset by each half cycle of downward displacement.

The effects of cyclic axial shaft loading and cyclic soil shaking have therefore been explained in terms of a conceptual shear zone model that surrounds the drilled shaft. The behaviour of the shear zone depends upon the type and magnitude of axial load applied to the shaft and on the level of shaking within the surrounding soil mass.

Chapter Nine

SUMMARY AND RECOMMENDATIONS

Deep foundations are subjected to variations in load during an earthquake. Extra loads may be exerted on the foundation head by the inertial actions of the supported structure and they may be exerted along the buried length of the foundation by the dynamic actions of the surrounding soil mass. The loads are usually of short duration and of a magnitude lower than the static capacity of the foundation, but the cyclic nature of these loads has been found to degrade the strength of the foundation and to cause failure at loads less than the static capacity.

This study investigated the specific case of drilled shaft foundations embedded in a cohesionless soil deposit and subjected to the dynamic loads typical of a seismic event. The study was experimentally based and the methodology, findings and recommendations are summarised in this chapter.

9.1 FOUNDATION LOADS

During an earthquake, the earth's crust ruptures and releases stored strain energy in the form of seismic waves. These waves radiate out from the point of rupture and are felt at the surface as an earthquake.

The majority of the seismic energy is transmitted as shear (s) waves and successive layering of the geologic material near the earth's surface means that these shear waves are refracted towards the vertical as they approach the surface. When they reach the surface, they are felt as horizontal accelerations and displacements. The accelerations and displacements are cyclic in nature and may be represented by an equivalent number of horizontal accelerations or displacements, where the amplitude, frequency and number of cycles may be chosen to represent the magnitude of the seismic event.

The response of the ground during an earthquake depends upon the properties of the ground itself. If the ground is soft soil then the seismic waves may be amplified as they approach the surface.

If a deep foundation is embedded in the soil mass, then it too will be subjected to dynamic loads as the soil reacts to the imposed accelerations. Further loads are applied to the foundation as it resists the inertial displacements and accelerations of the supported structure.

9.2 MODEL STUDY

The seismic response of drilled shaft foundations was investigated experimentally by constructing and load testing several similar model drilled shafts under different combinations of axial and shear load. The model drilled shafts were tested in laboratory prepared cohesionless soil deposits.

The experimental study was performed in two distinct stages. The first stage had different combinations of cyclic axial load and constant mean load applied to the head of the shaft while it was embedded in a static soil deposit. The second stage of testing had either constant or cyclic axial load applied to the head of the shaft while the shaft and the surrounding soil mass were simultaneously shaken at the base of the soil deposit.

Two cylindrical tanks, each 1.00 m diameter by 1.99 m high were constructed to contain the soil for the first stage of testing. A gate was constructed in the base of each tank, allowing one tank to be emptied directly into the other and thus avoiding double handling of the soil. Each soil deposit was prepared by air pluviation, with the soil falling from the full tank, into a funnel and hose system, then discharging through a diffuser into the bottom tank. This method produced near-homogeneous soil deposits with a relative density of approximately 31 percent.

The soil used for all the tests in this study was a commercially available, industrial grade 30/60 silica sand. The reasons for selecting this soil were: (a) It is a generic

particulate material that should qualitatively simulate the behaviour of a range of different soils. (b) It is suitable for air pluviation. (c) It is suitable for being reused many times without degradation. (d) It should be possible to obtain additional supplies of the material for future testing. (e) It is very clean and minimal dust is generated during air pluviation.

Twenty-seven model drilled shaft foundations were tested in the first stage of the study. Each foundation was nominally the same size at 95 mm diameter by 1450 mm buried length. The foundations were constructed from Portland Cement concrete and reinforced with a single 16 mm diameter deformed steel reinforcing rod that was placed centrally within each shaft.

Construction of each shaft involved a casing being buried in the soil as the deposit was being prepared. When the deposit was complete, the reinforcing rod and the concrete were placed in the casing, then the casing was removed. The concrete was left to cure for 24 hours before testing.

Loads were applied to the model drilled shaft by a hydraulic actuator connected to a closed-loop electro-hydraulic control system. The loads were generated by a PC, downloaded to a waveform generator, then downloaded to the control system. The load and displacement data were automatically recorded via a high-speed data acquisition system connected to the PC. Soil stress measurements were also automatically recorded with a stress transducer buried alongside the drilled shaft.

Each load test had the selected mean load applied to the drilled shaft and kept constant for 100 seconds before the selected cyclic axial load was applied. Twenty cycles of sinusoidal load were applied at a frequency of 1 Hz then the drilled shaft was immediately failed in uplift to determine its residual uplift capacity after cyclic loading. The residual uplift capacity was compared to reference values for a drilled shaft loaded monotonically to failure with no cyclic loading.

Stage II of the experimental study had cyclic base shaking applied to the soil mass while the embedded drilled shaft was simultaneously subjected to either constant or cyclic axial loads. A new laminar tank was constructed for these tests so that the soil

mass could deflect in shear and thus create a free-field soil response to the horizontal shaking. The laminar tank was constructed from 50 mm thick steel channel laminates that were stacked up and confined within a steel frame. The tank had internal dimensions of 0.8 m by 1.8 m by 2.0 m high. The laminates were separated by Teflon sliders to reduce friction and the tank was lined internally with a rubber membrane to contain the soil.

The same industrial grade silica sand was used for the Stage II tests and, again, the deposits were prepared by air pluviation. However, changes were made to the preparation method for the second stage of testing. The increased tank size meant that a hopper and storage system was required for these tests and the increased time of sample preparation meant that changes were required for the diffuser. To reduce preparation time, the diffuser size and flow-rate were increased, which gave an average relative density for each deposit of approximately 46 percent.

Changes were also made to the drilled shaft for the second stage of testing. To avoid the 24 hour curing period required for the cast in-situ reinforced concrete shaft, an artificial concrete shaft was constructed from steel tube that was coated in sand encrusted epoxy resin. The resin was added to model the roughness of the cast in-situ concrete. The steel drilled shaft also had a diameter of 95 mm and a buried length of 1450 mm and the gauge of the steel was chosen to give the steel shaft a flexural stiffness similar to that of the reinforced concrete shaft. The same artificial drilled shaft was used for the 44 tests performed in the laminar tank.

Axial loads were applied to the model drilled shafts with the same hydraulic actuator used in the Stage I tests. The shaking was applied to the soil deposit via a shaking table. The laminar tank was bolted to the 4.0 m by 2.0 m shaking table and subjected to cyclic horizontal base displacements. The displacements of the table were controlled by a separate closed-loop servo-hydraulic actuator, running on a separate PC.

The following measurements were made during each test and the results recorded on a PC-based data acquisition system:

- Shaking Table Displacement – with a linear potentiometer attached to the table

- Shaking Table Acceleration – with an accelerometer attached to the table
- Tank Acceleration – with an accelerometer attached to the top of the tank
- Tank Displacement – with an array of linear potentiometers alongside the tank.
- Soil Surface Settlement - with a linear potentiometer attached to the tank frame

Manual measurements were also taken of the total settlement occurring at different depths during each test.

The laminar tank performed as designed under cyclic base shaking. The response was a predominantly shear response and compared favourably with the calculated theoretical shear response of a similar soil layer. The deflected shape of the tank can be assumed as linear during shaking so the shear strain during shaking can be assumed as constant over the depth of the soil deposit. A parameter called the Average Peak Shear Strain (APSS) has been developed to quantify the soil response to cyclic shear loading. The APSS is taken as the peak shear strain at each half cycle of loading, averaged over the height of the soil column and averaged over the number of cycles of loading. The APSS values for these tests ranged from 0.10 percent to 1.56 percent.

The following parameters were investigated during the drilled shaft tests in the laminar tank.

- Shear load Amplitude. Similar axial loads were applied to drilled shafts while the amplitude of the shaking was changed for different tests.
- Dynamic Uplift Capacity. The uplift capacity of the drilled shaft during cyclic soil shaking was determined. Constant axial load was applied to the shaft while the soil mass was subjected different magnitudes of cyclic shaking and the axial load causing failure was determined.
- Dynamic Cyclic Uplift Capacity. The uplift capacity was determined under combined cyclic axial shaft loading and cyclic soil shaking.
- Phase Difference. The effects of phase difference between peak axial load and peak soil displacement were investigated.

9.3 TEST RESULTS

Stage 1

The test results showed that the drilled shaft may fail during cyclic axial loading at load magnitudes that are less than the equivalent static uplift capacity. The cyclic load causing failure was found to depend upon the mean load on the drilled shaft. There is little degradation of shaft capacity if the shaft is subjected to one-way loading, with the direction of applied load not changing during the test, i.e. cycling in compression only or uplift only. If however, the shaft is subjected to two-way loading, where the load is reversed twice in each cycle, then the model drilled shaft may suffer some degradation in uplift capacity and fail at uplift load magnitudes that are less that the static uplift capacity. The worst case load configuration occurs at zero mean, where the shaft fails at an uplift load magnitude that is 67% of the equivalent static uplift capacity.

If the model drilled shaft remains stable under the applied loads then little change is observed in its uplift capacity.

Stage 2

The test results showed that when the soil is shaken, its density increases with each cycle and its overall stiffness also increases. If a drilled shaft is embedded in that soil and it carries no axial load then its uplift capacity is found to increase after the soil around it is shaken. The amount by which the capacity increases depends upon the level of soil shaking. Greater levels of shaking bring greater increases in uplift capacity. They also bring greater amounts of soil settlement.

If the drilled shaft carries a constant axial load while the soil around it is shaking then it may fail in uplift during the test. The load magnitude causing uplift failure depends upon the level of soil shaking but in all cases is less than the static uplift capacity. These tests showed that an axial load of only 25 percent of the equivalent static capacity will cause the shaft to fail during strong soil shaking.

If the drilled shaft carries a cyclic axial load while the soil around it is shaking then it may fail in uplift during the test. The cyclic axial load causing uplift failure in these tests was 40 percent of the equivalent static capacity. All the cyclic axial load tests were performed at the same level of shaking so the effect of this parameter is unknown from these tests. The phase difference between peak axial load and peak soil displacement had a small effect on the point of instability of the drilled shaft. When the phase difference was changed from 0 degrees to 90 degrees, the load required to fail the drilled shaft increased by approximately 10 percent

9.4 CONCLUSIONS

The capacity of a drilled shaft foundation is adversely affected by seismic loading. If the drilled shaft is subjected to cyclic axial loads, as it is when the superstructure responds to an earthquake, then the drilled shaft may fail at loads that are well below its static design capacity. The worst case loading configuration for this model drilled shaft occurs about zero mean load, where the uplift capacity may be reduced to only 67 percent of the static capacity. The tests performed in this study show that the mean load on the shaft is an important parameter in determining its stability under cyclic axial loading. It was found that one-way loading has little adverse effect on the stability of the drilled shaft but two-way loading leads to capacity reductions during loading. The data from these tests has been used to develop a parameter called the Level of Load Reversal. The LLR is the amount by which the load is reversed during the test. Relationships have then been found between the LLR and the reduction in uplift capacity of the drilled shaft. It was found that the higher the LLR, the greater the reduction in uplift capacity.

The second stage tests showed that the uplift capacity of a drilled shaft increases if the soil around it is shaken under simulated seismic shaking. The reason for the capacity increase is that the soil settles and stiffens up as it densifies during inelastic shear straining. The denser and stiffer soil is more resistant to dilation of the material around the drilled shaft so a greater uplift load is required to cause failure.

If the drilled shaft is simultaneously subjected to a constant axial uplift load then it may fail in uplift at a load that is considerably less than the equivalent static uplift capacity. The reason for the reduced uplift capacity may be that the soil around the drilled shaft softens as it shears inelastically so it then can allow greater shear strains for small increases in shear stress. The softening of the soil may also allow dilation to occur more easily around the drilled shaft so the uplift capacity will be reduced.

If the drilled shaft is simultaneously subjected to a cyclic axial load then it will suffer the same degradation in uplift capacity as that seen under constant axial load. The mechanisms causing that degradation will be the same. The cyclic load amplitude required to fail the drilled shaft will be greater than the corresponding constant axial load because the uplift part of the load cycle is partially offset by the compression part of the loading cycle. The cumulative axial displacements will then be smaller so there will be a smaller amount of soil degradation around the shaft.

RECOMMENDATIONS

The results from these tests show that there can be significant reductions in the uplift capacity of a drilled shaft during seismic loading. Based on the results of these tests it is recommended that drilled shafts in seismic areas should be designed with an increased factor of safety to account for the reductions in capacity associated with fluctuating axial loads. If it is suspected that the foundation loads could be in uplift during the seismic event then particular care should be taken with regard loss of capacity. If the drilled shaft is founded in a soft soil then a careful analysis should be performed to determine the expected maximum shear strains in the soil as large shear strains have a highly detrimental effect on the capacity of a drilled shaft.

With regard to future research in this area, it is recommended that further testing be focussed on the effect of shear strain magnitude within the soil. These tests were performed under large inelastic shear strains and it is important to determine whether the same reductions in drilled shaft capacity are seen at lower shear strains. Further research is also recommended into the stress distribution in the soil around the drilled shaft during both cyclic axial loading and cyclic soil shaking.

Appendix A

PROPERTIES OF SILICA SAND

Particle Size Distribution

Mass of Sample = 99.56 gm

Table A1 – Particle Size Distribution for Silica Sand

Sieve Diameter (mm)	Mass Retained (gm)	Percent Retained (%)	Percent Passing (%)
2.36	0	0	100
1.18	0	0	100
0.60	1.66	1.67	98.33
0.30	88.00	88.39	9.94
0.15	9.86	9.90	0.04
-	0.04	0.04	0.00

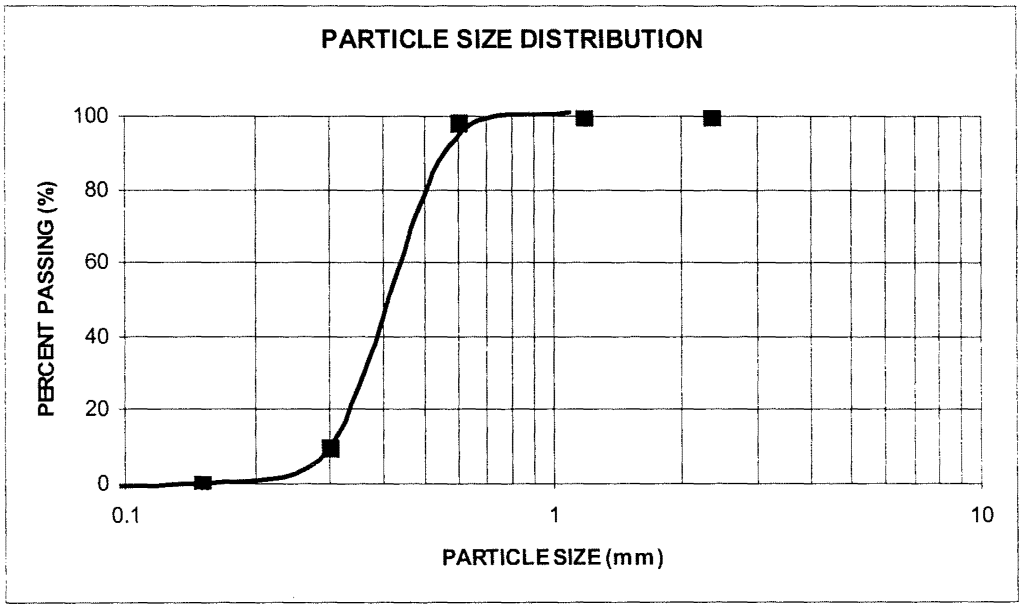

Figure A1 – Particle Size Distribution for Silica Sand

D_{10} = 0.30 mm

D_{60} = 0.45 mm

Density of Solid Particles

TableA2 – Density of Solid Particles

Test No.	Mass Jar+Lid (gm)	Jar+Lid+ Sample (gm)	Jar+Lid+Sample +Water (gm)	Jar+Lid+Water (gm)	Density (t/m^3)
1	883.74	1132.70	4180.86	4025.74	2.65
2	883.74	1132.56	4180.59	4025.74	2.65

$\therefore \rho_s$ = **2.65 t/m^3**

Void Ratios

Table A3 – Maximum Void Ratio

Test No.	Sample Mass (gm)	Sample Volume (cm^3)	Density (t/m^3)	Void Ratio
1	161.09	110.08	1.46	0.81
2	157.26	110.08	1.43	0.85
3	159.62	110.08	1.45	0.83
4	160.43	110.08	1.46	0.82

$\therefore e_{max}$ = **0.83**

Table A4 – Minimum Void Ratio

Test No.	Sample Mass (gm)	Sample Volume (cm^3)	Density (t/m^3)	Void Ratio
1	496.54	286.60	1.73	0.53
2	473.84	272.12	1.74	0.52
3	488.44	282.52	1.73	0.53
4	467.08	269.99	1.73	0.53

$\therefore e_{min}$ = **0.53**

Steady State Friction Angle

$\phi_{ss} = 33°$ (angle of repose of free-standing mound of sand)

Appendix B

STATIC SOIL TEST RESULTS

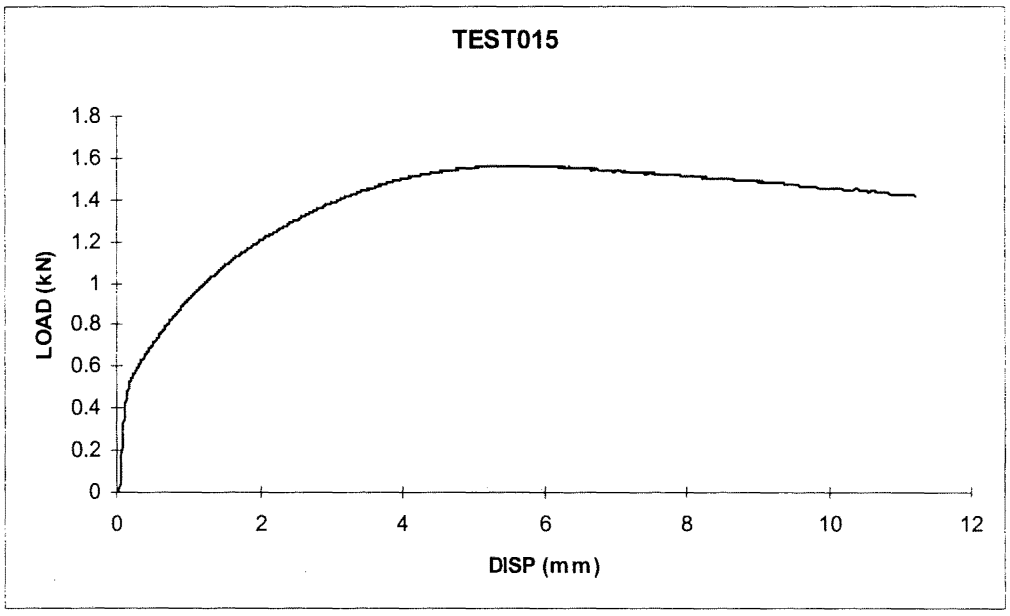

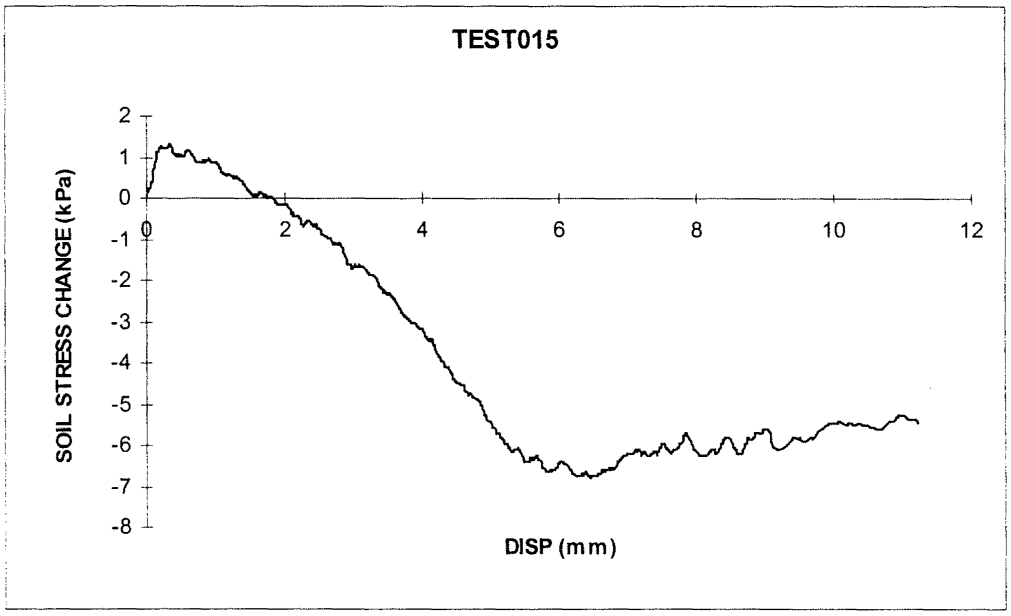

Figure B1 - Results of Test 015 – Monotonic Uplift

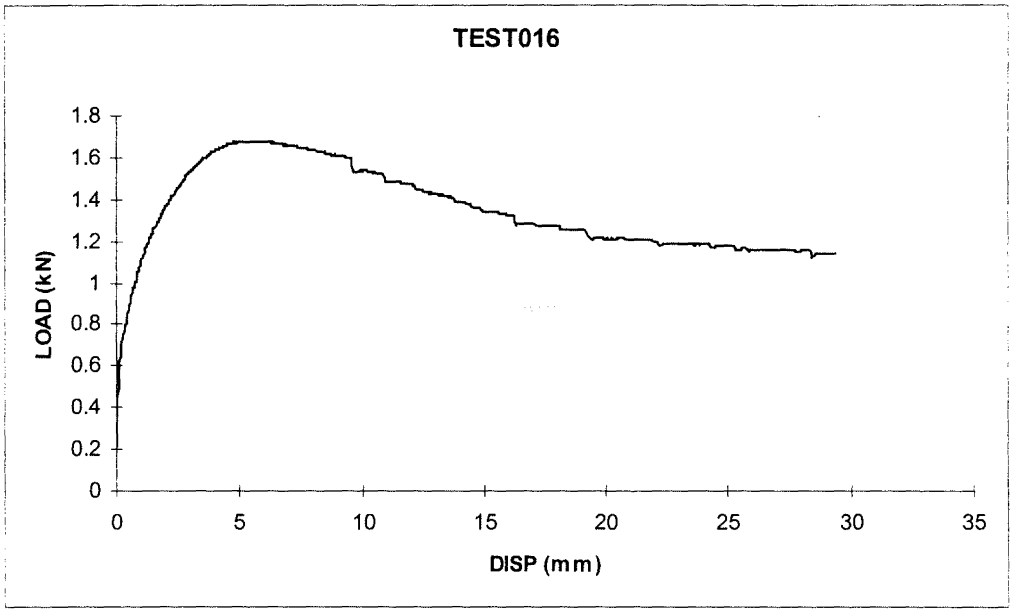

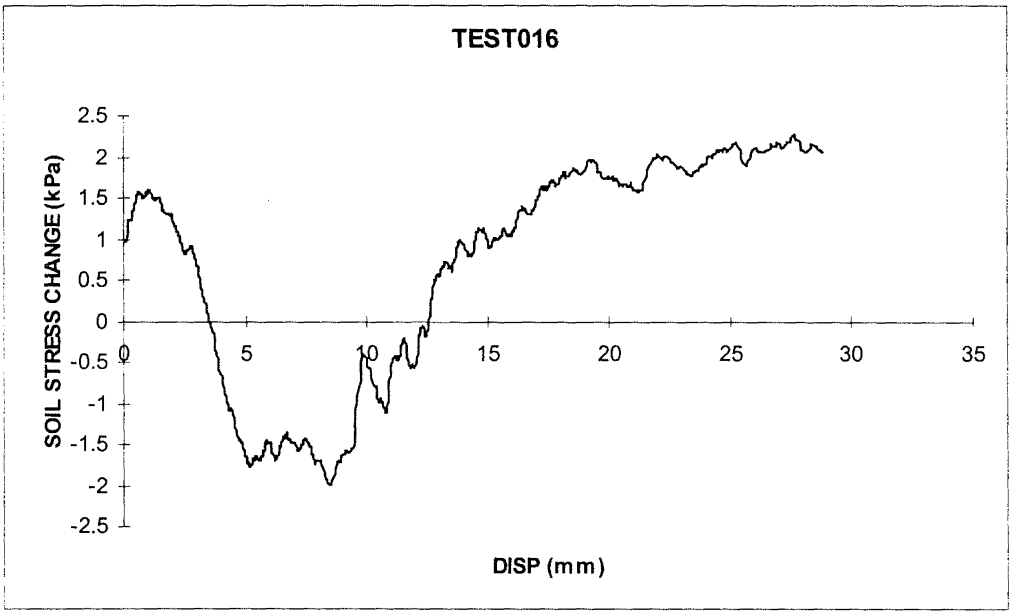

Figure B2 - Results of Test 016 – Monotonic Uplift

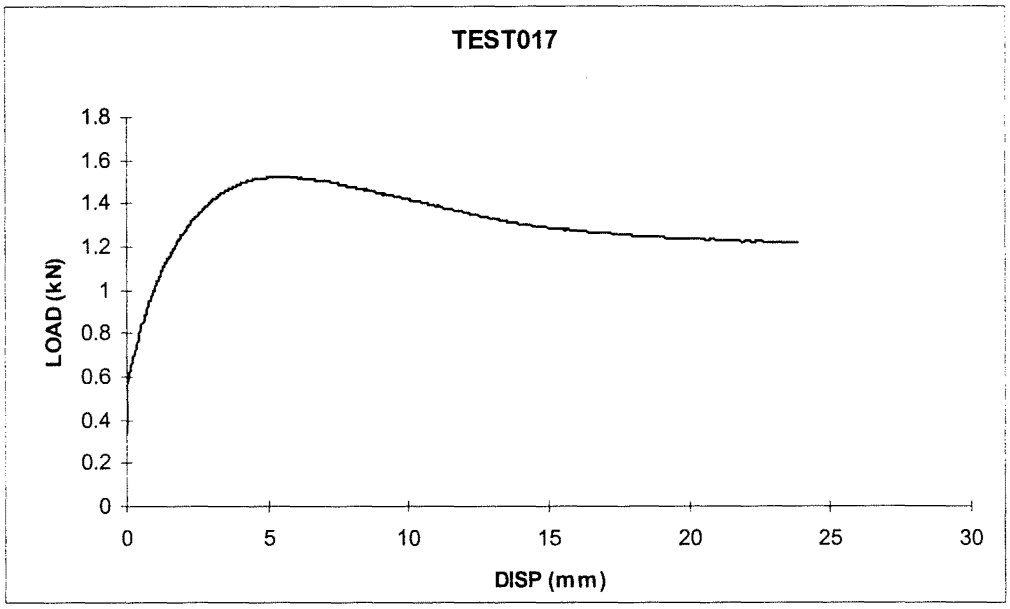

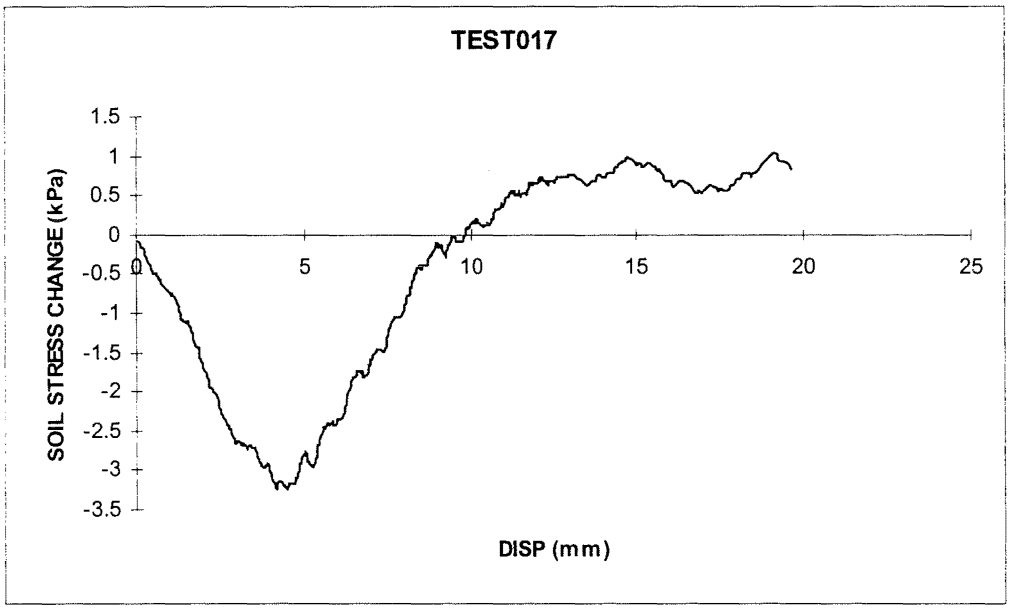

Figure B3 - Results of Test 017 – Monotonic Uplift

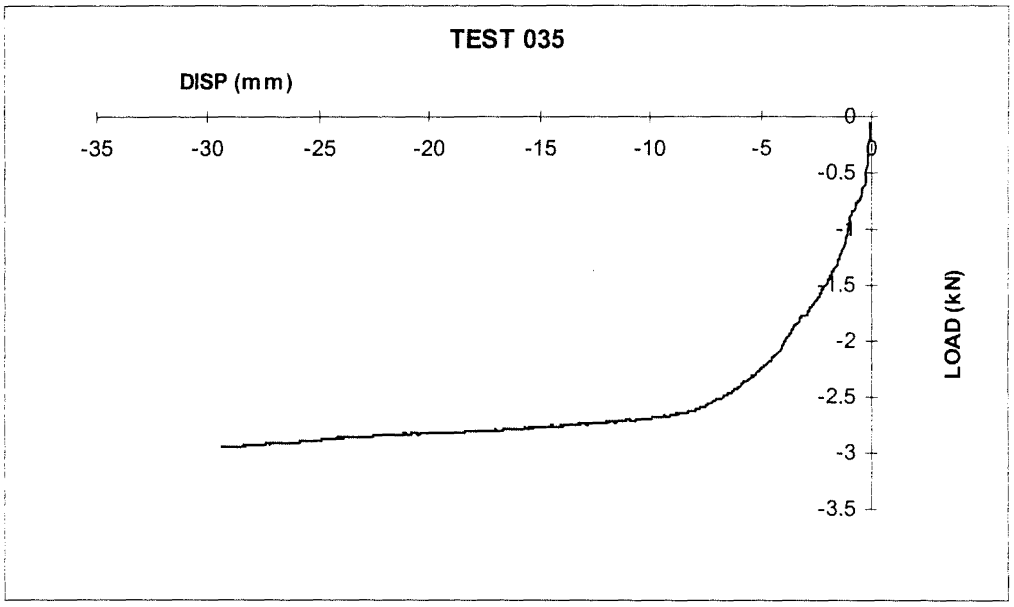

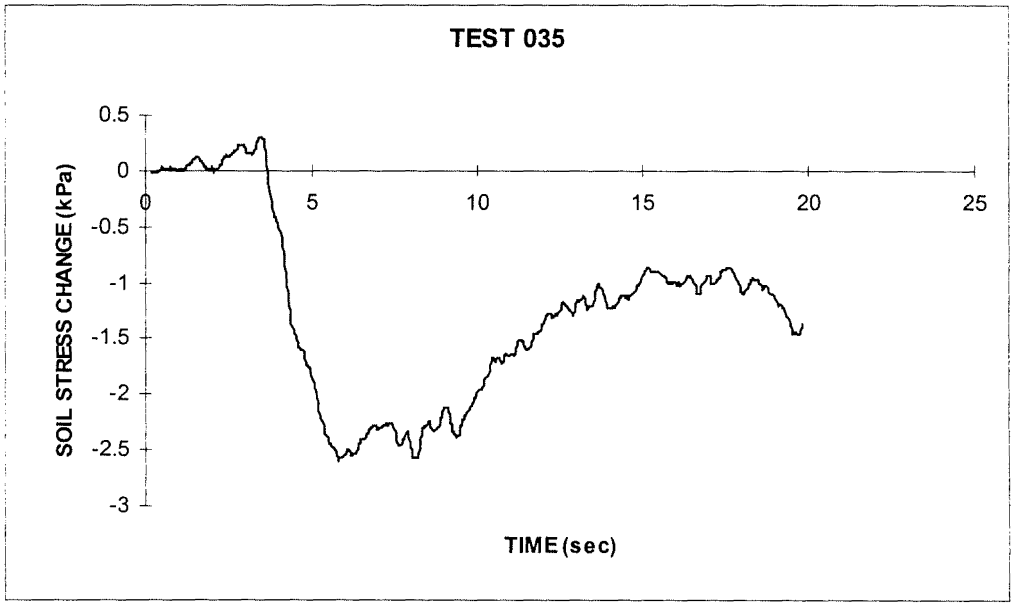

Figure B4 - Results of Test 035 – Monotonic Compression

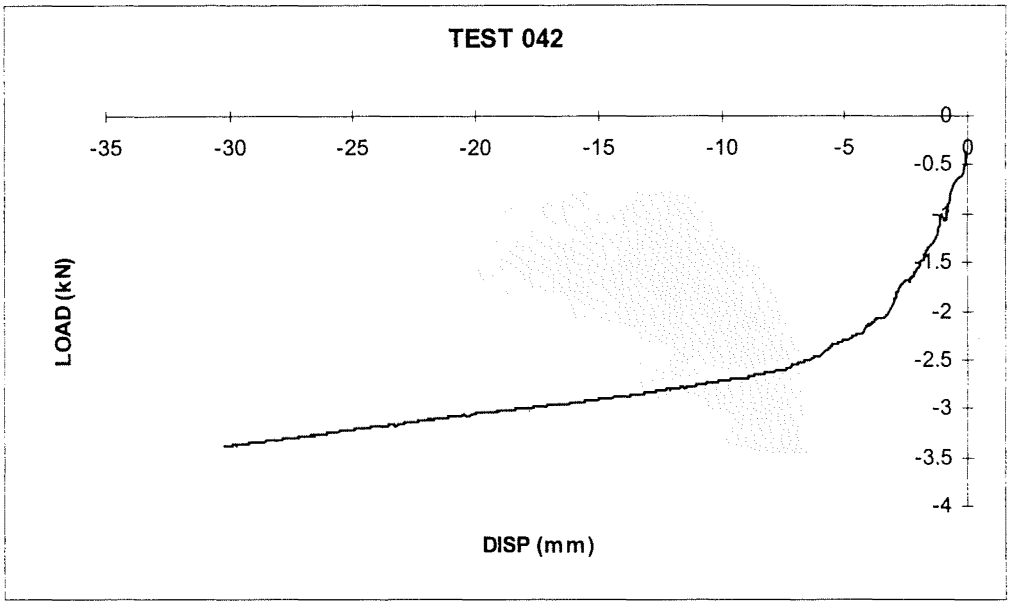

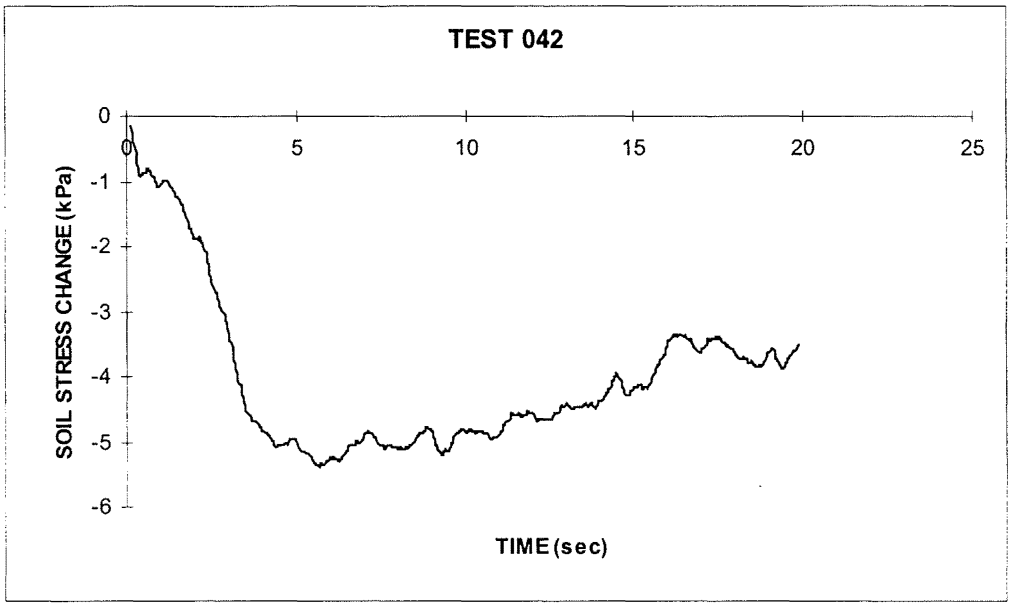

Figure B5 - Results of Test 042 – Monotonic Compression

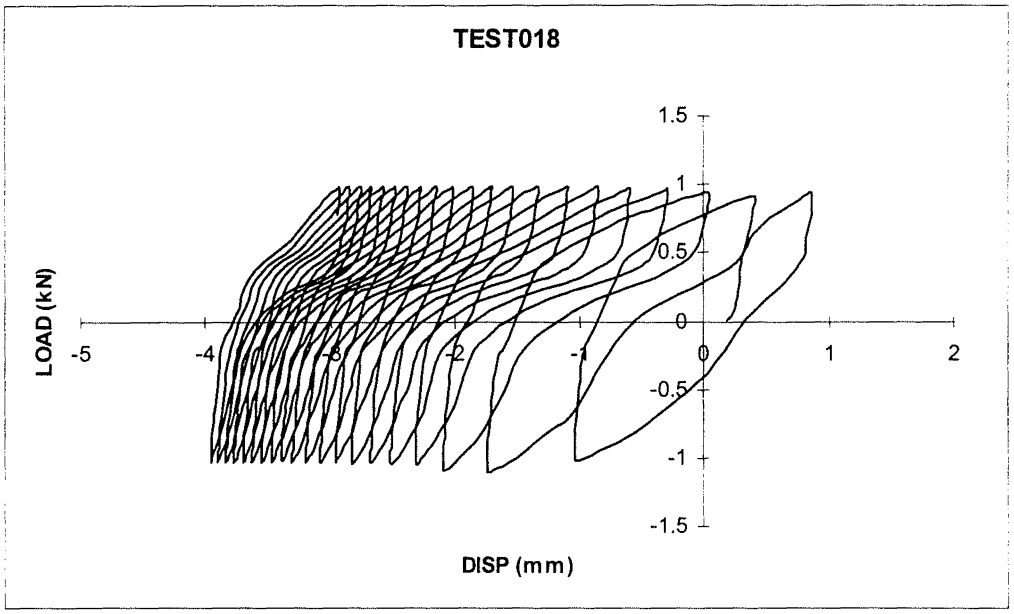

Figure B6- Results of Test 018 – Cyclic Axial Load

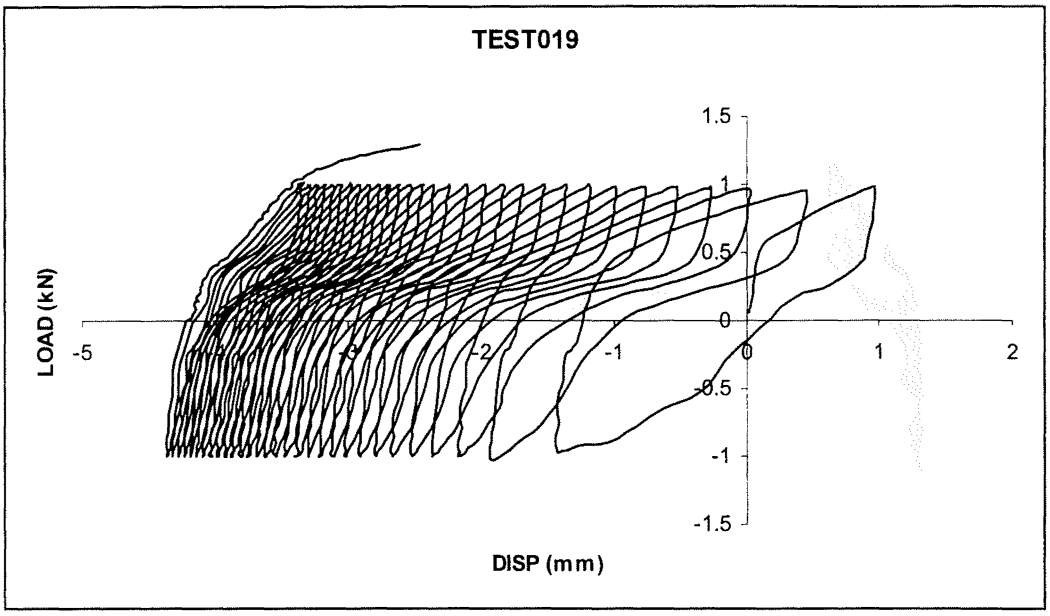

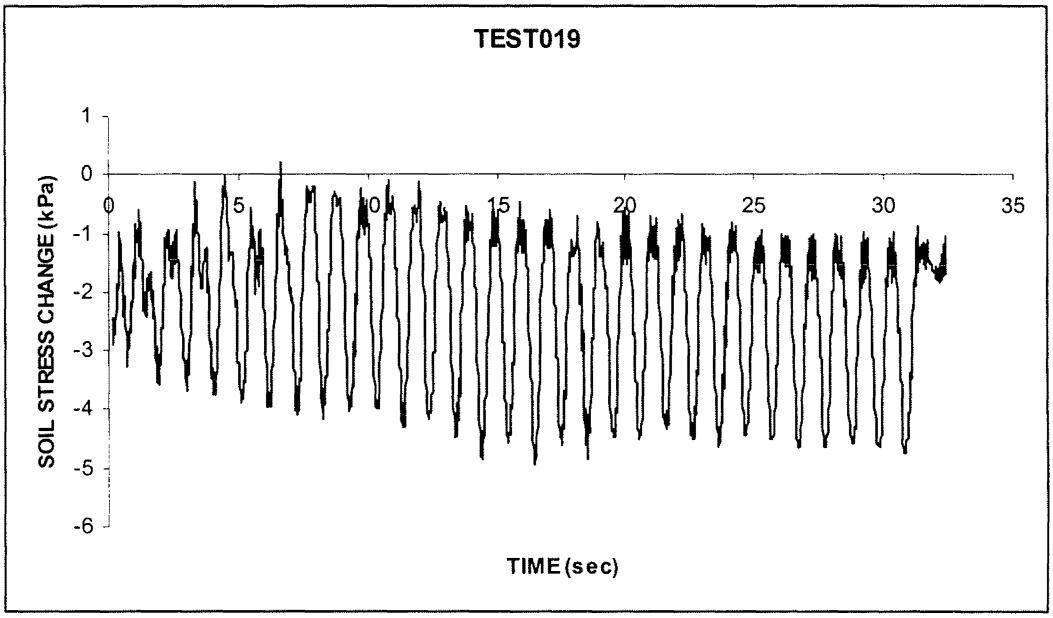

Figure B7 - Results of Test 019 – Cyclic Axial Load

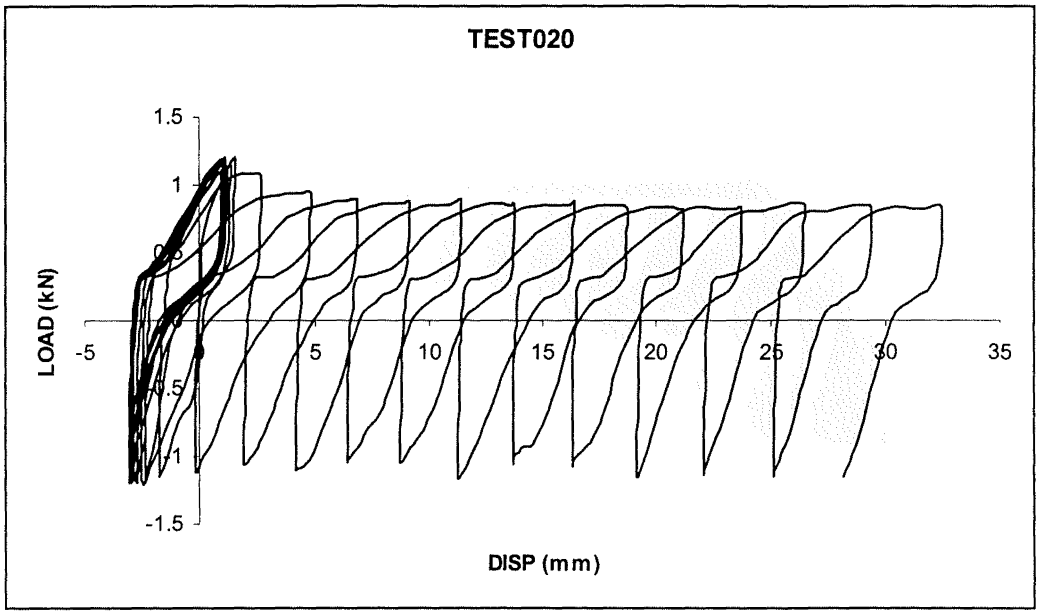

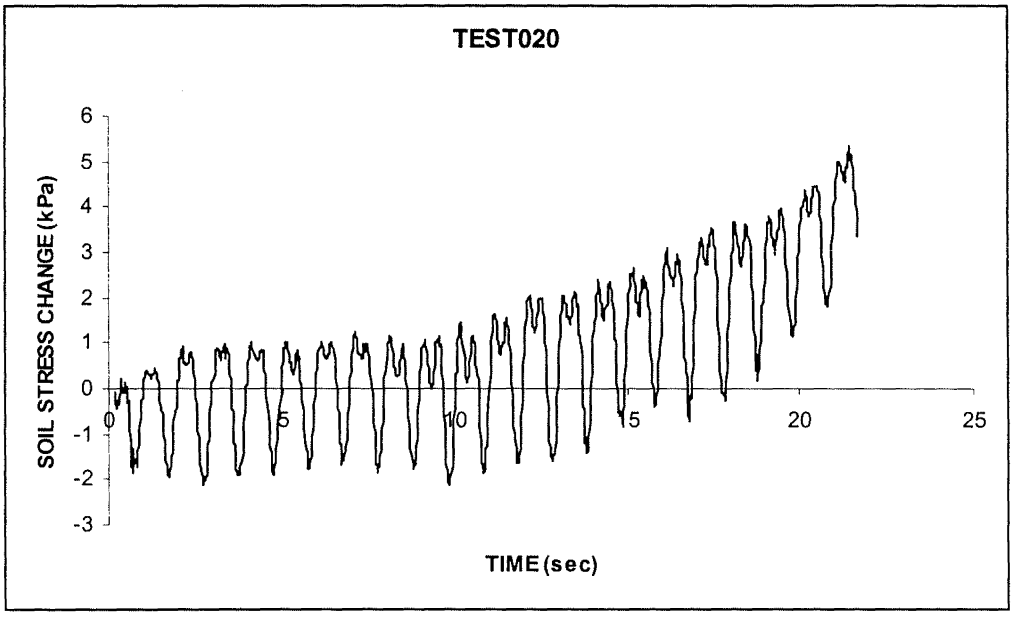

Figure B8 - Results of Test 020 – Cyclic Axial Load

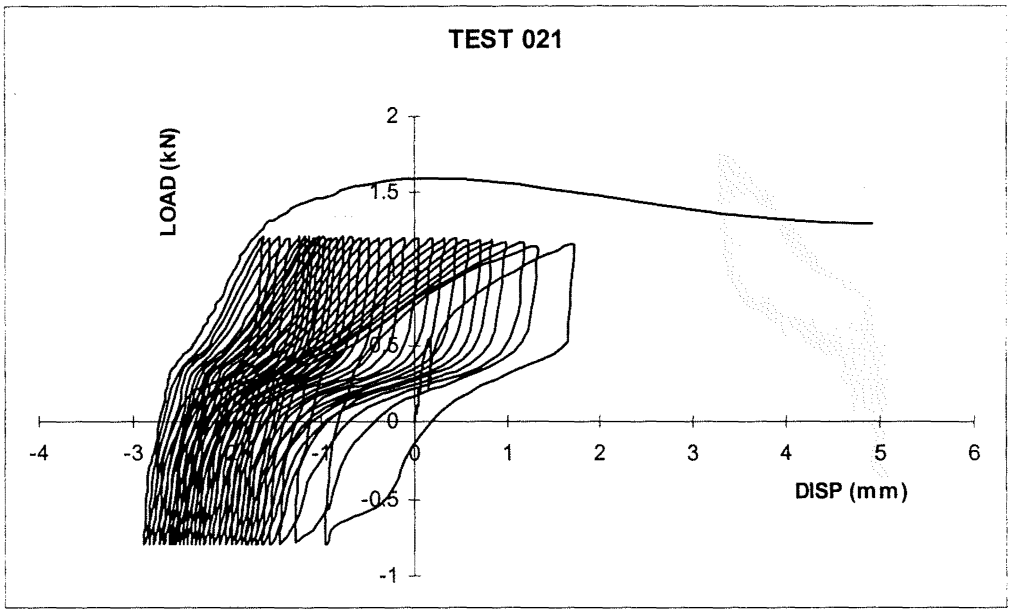

Figure B9 - Results of Test 021 – Cyclic Axial Load

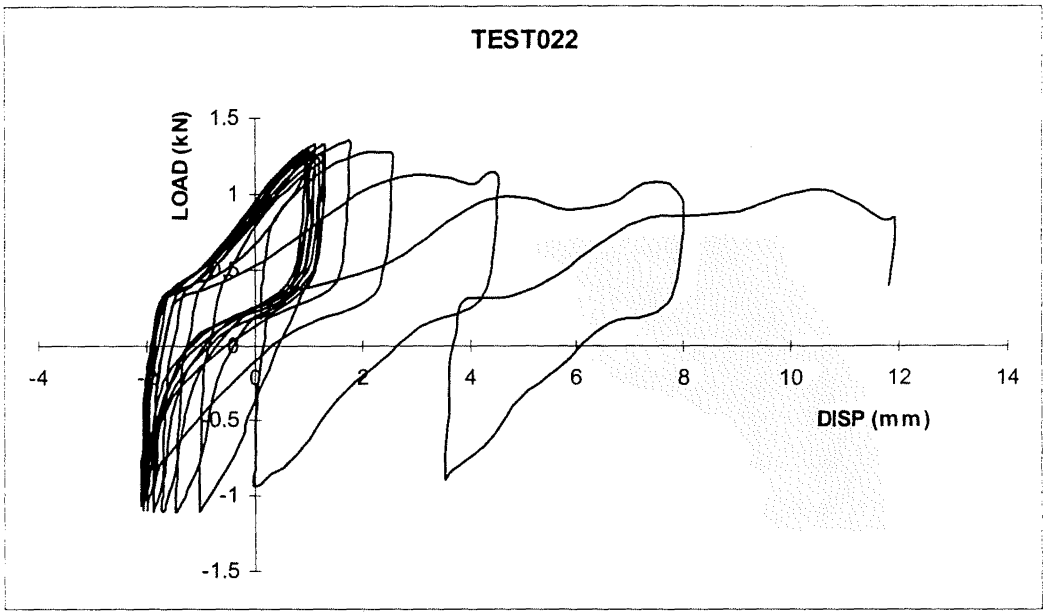

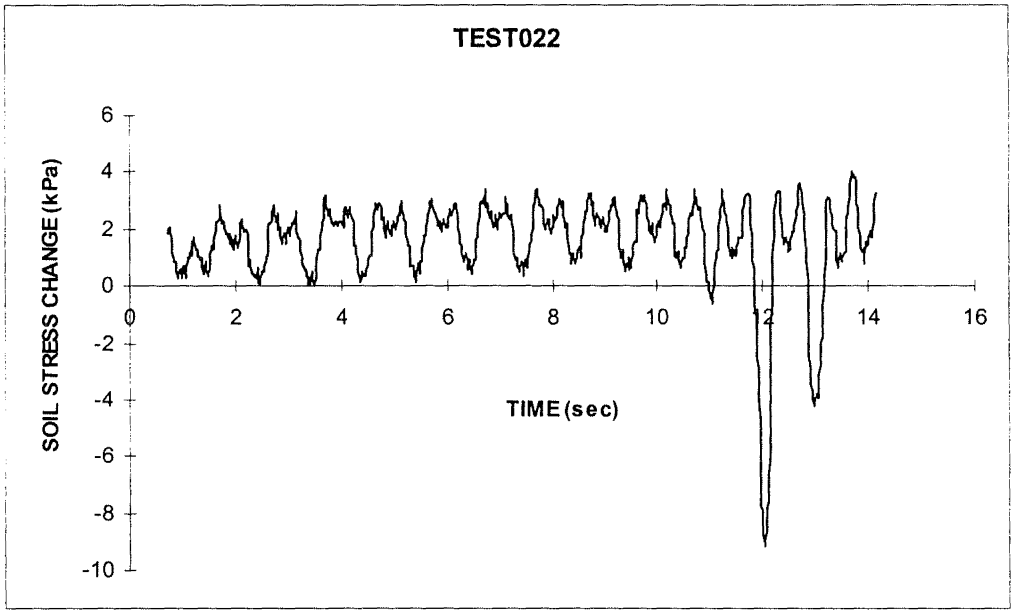

Figure B10 - Results of Test 022 – Cyclic Axial Load

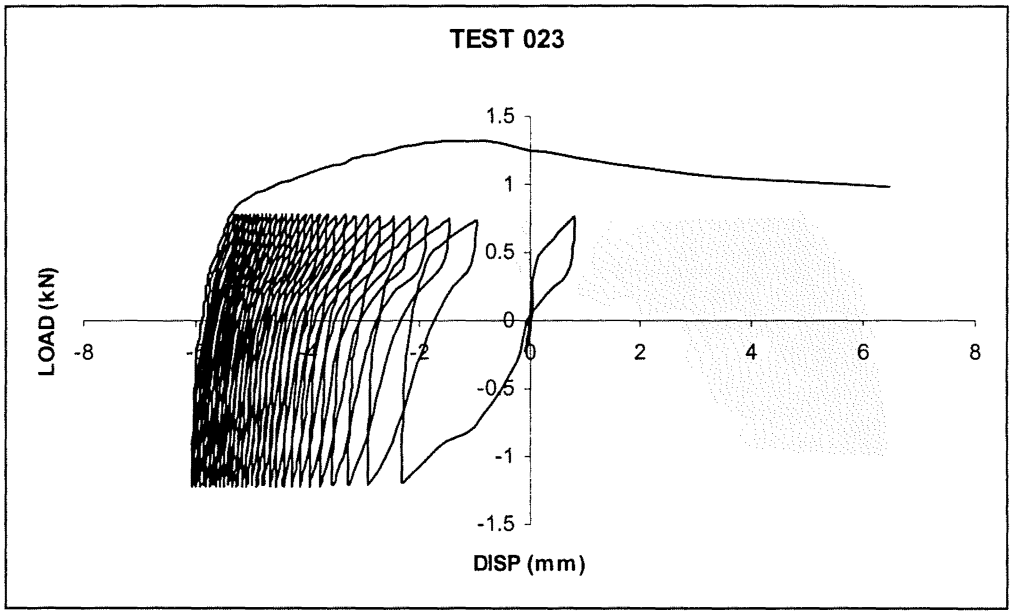

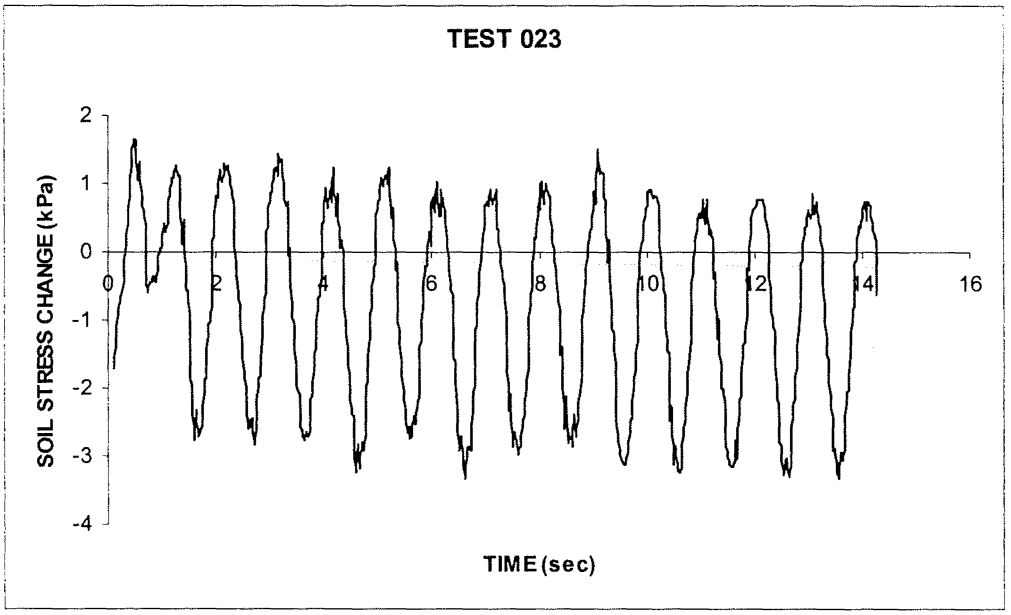

Figure B11 - Results of Test 023 – Cyclic Axial Load

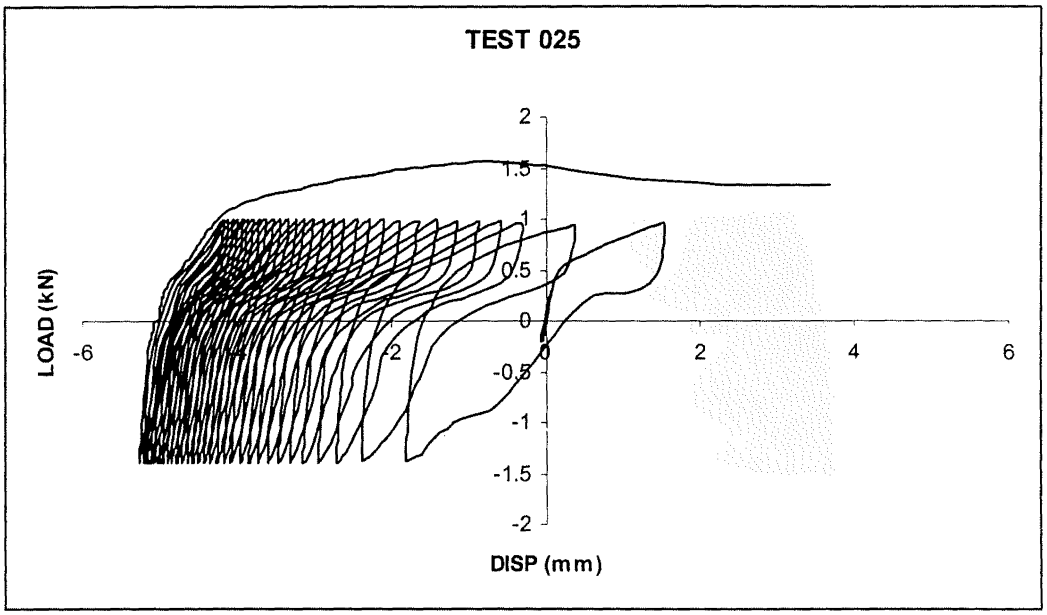

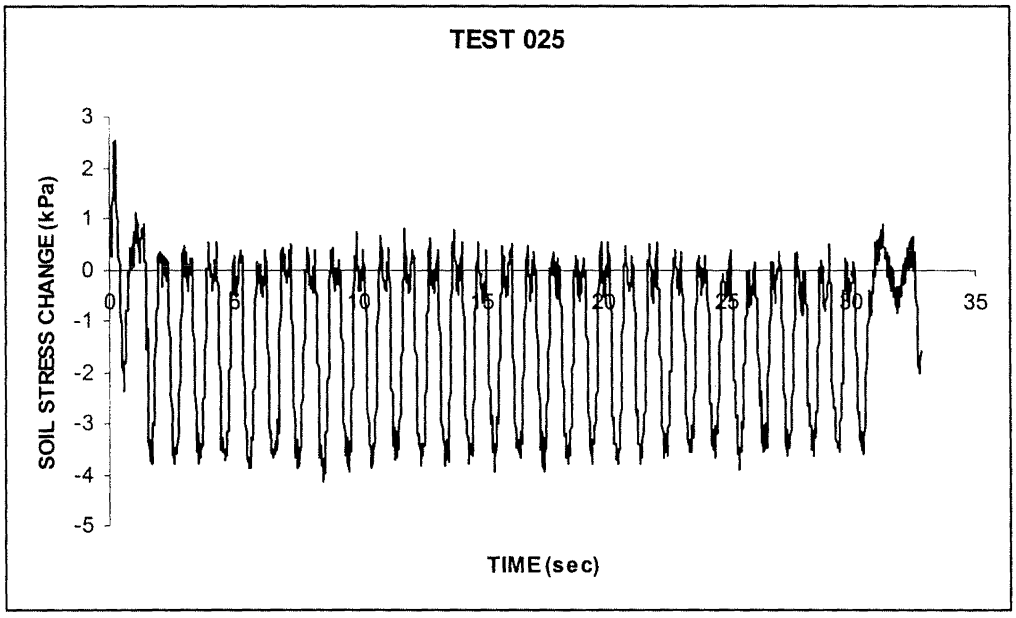

Figure B12 - Results of Test 025 – Cyclic Axial Load

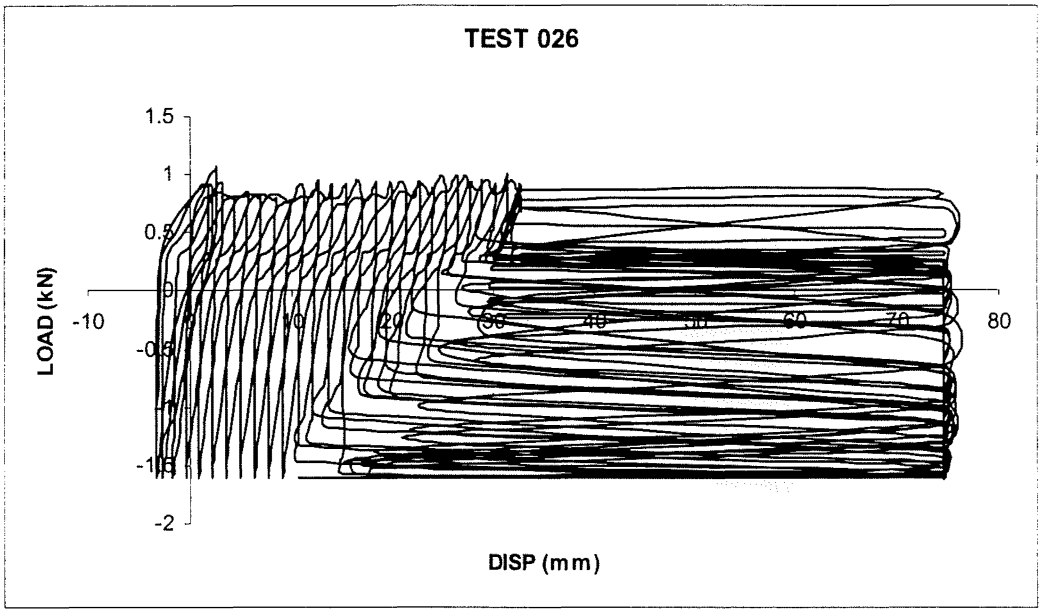

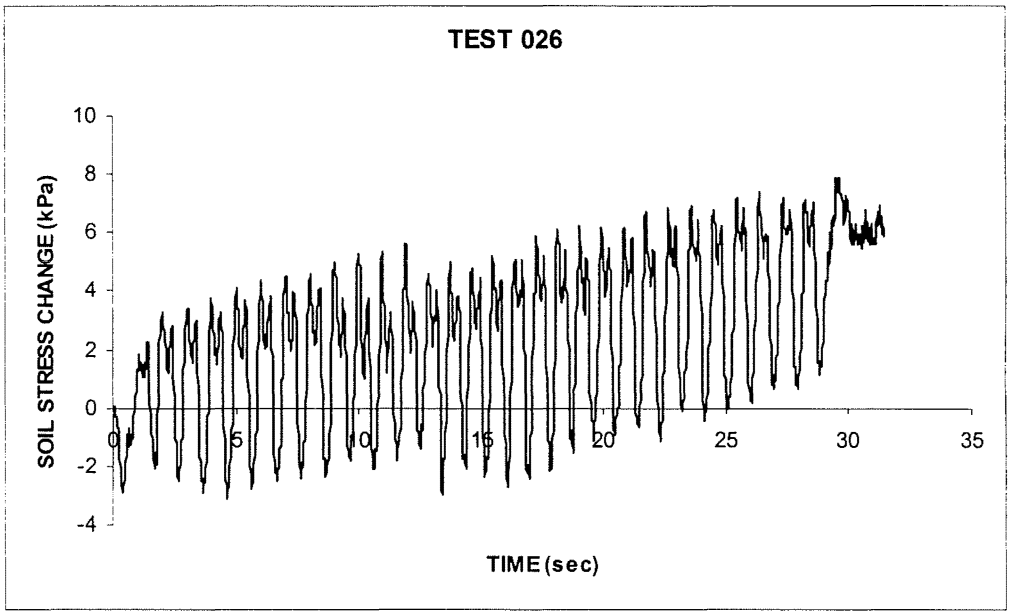

Figure B13 - Results of Test 026 – Cyclic Axial Load

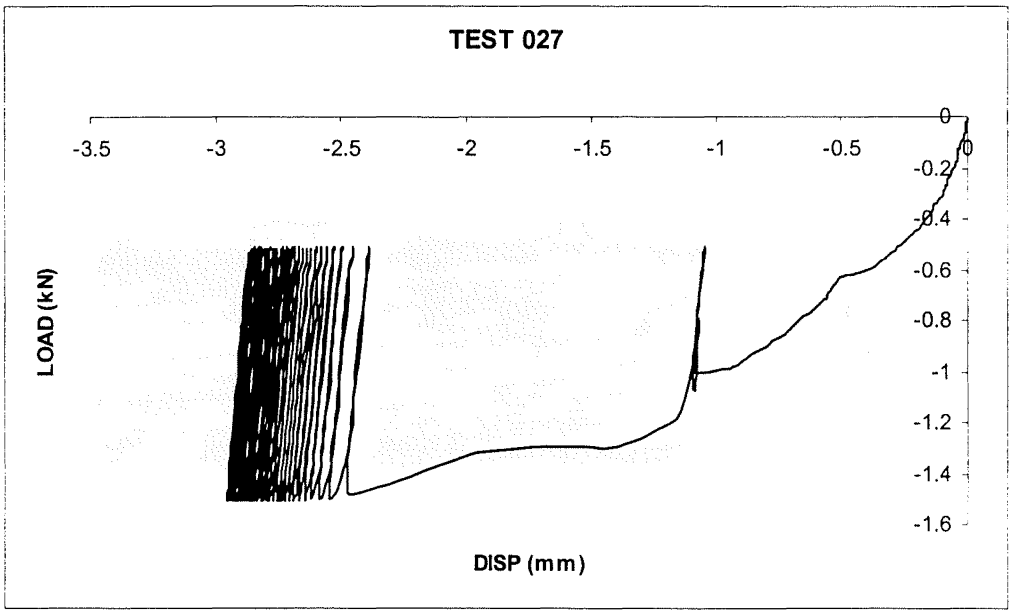

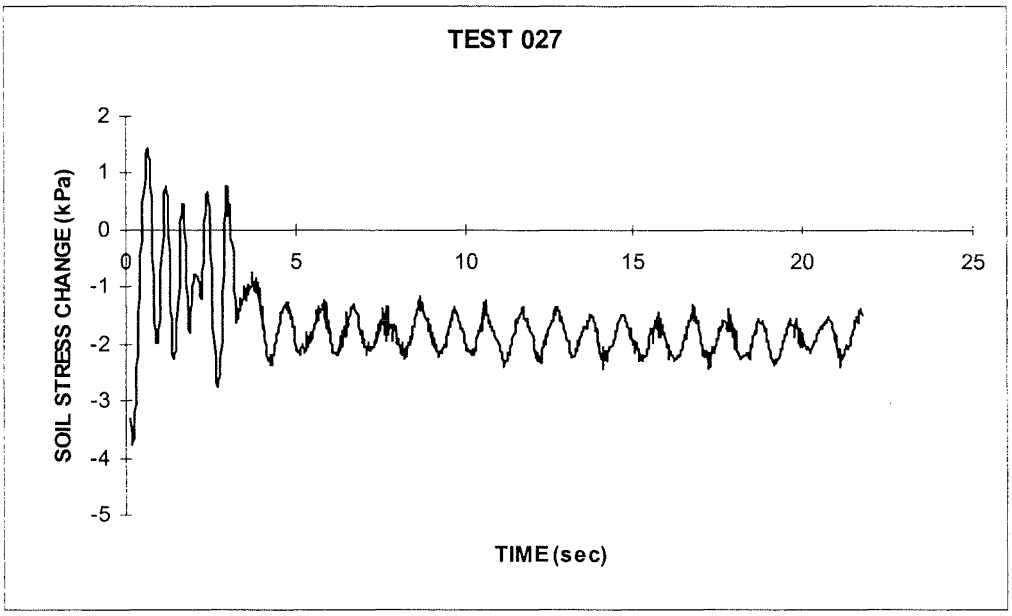

Figure B14 - Results of Test 027 – Cyclic Axial Load

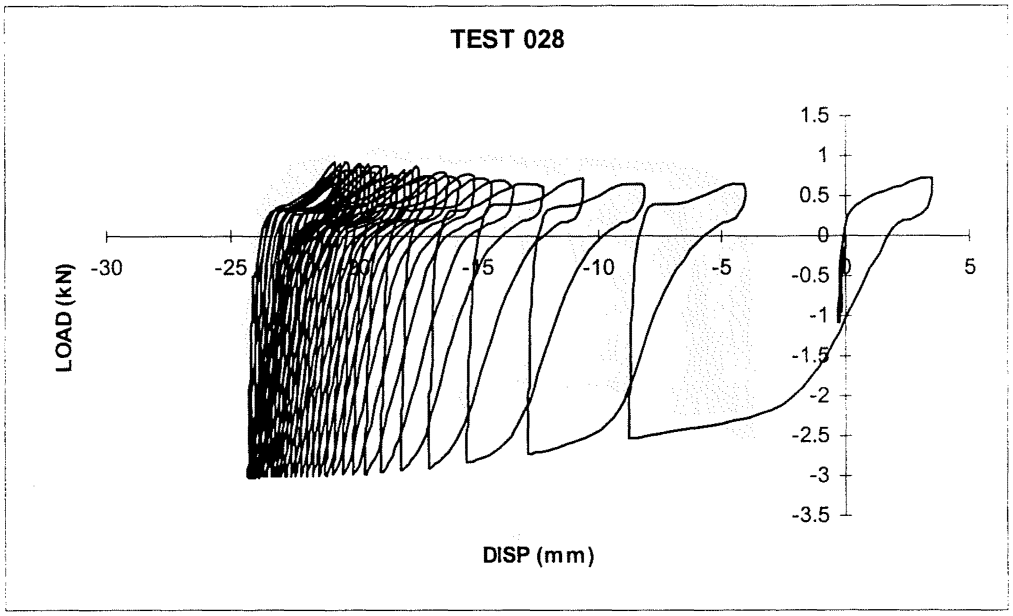

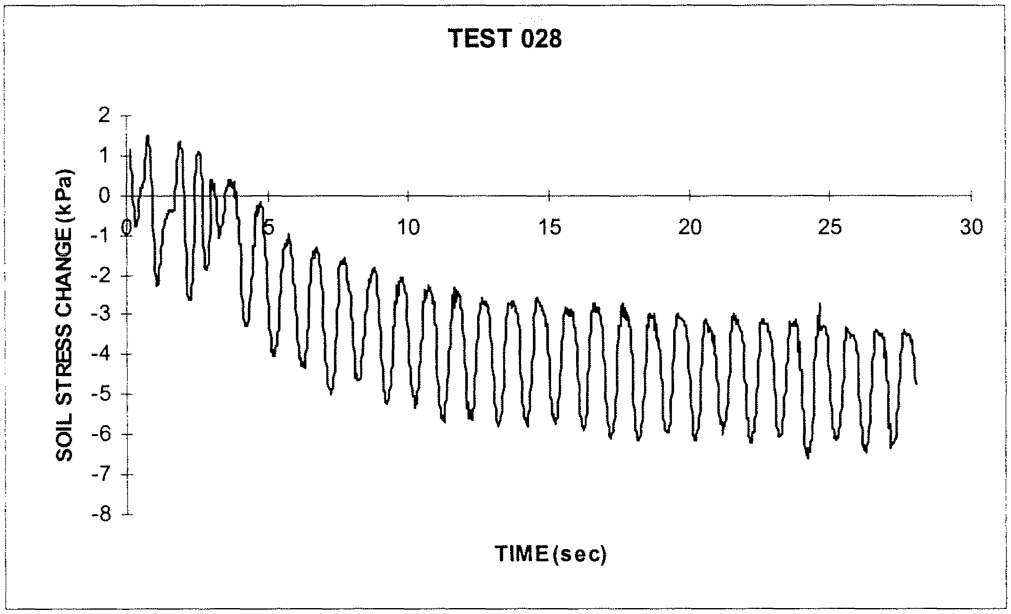

Figure B15 - Results of Test 028 – Cyclic Axial Load

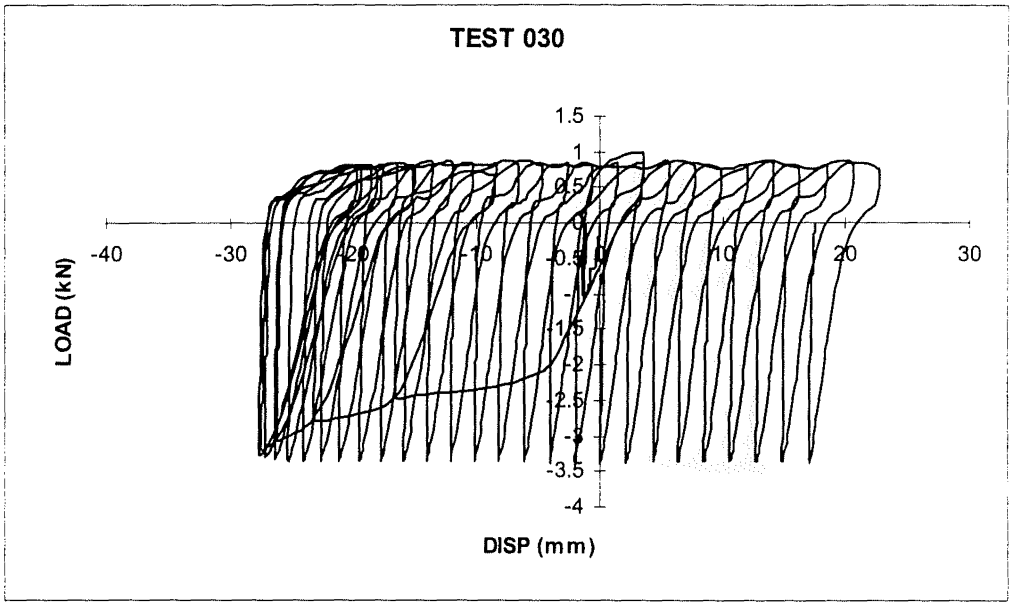

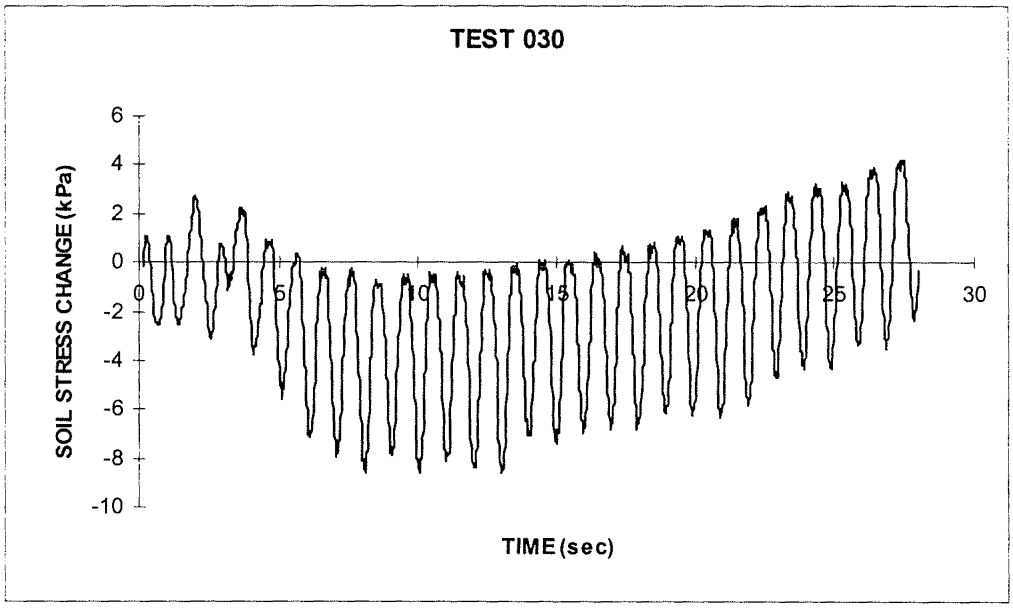

Figure B16 - Results of Test 030 – Cyclic Axial Load

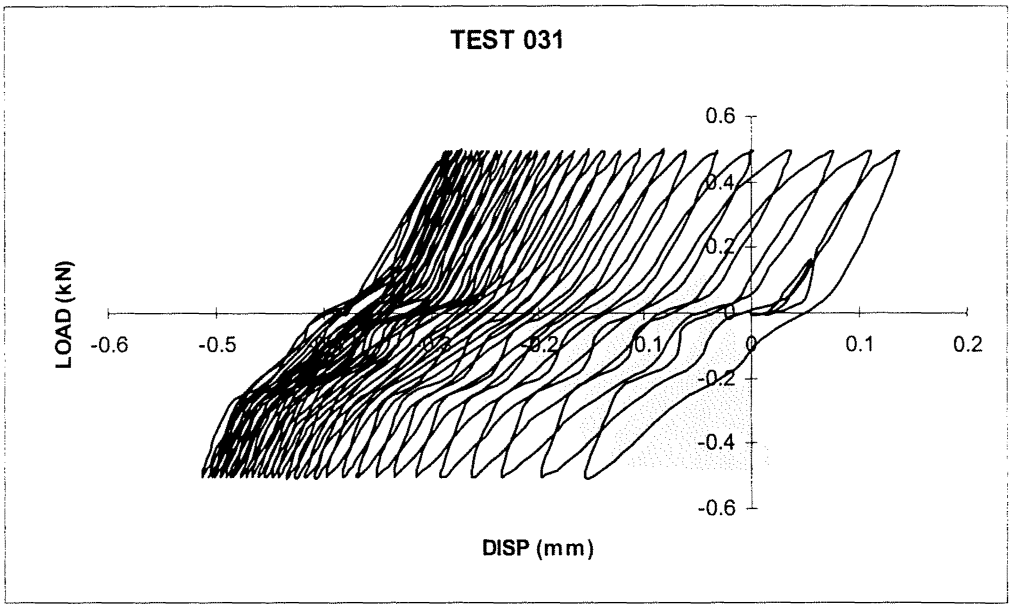

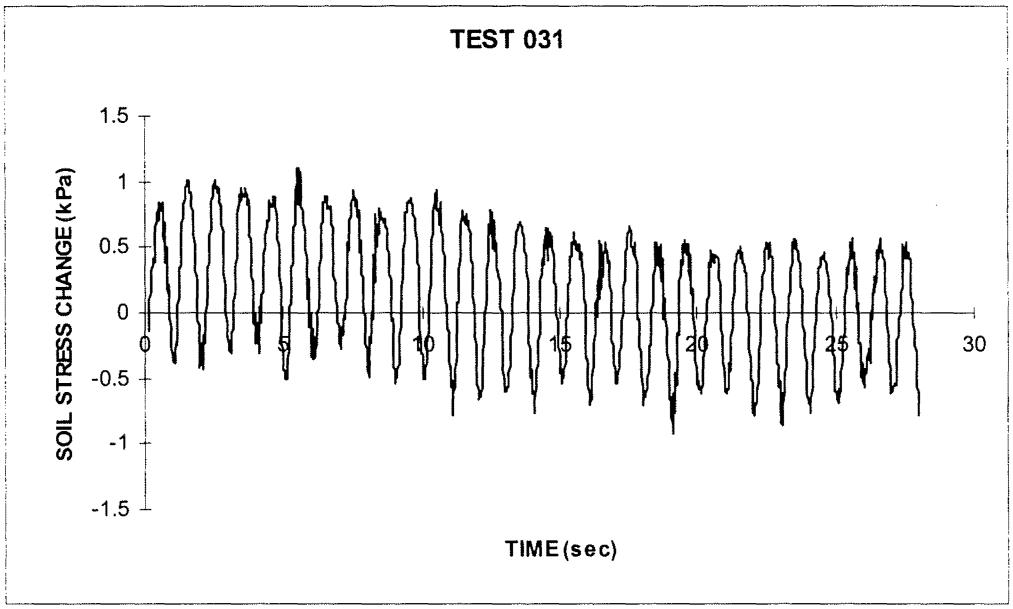

Figure B17 - Results of Test 031 – Cyclic Axial Load

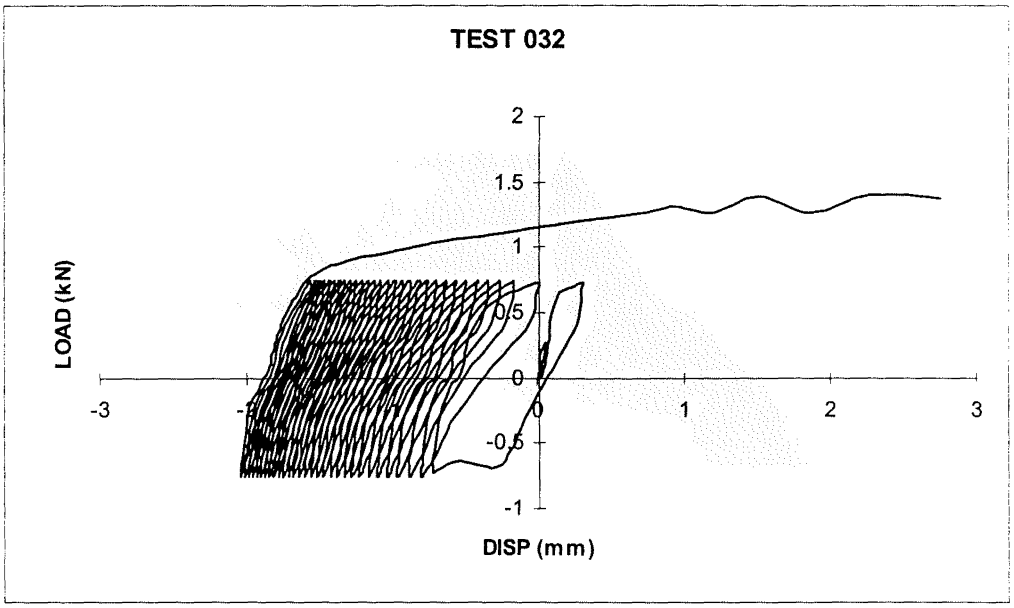

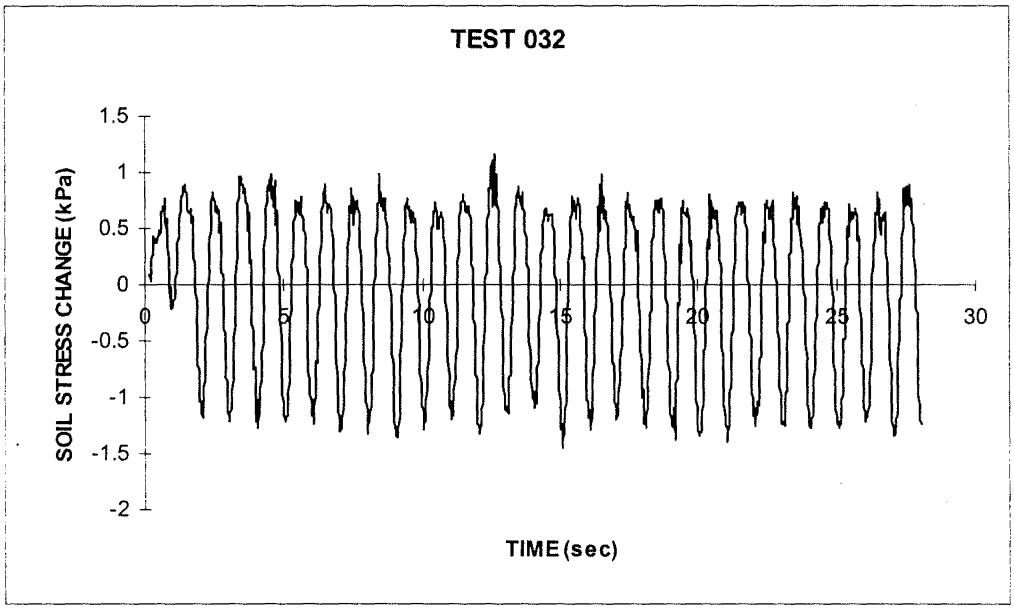

Figure B18 - Results of Test 032 – Cyclic Axial Load

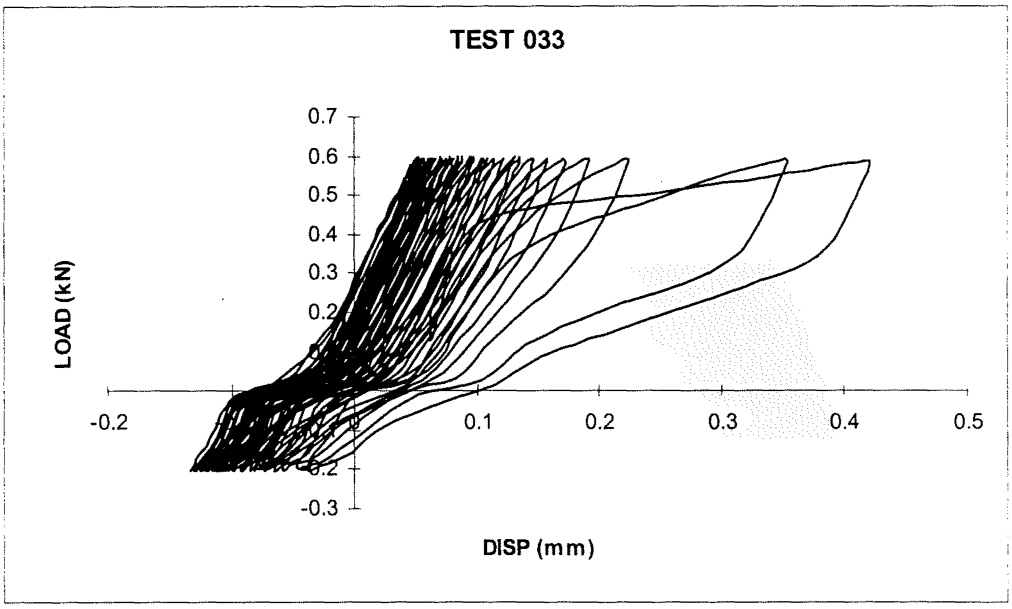

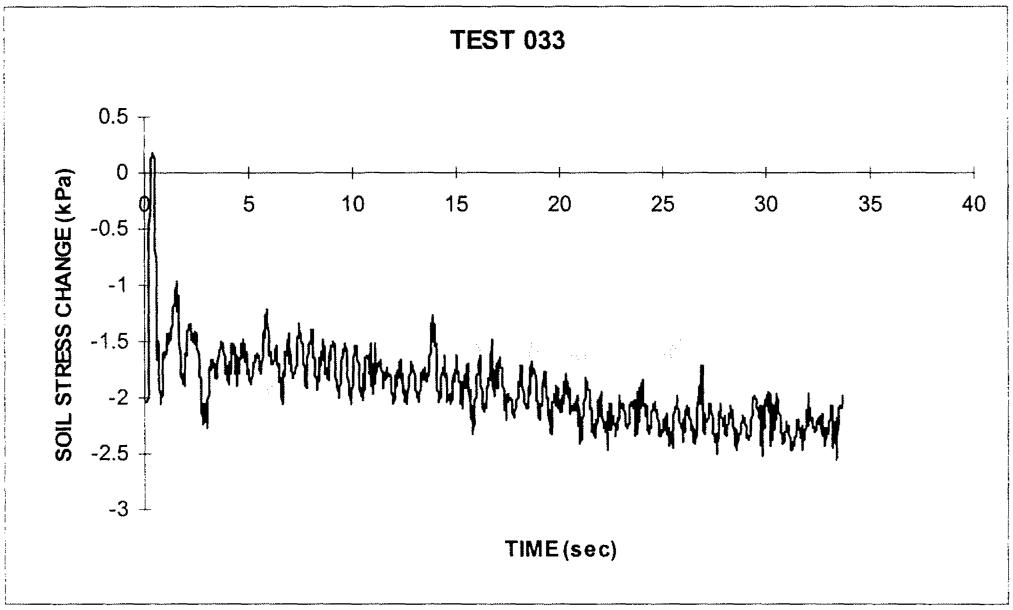

Figure B19 - Results of Test 033 – Cyclic Axial Load

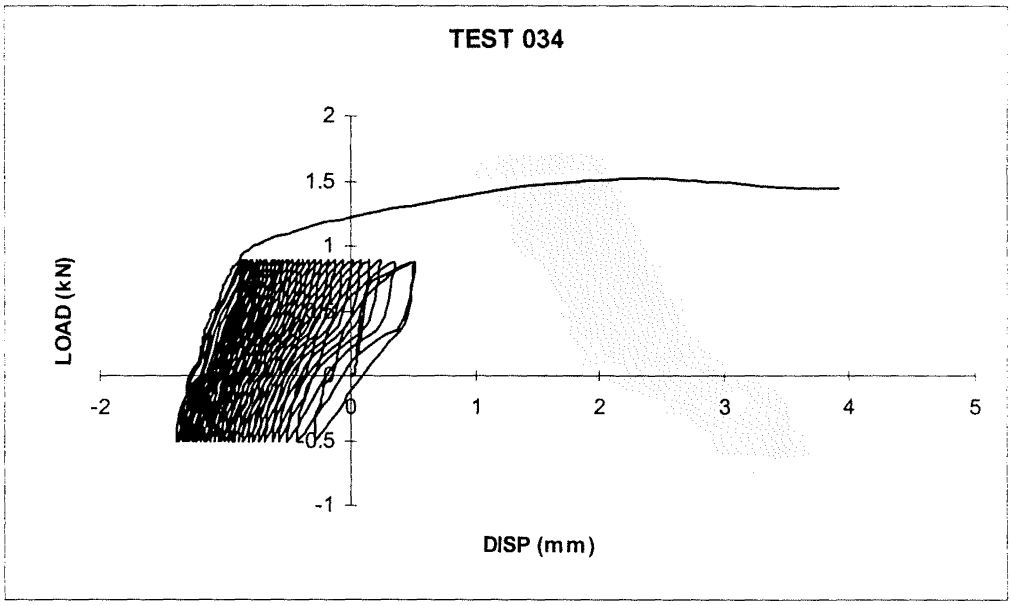

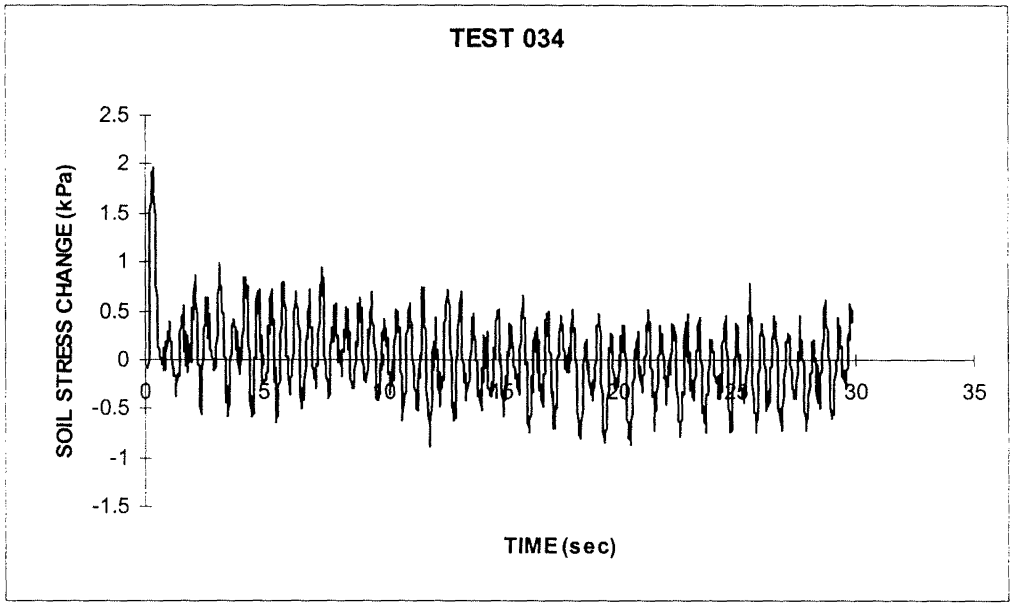

Figure B20 - Results of Test 034 – Cyclic Axial Load

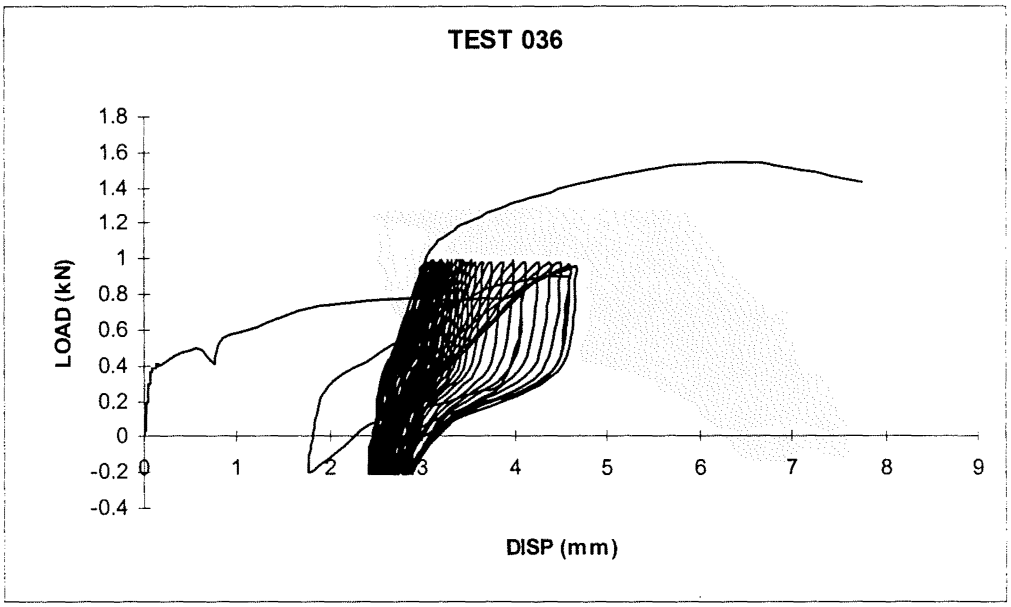

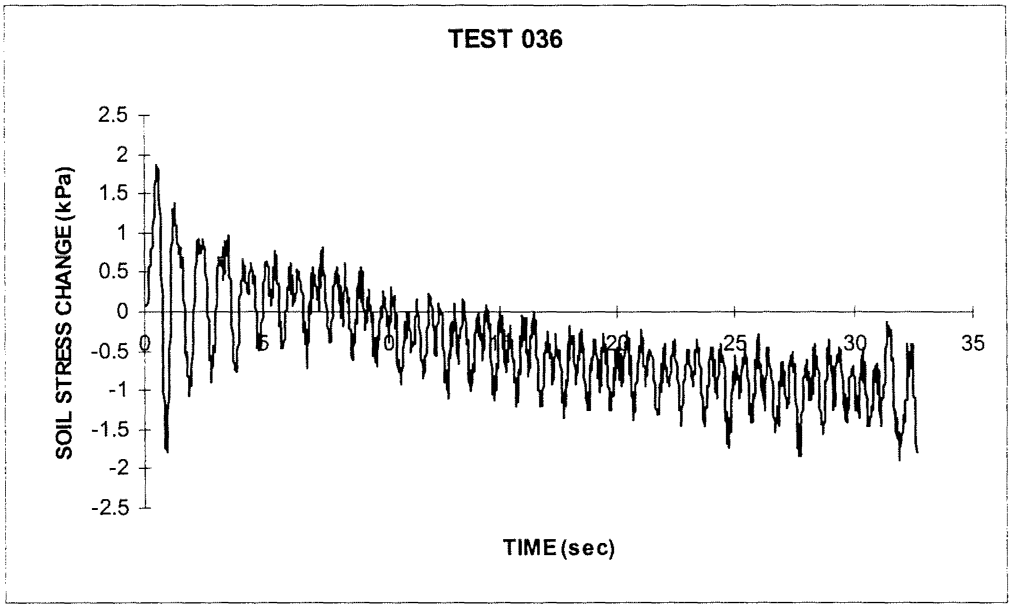

Figure B21 - Results of Test 036 – Cyclic Axial Load

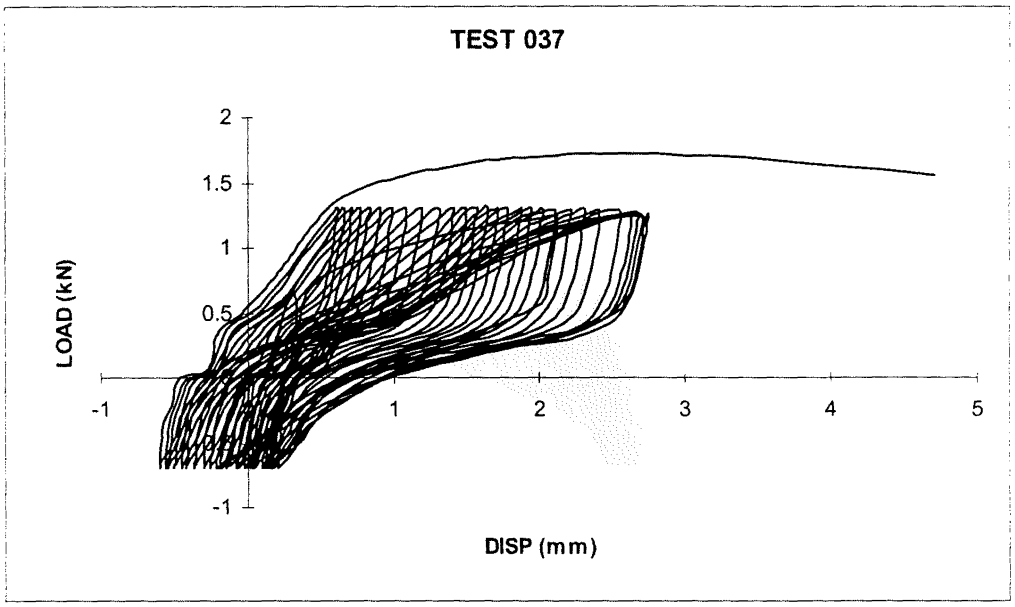

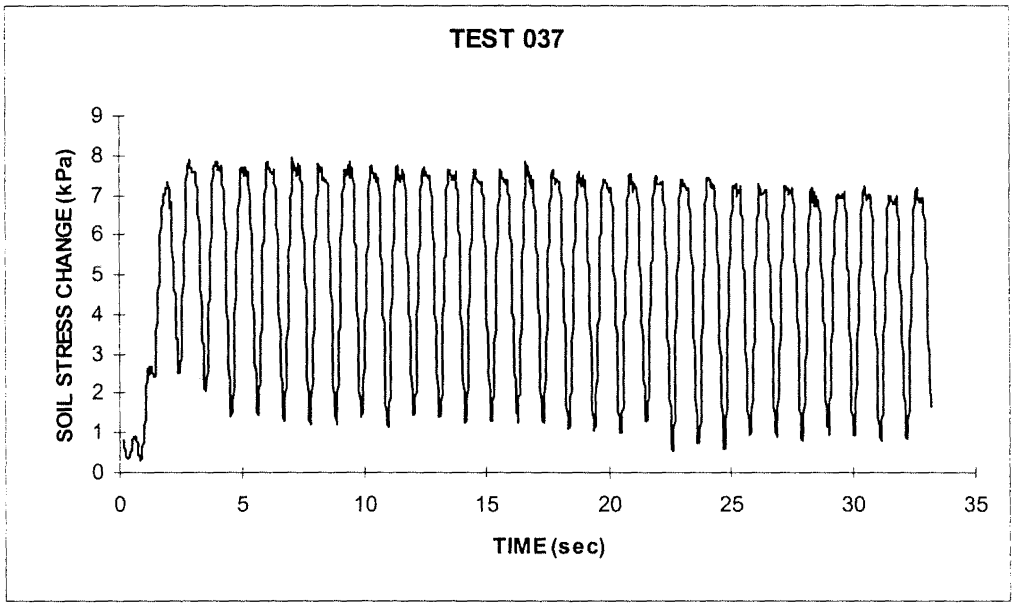

Figure B22 - Results of Test 037 – Cyclic Axial Load

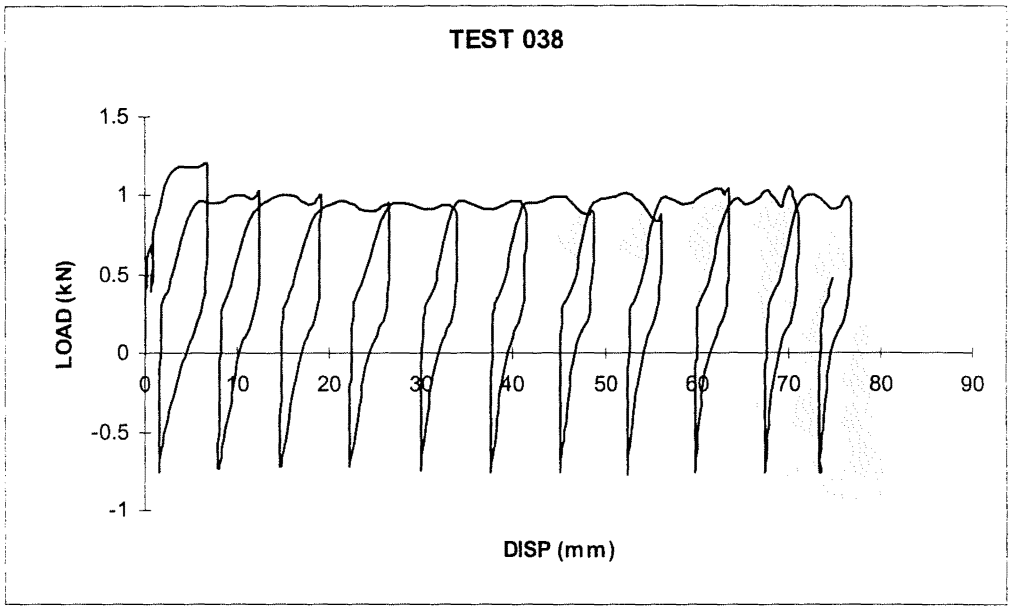

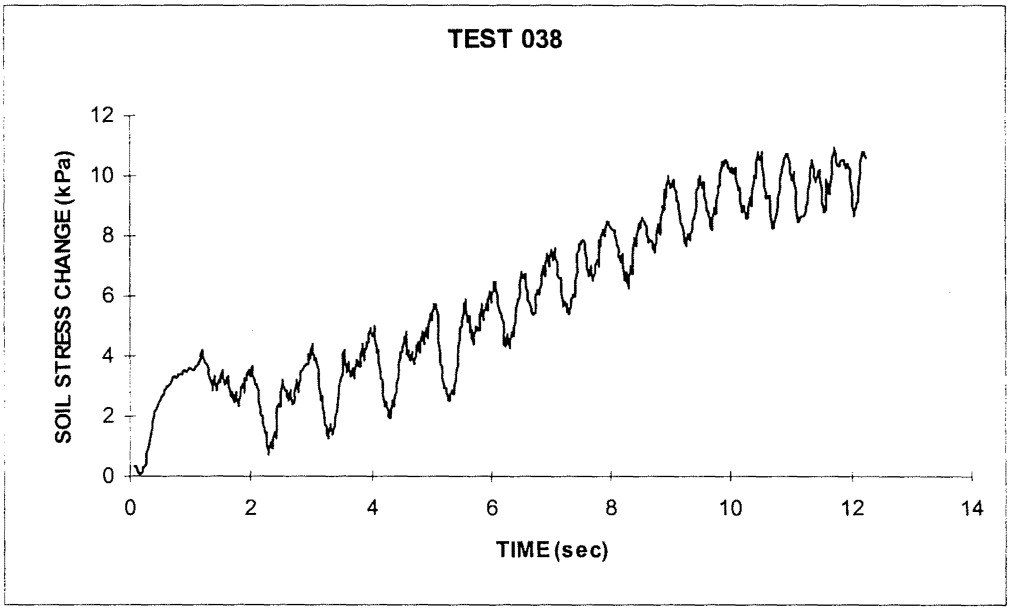

Figure B23 - Results of Test 038 – Cyclic Axial Load

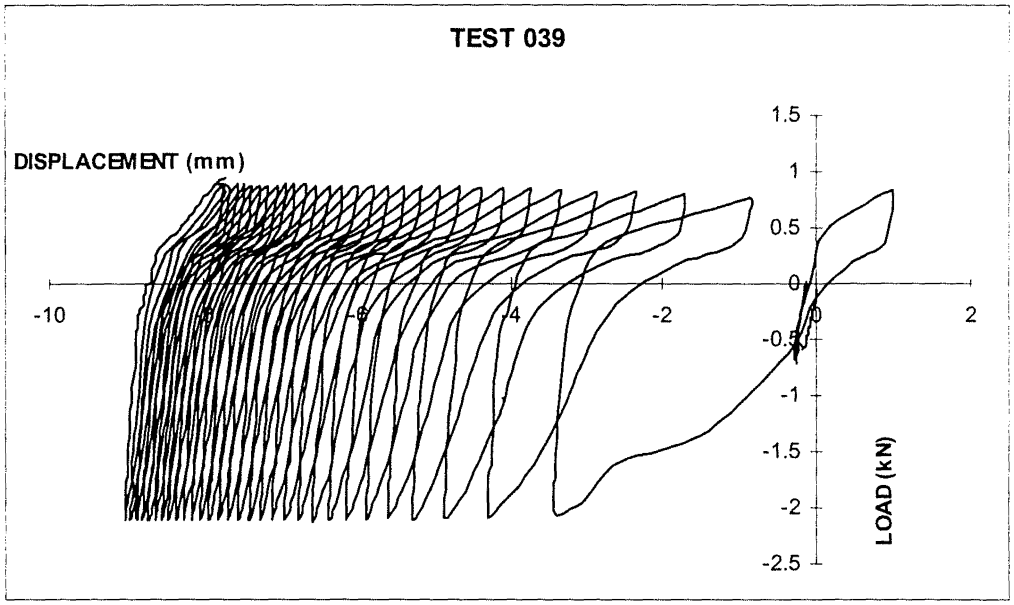

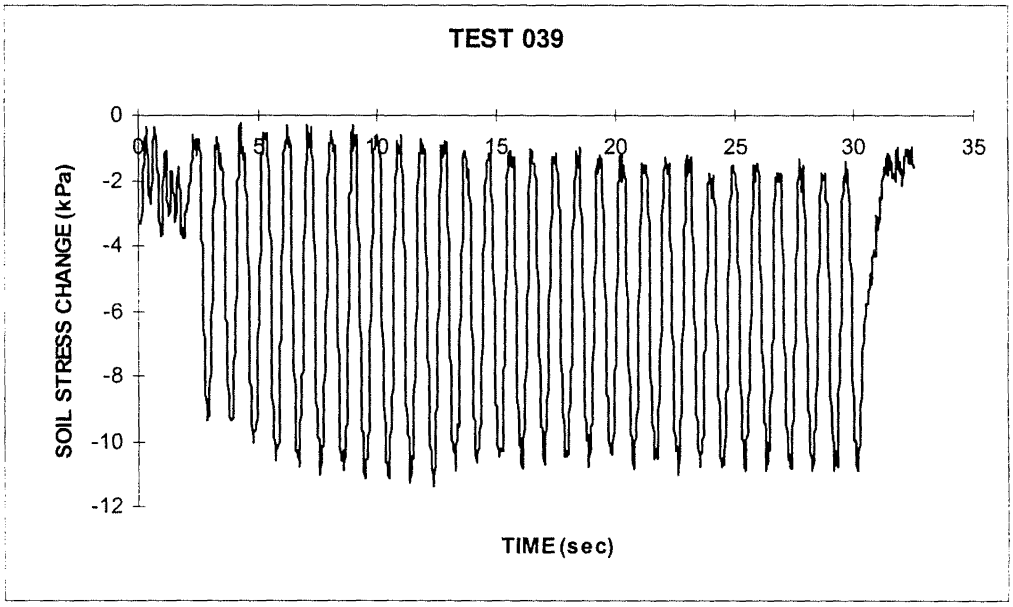

Figure B24 - Results of Test 039 – Cyclic Axial Load

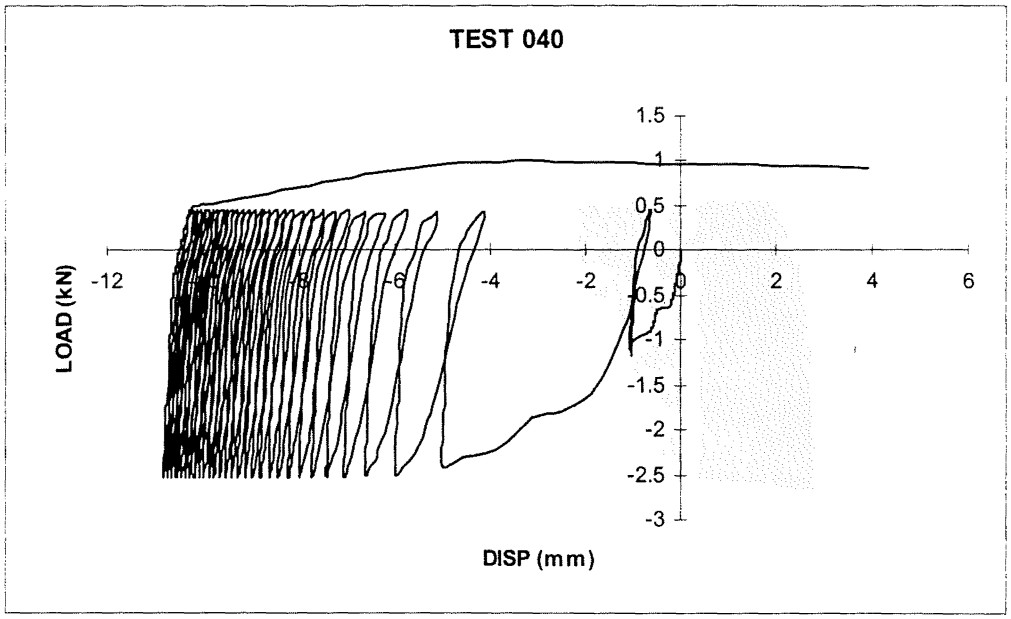

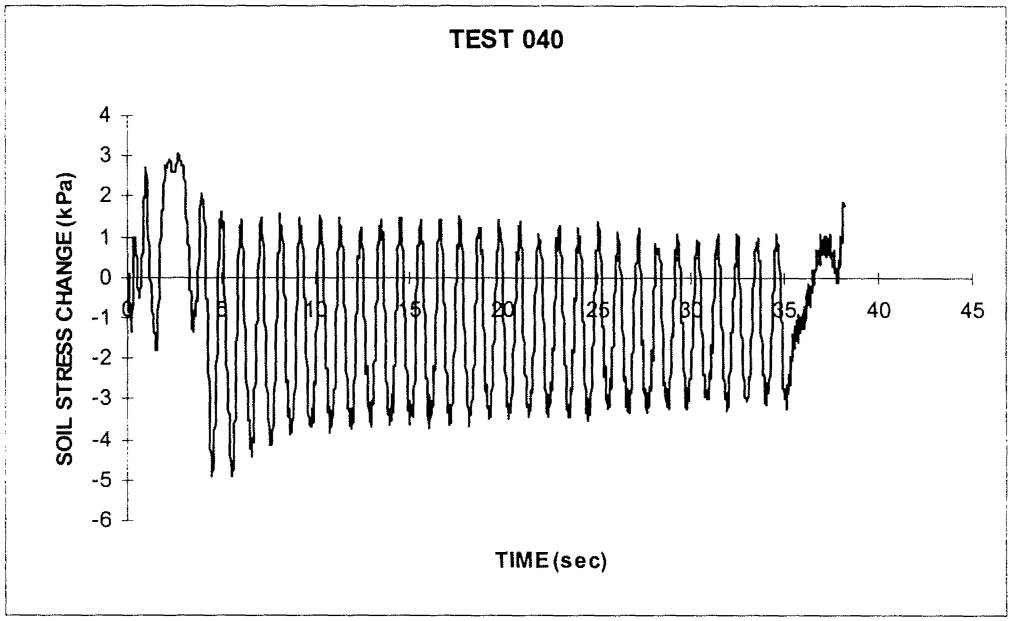

Figure B25 - Results of Test 040 – Cyclic Axial Load

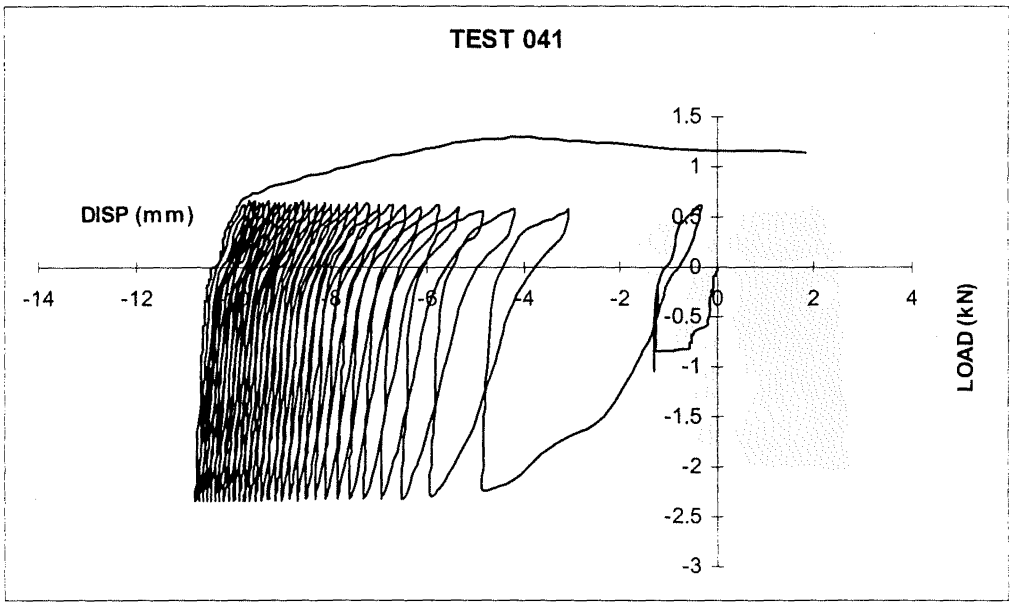

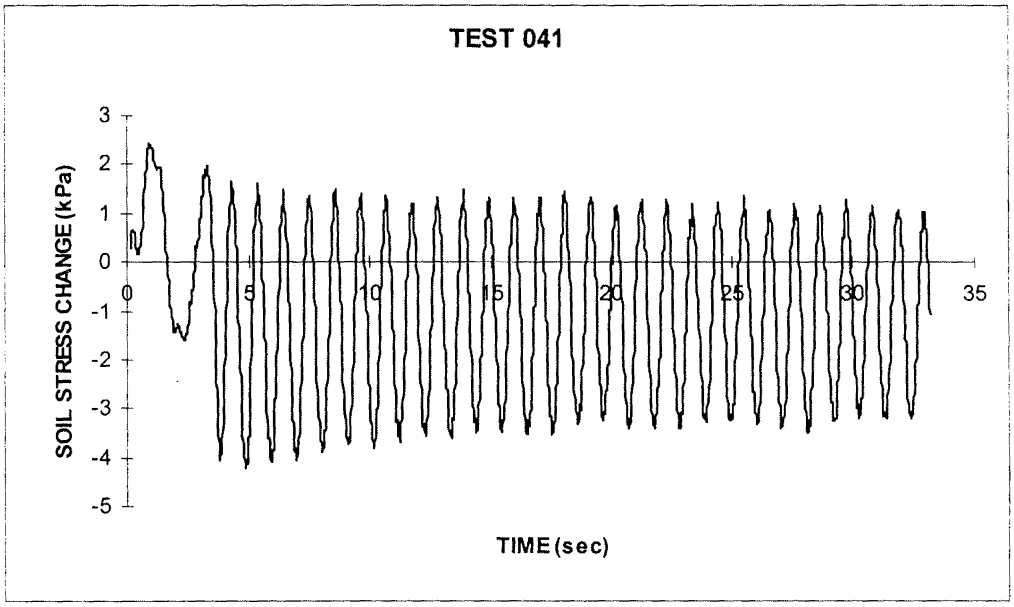

Figure B26 - Results of Test 041 – Cyclic Axial Load

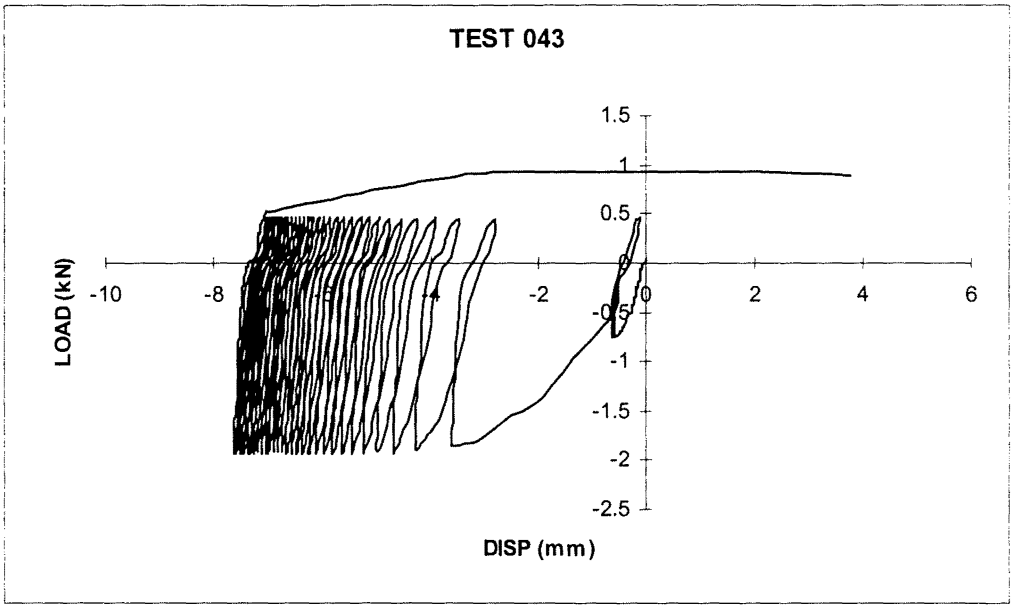

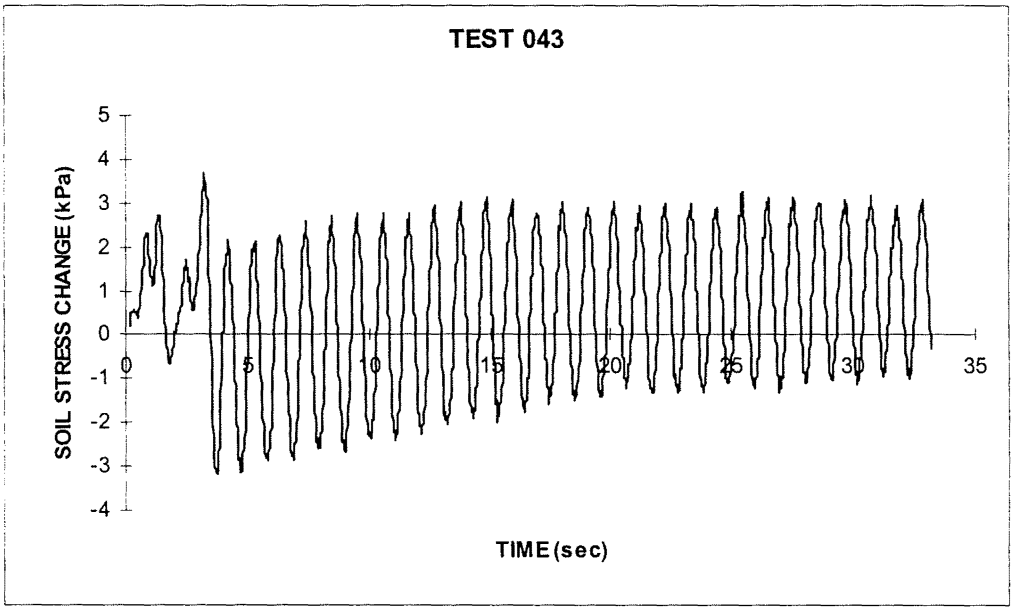

Figure B27 - Results of Test 043 – Cyclic Axial Load

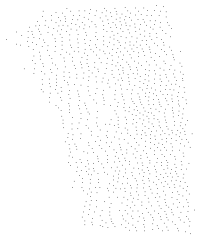

Appendix C

DYNAMIC SOIL TEST RESULTS

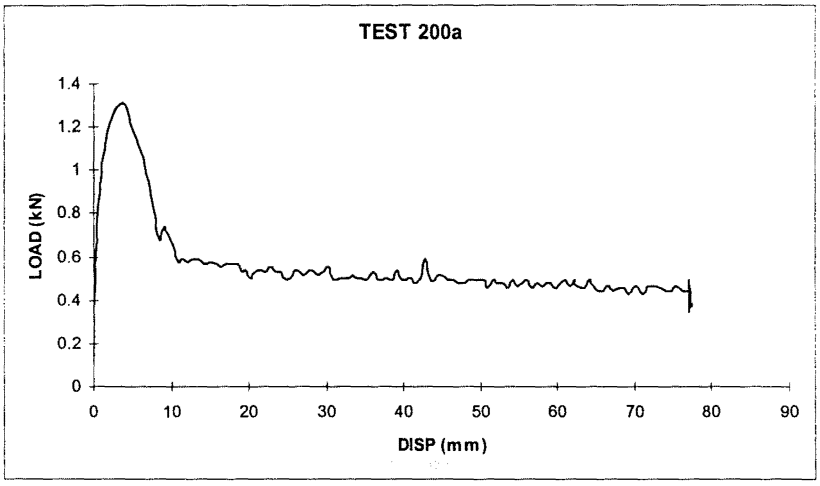

Figure C1 - Test 200a – Monotonic Uplift (No Shaking)

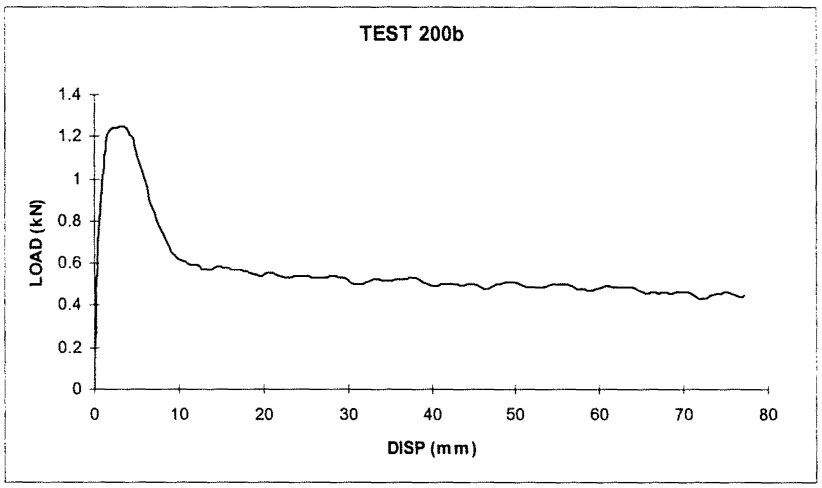

Figure C2 - Test 200b – Monotonic Uplift (No Shaking)

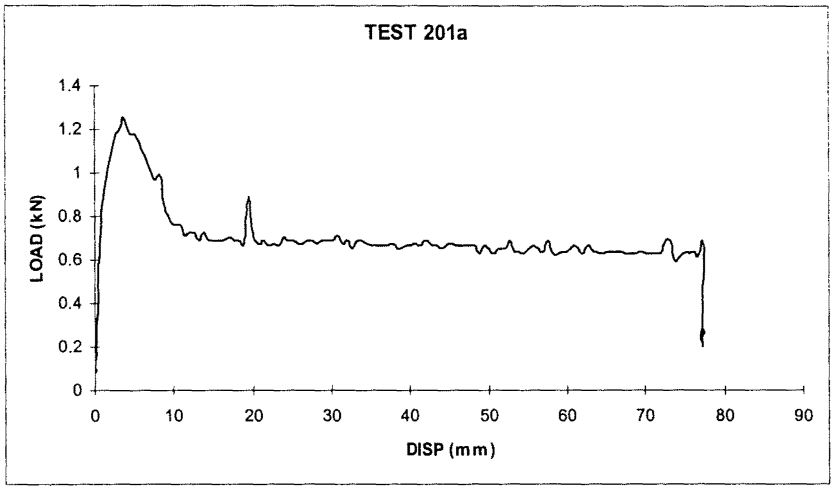

Figure C3 - Test 201a – Monotonic Uplift (No Shaking)

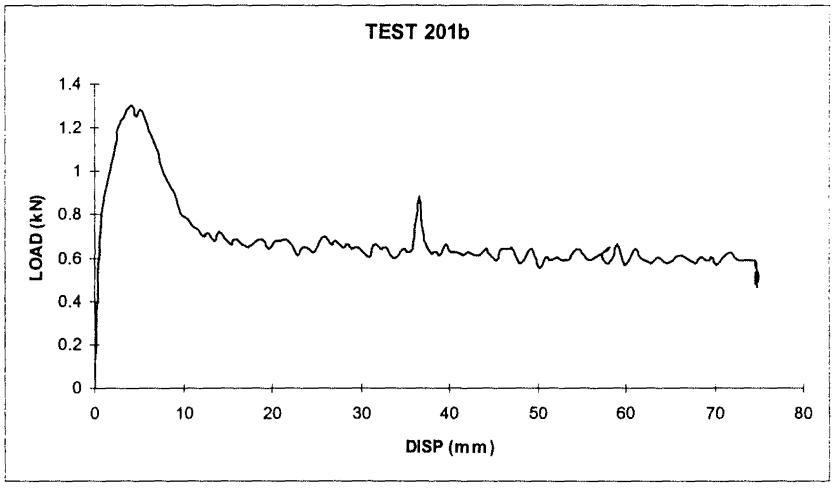

Figure C4 - Test 201b – Monotonic Uplift (No Shaking)

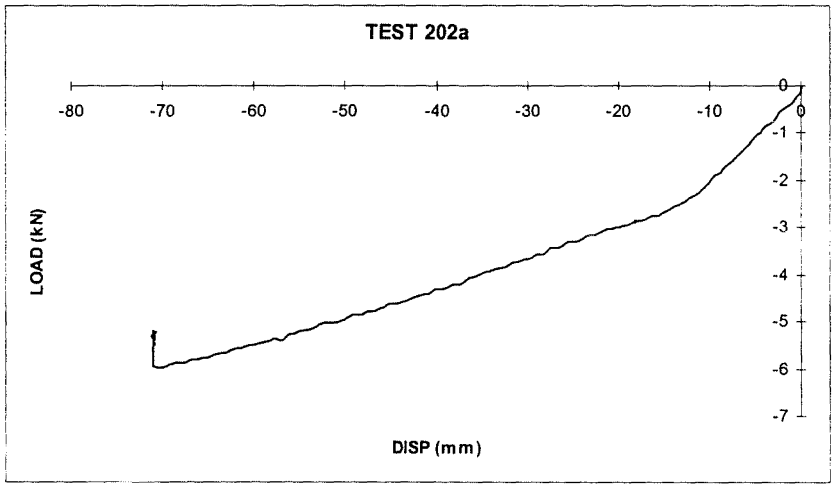

Figure C5 - Test 202a – Monotonic Compression (No Shaking)

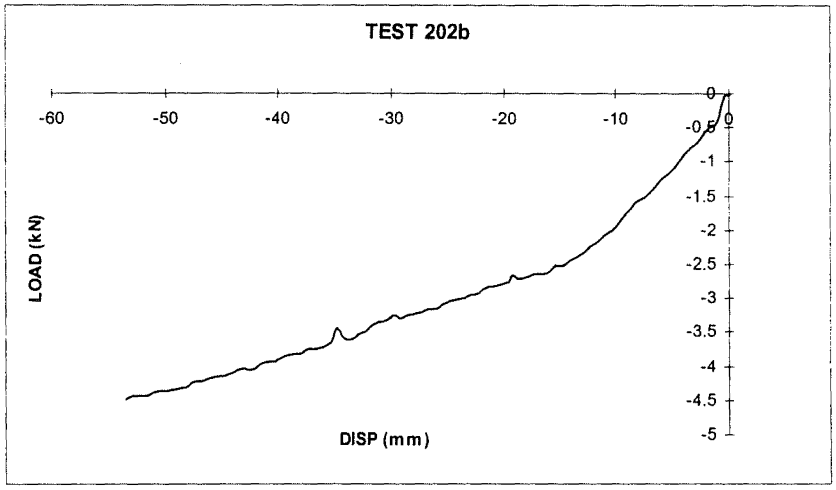

Figure C6 - Test 202b – Monotonic Compression (No Shaking)

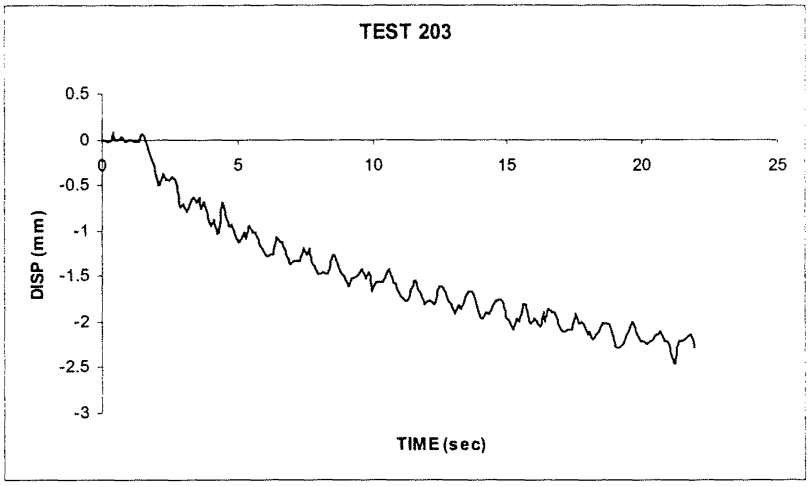

Figure C7 - Test 203 – Shaft Displacement Under Constant Axial Load (0.32 kN) and Cyclic Soil Shaking

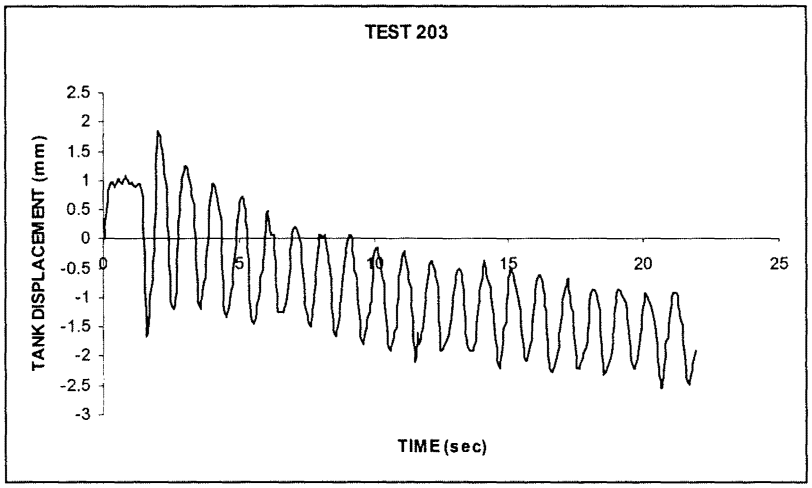

Figure C8 - Test 203 – Tank Displacement Under Cyclic Shaking

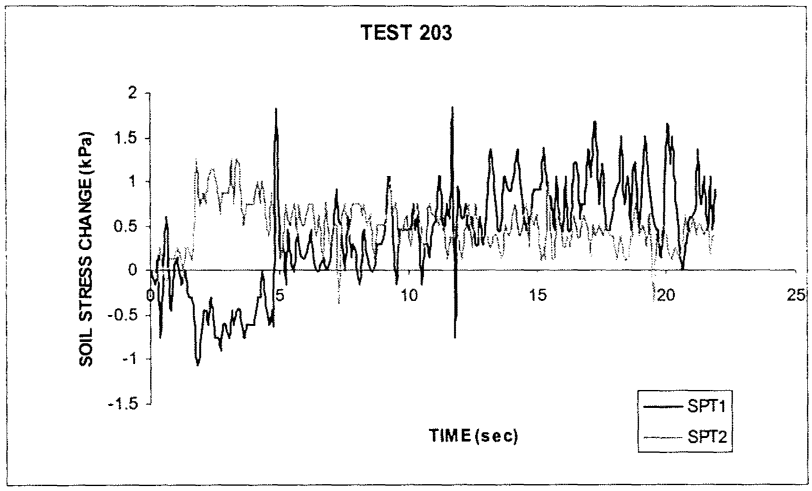

Figure C9 - Test 203 – Change in Soil Stress During Combined Loading
Depth of Burial – SPT1 = 1000 mm, SPT2 = 500mm
NOTE: Both Stress Transducers at 20 mm from shaft sidewall

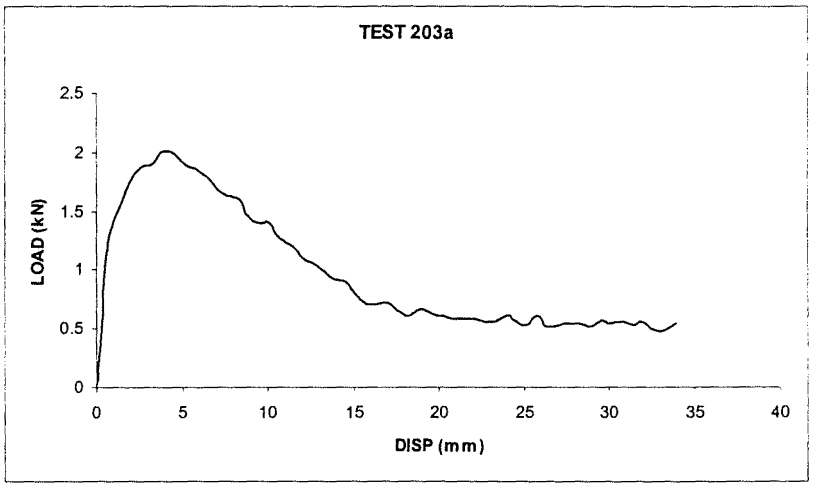

Figure C10 - Test 203a – Monotonic Uplift after Combined Loading

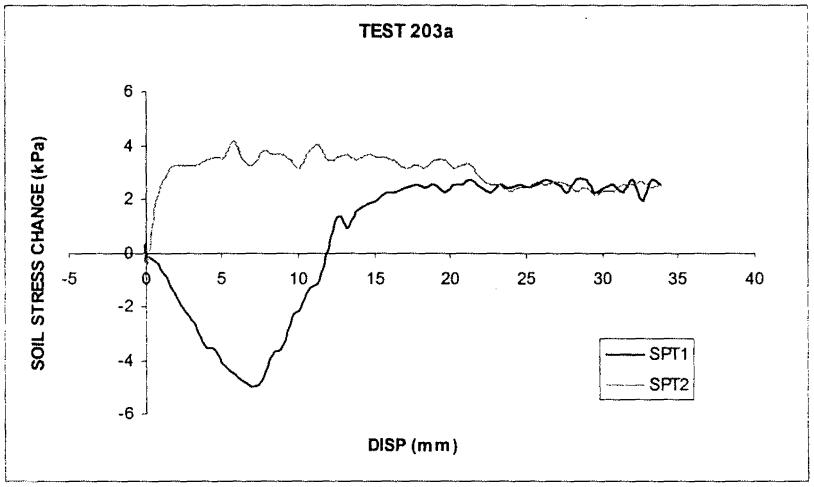

Figure C11 - Test 203a – Change in Soil Stress during Monotonic Uplift

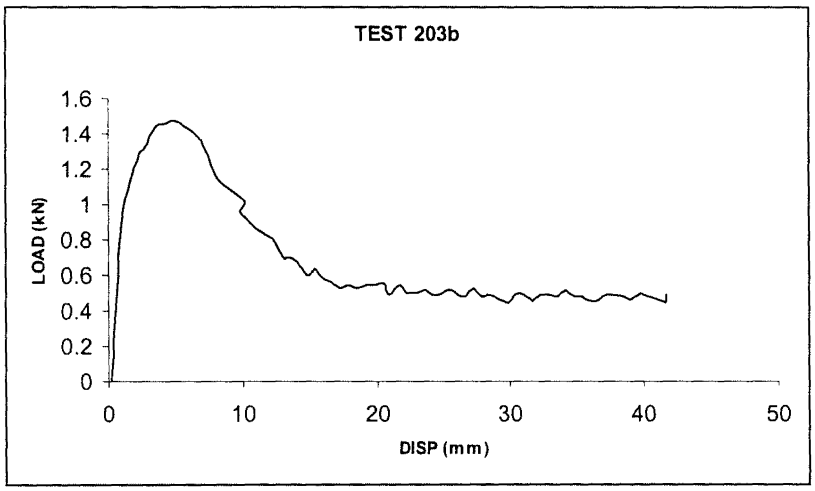

Figure C12 - Test 203b – Monotonic Uplift after Cyclic Shaking only

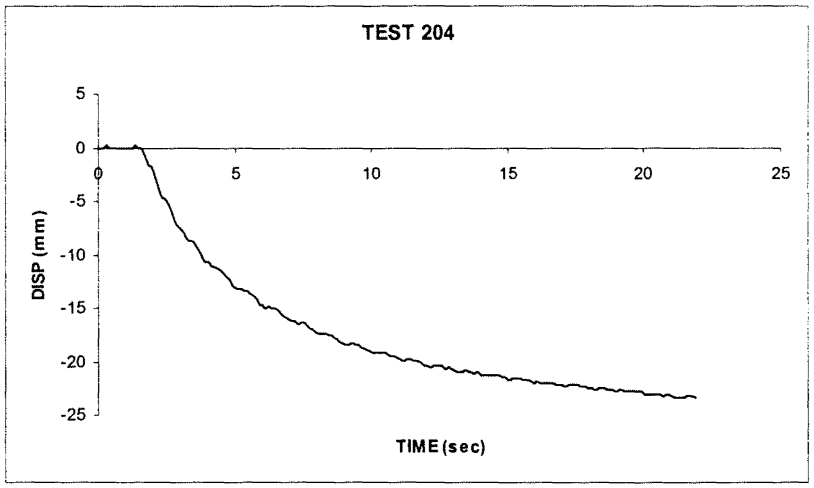

Figure C13 - Test 204 – Shaft Displacement Under Constant Axial Load (0.32 kN) and Cyclic Soil Shaking

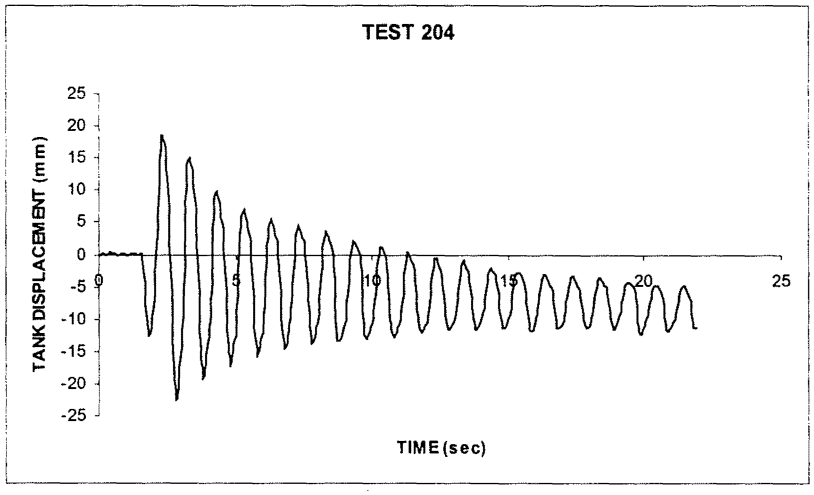

Figure C14 - Test 204 – Tank Displacement Under Cyclic Shaking

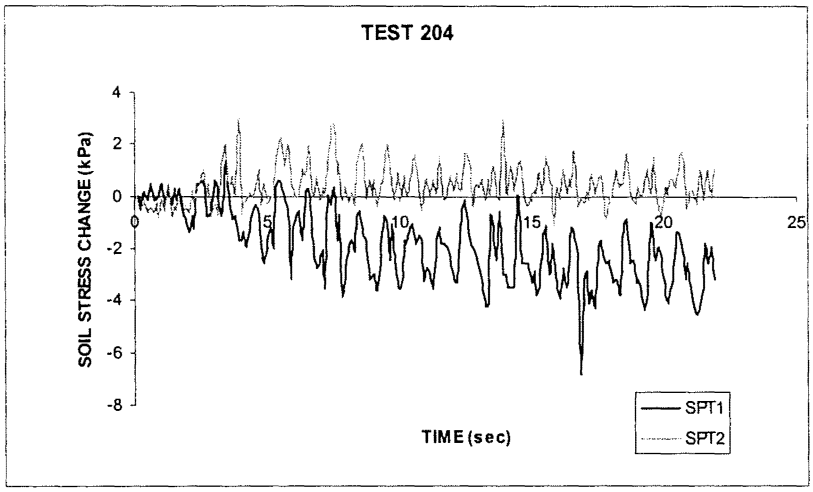

Figure C15 - Test 204 – Change in Soil Stress During Combined Loading
Depth of Burial – SPT1 = 1000 mm, SPT2 = 500mm
NOTE: Both Stress Transducers at 20 mm from shaft sidewall

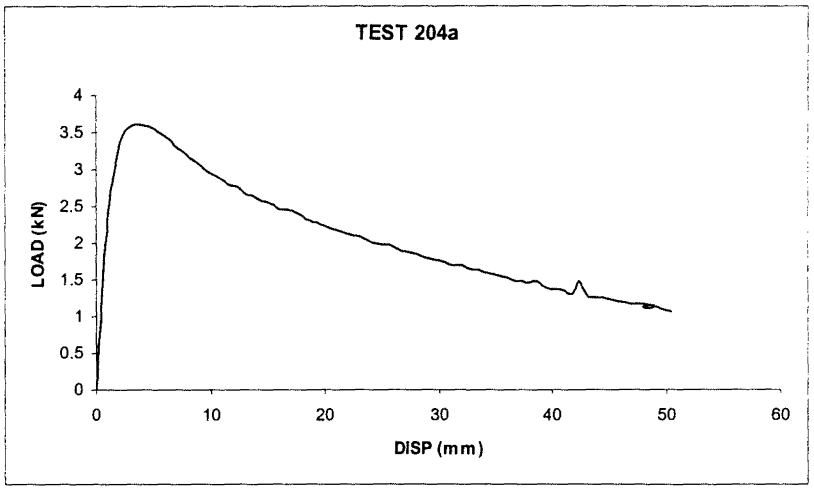

Figure C16 - Test 204a – Monotonic Uplift after Combined Loading

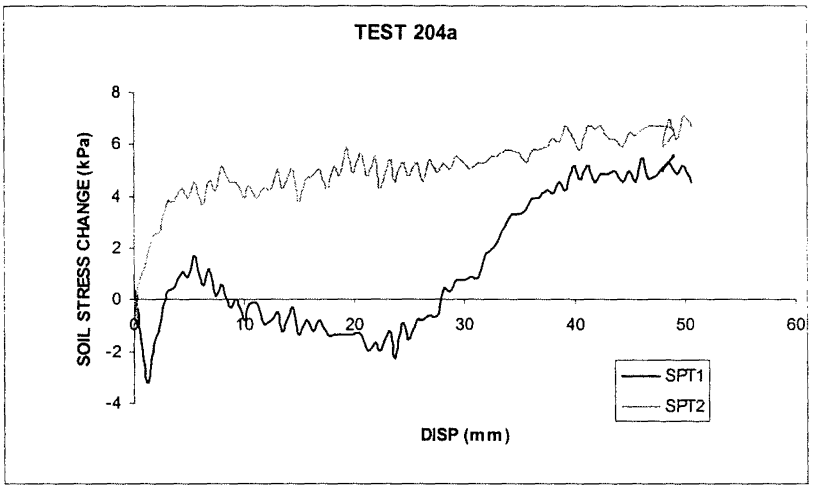

Figure C17 - Test 204a – Change in Soil Stress during Monotonic Uplift

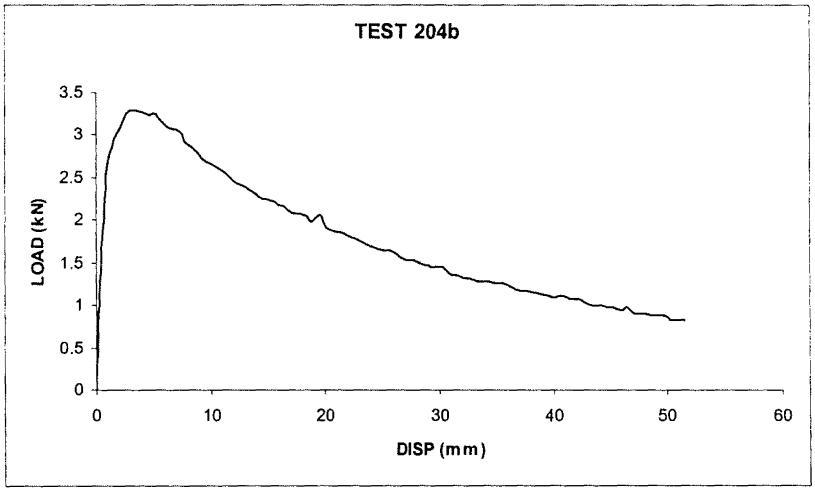

Figure C18 - Test 204b – Monotonic Uplift after Cyclic Shaking only

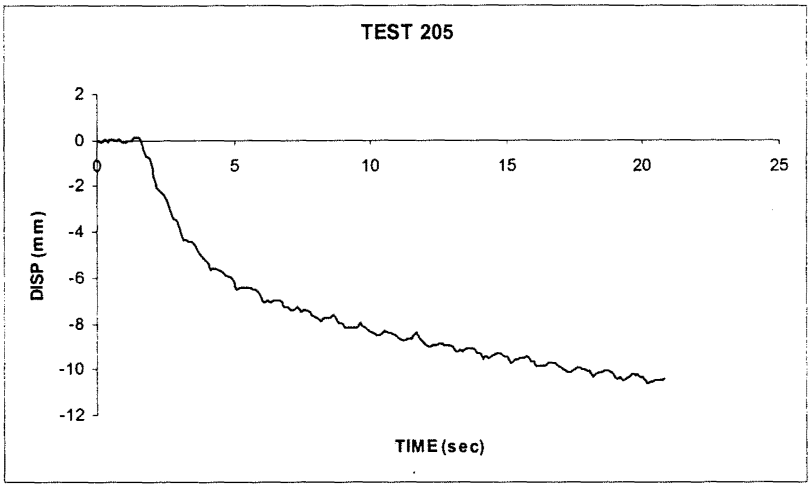

Figure C19 - Test 205 – Shaft Displacement Under Constant Axial Load (0.32 kN) and Cyclic Soil Shaking

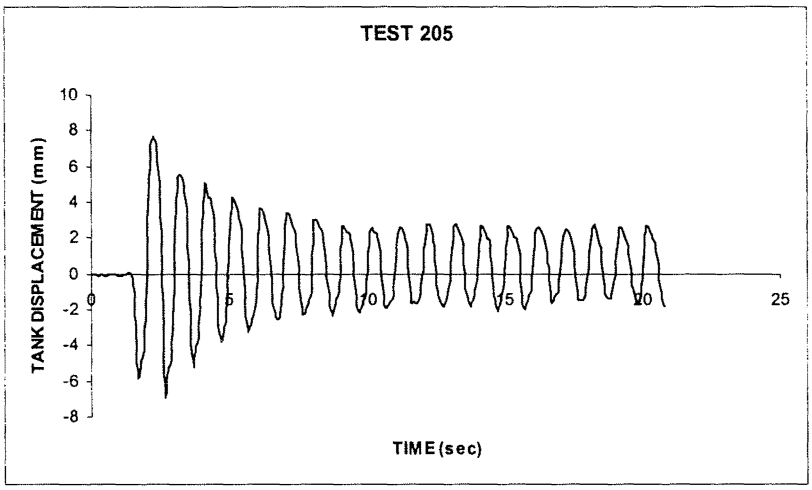

Figure C20 - Test 205 – Tank Displacement Under Cyclic Shaking

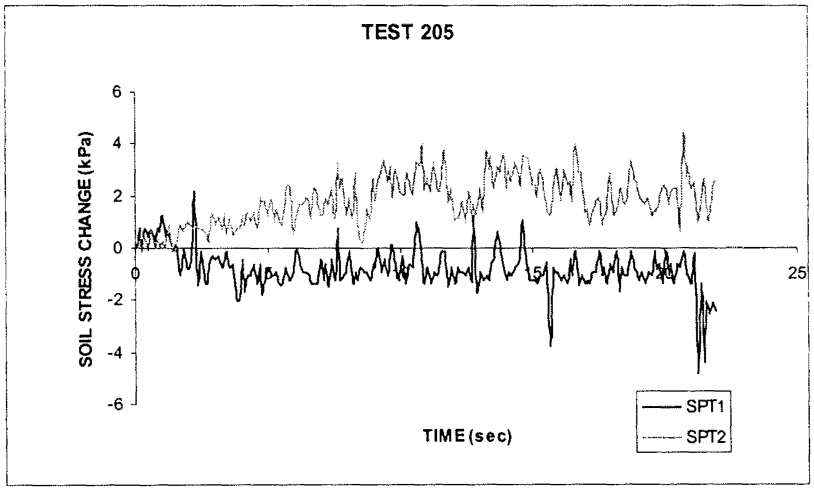

Figure C21 - Test 205 – Change in Soil Stress During Combined Loading
Depth of Burial – SPT1 = 1000 mm, SPT2 = 500mm
NOTE: Both Stress Transducers at 20 mm from shaft sidewall

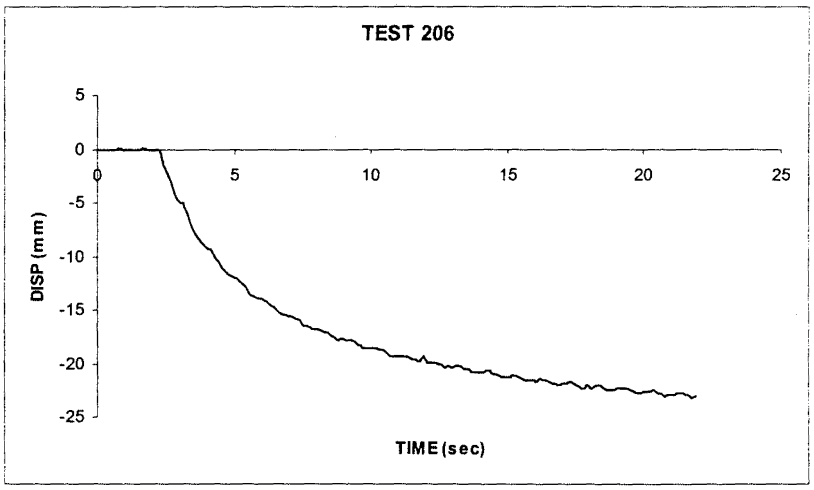

Figure C22 - Test 206 – Shaft Displacement Under Constant Axial Load (0.32 kN) and Cyclic Soil Shaking

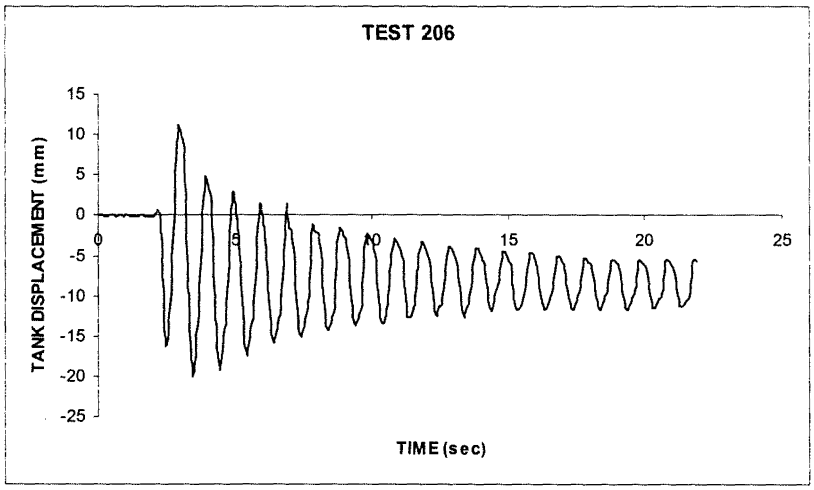

Figure C23 - Test 206 – Tank Displacement Under Cyclic Shaking

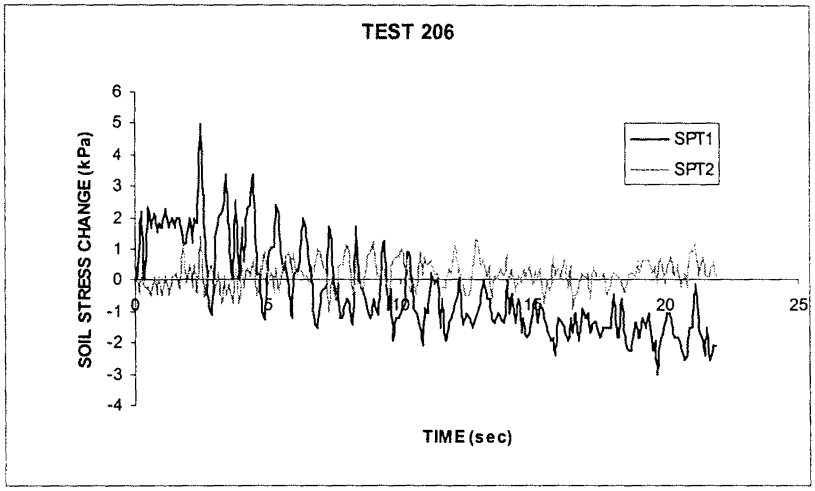

Figure C24 - Test 206 – Change in Soil Stress During Combined Loading
Depth of Burial – SPT1 = 1000 mm, SPT2 = 500mm
NOTE: Both Stress Transducers at 20 mm from shaft sidewall

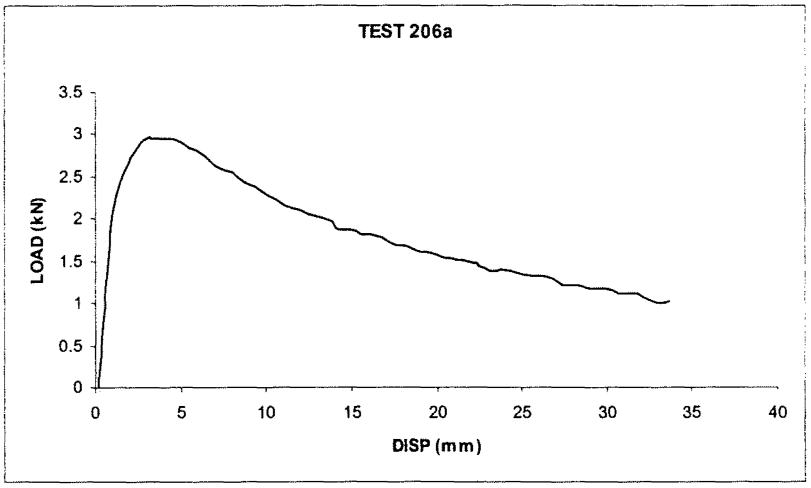

Figure C25 - Test 206a – Monotonic Uplift after Combined Loading

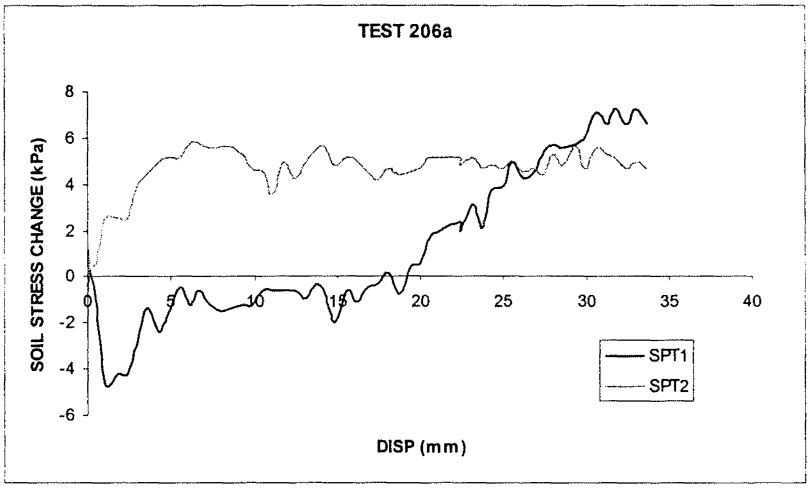

Figure C26 - Test 206a – Change in Soil Stress during Monotonic Uplift

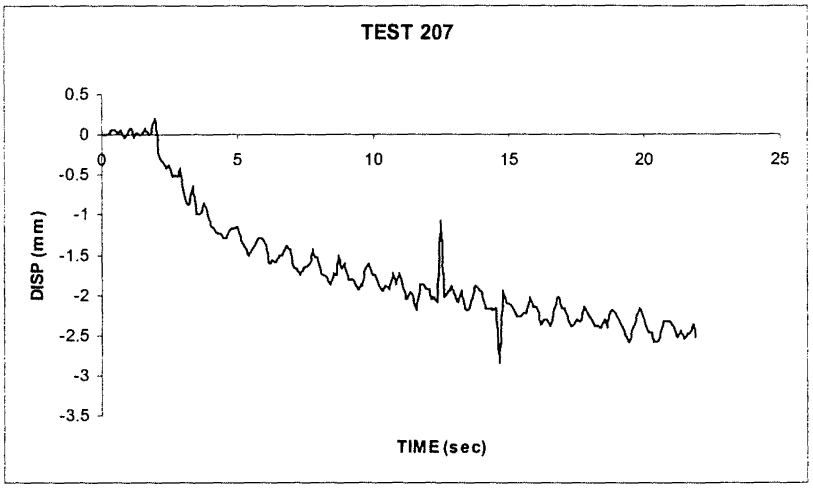

Figure C27 - Test 207 – Shaft Displacement Under Constant Axial Load (0.64 kN) and Cyclic Soil Shaking

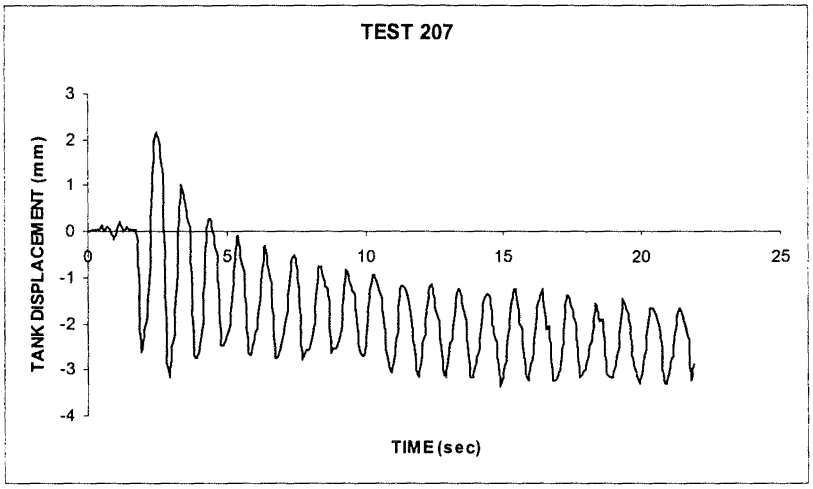

Figure C28 - Test 207 – Tank Displacement Under Cyclic Shaking

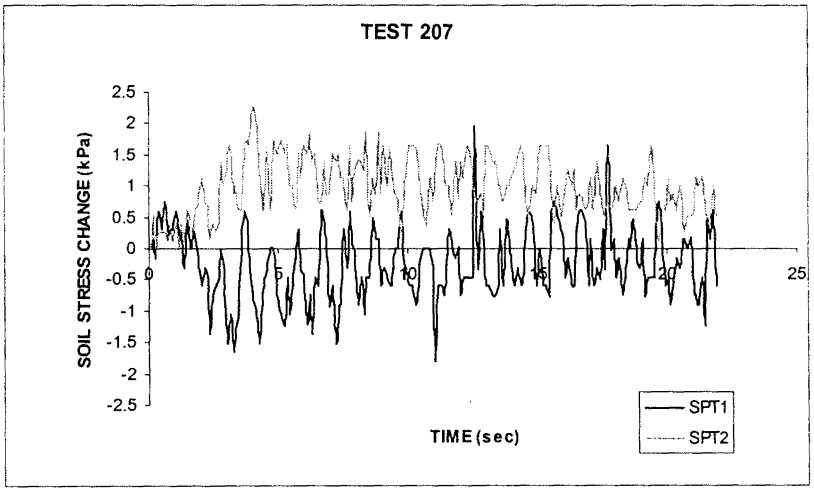

Figure C29 - Test 207 – Change in Soil Stress During Combined Loading
Depth of Burial – SPT1 = 1000 mm, SPT2 = 500mm
NOTE: Both Stress Transducers at 20 mm from shaft sidewall

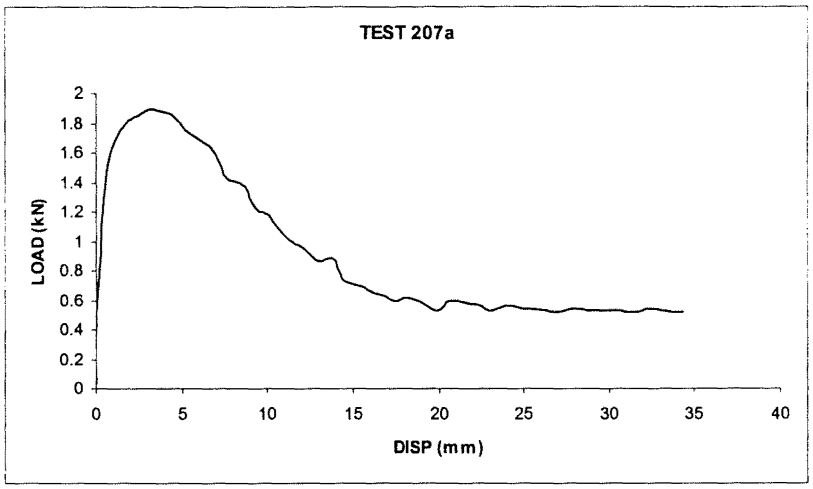

Figure C30 - Test 207a – Monotonic Uplift after Combined Loading

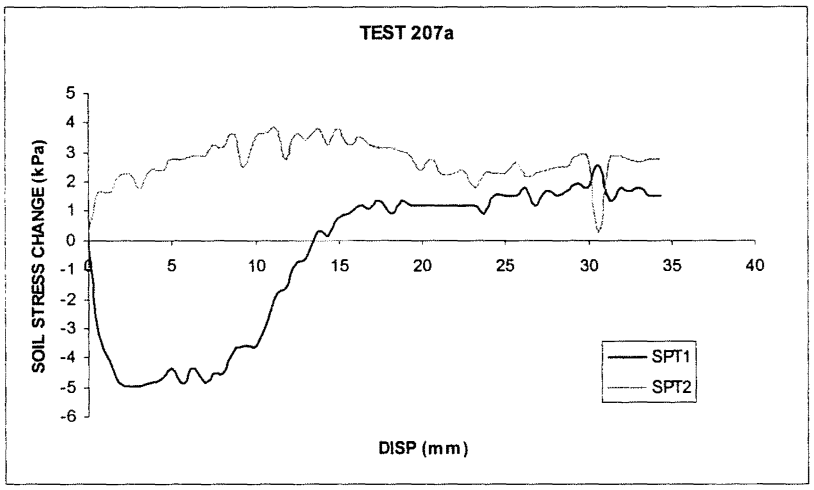

Figure C31 - Test 207a – Change in Soil Stress during Monotonic Uplift

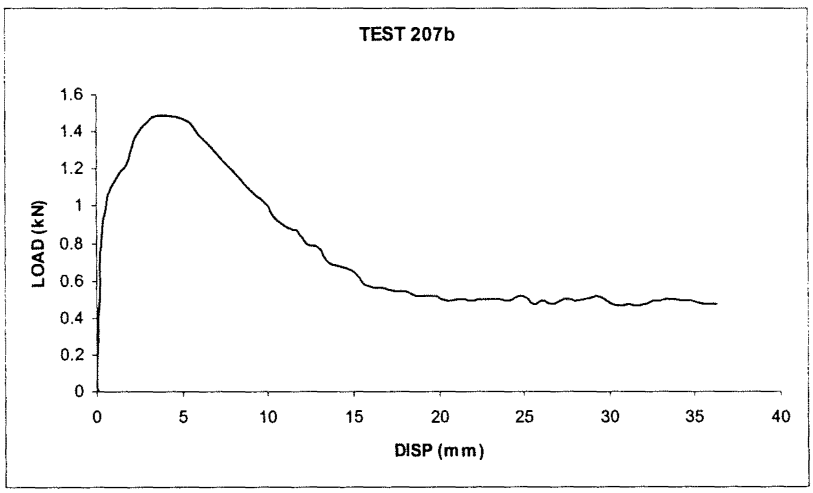

Figure C32 - Test 207b – Monotonic Uplift after Cyclic Shaking only

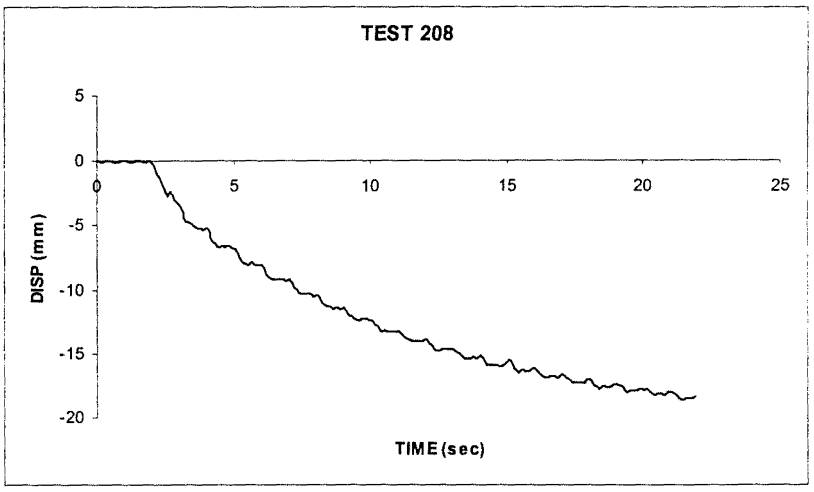

Figure C33 - Test 208 – Shaft Displacement Under Constant Axial Load (0.64 kN) and Cyclic Soil Shaking

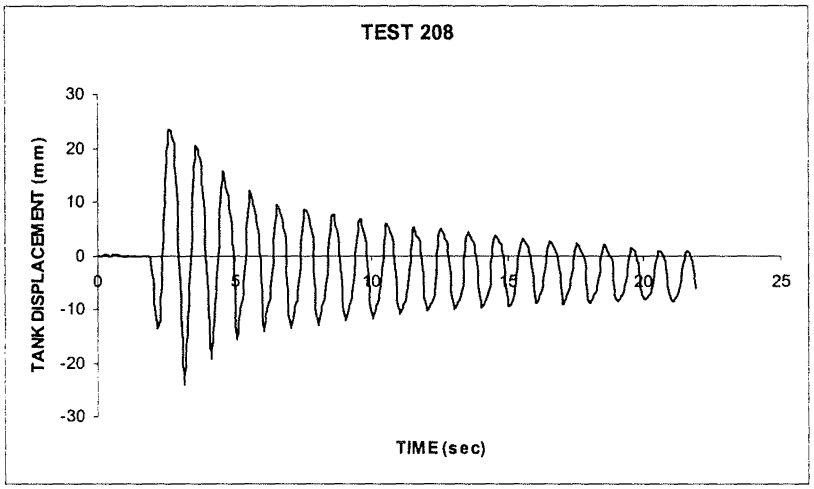

Figure C34 - Test 208 – Tank Displacement Under Cyclic Shaking

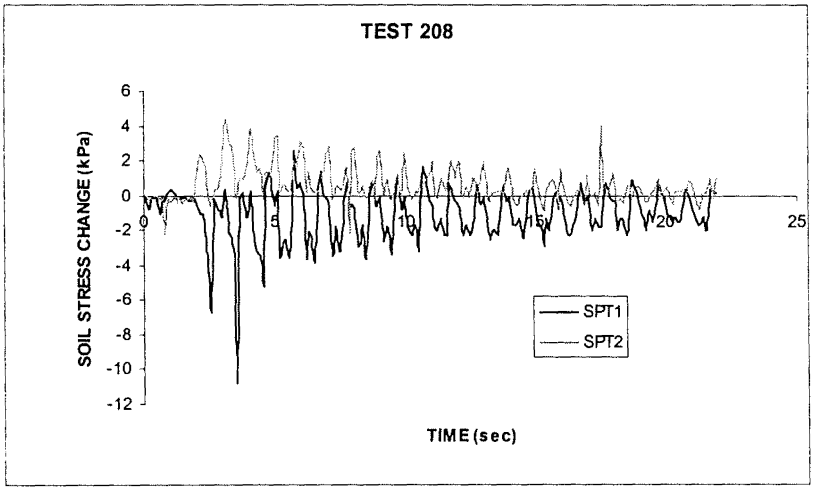

Figure C35 - Test 208 – Change in Soil Stress During Combined Loading
Depth of Burial – SPT1 = 1000 mm, SPT2 = 500mm
NOTE: Both Stress Transducers at 20 mm from shaft sidewall

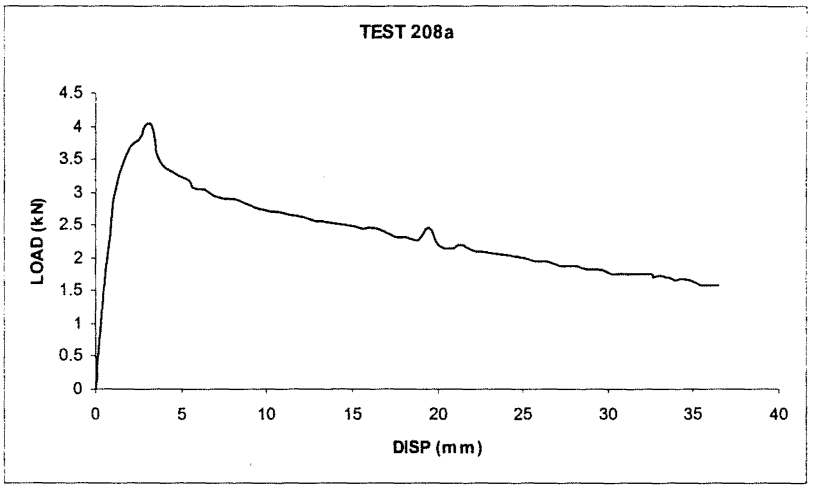

Figure C36 - Test 208a – Monotonic Uplift after Combined Loading

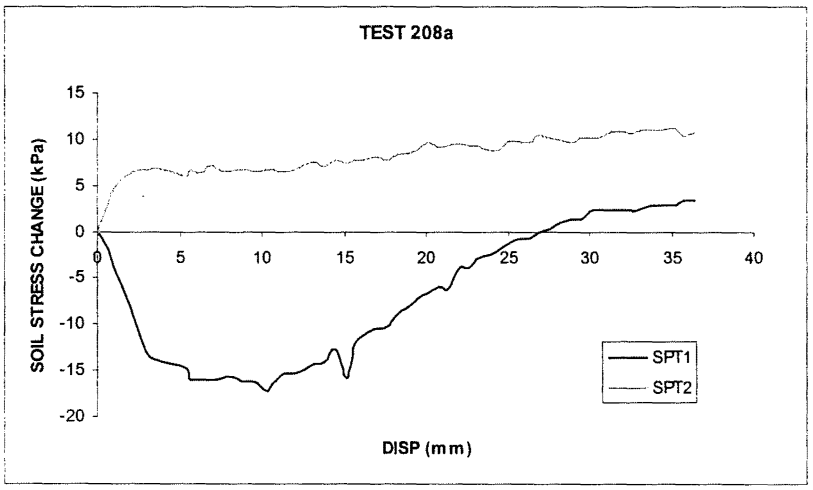

Figure C37 - Test 208a – Change in Soil Stress during Monotonic Uplift

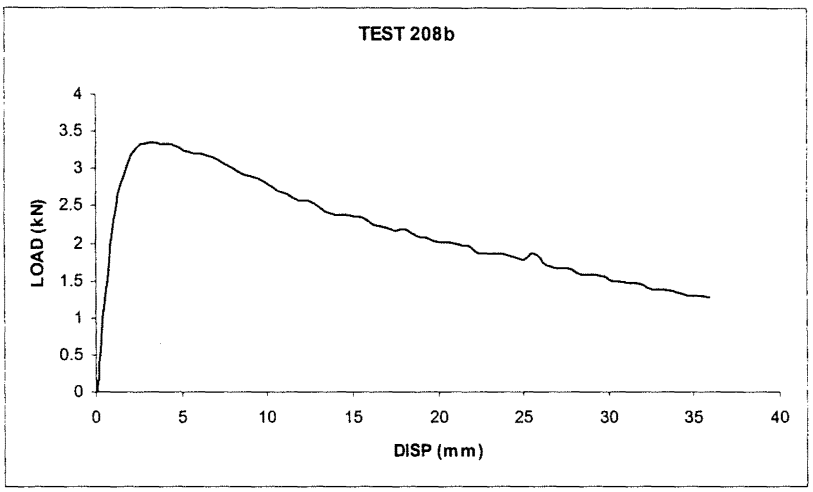

Figure C38 - Test 208b – Monotonic Uplift after Cyclic Shaking only

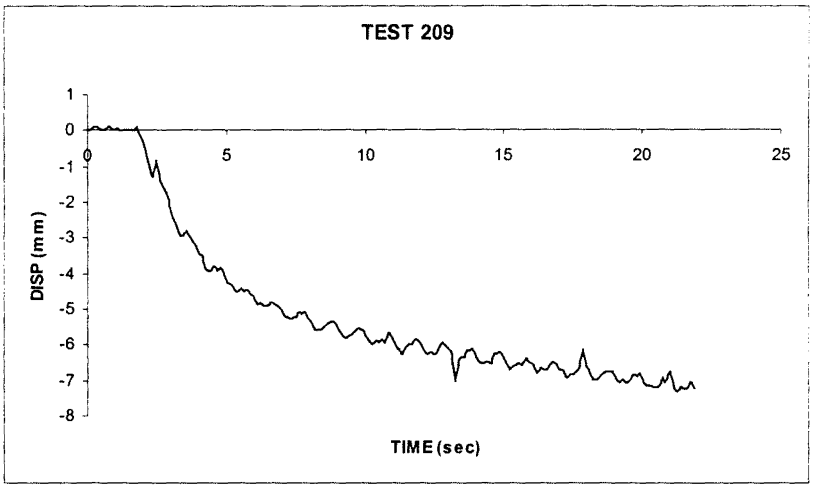

Figure C39 - Test 209 – Shaft Displacement Under Constant Axial Load (0.64 kN) and Cyclic Soil Shaking

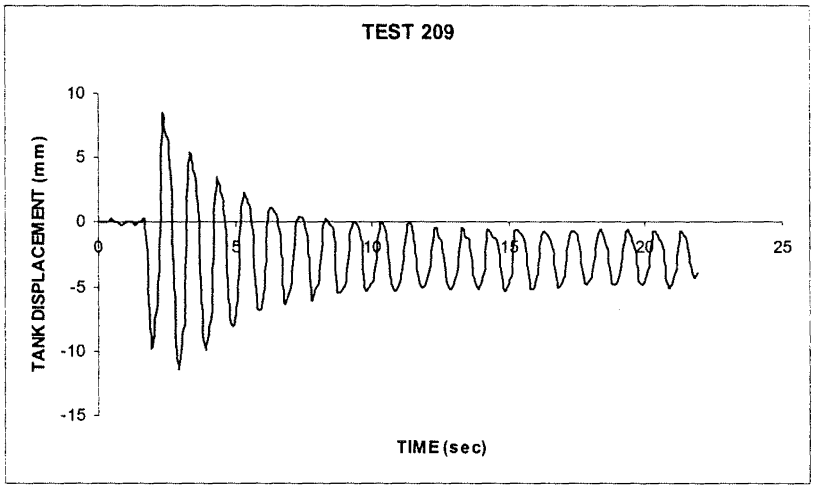

Figure C40 - Test 209 – Tank Displacement Under Cyclic Shaking

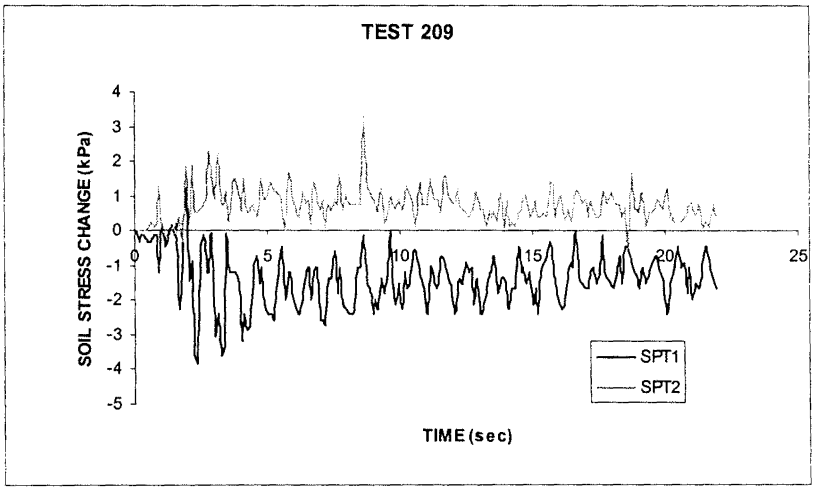

Figure C41 - Test 209 – Change in Soil Stress During Combined Loading
Depth of Burial – SPT1 = 1000 mm, SPT2 = 500mm
NOTE: Both Stress Transducers at 20 mm from shaft sidewall

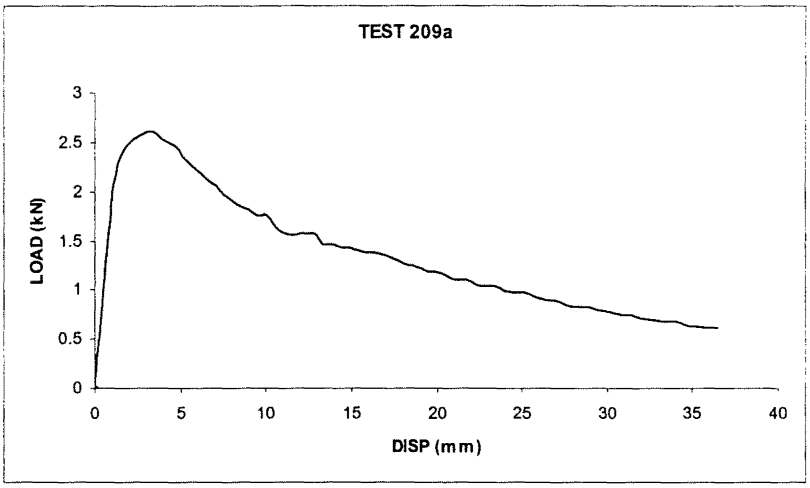

Figure C42 - Test 209a – Monotonic Uplift after Combined Loading

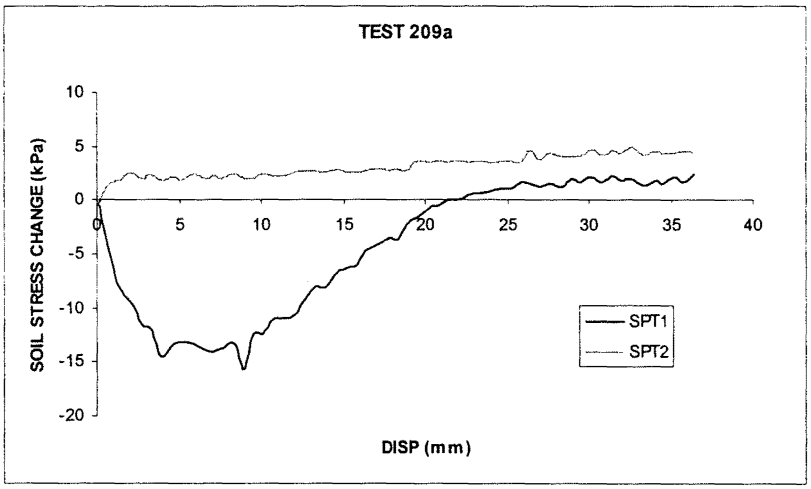

Figure C43 - Test 209a – Change in Soil Stress during Monotonic Uplift

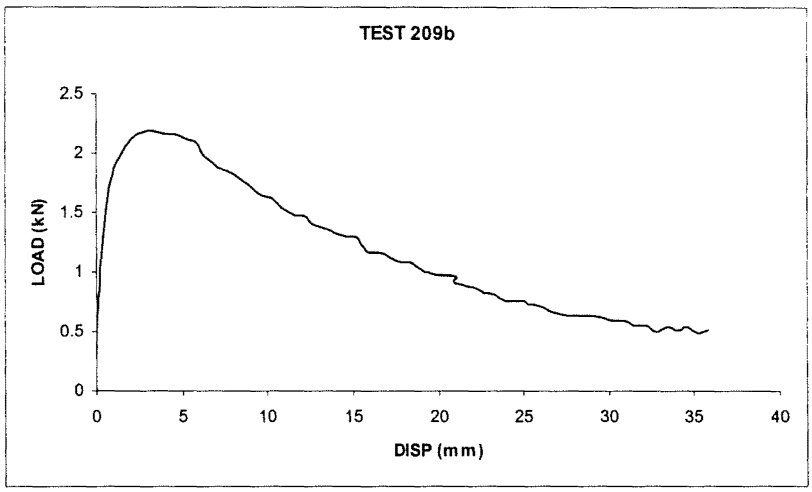

Figure C44 - Test 209b – Monotonic Uplift after Cyclic Shaking only

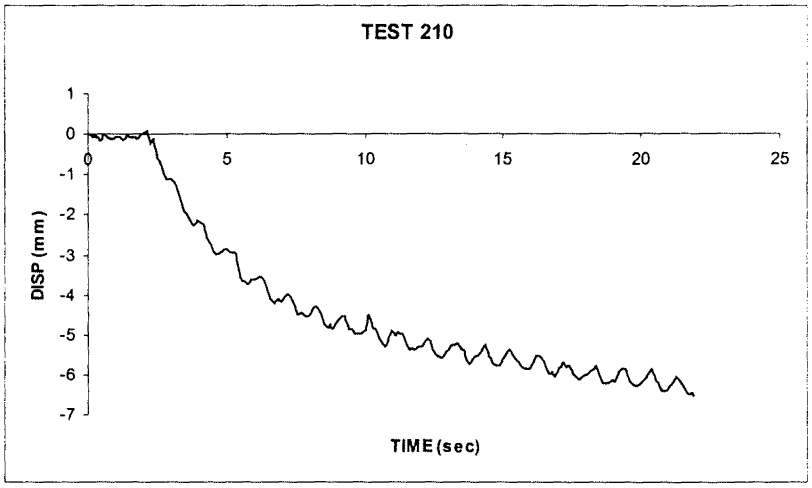

Figure C45 - Test 210 – Shaft Displacement Under Constant Axial Load (0.64kN) and Cyclic Soil Shaking

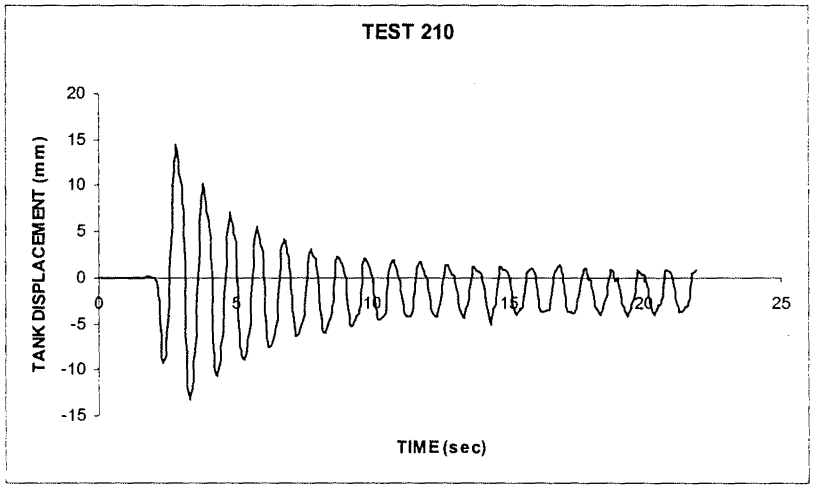

Figure C46 - Test 210 – Tank Displacement Under Cyclic Shaking

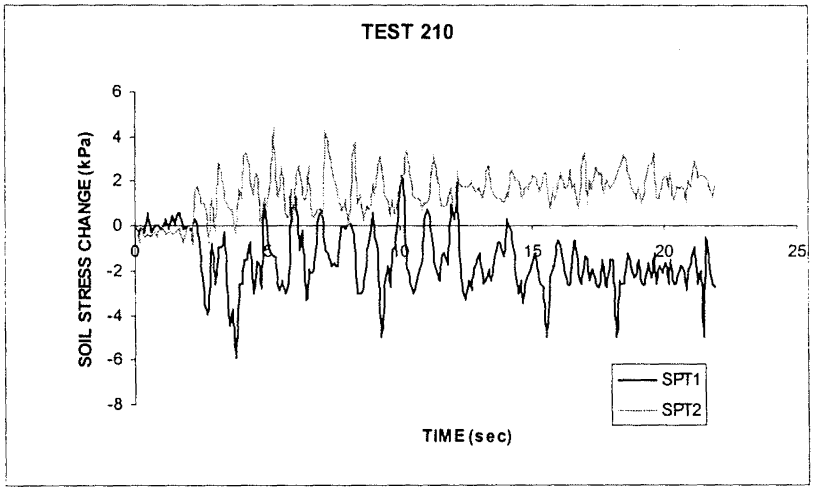

Figure C47 - Test 210 – Change in Soil Stress During Combined Loading
Depth of Burial – SPT1 = 1000 mm, SPT2 = 500mm
NOTE: Both Stress Transducers at 20 mm from shaft sidewall

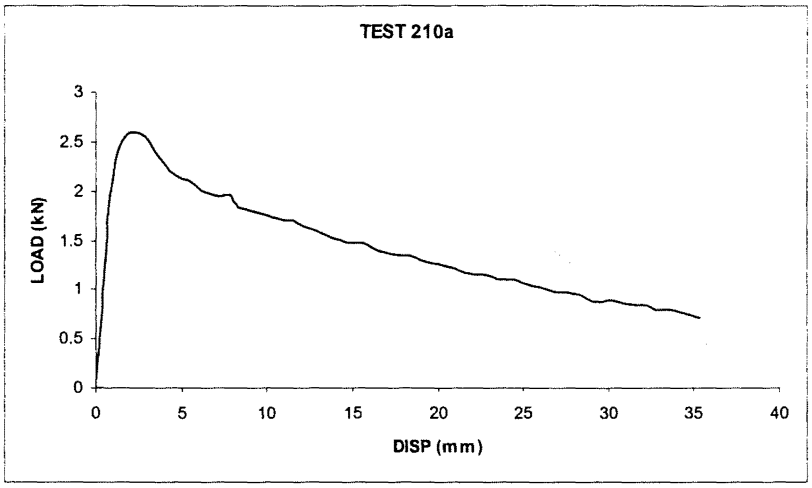

Figure C48 - Test 210a – Monotonic Uplift after Combined Loading

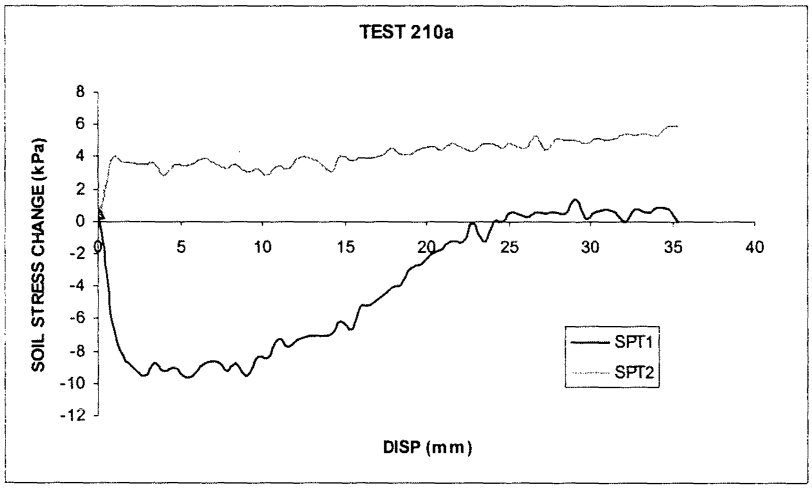

Figure C49 - Test 210a – Change in Soil Stress during Monotonic Uplift

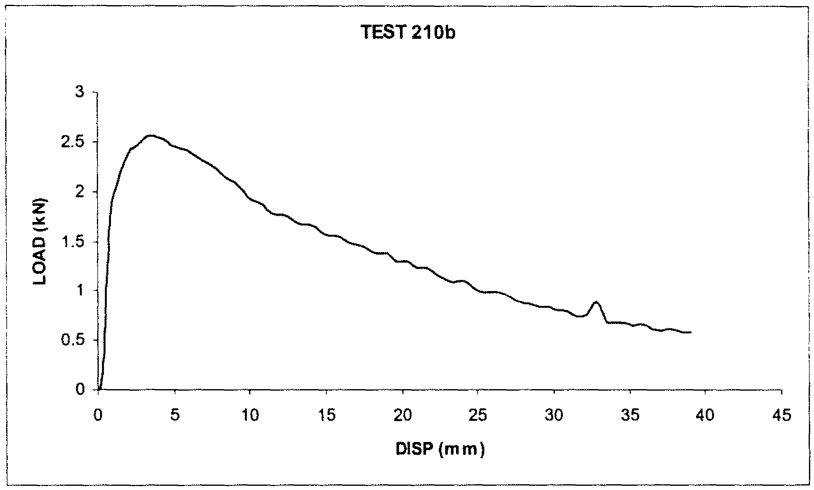

Figure C50 - Test 210b – Monotonic Uplift after Cyclic Shaking only

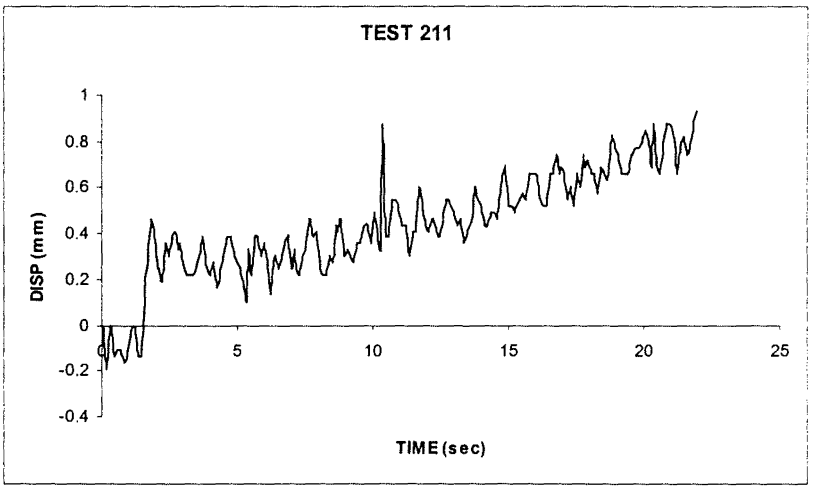

Figure C51 - Test 211 – Shaft Displacement Under Constant Axial Load (0.96 kN) and Cyclic Soil Shaking

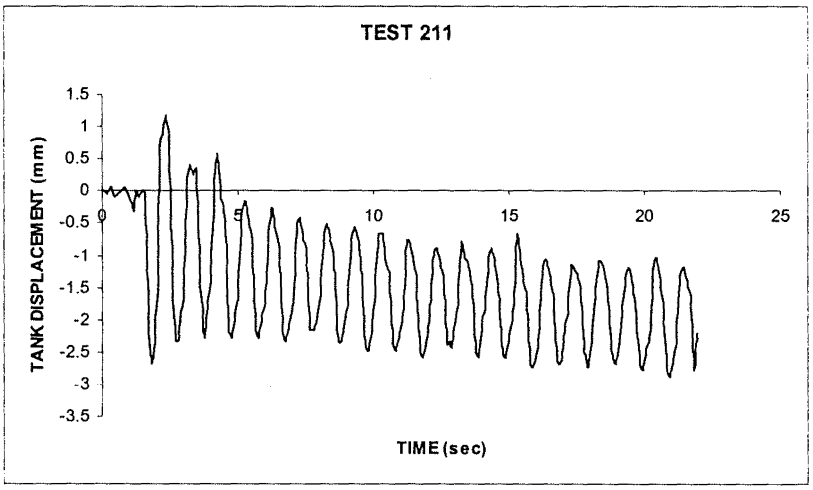

Figure C52 - Test 211 – Tank Displacement Under Cyclic Shaking

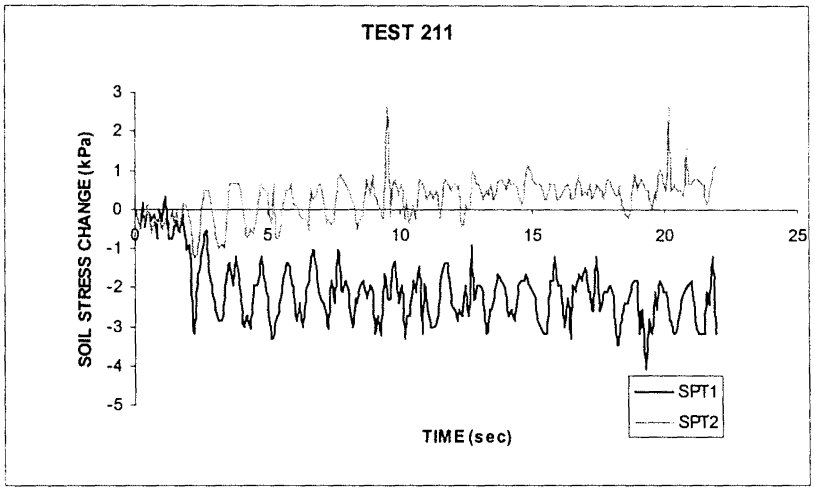

Figure C53 - Test 211 – Change in Soil Stress During Combined Loading
Depth of Burial – SPT1 = 1000 mm, SPT2 = 500mm
NOTE: Both Stress Transducers at 20 mm from shaft sidewall

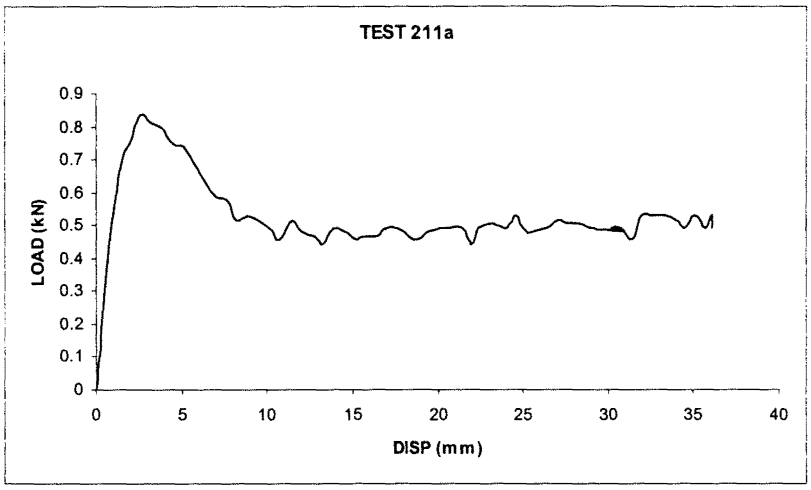

Figure C54 - Test 211a – Monotonic Uplift after Combined Loading

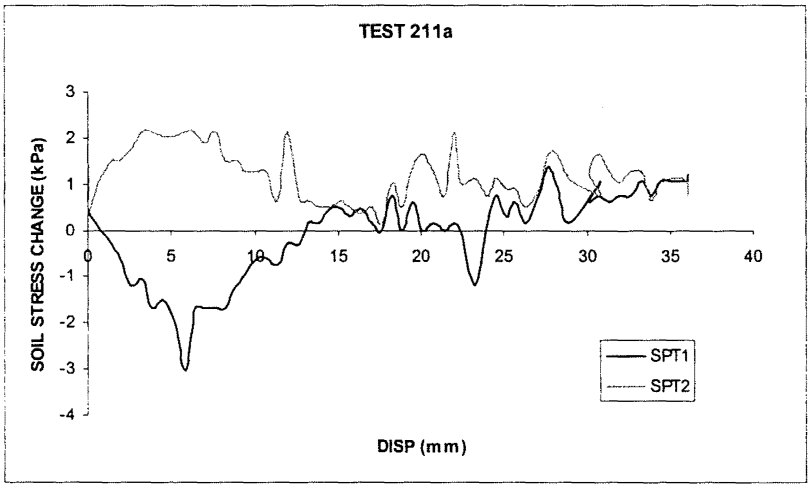

Figure C55 - Test 211a – Change in Soil Stress during Monotonic Uplift

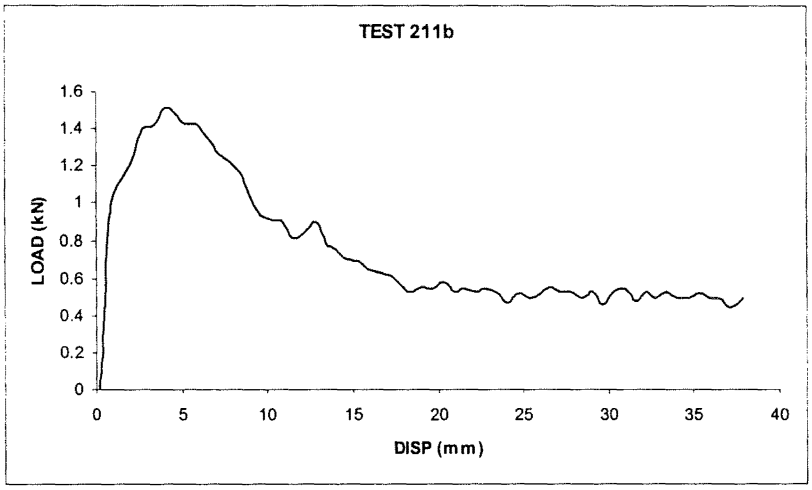

Figure C56 - Test 211b – Monotonic Uplift after Cyclic Shaking only

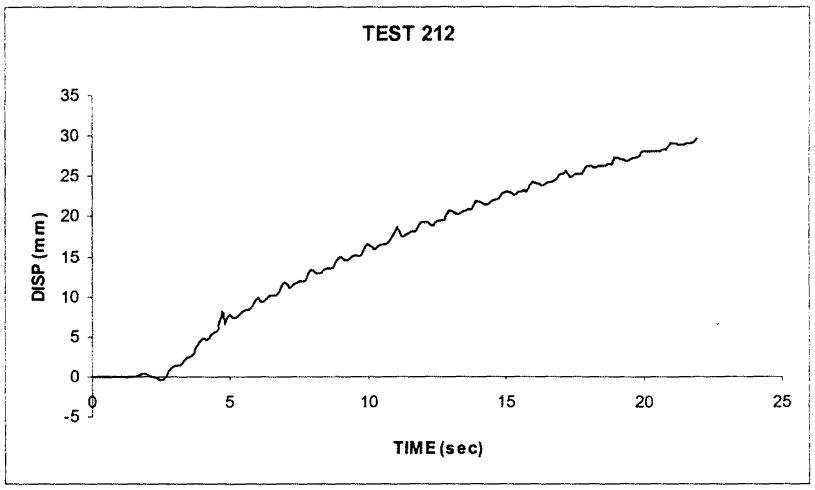

Figure C57 - Test 212 – Shaft Displacement Under Constant Axial Load (0.96 kN) and Cyclic Soil Shaking

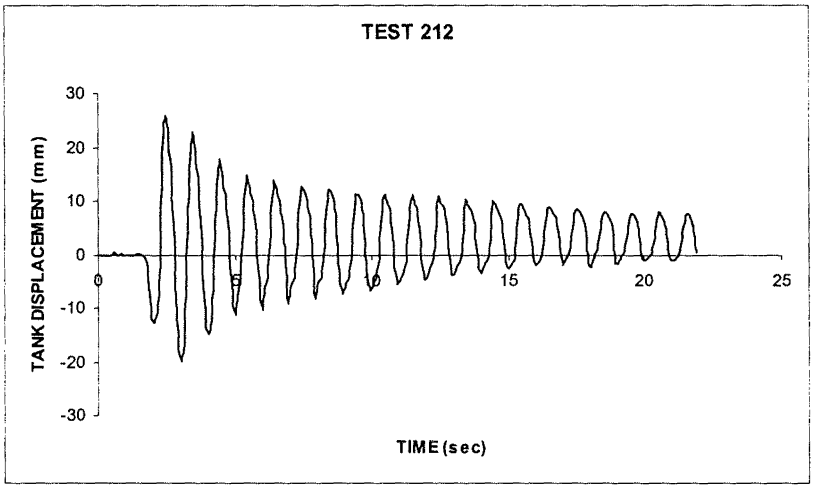

Figure C58 - Test 212 – Tank Displacement Under Cyclic Shaking

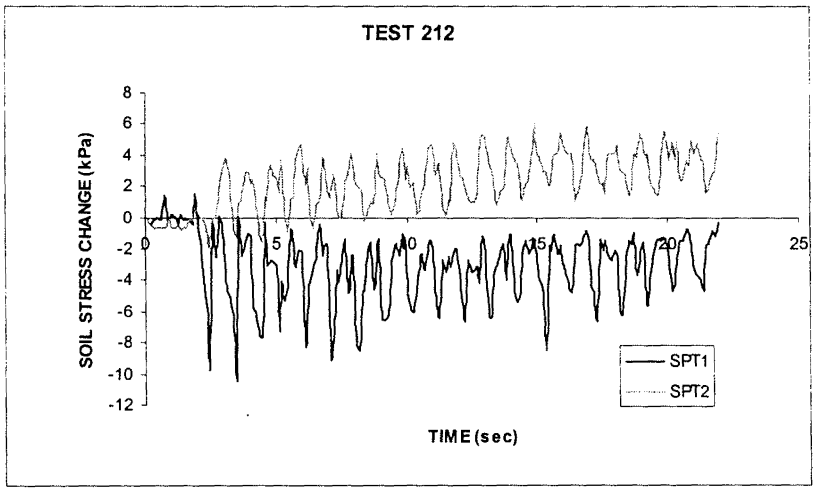

Figure C59 - Test 212 – Change in Soil Stress During Combined Loading
Depth of Burial – SPT1 = 1000 mm, SPT2 = 500mm
NOTE: Both Stress Transducers at 20 mm from shaft sidewall

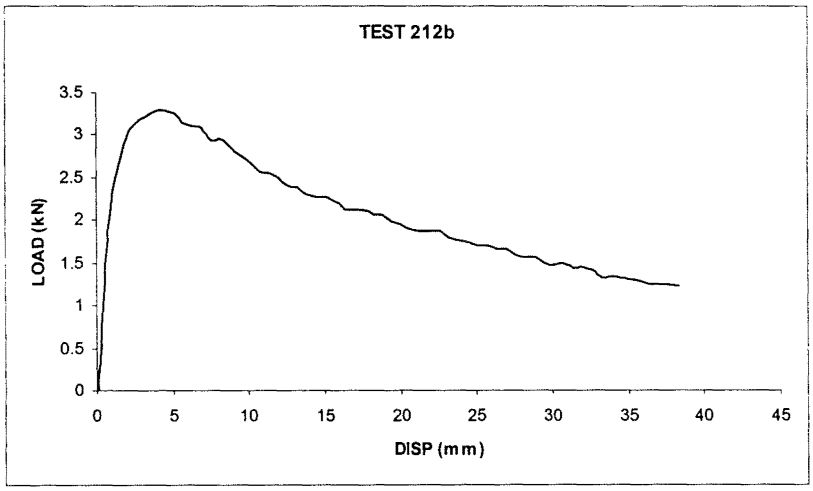

Figure C60 - Test 212b – Monotonic Uplift after Cyclic Shaking only

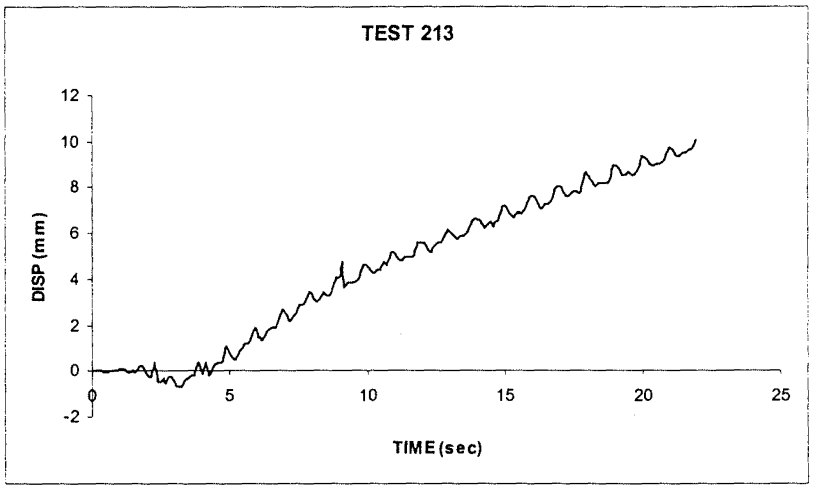

Figure C61 - Test 213 – Shaft Displacement Under Constant Axial Load (0.96 kN) and Cyclic Soil Shaking

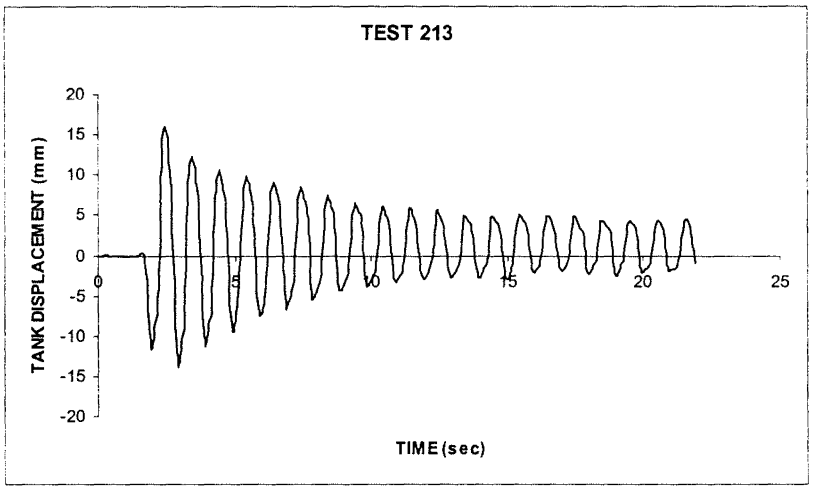

Figure C62 - Test 213 – Tank Displacement Under Cyclic Shaking

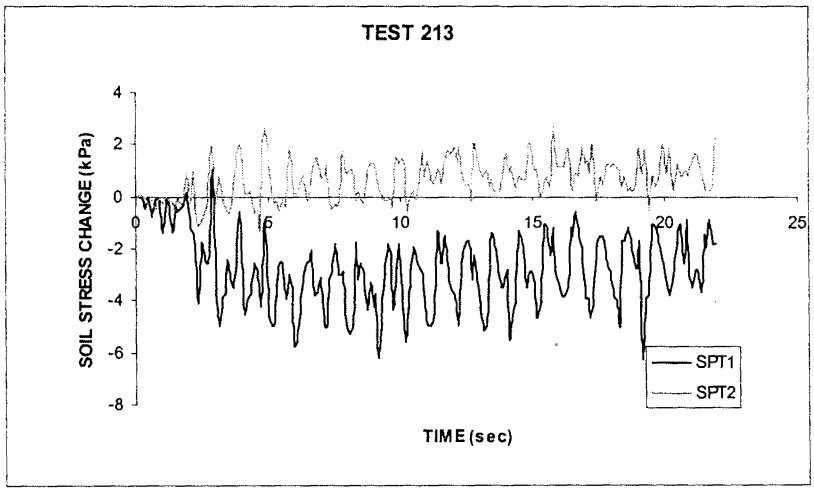

Figure C63 - Test 213 – Change in Soil Stress During Combined Loading
Depth of Burial – SPT1 = 1000 mm, SPT2 = 500mm
NOTE: Both Stress Transducers at 20 mm from shaft sidewall

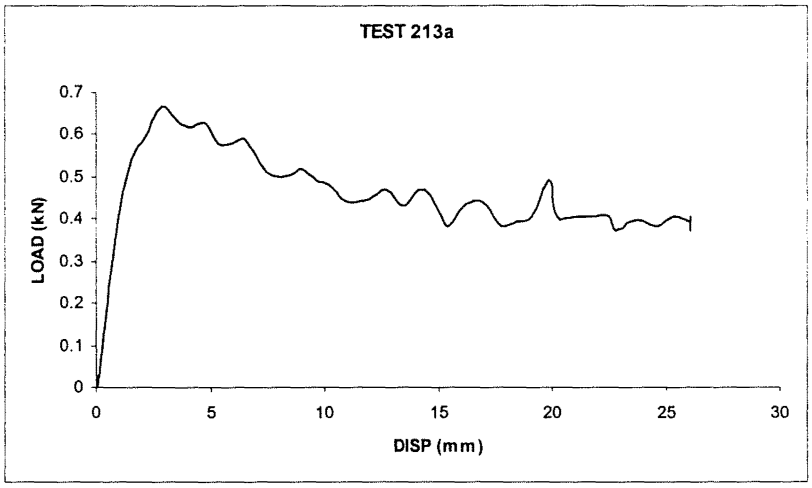

Figure C64 - Test 213a – Monotonic Uplift after Combined Loading

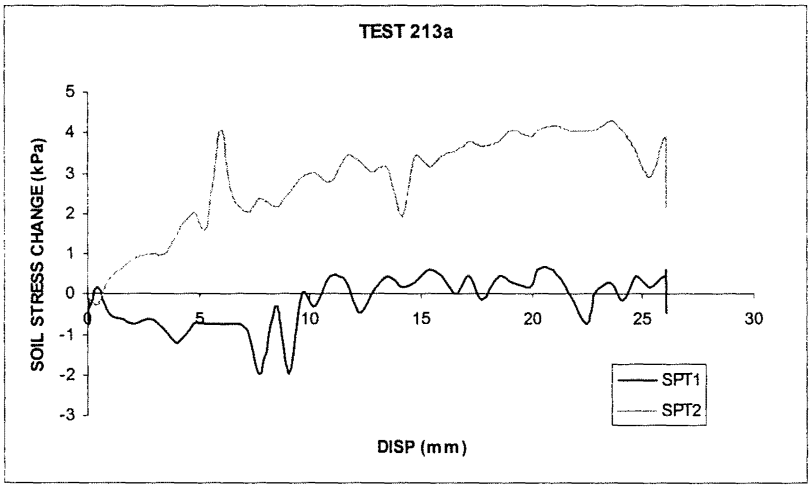

Figure C65 - Test 213a – Change in Soil Stress during Monotonic Uplift

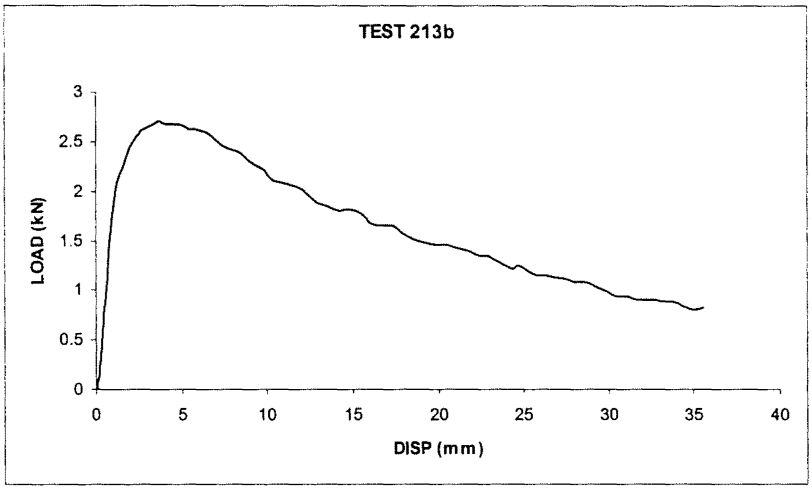

Figure C66 - Test 213b – Monotonic Uplift after Cyclic Shaking only

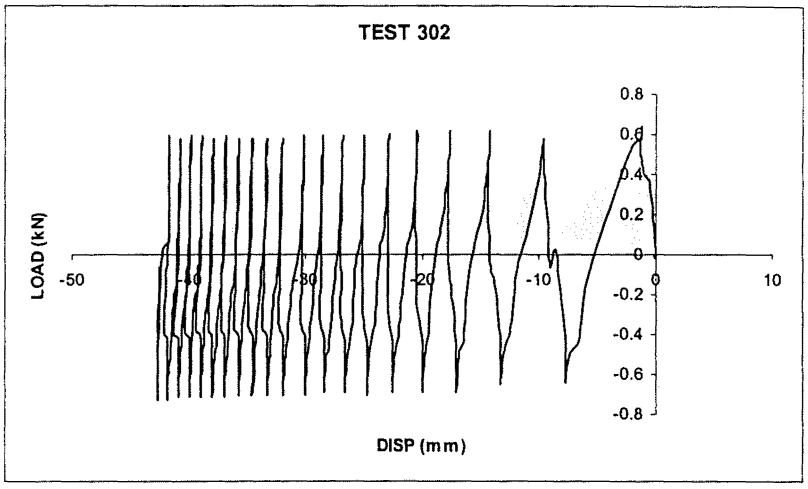

Figure C67 - Test 302 – Shaft Load v Displacement Under Cyclic Axial Load (+/-0.64 kN) and Cyclic Soil Shaking (Phase Angle = 90°)

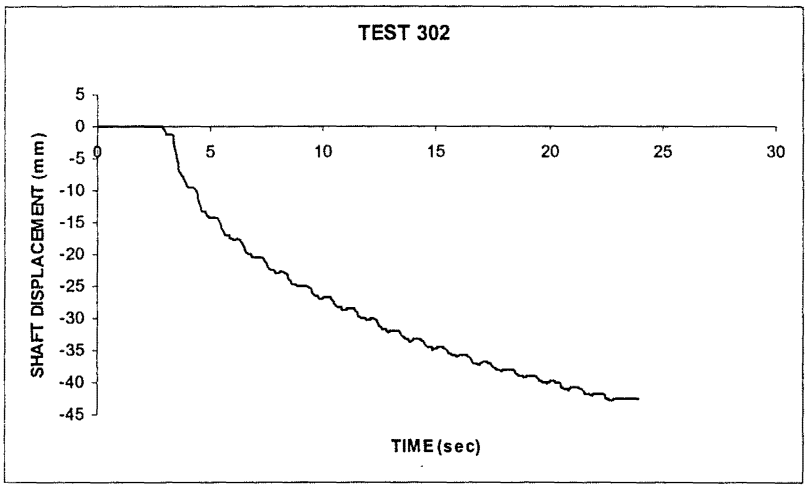

Figure C68 - Test 302 – Shaft Displacement Under Cyclic Axial Load (+/-0.64 kN) and Cyclic Soil Shaking

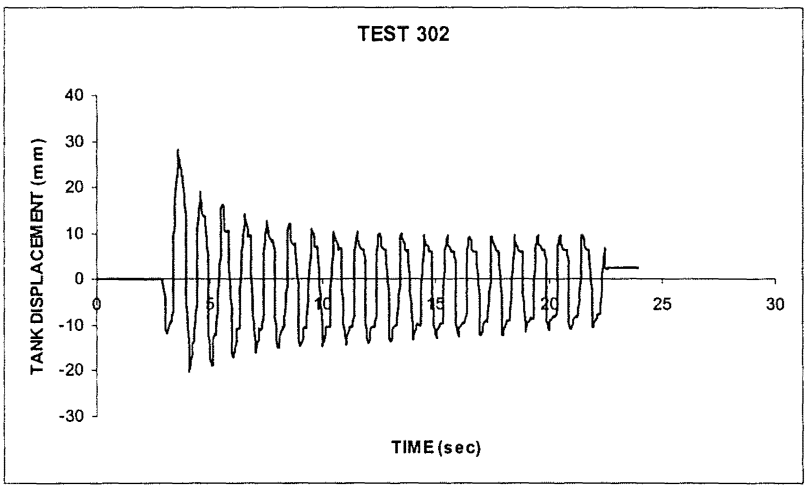

Figure C69 - Test 302 – Tank Displacement Under Cyclic Soil Shaking

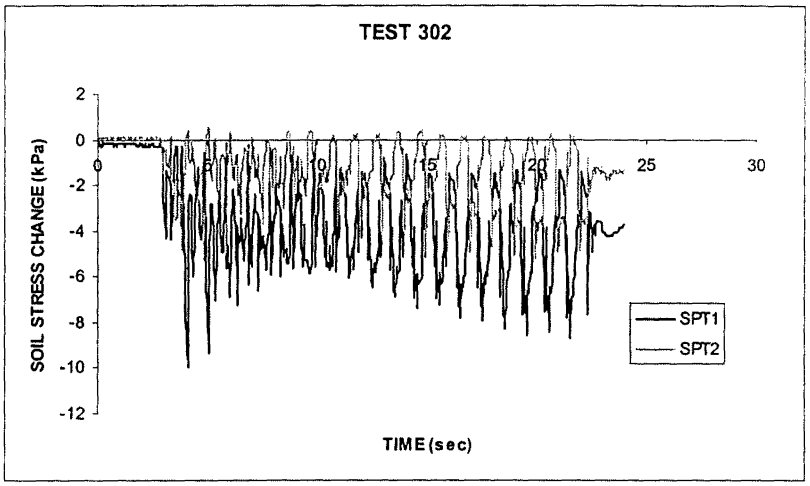

Figure C70 - Test 302 – Change in Soil Stress During Combined Loading
Depth of Burial – SPT1 = 1000 mm, SPT2 = 500mm
NOTE: Both Stress Transducers at 20 mm from shaft sidewall

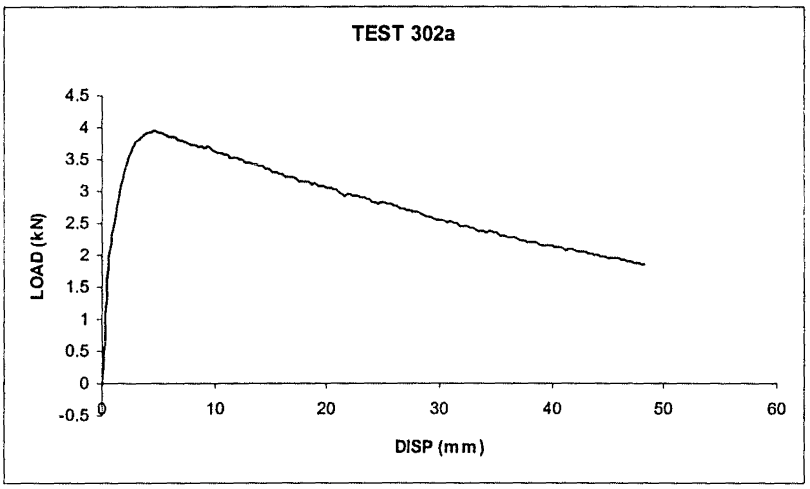

Figure C71 - Test 302a – Monotonic Uplift after Combined Loading

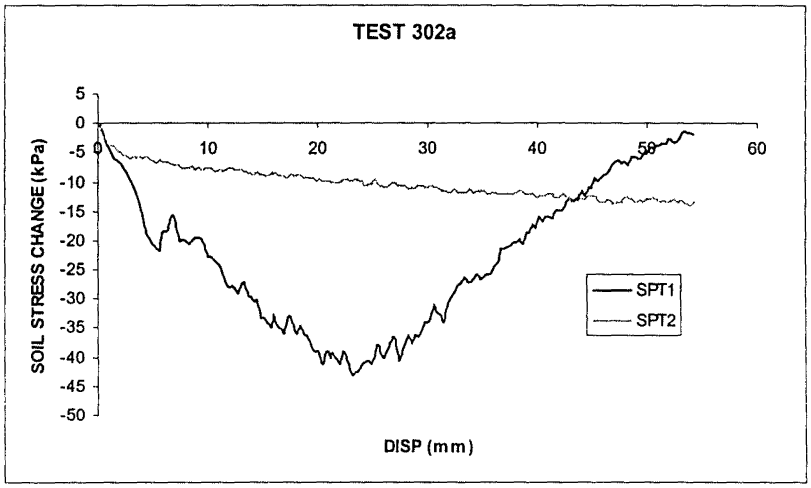

Figure C72 - Test 302a – Change in Soil Stress during Monotonic Uplift

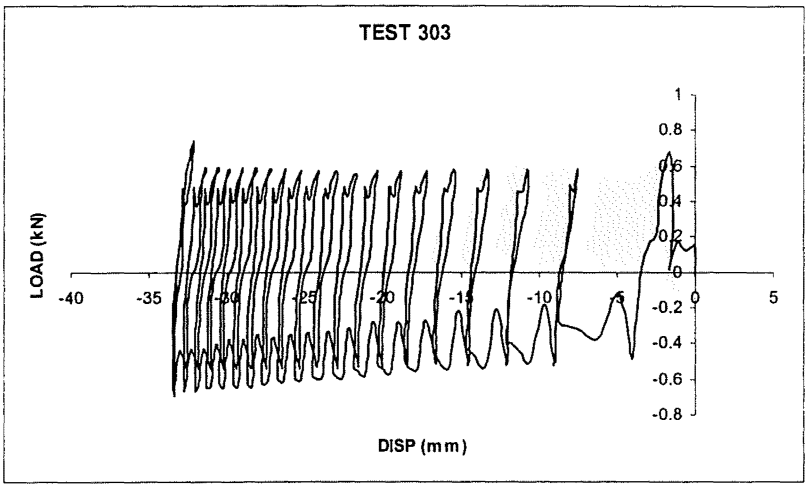

Figure C73 - Test 303 – Shaft Load v Displacement Under Cyclic Axial Load (+/-0.64 kN) and Cyclic Soil Shaking (Phase Angle = 0°)

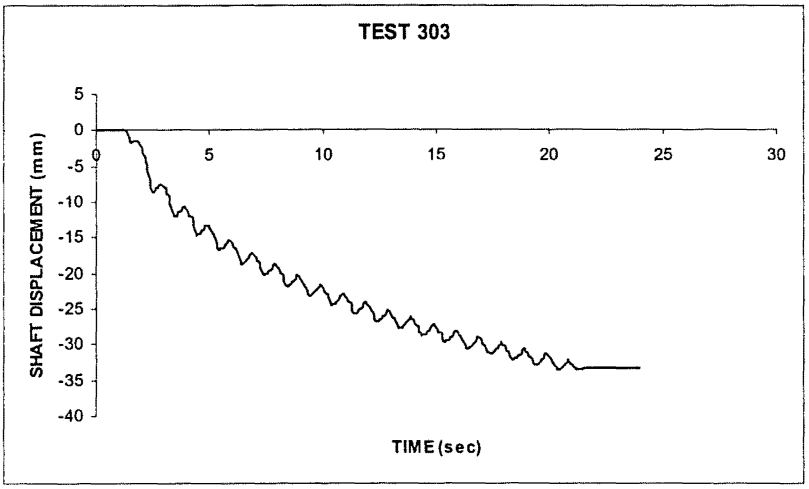

Figure C74 - Test 303 – Shaft Displacement Under Cyclic Axial Load (+/-0.64 kN) and Cyclic Soil Shaking

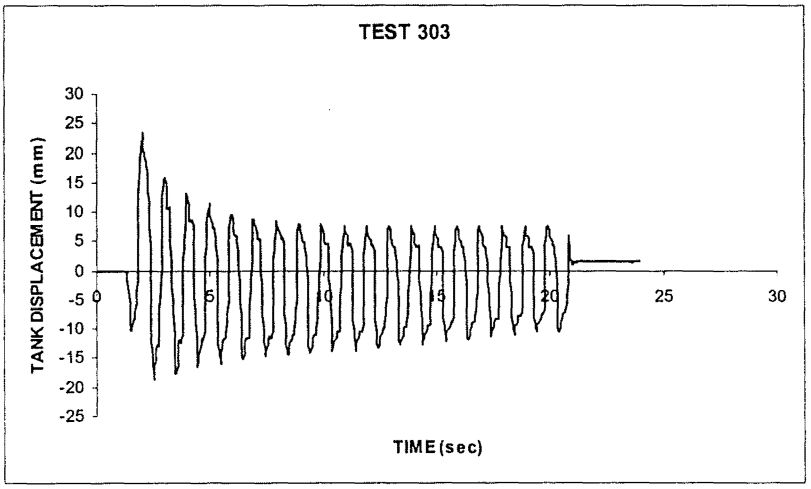

Figure C75 - Test 303 – Tank Displacement Under Cyclic Soil Shaking

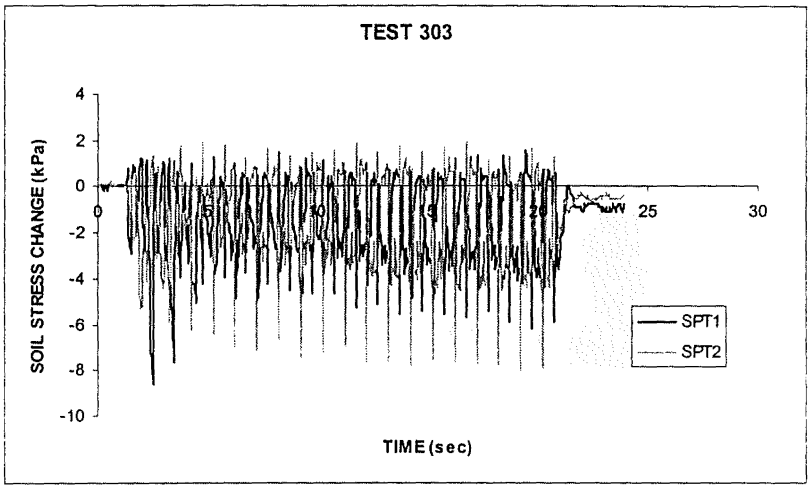

Figure C76 - Test 303 – Change in Soil Stress During Combined Loading
Depth of Burial – SPT1 = 1000 mm, SPT2 = 500mm
NOTE: Both Stress Transducers at 20 mm from shaft sidewall

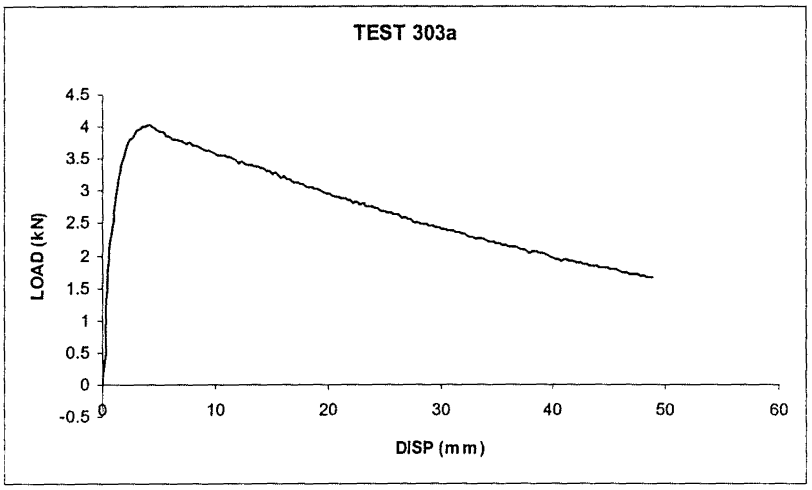

Figure C77 - Test 303a – Monotonic Uplift after Combined Loading

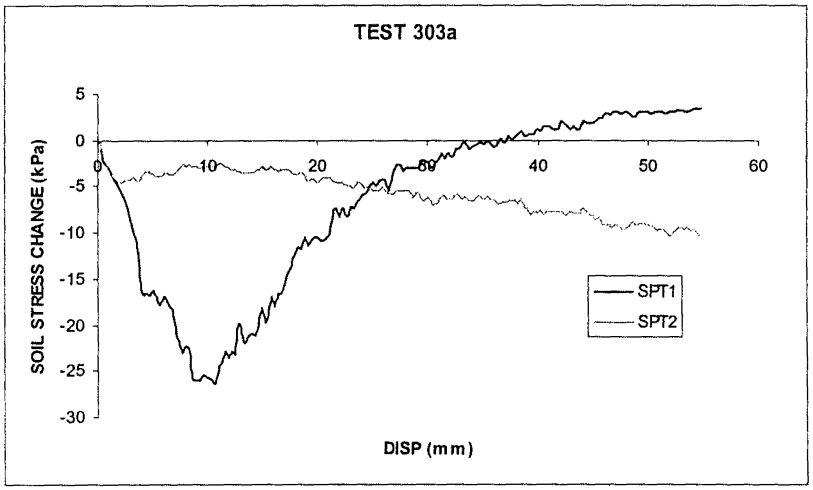

Figure C78 - Test 303a – Change in Soil Stress during Monotonic Uplift

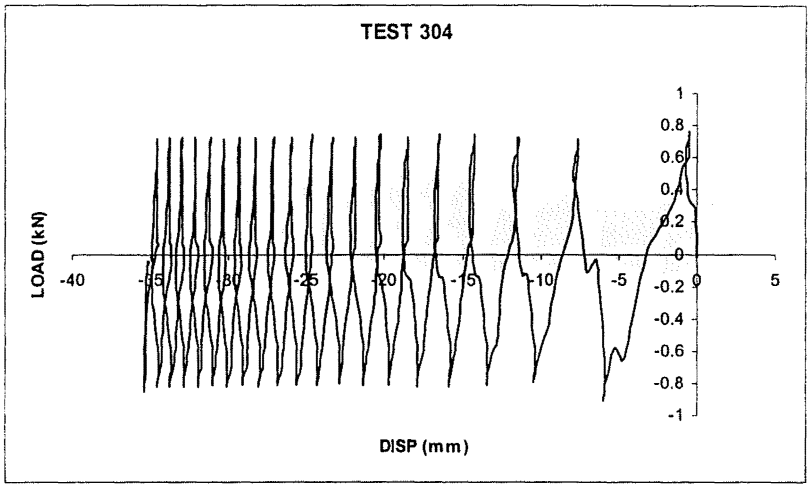

Figure C79 - Test 304 – Shaft Load v Displacement Under Cyclic Axial Load (+/-0.77 kN) and Cyclic Soil Shaking (Phase Angle = 90°)

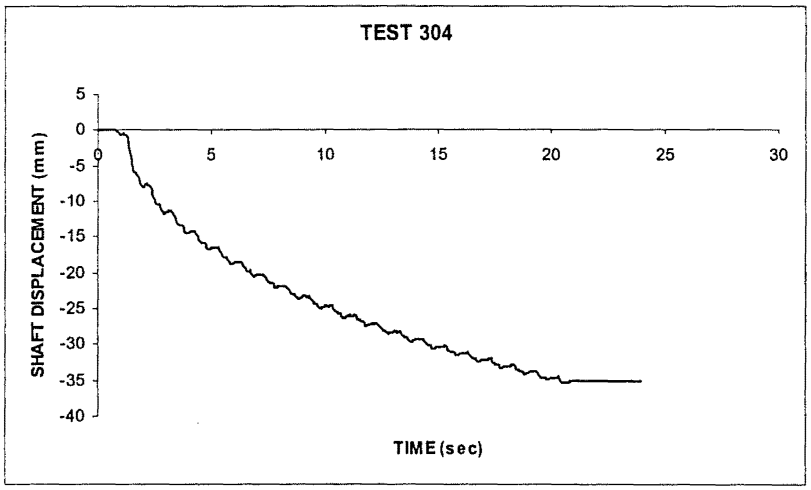

Figure C80 - Test 304 – Shaft Displacement Under Cyclic Axial Load (+/-0.77 kN) and Cyclic Soil Shaking

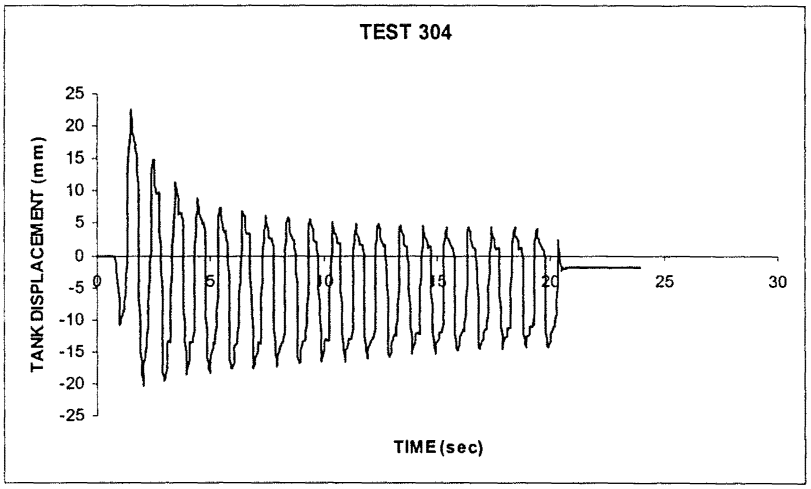

Figure C81 - Test 304 – Tank Displacement Under Cyclic Soil Shaking

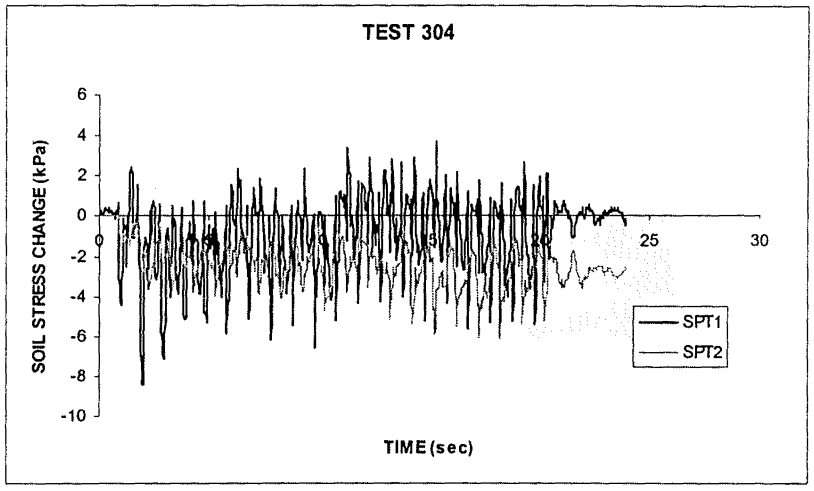

Figure C82 - Test 304 – Change in Soil Stress During Combined Loading
Depth of Burial – SPT1 = 1000 mm, SPT2 = 500mm
NOTE: Both Stress Transducers at 20 mm from shaft sidewall

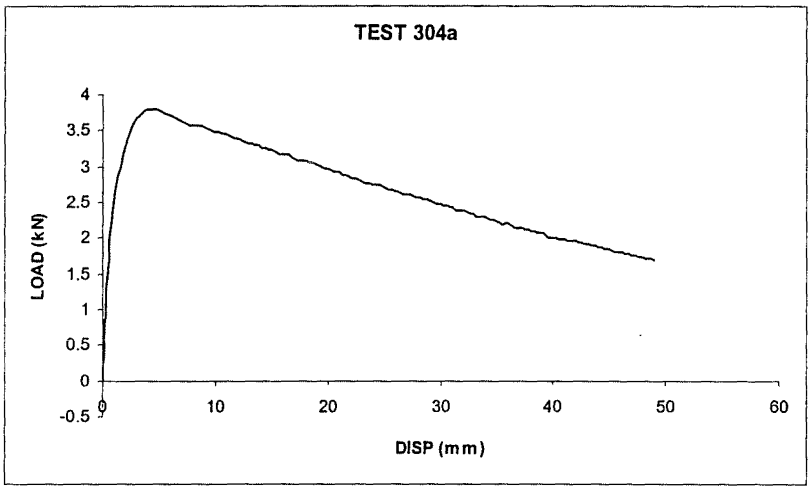

Figure C83 - Test 304a – Monotonic Uplift after Combined Loading

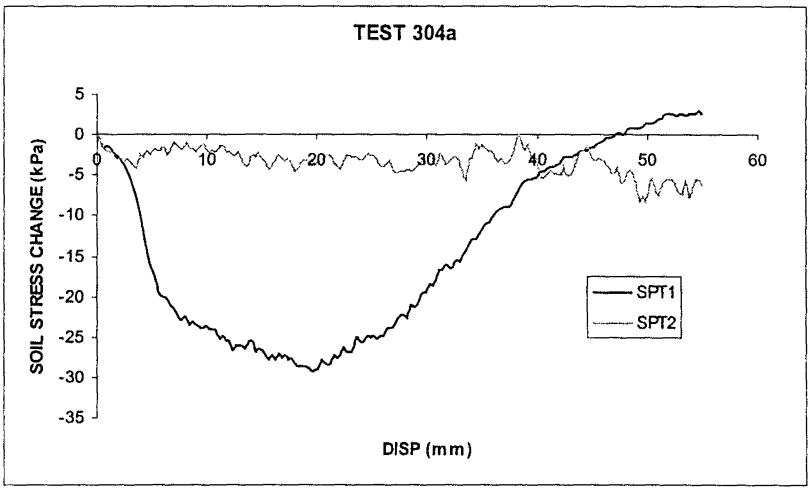

Figure C84 - Test 304a – Change in Soil Stress during Monotonic Uplift

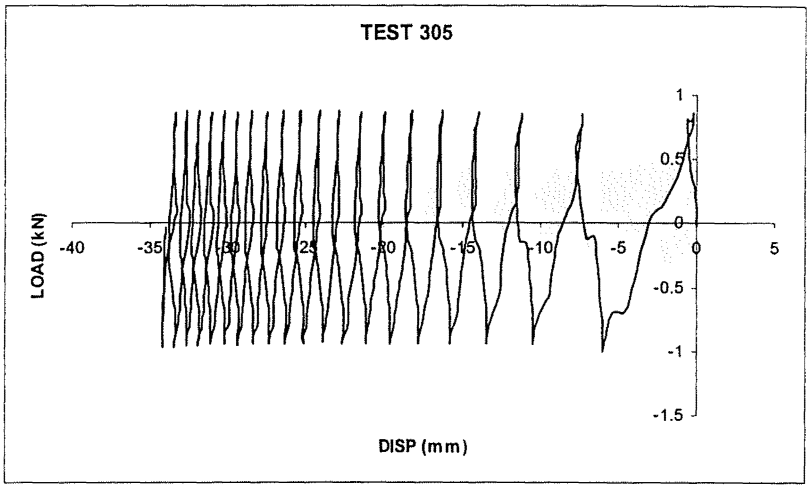

Figure C85 - Test 305 – Shaft Load v Displacement Under Cyclic Axial Load (+/-0.90 kN) and Cyclic Soil Shaking (Phase Angle = 90°)

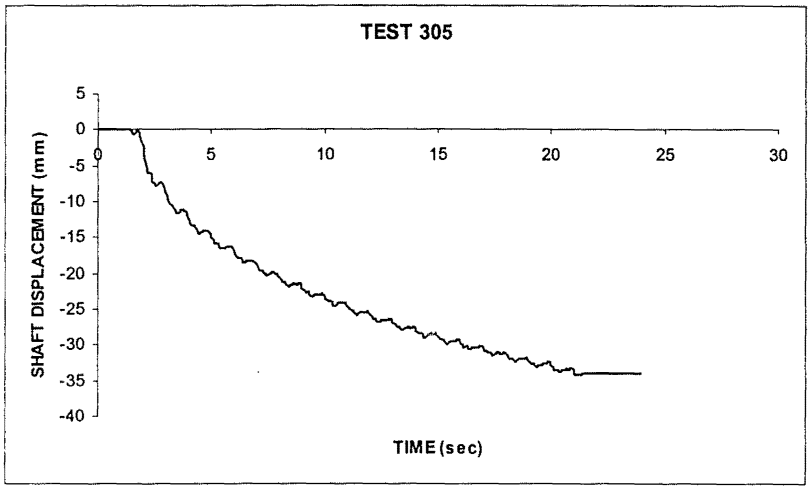

Figure C86 - Test 305 – Shaft Displacement Under Cyclic Axial Load (+/-0.90 kN) and Cyclic Soil Shaking

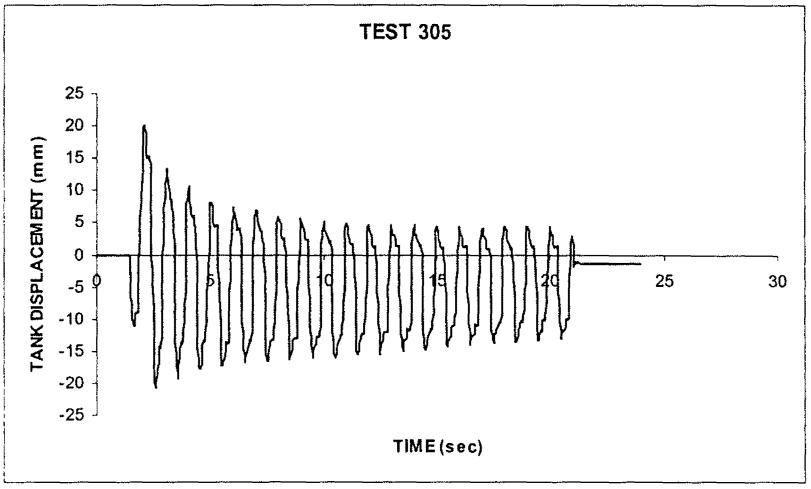

Figure C87 - Test 305 – Tank Displacement Under Cyclic Soil Shaking

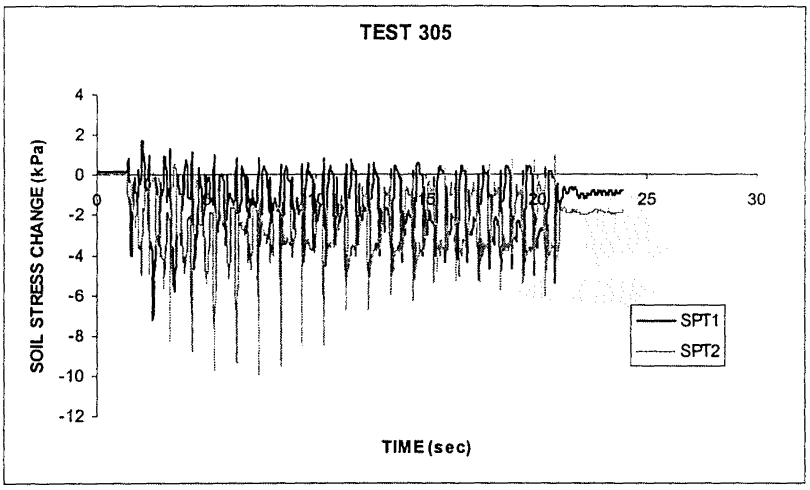

Figure C88 - Test 305 – Change in Soil Stress During Combined Loading
Depth of Burial – SPT1 = 1000 mm, SPT2 = 500mm
NOTE: Both Stress Transducers at 20 mm from shaft sidewall

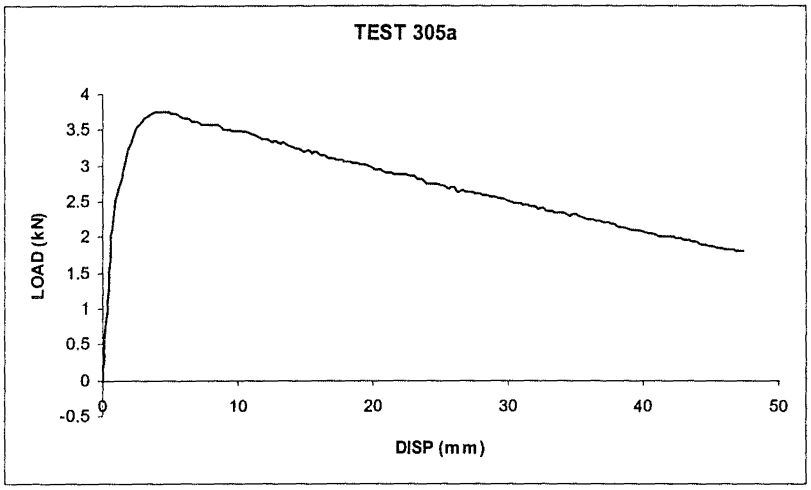

Figure C89 - Test 305a – Monotonic Uplift after Combined Loading

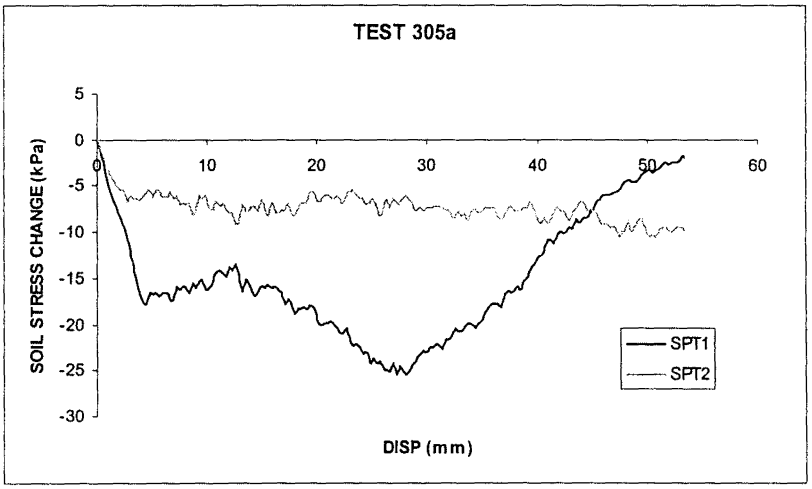

Figure C90 - Test 305a – Change in Soil Stress during Monotonic Uplift

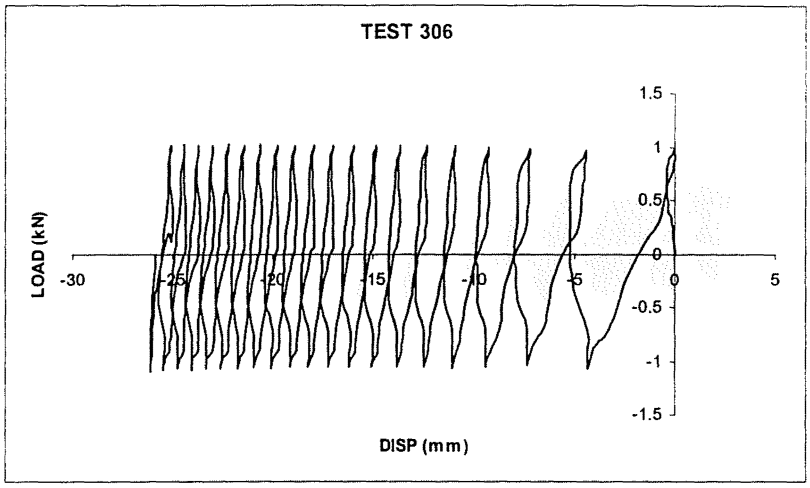

Figure C91 - Test 306 – Shaft Load v Displacement Under Cyclic Axial Load (+/-1.02 kN) and Cyclic Soil Shaking (Phase Angle = 90°)

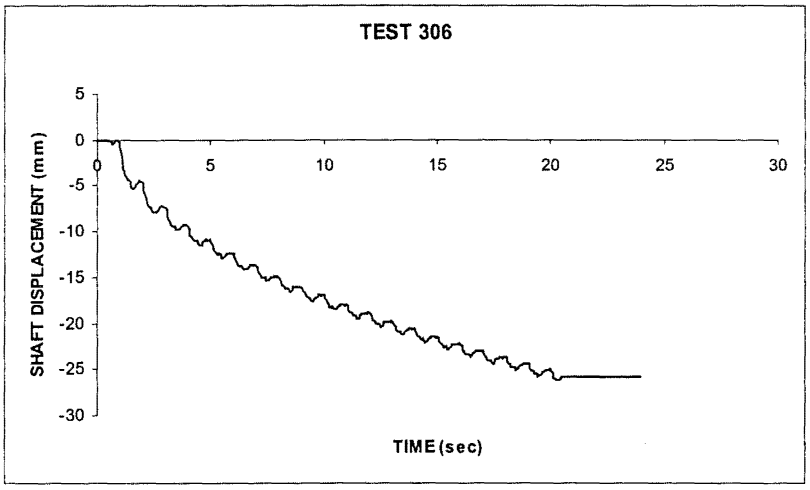

Figure C92 - Test 306 – Shaft Displacement Under Cyclic Axial Load (+/-1.02 kN) and Cyclic Soil Shaking

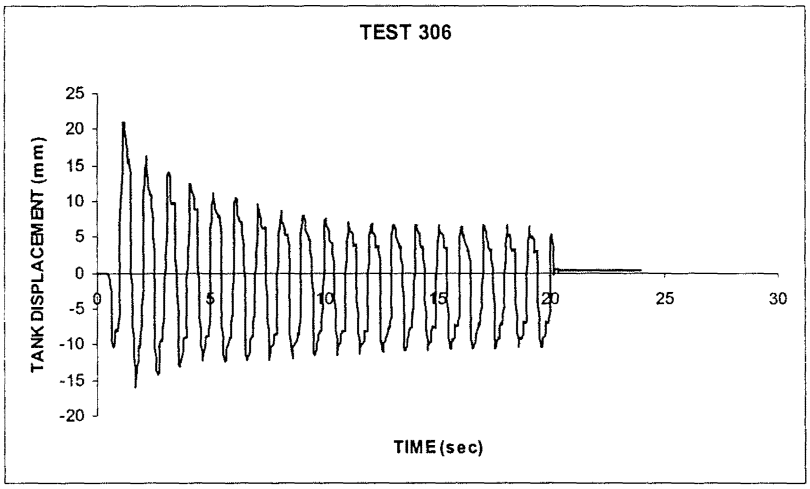

Figure C93 - Test 306 – Tank Displacement Under Cyclic Soil Shaking

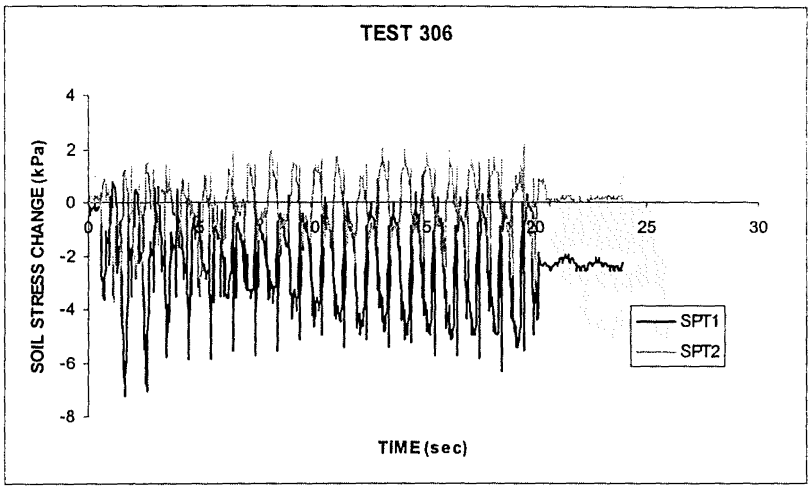

Figure C94 - Test 306 – Change in Soil Stress During Combined Loading
Depth of Burial – SPT1 = 1000 mm, SPT2 = 500mm
NOTE: Both Stress Transducers at 20 mm from shaft sidewall

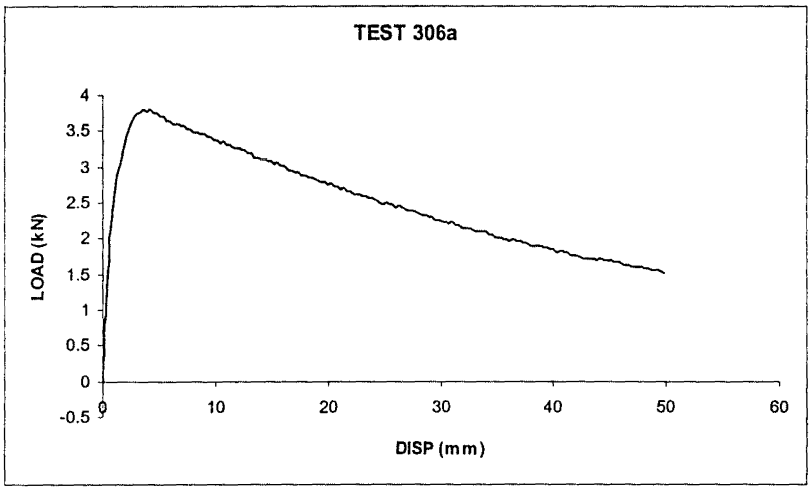

Figure C95 - Test 306a – Monotonic Uplift after Combined Loading

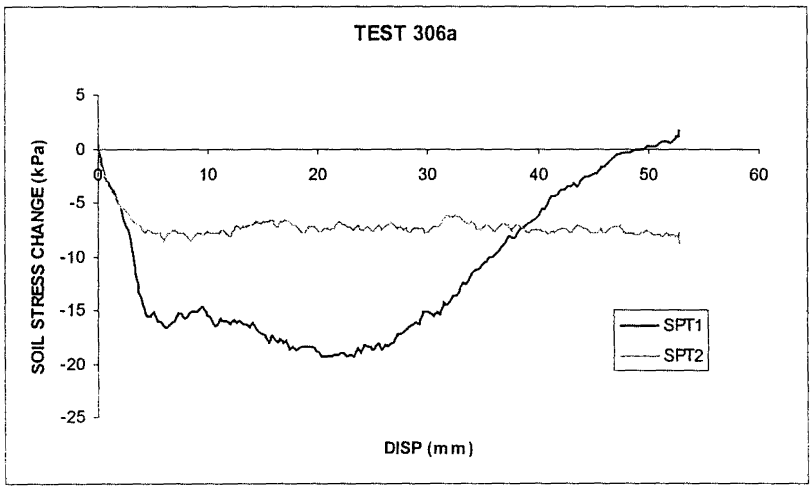

Figure C96 - Test 306a – Change in Soil Stress during Monotonic Uplift

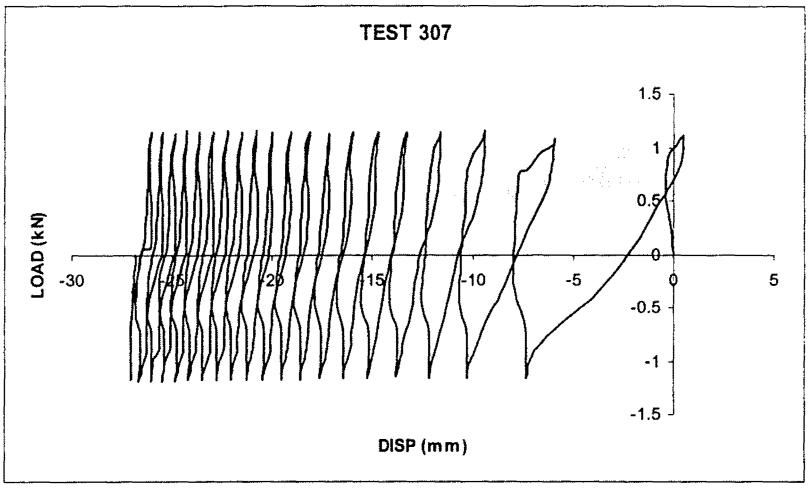

Figure C97 - Test 307 – Shaft Load v Displacement Under Cyclic Axial Load (+/-1.15 kN) and Cyclic Soil Shaking (Phase Angle = 90°)

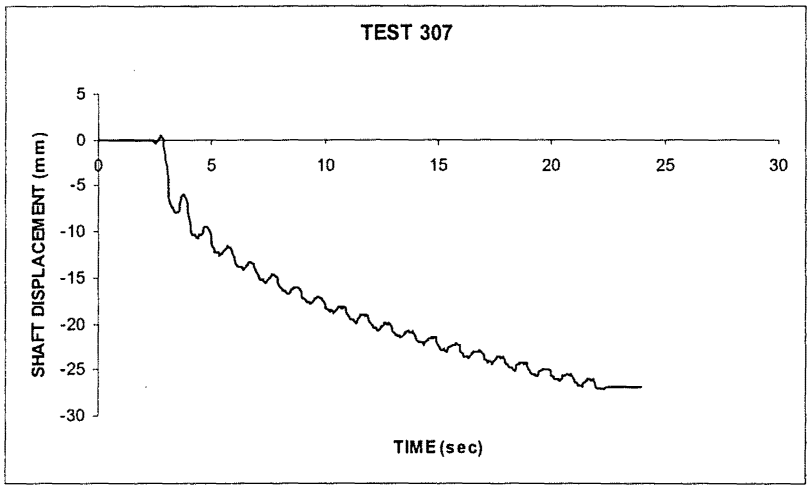

Figure C98 - Test 307 – Shaft Displacement Under Cyclic Axial Load (+/-1.15 kN) and Cyclic Soil Shaking

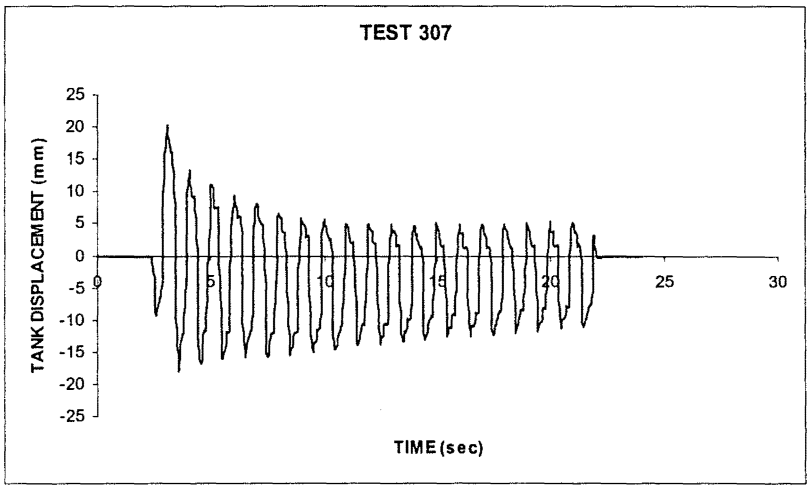

Figure C99 - Test 307 – Tank Displacement Under Cyclic Soil Shaking

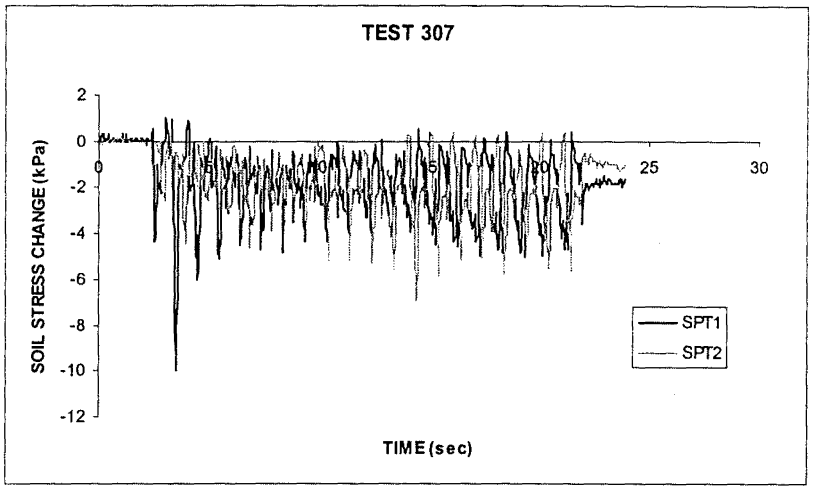

Figure C100 - Test 307 – Change in Soil Stress During Combined Loading
Depth of Burial – SPT1 = 1000 mm, SPT2 = 500mm
NOTE: Both Stress Transducers at 20 mm from shaft sidewall

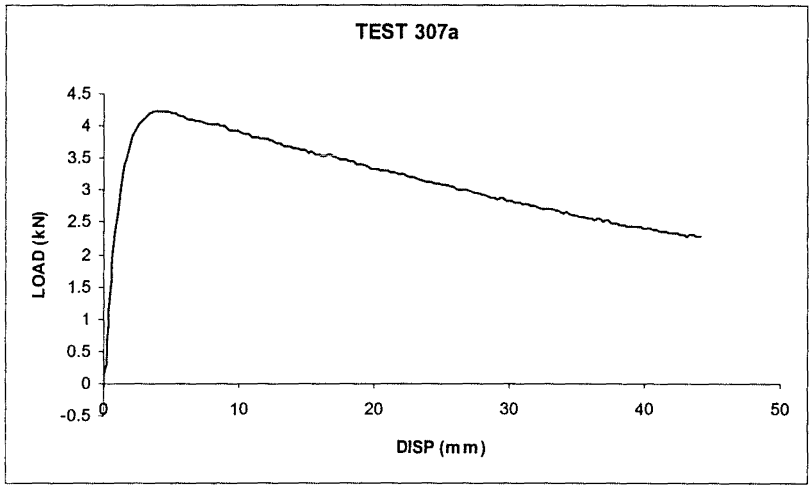

Figure C101 - Test 307a – Monotonic Uplift after Combined Loading

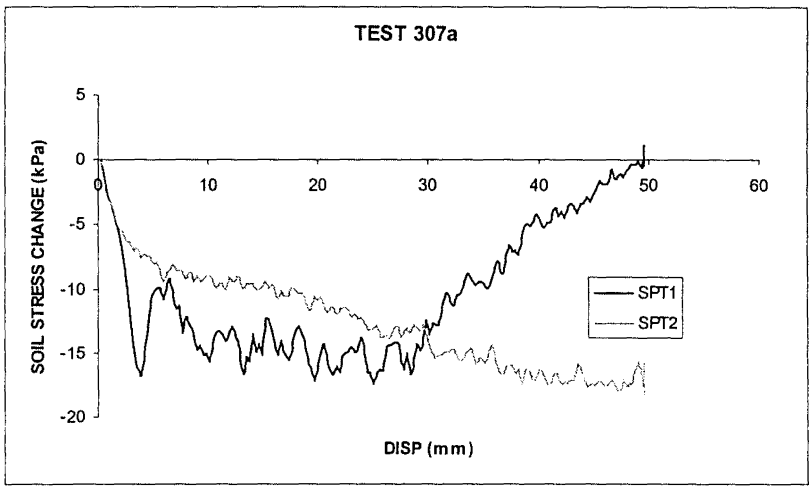

Figure C102 - Test 307a – Change in Soil Stress during Monotonic Uplift

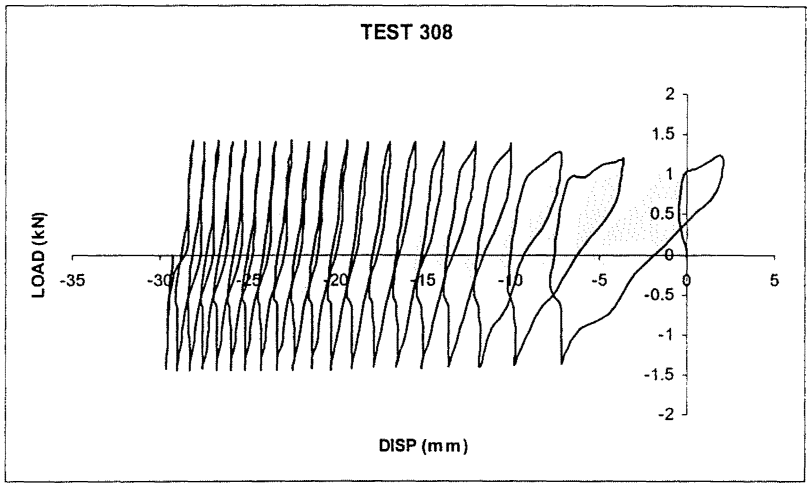

Figure C103 - Test 308 – Shaft Load v Displacement Under Cyclic Axial Load (+/-1.41 kN) and Cyclic Soil Shaking (Phase Angle = 90°)

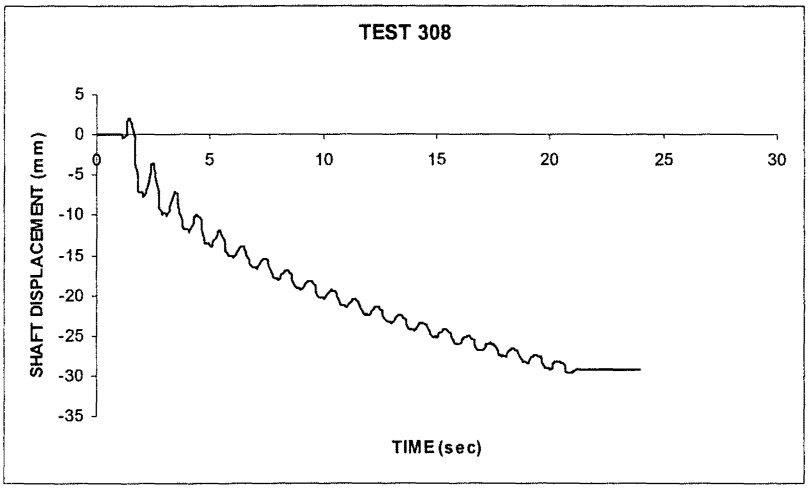

Figure C104 - Test 308 – Shaft Displacement Under Cyclic Axial Load (+/-1.41 kN) and Cyclic Soil Shaking

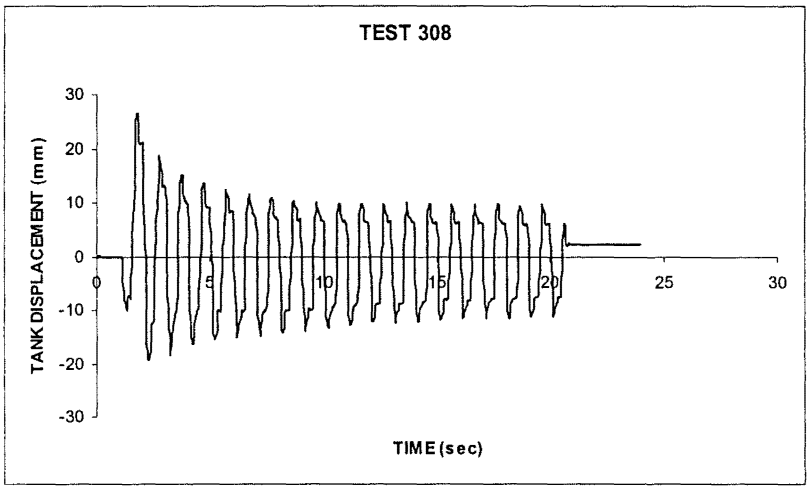

Figure C105 - Test 308 – Tank Displacement Under Cyclic Soil Shaking

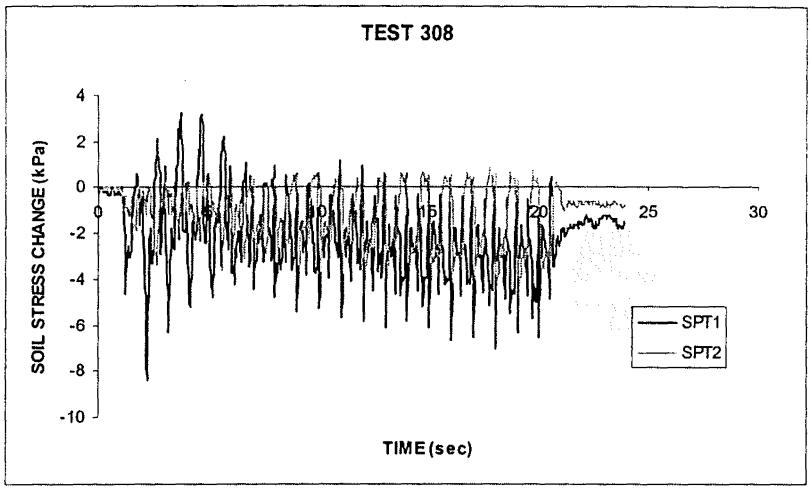

Figure C106 - Test 308 – Change in Soil Stress During Combined Loading
Depth of Burial – SPT1 = 1000 mm, SPT2 = 500mm
NOTE: Both Stress Transducers at 20 mm from shaft sidewall

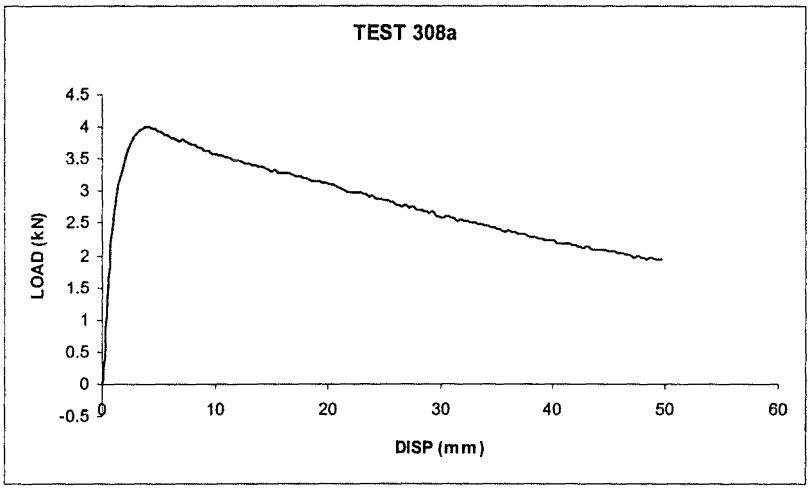

Figure C107 - Test 308a – Monotonic Uplift after Combined Loading

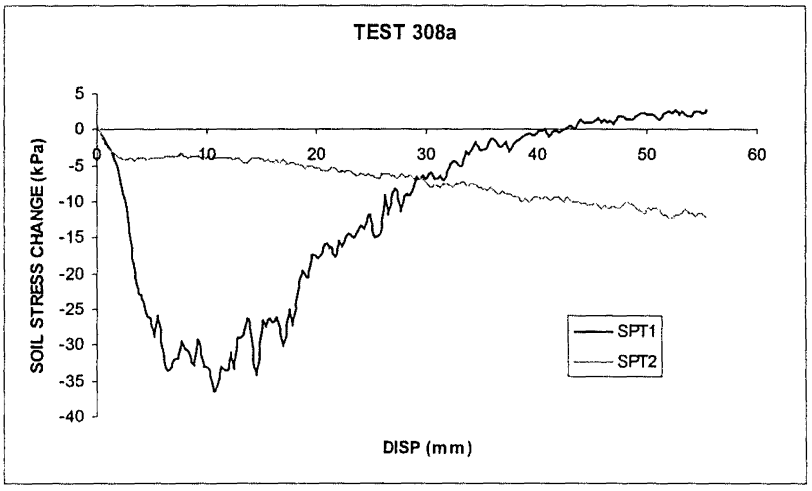

Figure C108 - Test 308a – Change in Soil Stress during Monotonic Uplift

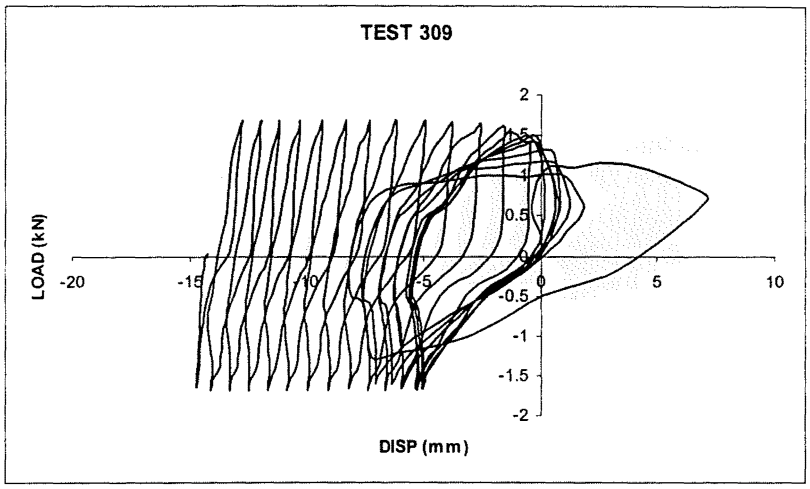

Figure C109 - Test 309 – Shaft Load v Displacement Under Cyclic Axial Load (+/-1.66 kN) and Cyclic Soil Shaking (Phase Angle = 90°)

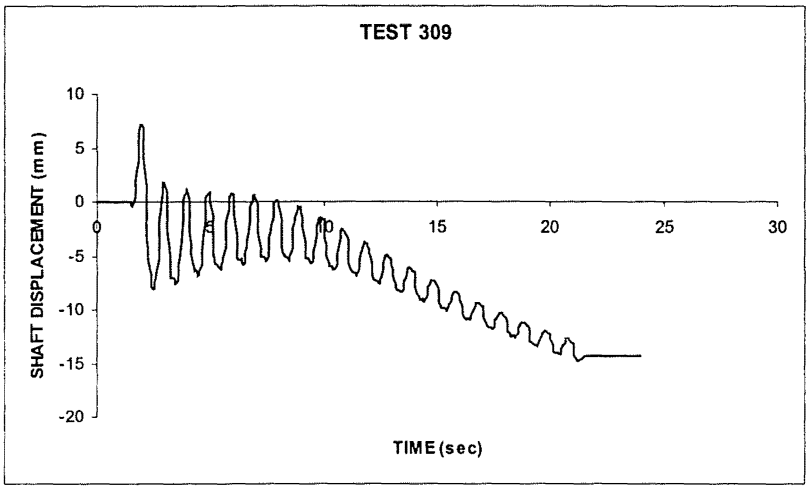

Figure C110 - Test 309 – Shaft Displacement Under Cyclic Axial Load (+/-1.66 kN) and Cyclic Soil Shaking

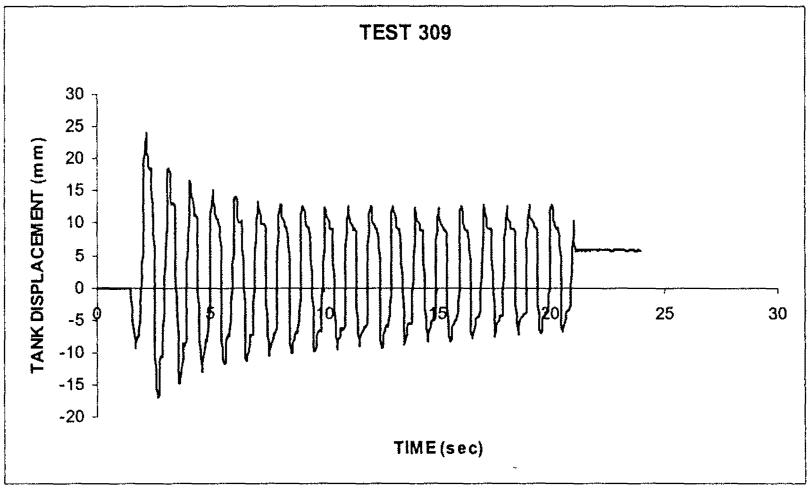

Figure C111 - Test 309 – Tank Displacement Under Cyclic Soil Shaking

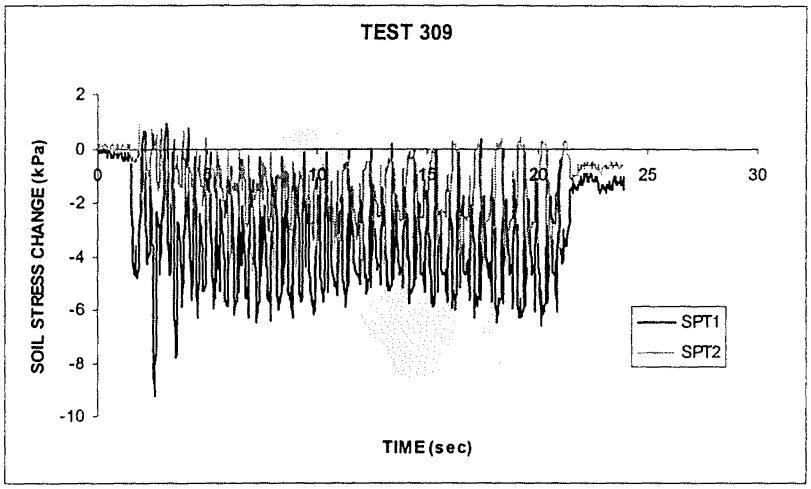

Figure C112 - Test 309 – Change in Soil Stress During Combined Loading
Depth of Burial – SPT1 = 1000 mm, SPT2 = 500mm
NOTE: Both Stress Transducers at 20 mm from shaft sidewall

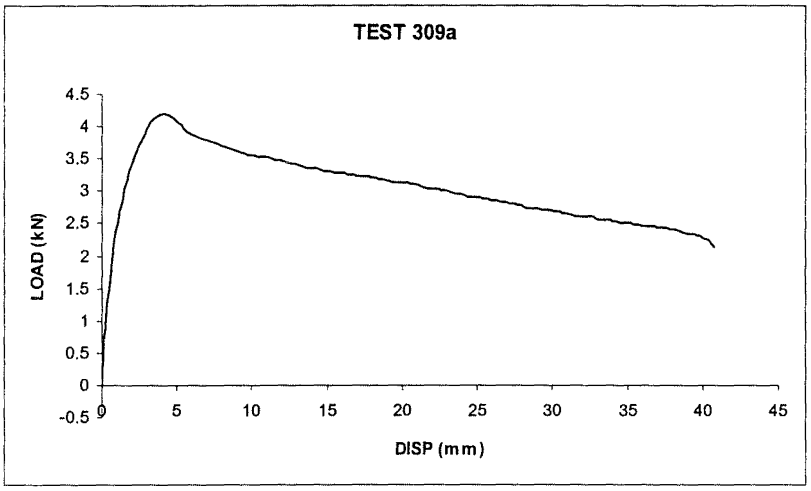

Figure C113 - Test 309a – Monotonic Uplift after Combined Loading

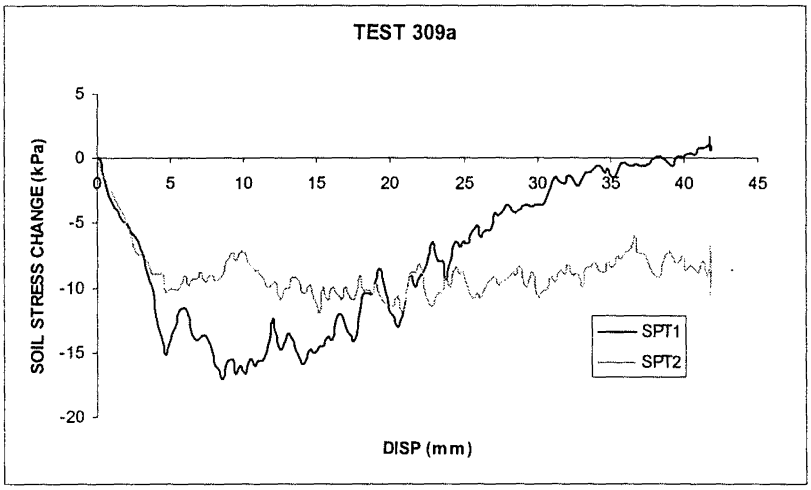

Figure C114 - Test 309a – Change in Soil Stress during Monotonic Uplift

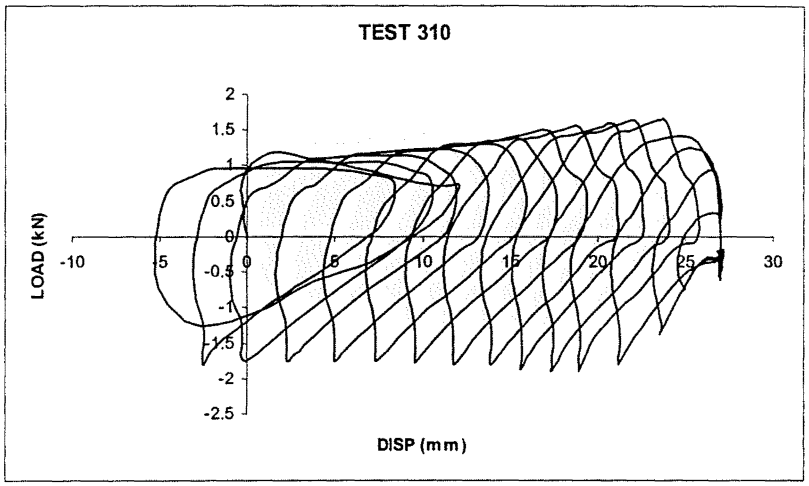

Figure C115 - Test 310 – Shaft Load v Displacement Under Cyclic Axial Load (+/-1.92 kN) and Cyclic Soil Shaking (Phase Angle = 90°)

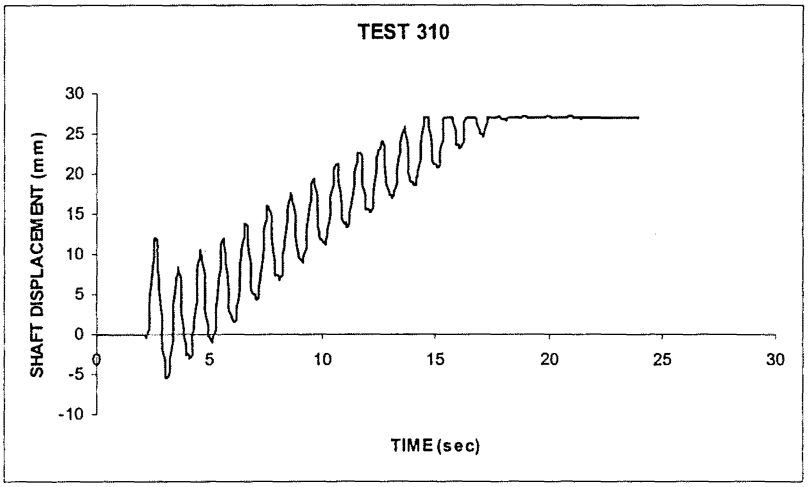

Figure C116 - Test 310 – Shaft Displacement Under Cyclic Axial Load (+/-1.92 kN) and Cyclic Soil Shaking

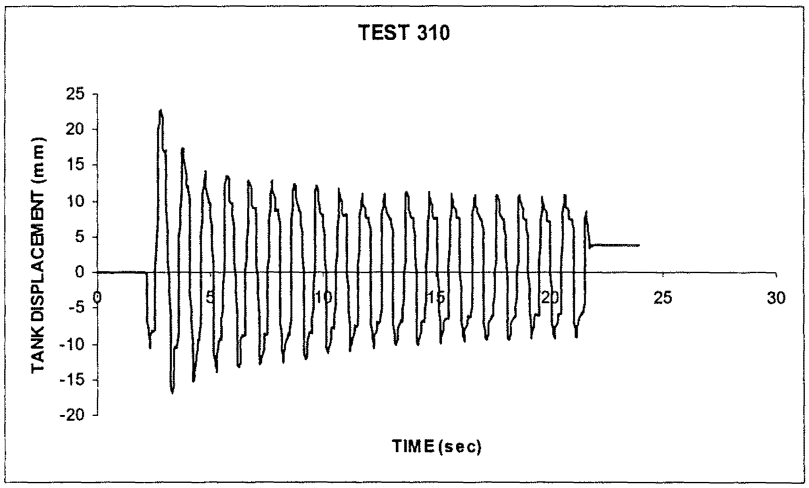

Figure C117 - Test 310 – Tank Displacement Under Cyclic Soil Shaking

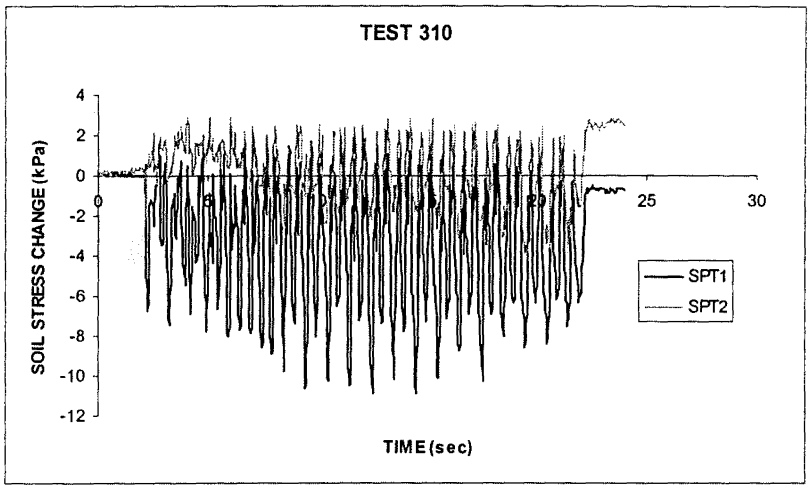

Figure C118 - Test 310 – Change in Soil Stress During Combined Loading
Depth of Burial – SPT1 = 1000 mm, SPT2 = 500mm
NOTE: Both Stress Transducers at 20 mm from shaft sidewall

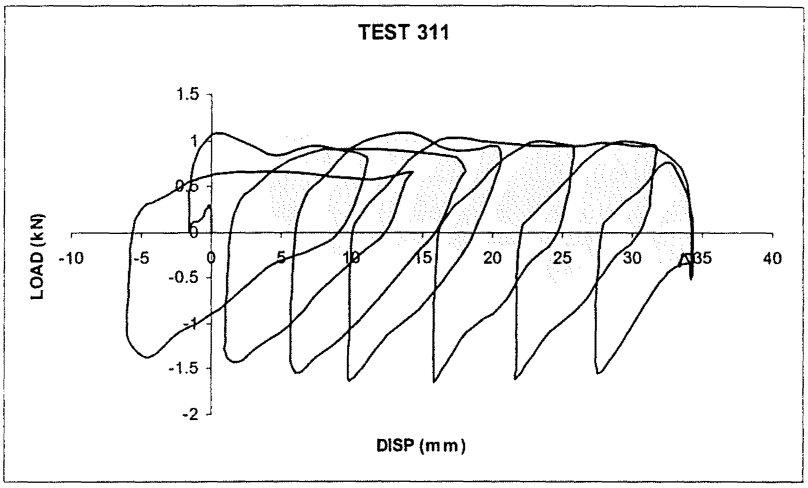

Figure C119 - Test 311 – Shaft Load v Displacement Under Cyclic Axial Load (+/-1.92 kN) and Cyclic Soil Shaking (Phase Angle = 0°)

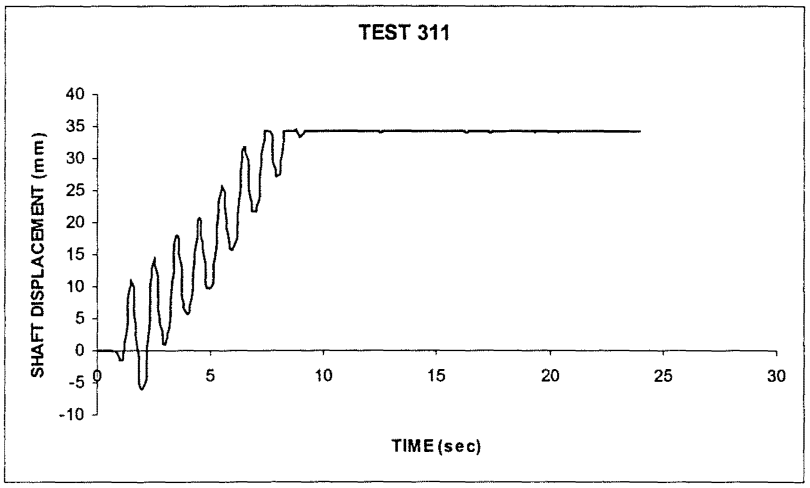

Figure C120 - Test 311 – Shaft Displacement Under Cyclic Axial Load (+/-1.92 kN) and Cyclic Soil Shaking

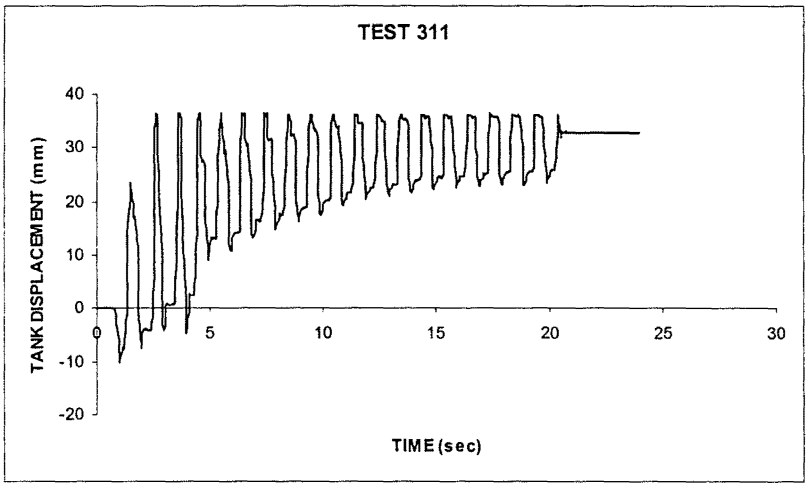

Figure C121 - Test 311 – Tank Displacement Under Cyclic Soil Shaking

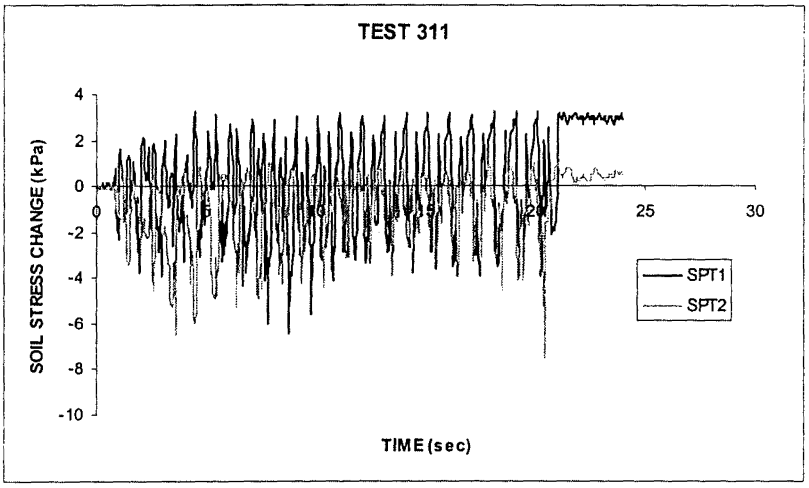

Figure C122 - Test 311 – Change in Soil Stress During Combined Loading
Depth of Burial – SPT1 = 1000 mm, SPT2 = 500mm
NOTE: Both Stress Transducers at 20 mm from shaft sidewall

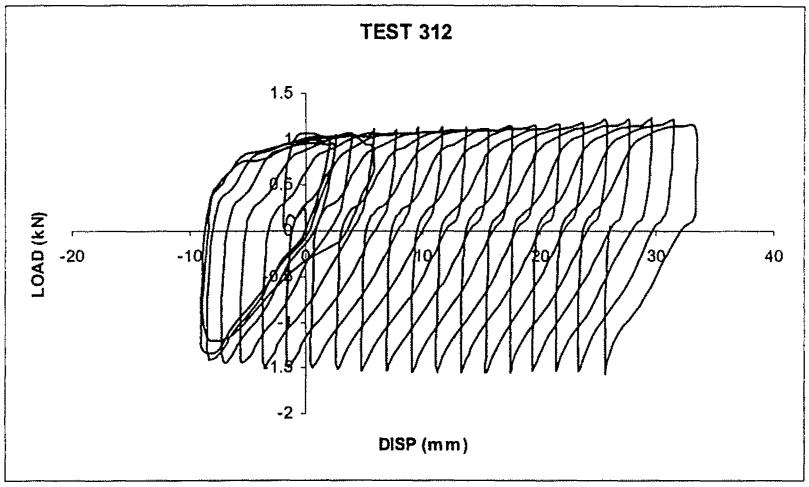

Figure C123 - Test 312 – Shaft Load v Displacement Under Cyclic Axial Load (+/-1.66 kN) and Cyclic Soil Shaking (Phase Angle = 0°)

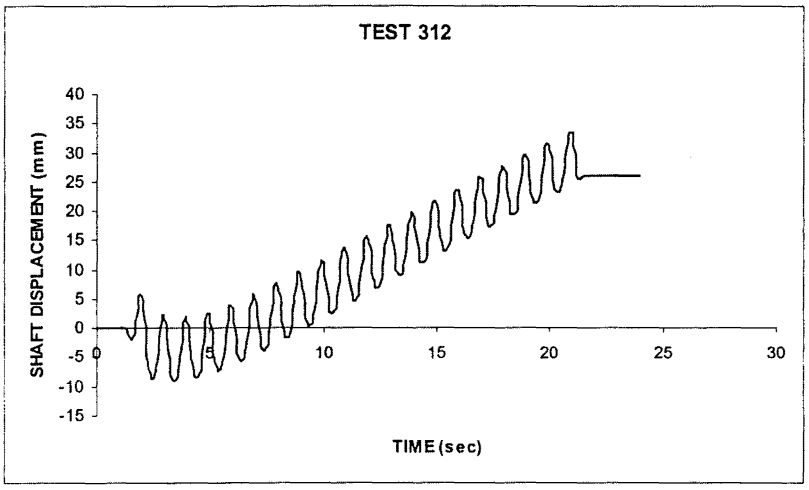

Figure C124 - Test 312 – Shaft Displacement Under Cyclic Axial Load (+/-1.66 kN) and Cyclic Soil Shaking

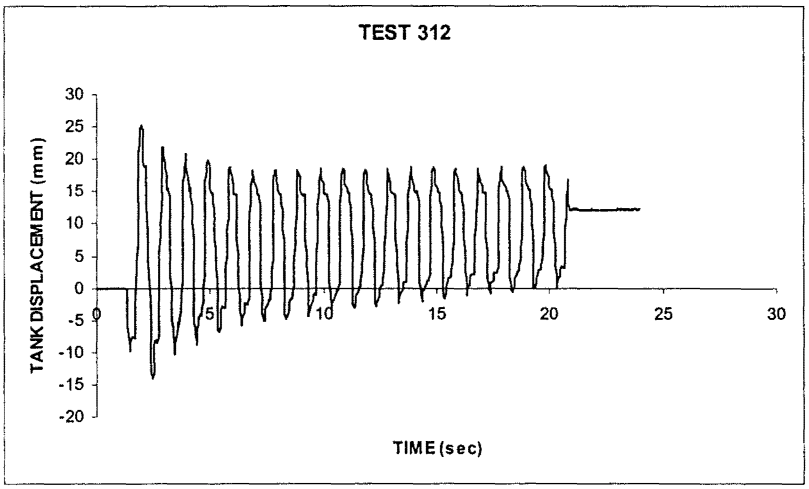

Figure C125 - Test 312 – Tank Displacement Under Cyclic Soil Shaking

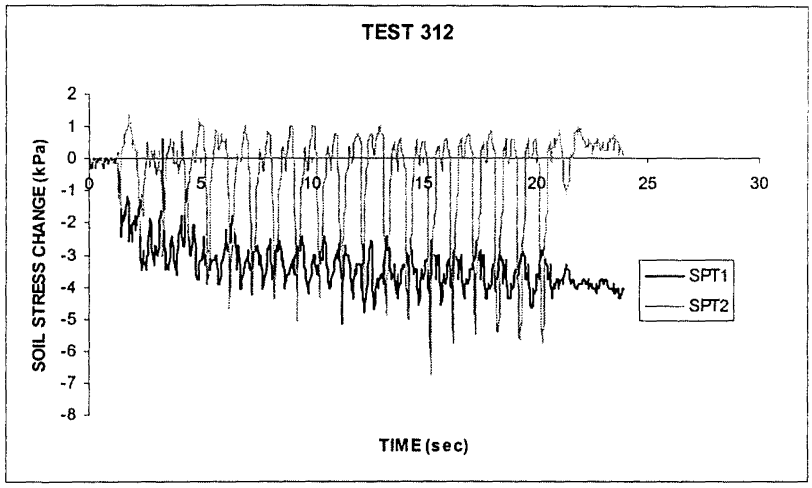

Figure C126 - Test 312 – Change in Soil Stress During Combined Loading
Depth of Burial – SPT1 = 1000 mm, SPT2 = 500mm
NOTE: Both Stress Transducers well clear of shaft sidewall (measuring far-field response)

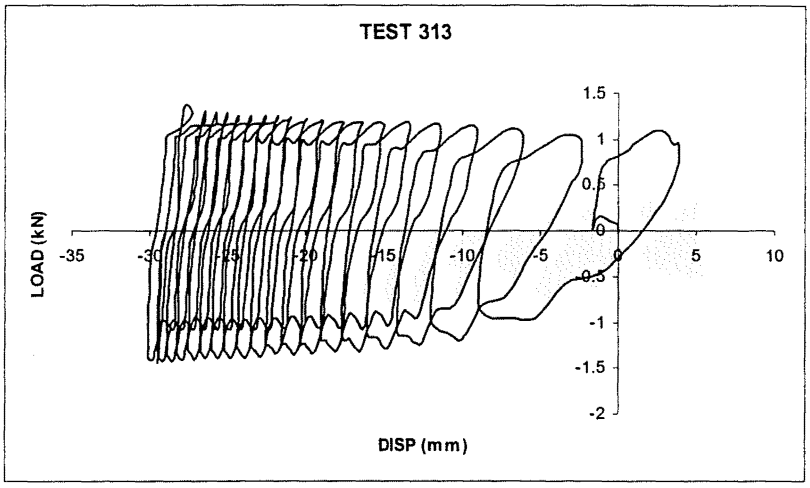

Figure C127 - Test 313 – Shaft Load v Displacement Under Cyclic Axial Load (+/-1.41 kN) and Cyclic Soil Shaking (Phase Angle = 0°)

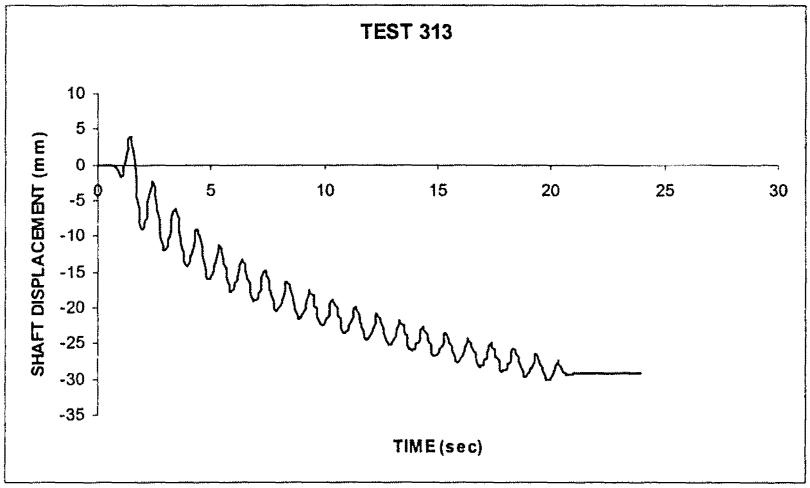

Figure C128 - Test 313 – Shaft Displacement Under Cyclic Axial Load (+/-1.41 kN) and Cyclic Soil Shaking

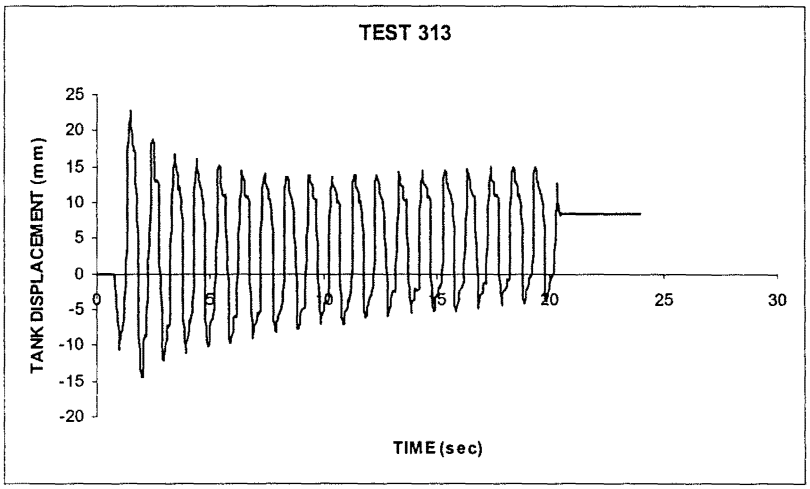

Figure C129 - Test 313 – Tank Displacement Under Cyclic Soil Shaking

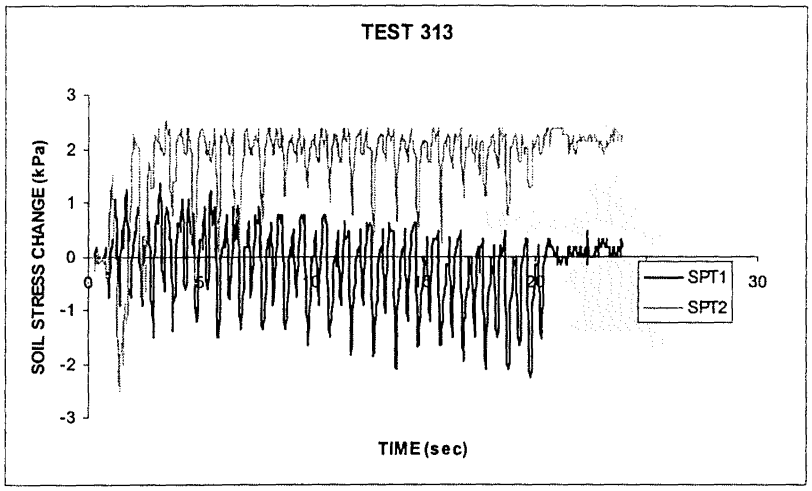

Figure C130 - Test 313 – Change in Soil Stress During Combined Loading
Depth of Burial – SPT1 = 850 mm, SPT2 = 300mm
NOTE: Both Stress Transducers well clear of shaft sidewall (measuring far-field response)

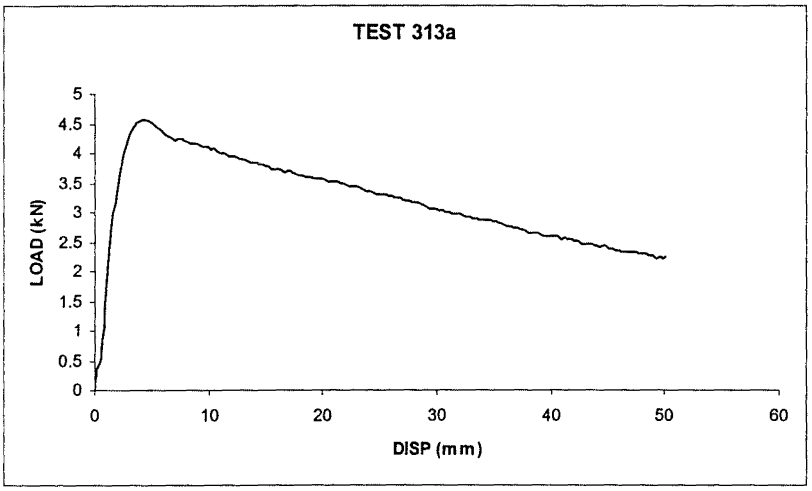

Figure C131 - Test 313a – Monotonic Uplift after Combined Loading

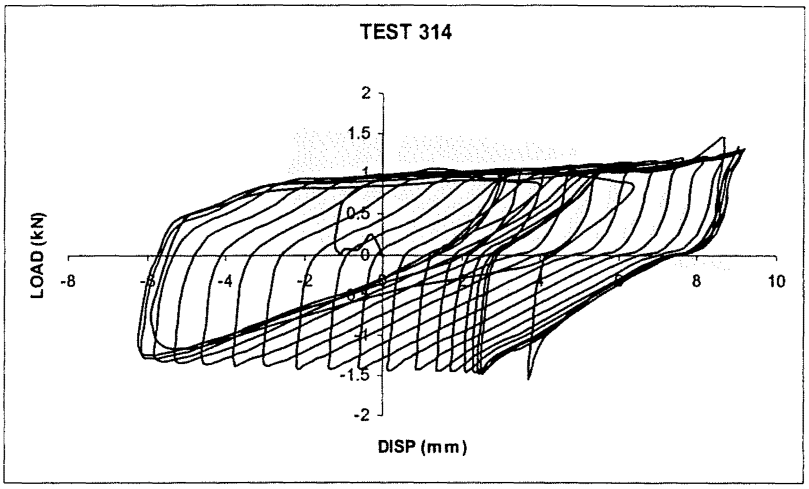

Figure C132 - Test 314 – Shaft Load v Displacement Under Cyclic Axial Load (+/-1.54 kN) and Cyclic Soil Shaking (Phase Angle = 0°)

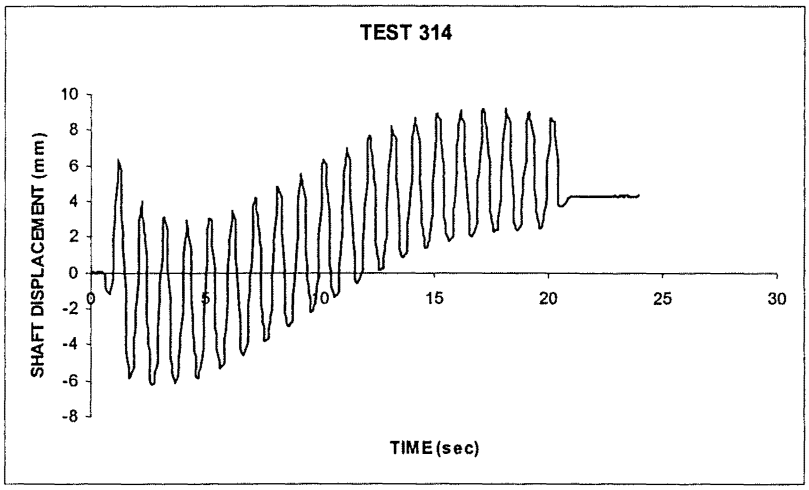

Figure C133 - Test 314 – Shaft Displacement Under Cyclic Axial Load (+/-1.54 kN) and Cyclic Soil Shaking

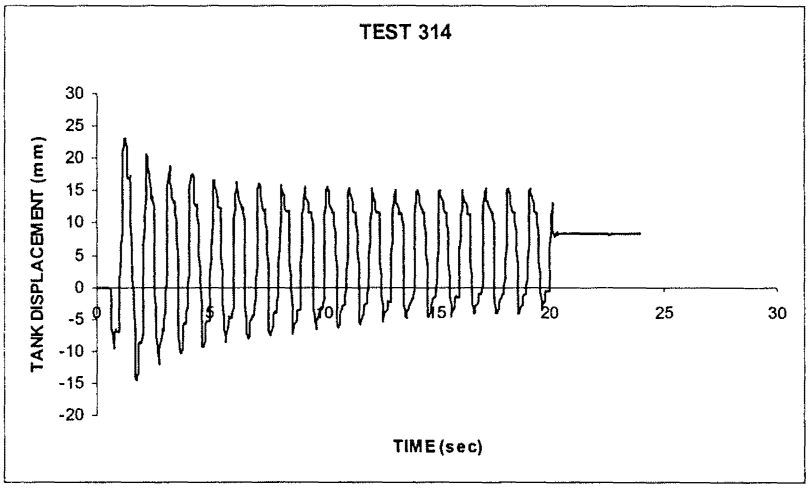

Figure C134 - Test 314 – Tank Displacement Under Cyclic Soil Shaking

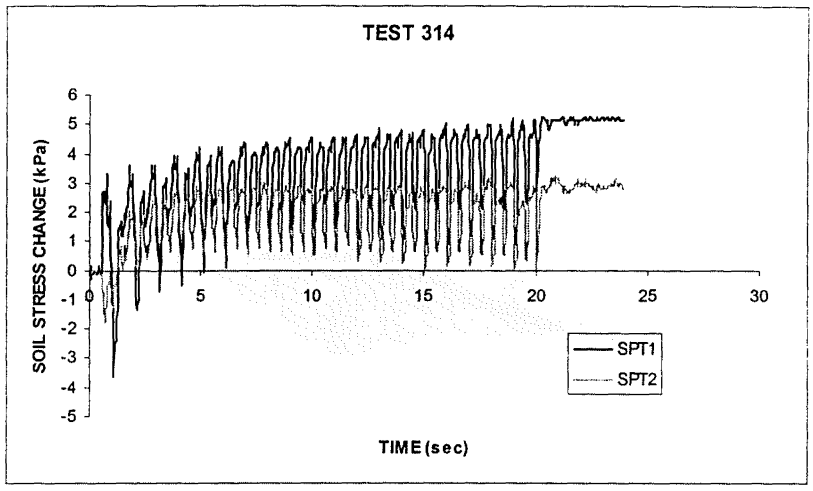

Figure C135 - Test 314 – Change in Soil Stress During Combined Loading
Depth of Burial – SPT1 = 1100 mm, SPT2 = 550mm
NOTE: Both Stress Transducers well clear of shaft sidewall (measuring far-field response)

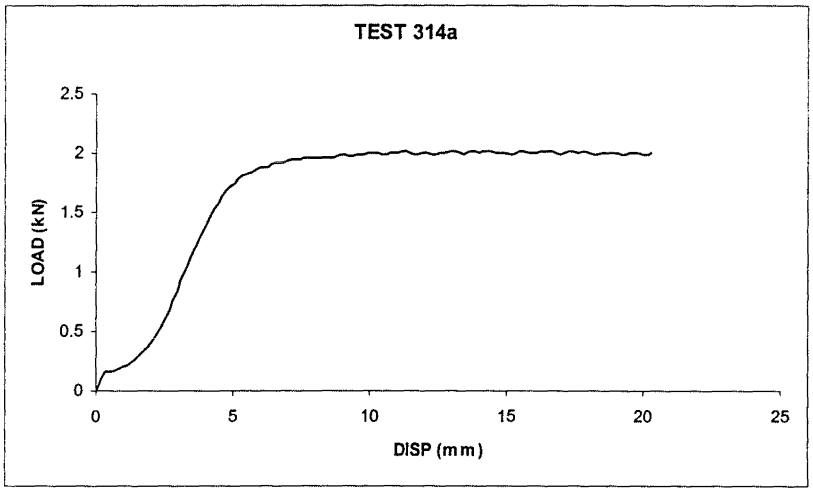

Figure C136 - Test 314a – Monotonic Uplift after Combined Loading

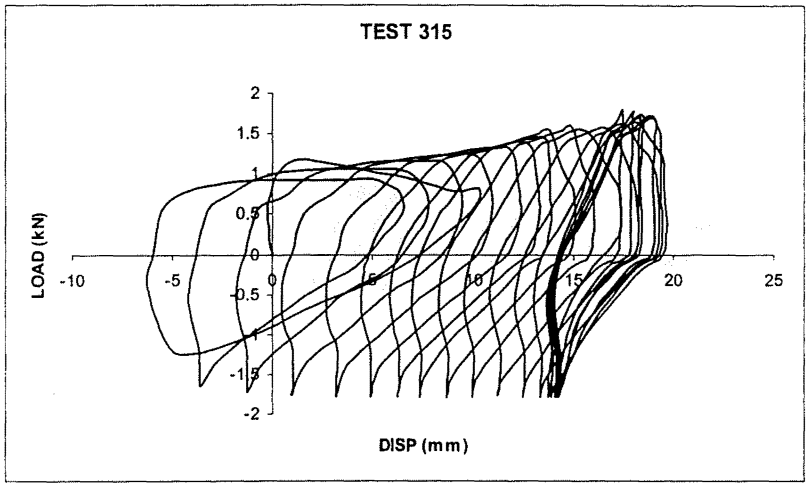

Figure C137 - Test 315 – Shaft Load v Displacement Under Cyclic Axial Load (+/-1.79 kN) and Cyclic Soil Shaking (Phase Angle = 90°)

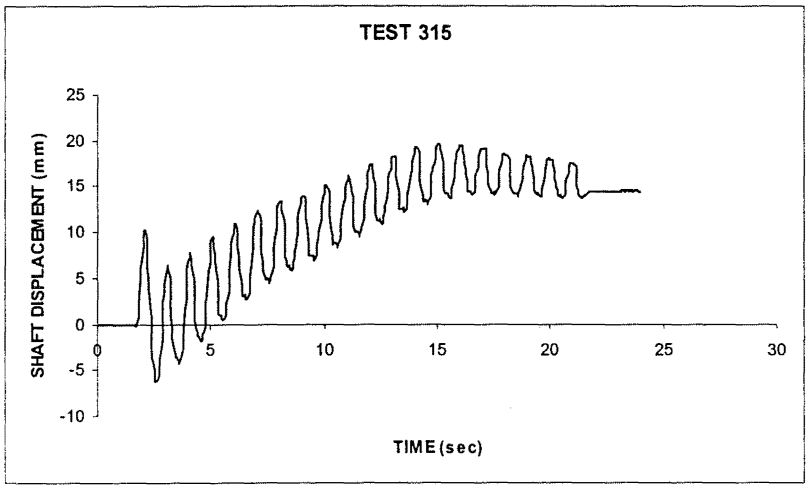

Figure C138 - Test 315 – Shaft Displacement Under Cyclic Axial Load (+/-1.79 kN) and Cyclic Soil Shaking

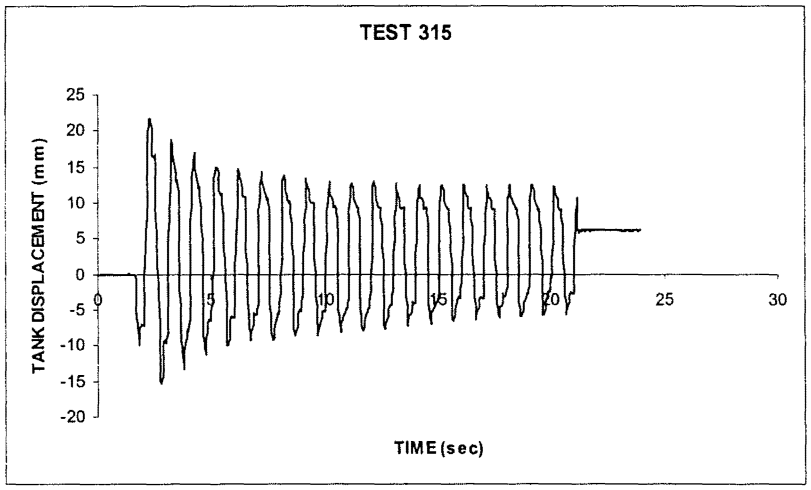

Figure C139 - Test 315 – Tank Displacement Under Cyclic Soil Shaking

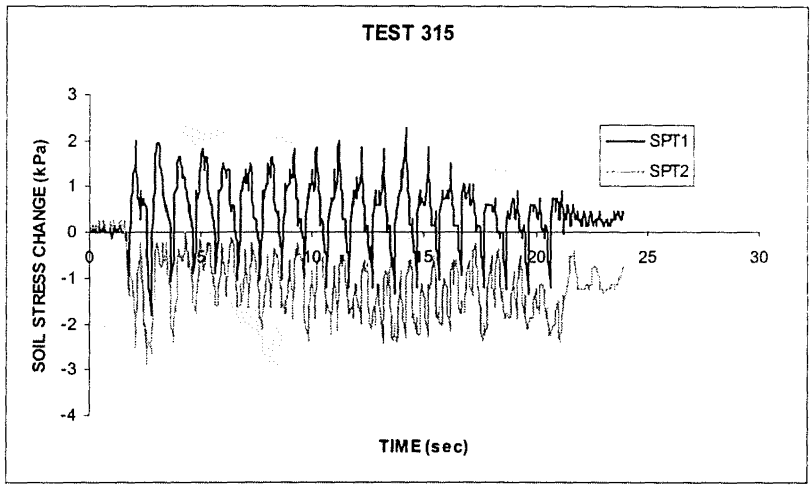

Figure C140 - Test 315 – Change in Soil Stress During Combined Loading
Depth of Burial – SPT1 = 750 mm, SPT2 = 200mm
NOTE: Both Stress Transducers well clear of shaft sidewall (measuring far-field response)

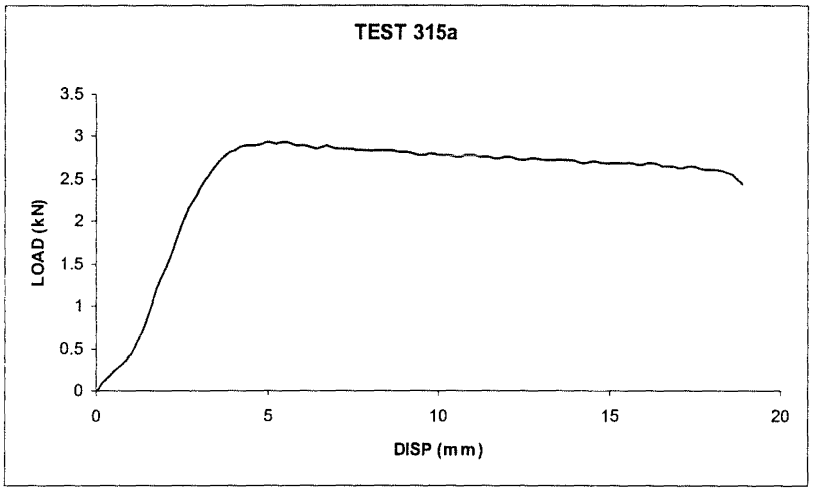

Figure C141 - Test 315a – Monotonic Uplift after Combined Loading

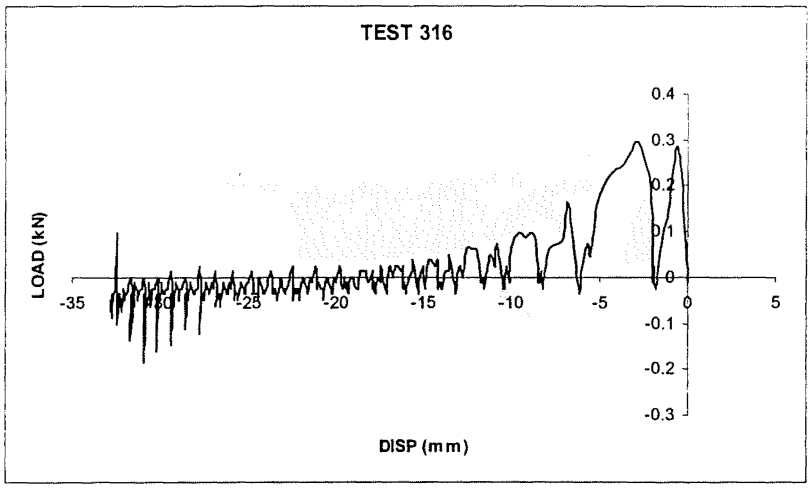

Figure C142 - Test 316 – Shaft Load v Displacement Under Cyclic Axial Load (+/-1.15 kN) and Cyclic Soil Shaking (Phase Angle = 0°)

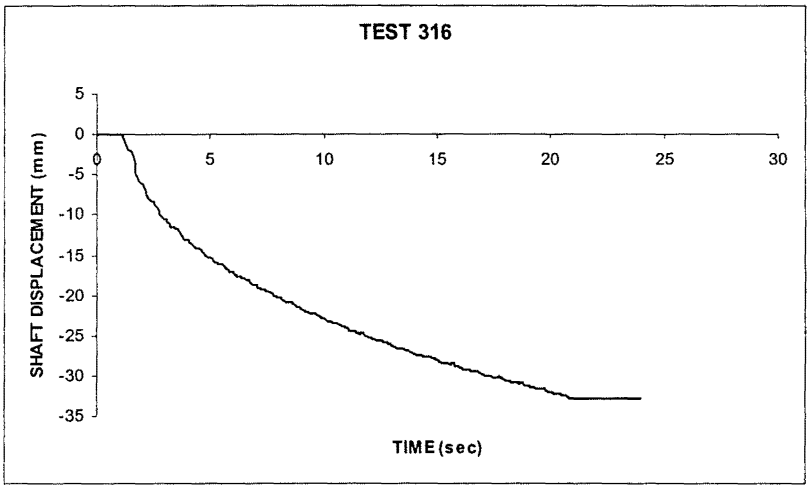

Figure C143 - Test 316 – Shaft Displacement Under Cyclic Axial Load (+/-1.15 kN) and Cyclic Soil Shaking

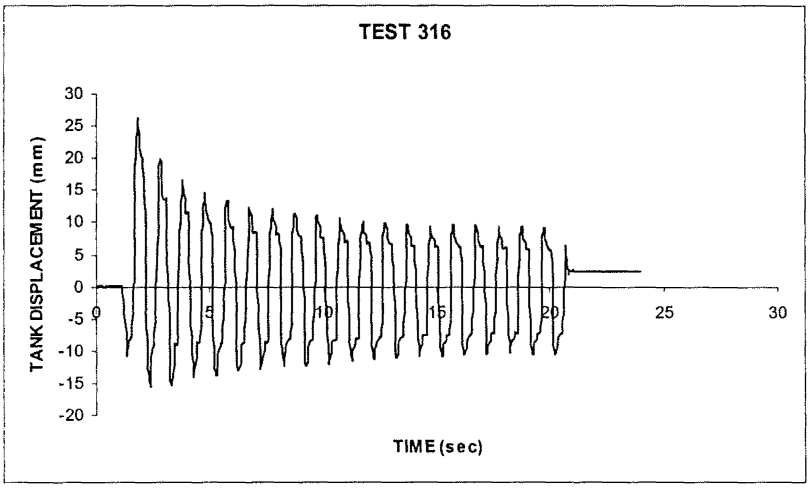

Figure C144 - Test 316 – Tank Displacement Under Cyclic Soil Shaking

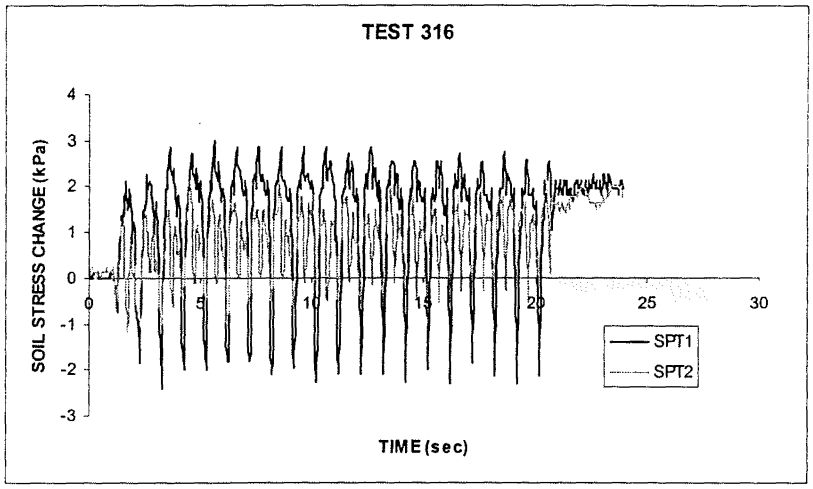

Figure C145 - Test 316 – Change in Soil Stress During Combined Loading
Depth of Burial – SPT1 = 1000 mm, SPT2 = 400mm
NOTE: Both Stress Transducers well clear of shaft sidewall (measuring far-field response)

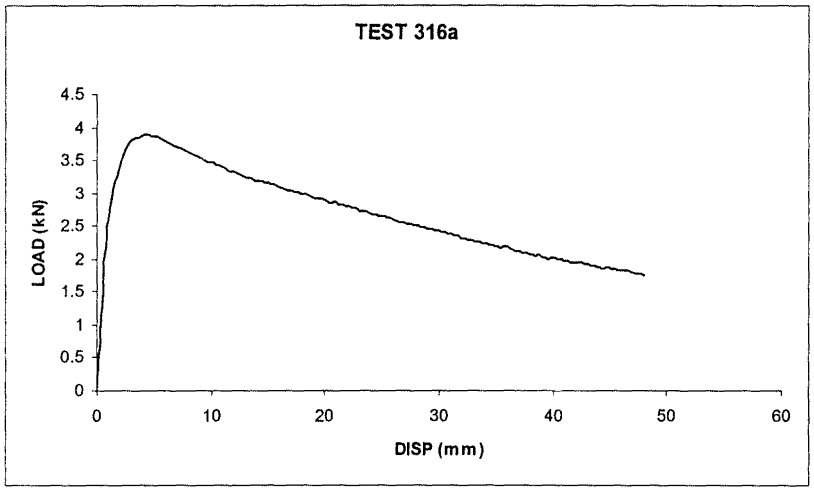

Figure C146 - Test 316a – Monotonic Uplift after Combined Loading

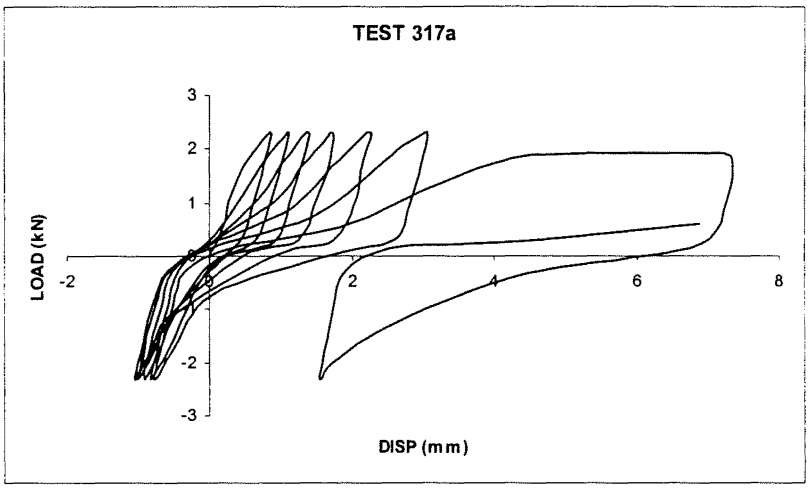

Figure C157 - Test 317a – Cyclic Axial Loading (+/- 2.31 kN) in Compacted Soil Deposit

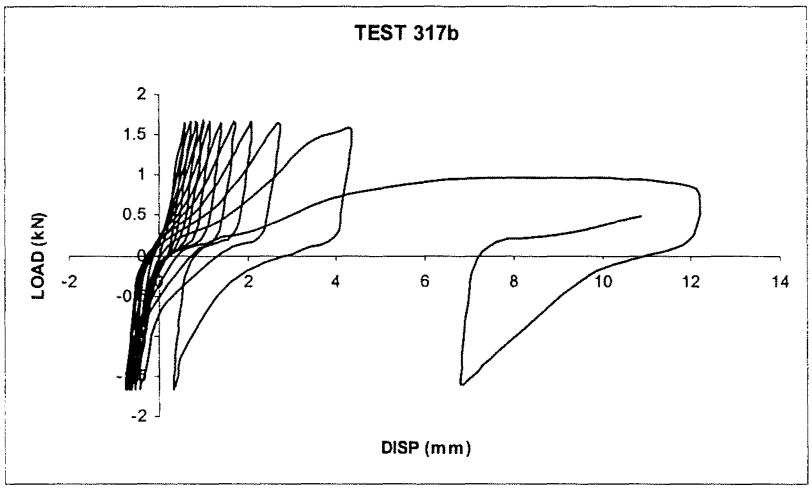

Figure C158 - Test 317b – Cyclic Axial Loading (+/- 1.65 kN) in Compacted Soil Deposit

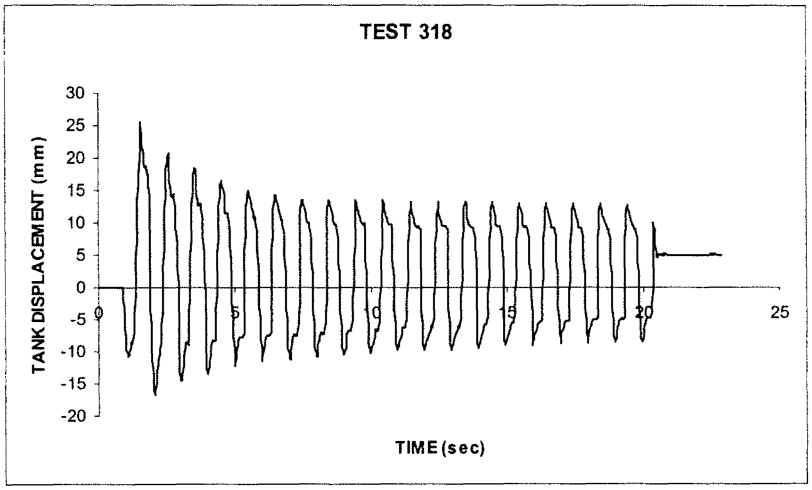

Figure C159 - Test 318 – Tank Displacement Under Cyclic Soil Shaking

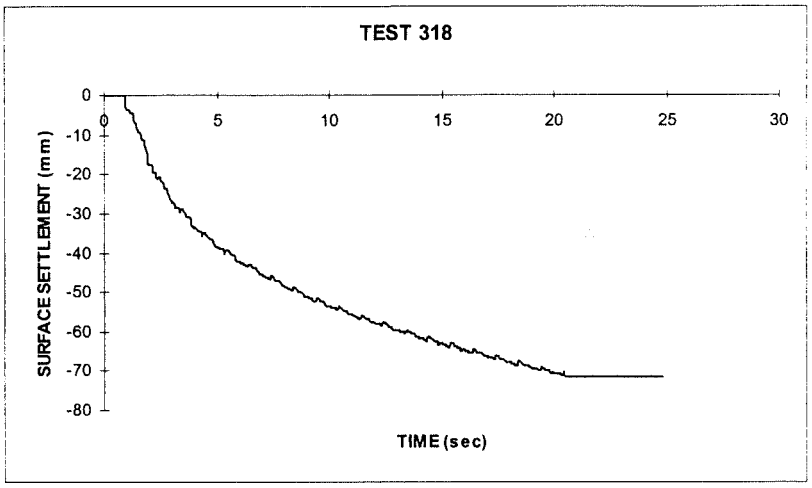

Figure C160 - Test 318 – Surface Settlement Under Cyclic Soil Shaking

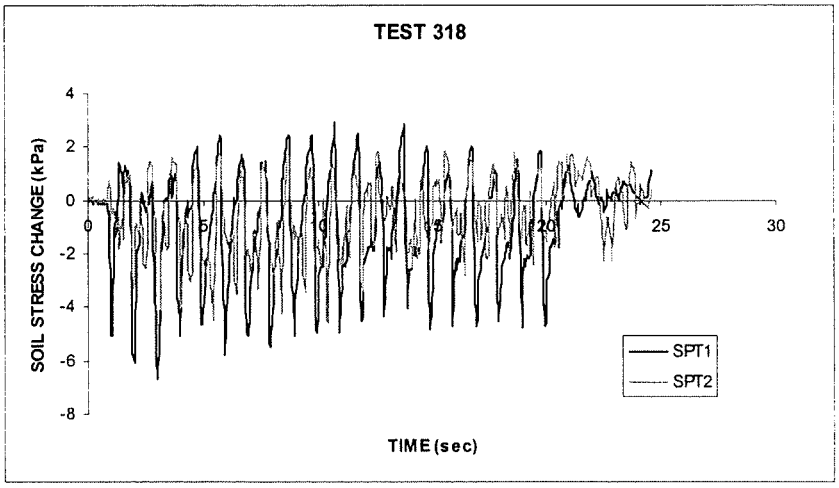

Figure C161 - Test 318 – Change in Soil Stress During Cyclic Soil Shaking
Depth of Burial – SPT1 = 1150 mm, SPT2 = 600mm
NOTE: Both Stress Transducers well clear of shaft (measuring far-field response)

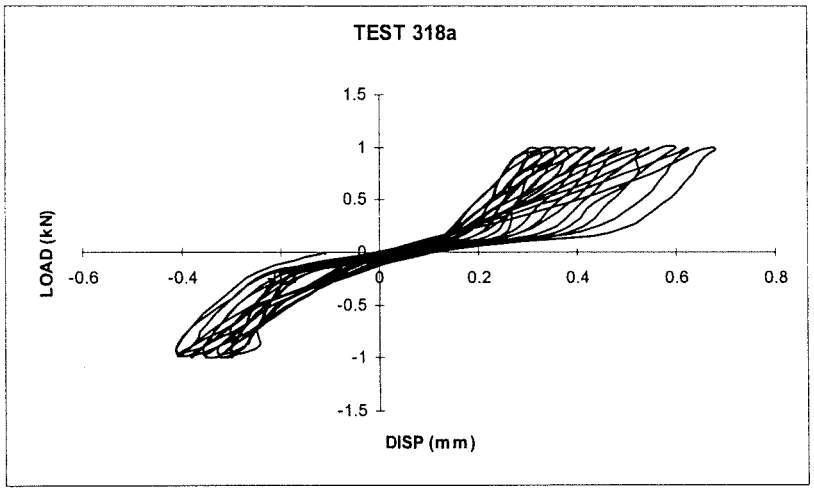

Figure C162 - Test 318a – Cyclic Axial Loading (+/- 0.99 kN) in Compacted Soil Deposit

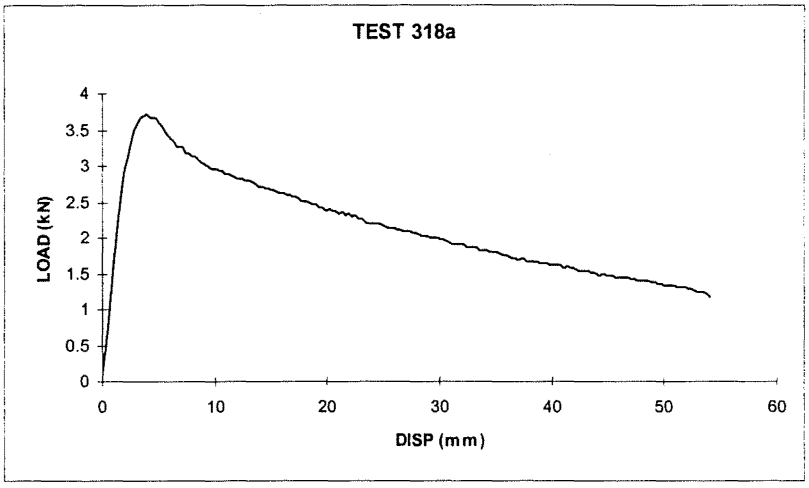

Figure C163 - Test 318a – Monotonic Uplift after Compaction and Cyclic Axial Loading

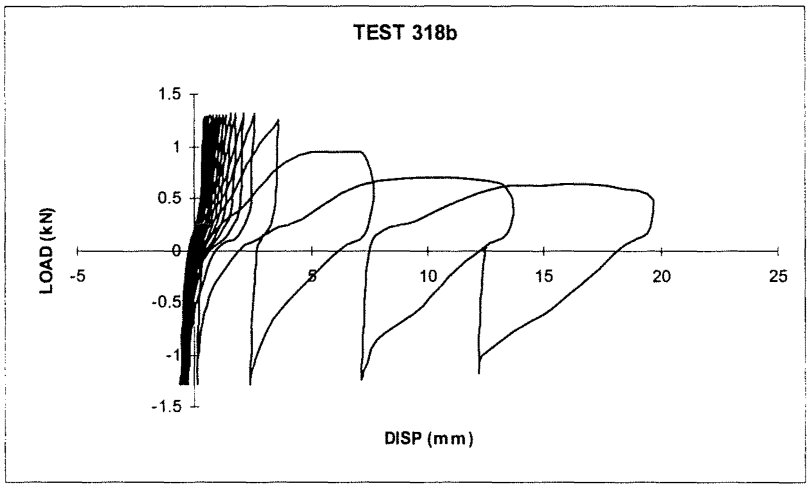

Figure C164 - Test 318b – Cyclic Axial Loading (+/- 1.28 kN) in Compacted Soil Deposit

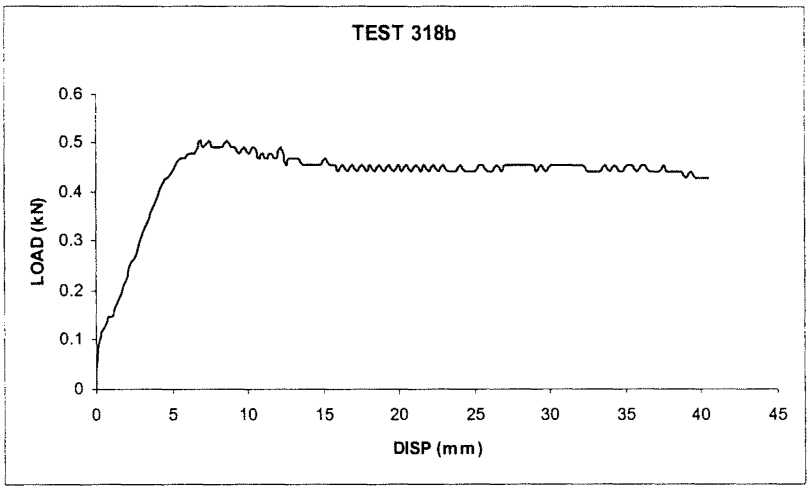

Figure C165 - Test 318b – Monotonic Uplift after Compaction and Cyclic Axial Loading

Original is missing pages LXXXIX to XCII

Appendix D

CALIBRATION OF INSTRUMENTATION

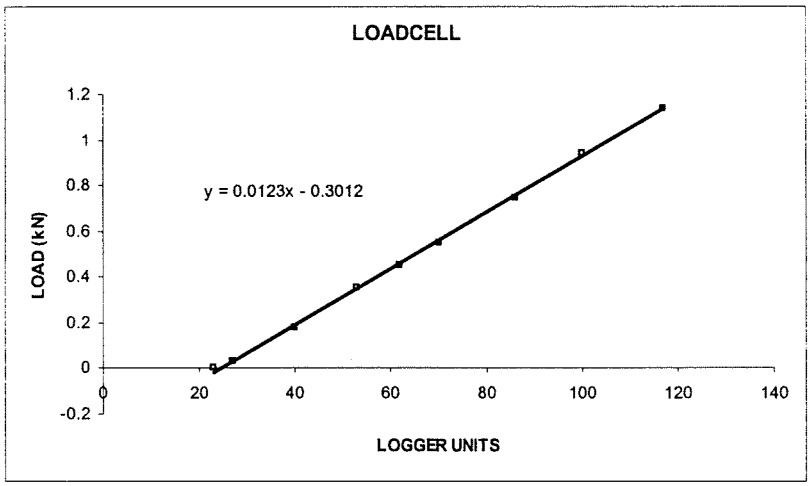

Figure D1 – Calibration Curve for Loadcell on Hydraulic Actuator

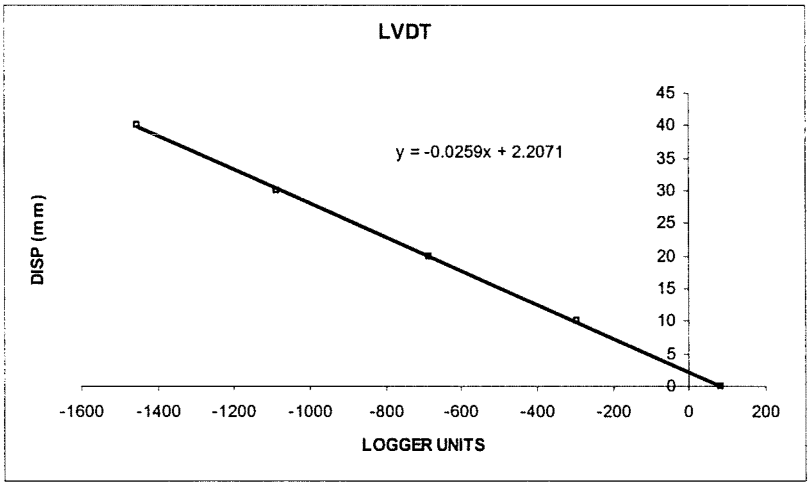

Figure D2 – Calibration Curve for LVDT on Hydraulic Actuator

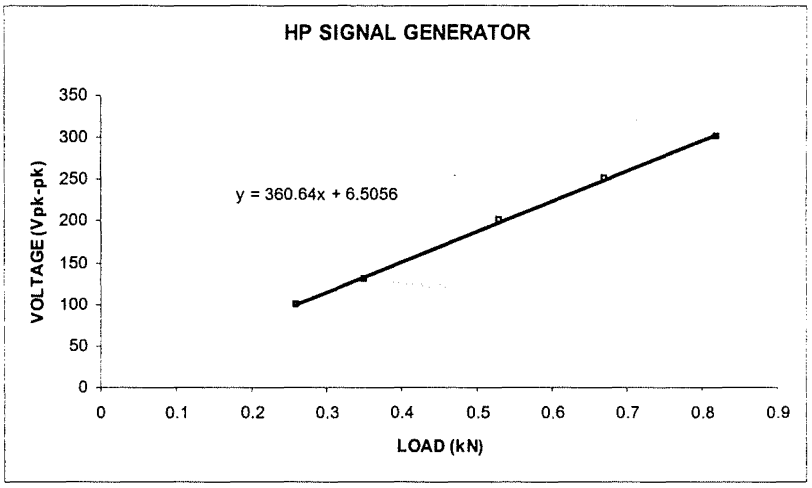

Figure D3 – Calibration Curve for Load Signal Generator

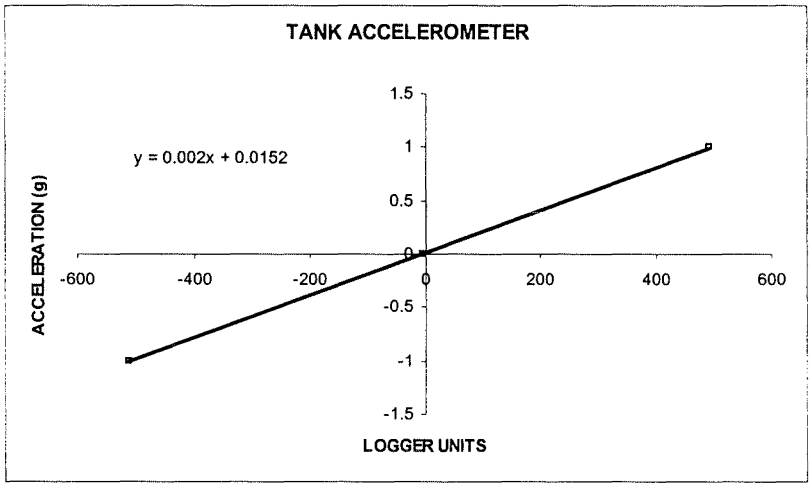

Figure D4 – Calibration Curve for Laminar Tank Accelerometer

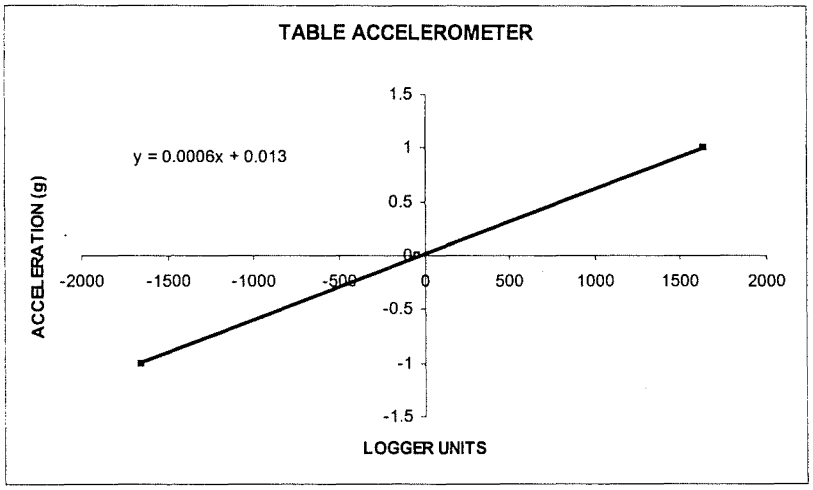

Figure D5 – Calibration Curve for Shaking Table Accelerometer

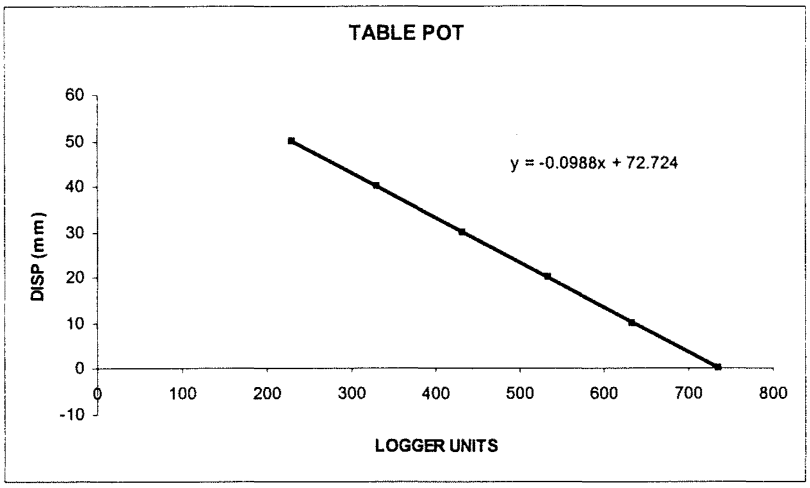

Figure D6 – Calibration Curve for Shaking Table Potentiometer

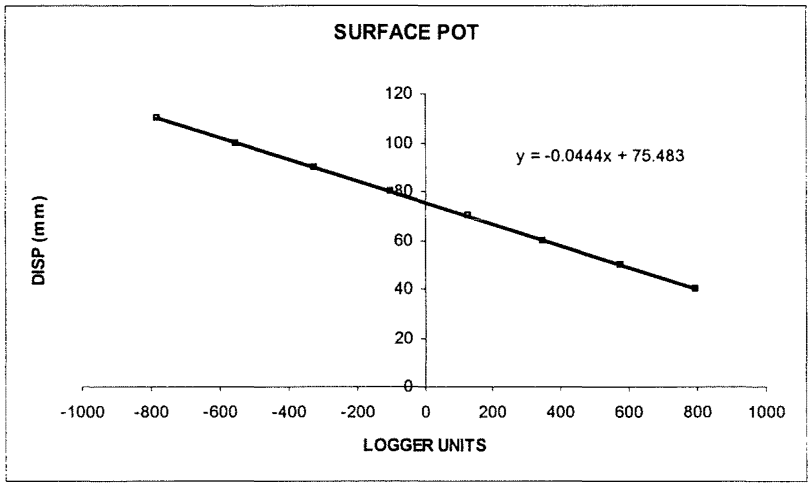

Figure D7 – Calibration Curve for Potentiometer at Soil Surface

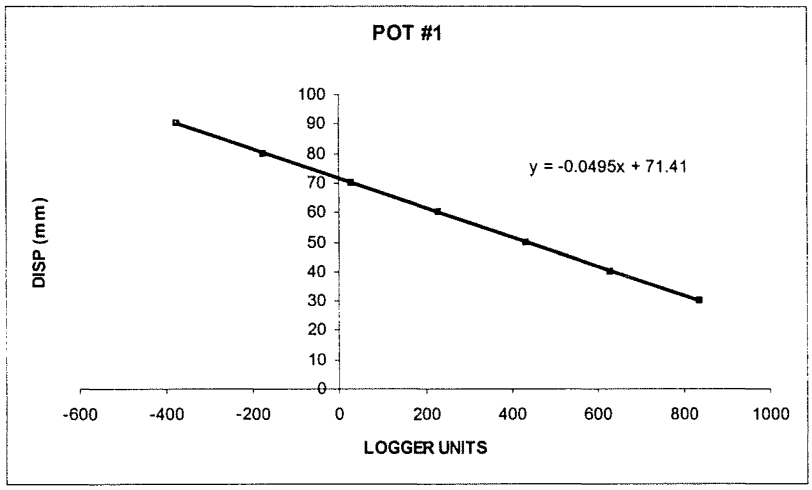

Figure D8 – Calibration Curve for Laminar Tank Potentiometer No. 1 (1990 mm above table)

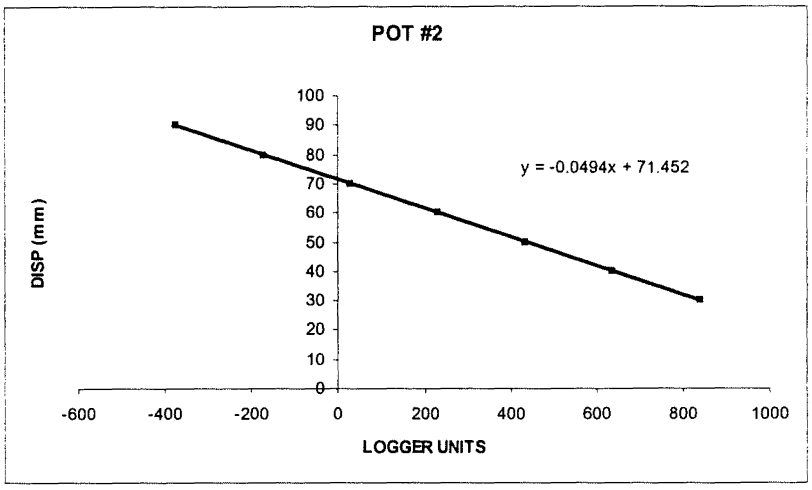

Figure D9 – Calibration Curve for Laminar Tank Potentiometer No. 2 (1780 mm above table)

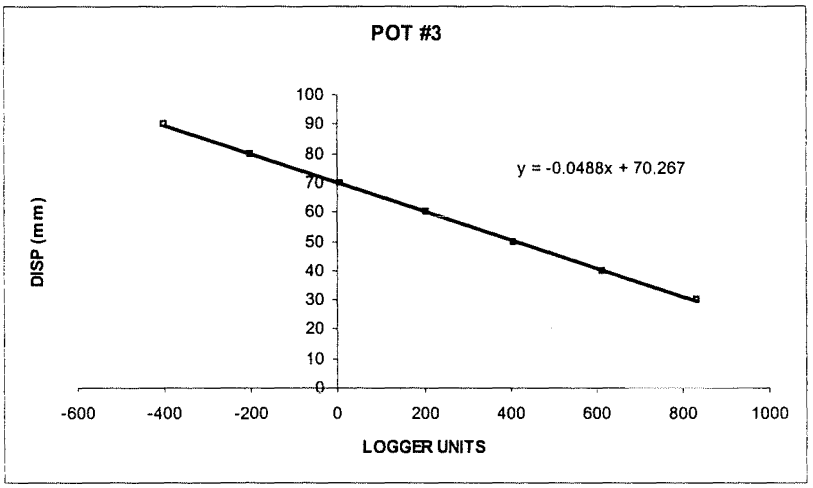

Figure D10 – Calibration Curve for Laminar Tank Potentiometer No. 3 (1575 mm above table)

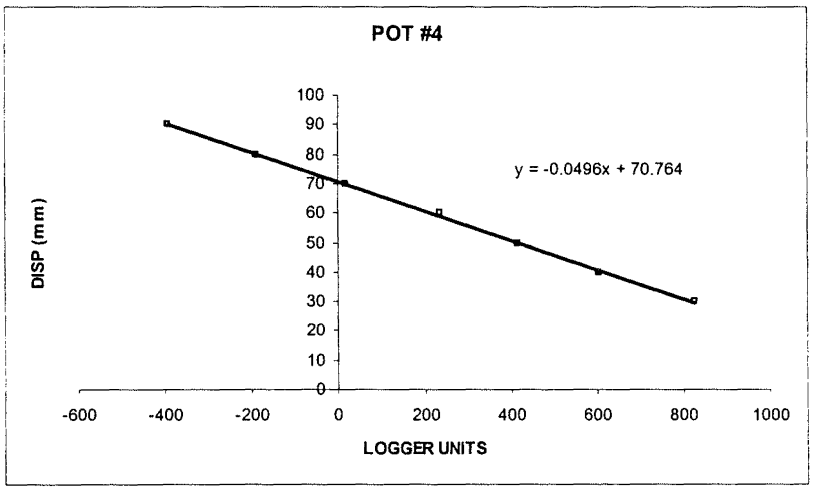

Figure 11 – Calibration Curve for Laminar Tank Potentiometer No. 4 (1250 mm above table)

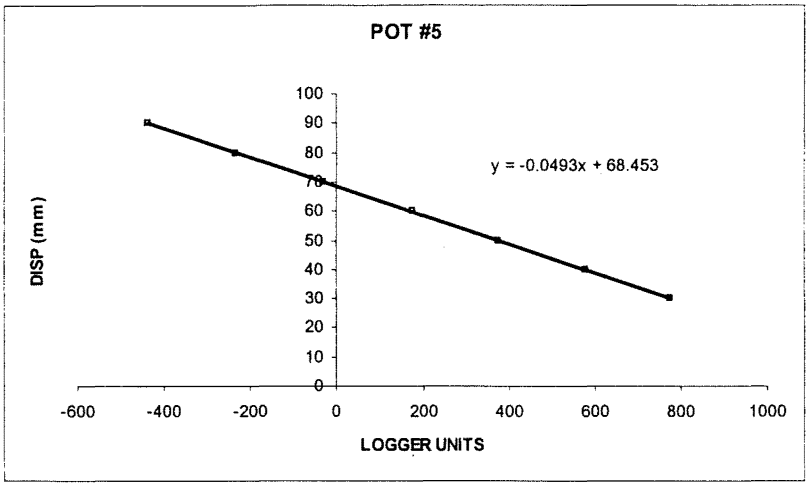

Figure D12 – Calibration Curve for Laminar Tank Potentiometer No. 5 (875 mm above table)

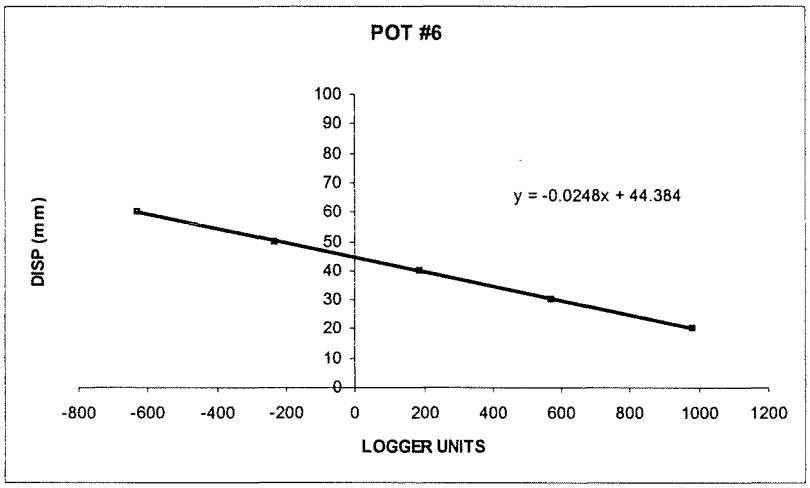

Figure D13 – Calibration Curve for Laminar Tank Potentiometer No. 6 (555 mm above table)

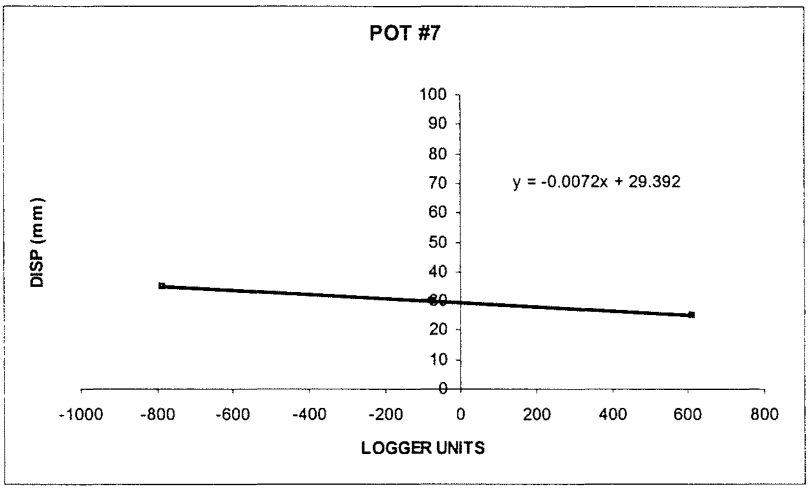

Figure D14 – Calibration Curve for Laminar Tank Potentiometer No. 7 (240 mm above table)

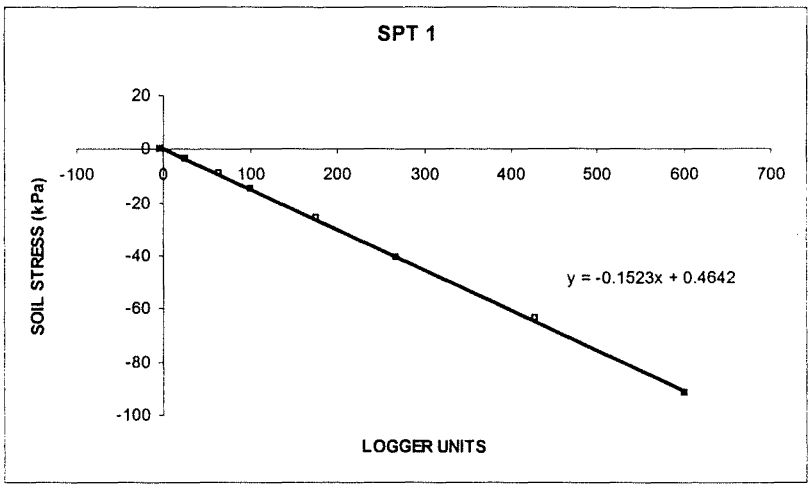

Figure D15 – Calibration Curve for Soil Pressure Transducer No. 1

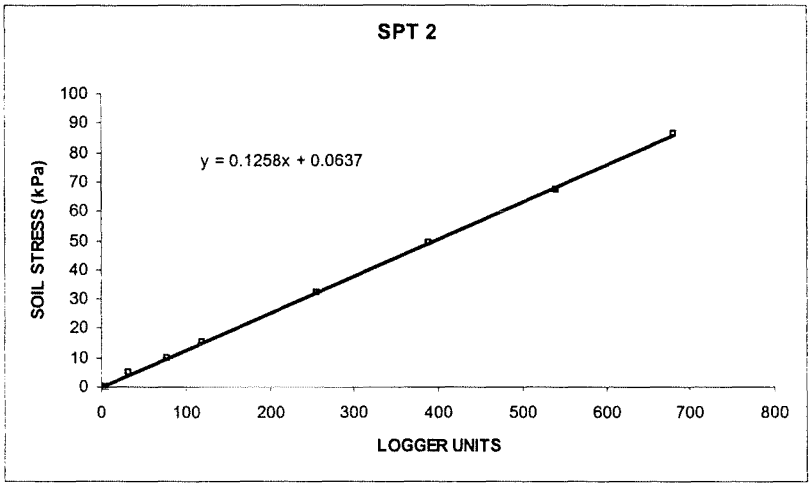

Figure D16 – Calibration Curve for Soil Pressure Transducer No. 2